Technische Universität München
Lehrstuhl für Entwicklungsgenetik

The role of FGFR2 in cerebellum development and depressive disorders

Sabit Delić

Vollständiger Abdruck der von der Fakultät Wissenschaftszentrum Weihenstephan für Ernährung, Landnutzung und Umwelt der Technischen Universität München zur Erlangung des akademischen Grades eines

Doktors der Naturwissenschaften

genehmigten Dissertation.

Vorsitzender:	Univ.-Prof. Dr. Siegfried Scherer
Prüfer der Dissertation:	1. Univ.-Prof. Dr. Wolfgang Wurst
	2. Univ.-Prof. Dr. Martin Hrabé de Angelis

Die Dissertation wurde am 11.06.2008 bei der Technischen Universität München eingereicht und durch die Fakultät Wissenschaftszentrum Weihenstephan für Ernährung, Landnutzung und Umwelt am 16.09.2008 angenommen.

1 SUMMARY / ZUSAMMENFASSUNG

The main goal of this study was to analyse genetic factors and pathway involved in depressive disorders using mice as animal models. Based on findings from other studies I concentrated on the two cell surface receptors Fibroblast growth factor receptor 2 (FGFR2) and purinergic receptor P2X, ligand-gated ion channel (P2RX7). The receptor FGFR2 is activated upon binding of extracellular FGFs and mediates its intracellular signalling via a tyrosine kinase domain. P2RX7 is a ligand gated ion channel. Extracellular ATP leads to changes in the P2RX7 conformation and to Ca^{2+} influx.

From literature it was known that components of the Fgf family are deregulated in depressive patients. However, it was not clear if this deregulation is causing depression or is just a consequence of the disorder. I inactivated FGFR2 in the entire CNS from day 11.5 of embryonic development in mice. These mice were viable and fertile and the adult mice showed dramatically altered behaviour indicating a general role of FGFR2 in CNS development and regulation of mouse behaviour. Unexpectedly, histological analysis revealed cerebellar malformations in these mice. I could show that these cerebellar phenotypes are due to developmental defects, probably caused by abnormal Bergmann glia development and morphology. Furthermore, I showed that *Fgfr2* is a good candidate gene for genetic predisposition for depressive disorders. The restricted inactivation of FGFR2 in forebrain neurons in adult mice altered depression-like behaviour and the response to acute fluoxetine administration. These data suggest that FGFR2 is not only involved in depressive disorders but also in mediating the acute response to fluoxetine, one of the most frequently used antidepressant drugs worldwide.

I generated a mouse model to study the role of P2RX7 in depressive disorders by using RNAi technology. Applying RNAi *in vivo* is a fast alternative to knockout animals and, in contrast to pharmacological inhibitors, RNAi can be used to target virtually all genes. I generated shRNA expressing mice with 88% reduction of *P2rx7* mRNA levels in the brain of adult transgenic animals. These mice are viable and fertile and the behavioural analysis is currently ongoing.

Das vorrangige Ziel meiner Doktorarbeit war die Analyse genetischer Faktoren bei der Entstehung depressiver Erkrankungen. Aufgrund von bereits veröffentlichten Studien habe ich mich dabei auf die beiden Gene Fibroblast growth factor receptor 2 (FGFR2) und purinergic receptor P2X, ligand-gated ion channel (P2RX7) konzentriert. Der Rezeptor FGFR2 wird durch die Bindung von extrazellulären FGFs aktiviert und vermittelt das intrazelluläre Signal durch eine Tyrosinkinasedomäne. P2RX7 dagegen ist ein ligandenabhängiger Ionenkanal. Die Bindung von extrazellulärem ATP an P2RX7 führt zu Konformationsänderungen und zu Ca^{2+} -Durchlässigkeit.

Aus der Literatur geht hervor, dass verschiedene Komponenten der FGF-Familie in depressiven Patienten dereguliert sind. Allerdings ist dabei nicht klar, ob diese Deregulierung Ursache oder Folge der Depression ist. Ich habe FGFR2 im gesamten zentralen Nervensystem (ZNS) von Tag E11.5 an im Maus-Embryo inaktiviert. Die Mäuse waren überlebensfähig und fertil und die erwachsenen Mäuse zeigten deutliche Auffälligkeiten in ihrem Verhalten, was eine generelle Rolle von FGFR2 in der Kontrolle des Mausverhaltens nahelegt. Unerwarteterweise haben histologische Analysen eine Fehlbildung des Kleinhirns gezeigt. Ich konnte zeigen, dass dieser Kleinhirndefekt bereits während der Entwicklung auftritt und wahrscheinlich durch gestörte Bergmann-Glia-Entwicklung und –Morphologie verursacht wird. Zusätzlich konnte ich deutliche Hinweise dafür finden, dass FGFR2 eine Rolle bei der genetischen Prädisposition für Depression spielt. Die eingeschränkte FGFR2-Inaktivierung in Vorderhirnneuronen von erwachsenen Mäusen führte zur Veränderung sowohl des depressionsbezogenen Verhaltens als auch der akuten Reaktion auf das häufig verwendete Antidepressivum Fluoxetin.

Mittels RNAi-Technik generierte ich ein Mausmodell zur Untersuchung von P2RX7-Funktionen in depressiven Krankheiten. Die Anwendung der RNAi-Methode ist eine schnelle Alternative zu herkömmlichen „knockout“-Mäusen und kann, im Gegensatz zu pharmakologischen Inhibitoren, prinzipiell auf alle Gene angewandt werden. Die hergestellte RNAi-Maus zeigt eine Reduktion des P2rx7-mRNA-Gehalts um 88% im Gehirn von erwachsenen Mäusen. Diese Mäuse sind fertil und werden nun in Verhaltenstest auf ein verändertes depressionsbezogenes Verhalten untersucht.

2 SCOPE OF THE WORK

The scope of this work was to analyse the role of FGFR2 during brain development and in depressive disorders. Furthermore, a new P2RX7 mouse model for depressive disorders was generated using RNAi technology.

Before exploring the role of FGF signalling in depressive disorders in mice, I first examined the expression of all four known *Fgfrs* in the adult mouse brain. Based on the findings of this expression analysis I decided to study both, the general role of FGFR2 during brain development and the role of FGFR2 in Depression.
Many studies showed already the importance of FGF signalling and its components during brain development. In this study I examined nonredundant functions of one of the FGF receptors, namely FGFR2. The analysis of FGFR2 function during brain development is done by disruption of the FGFR2 gene through Cre-mediated recombination in the whole CNS during embryogenesis (from embryonic day E11.5 on).
Several studies showed also a possible role for FGF signalling in mood disorders. Especially the expression of *Fgf2* and the two receptors *Fgfr2* and *Fgfr3* are thought to be reduced in depressive patients or in rats after antidepressant treatment. Significantly lower expression levels of *Fgfr2* were shown in depressive patients in cingulate cortex and in prefrontal cortex. These two forebrain regions are known to be involved in depressive disorders. In this study I analysed if the loss of FGFR2 leads to increased depression-like behaviour in mice. Therefore, I disrupted the *Fgfr2* gene by Cre-mediated recombination in forebrain neurons and tested these mice in several behavioural paradigms, including the forced swim test and the tail suspension test. These are the two commonly used tests for depression-like behaviour in mice.

Working on depression and studying depression-like behaviour in mice led to the idea to generate P2RX7 knockdown mice. Since recent studies linked the purine receptor P2RX7 to major depressive disorder in humans these mice could be used in behavioural paradigms to determine the involvement of P2RX7 in depression-like behaviour. I used the RNAi technology to generate a P2RX7 mutant mouse because it is faster than generating knockout mice. Not only that the generation of ES cell derived mice is accelerated but it is also possible to use heterozygote mice for analysis.

3 INTRODUCTION

3.1 FGF family – general overview

The Fibroblast growth factor (FGF) signalling system is composed of 22 Fibroblast growth factors and 4 Fibroblast growth factor receptors (FGFRs) and has important functions in many tissues including the nervous system (Ford-Perriss et al., 2001; Itoh and Ornitz, 2004). FGFs are polypeptide growth factors that are found in organisms ranging from nematodes to humans (Ornitz and Itoh, 2001). FGF receptors are tyrosine kinase transmembrane receptors. The four known FGF receptors (FGFR1-4) bind FGFs in combination with heparane sulphate proteoglycans. The FGF signalling activity is regulated by the distinct expression of FGFs and FGFRs and their binding specificity (Fortin et al., 2005; Ornitz et al., 1996; Zhang et al., 2006). Binding of two FGFs to the extracellular domains of a FGFR-dimer leads to intermolecular autophosphorylation of the intracellular FGFR domains (Bellot et al., 1991). The three major intracellular signalling pathways mitogen-activated protein kinase (MAPK), phosphatidylinositol 3 -OH kinase (PI3K) and phospholipaseC gamma (PLCgamma) are influenced by FGF signalling (Fig. 1) (Eswarakumar et al., 2005; Walsh et al., 1997). FGFR activation leads to a negative feedback loop by inducing expression of Sprouty family members (Liu et al., 2003). Sprouty proteins are antagonists of tyrosine kinase-containing receptors like FGFRs and are therefore inhibiting FGFR activity (Hanafusa et al., 2002; Mason et al., 2004). Similar negative feedback loops via Sef1 and MAPK phasphatase 3 (MKP3) are known (Echevarria et al., 2005; Furthauer et al., 2002). FGF signalling is further modified by indirect interactions between the FGFRs via a negative feedback loop (Liu et al., 2003). In mouse P1 mid-hindbrain tissue FGF8b mediated FGFR1 activation leads to an inhibition of *Fgfr2* and *Fgfr3* expression. Furthermore, FGFRs can directly interact with neuronal cell adhesion molecules (NCAM) linking FGF signalling to cell-cell interaction and axonal growth (Cavallaro et al., 2001; Doherty and Walsh, 1996; Kiselyov et al., 2005). Beside all these molecules which are directly mediating effects of FGFR activation there are also interactions between FGF signalling and NOTCH and WNT mediated signalling pathways described (Saarimaki-Vire et al., 2007; Wahl et al., 2007; Yoon et al., 2004). The importance of FGF signalling is demonstrated in mice by several knockout mutants. While depletion of FGFR1 or FGFR2 in mice results in embryonic lethality the loss of FGFR3 leads

to a less severe phenotype including bone malformations (Arman et al., 1998; Deng et al., 1996; Deng et al., 1994; Yamaguchi et al., 1994). Furthermore, several human disorders are caused by mutations and malfunctions of FGF family members (Evans et al., 2004; Kornmann et al., 1998; Nie et al., 2006; Wilkie, 2005).

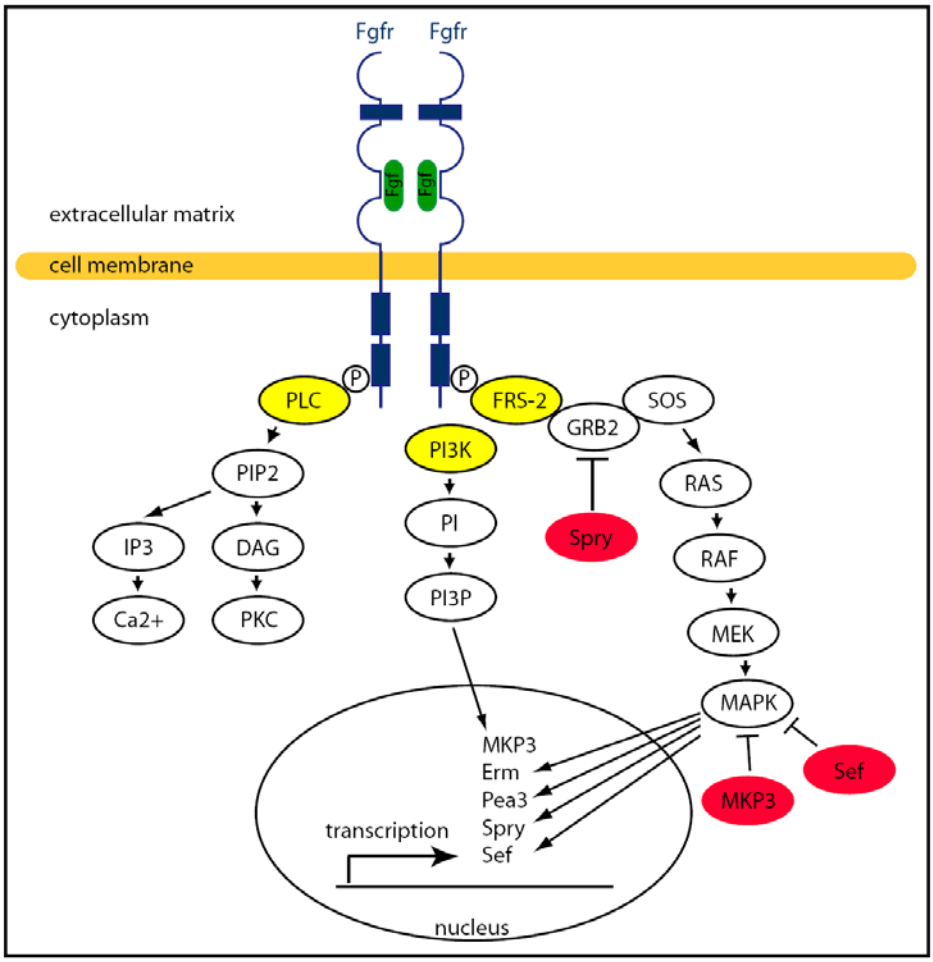

Figure 1. Upon binding of extracellular FGFs FGFR dimers can activate the PLCgamma, the PI3K and the MAPK signalling pathway (Blak, 2005).

PLCgamma binds to activated FGFR dimers and induces dissociation of Phosphatidylinositol 4,5-Bisphosphate (PIP2) into Inositol triphosphate (IP3) and diacylglycerol (DAG). IP3 stimulates Ca^{2+} release from the Endoplasmatic Reticulum. DAG together with Ca^{2+} activates proteine kinase C (PKC) (Mohammadi et al., 1992; Peters et al., 1992). Additionally the increased intracellular Ca^{2+} levels modulate the function of several other proteins and enzymes. FGFRs induce via PI3K activation the phosphorylation of Phosphoinositol (PI), resulting in the production of Phosphoinositol 3-phosphate (PI3P). PI3P activates transcription of *Mkp3*, a MAPK inhibitor (Camps et al., 1998; Kawakami et al., 2003; Muda et al., 1996). The MAPK signalling pathway is activated by phosphorylation of the adapter protein fibroblast growth factor receptor substrate 2 (FRS-2) (Kouhara et al., 1997). The signalling cascade via RAS/RAF leads to MAPK activation (Kolch et al., 1993; Moodie et al., 1993; Stokoe and McCormick, 1997). MAPK is translocated to the nucleus and induces the transcription of the transcription factors *polyomavirus enhancer activator 3 (Pea3)* and *Ets Related Molecule PEA3-like* (*Erm*) and the inhibitors *Sprouty1* (*Spry*) and *Sef*.

3.2 FGF signalling in cerebellum development

Anatomically the cerebellum belongs to the hindbrain and represents in adults the most rostral and dorsal part of the hindbrain (Fig. 2). In mice the cerebellum undergoes important morphological changes, including cell proliferation and cell migration, untill the third postnatal week (Komuro and Rakic, 1998). Midbrain and hindbrain development is regulated by a secondary organizing centre within the neural tube, the so called mid-/hindbrain organizer (MHO), which is located at the isthmic constriction, the interface between the midbrain and the hindbrain. The expression of a set of transcription factors and secreted molecules are characterising the MHO (Echevarria et al., 2003; Liu and Joyner, 2001; Rhinn and Brand, 2001; Wurst and Bally-Cuif, 2001). The position of the MHO along the anterior/posterior axis (a/p) is determined by the interaction of the two transcription factors *Orthodenticle like homeobox protein 2* (*Otx2*) and *Gastrulation brain homeobox protein 2* (*Gbx2*) at around embryonic day (E) 8 (Broccoli et al., 1999; Millet et al., 1999; Simeone, 2000). Subsequently, the expression of the four transcription factors *Paired domain homeobox proteins 2* and *5* (*Pax2/5*) and *Engrailed 1* and *2* (*En1/2*), which were shown to be necessary for the normal development of the MHR, is induced across the midbrain-/hindbrain boundary (Millen et al., 1994; Rowitch and McMahon, 1995; Wurst et al., 1994). Furthermore, the secreted growth factors *Sonic hedgehog* (*Shh*), Wingless-type MMTV integration site 1 (*Wnt1*) and *Fibroblast growth factor 8* (*Fgf8*) control the establishment and maintenance of the MHR. *Shh* is expressed along the floor plate of the neural tube whereas in the midbrain its expression is expanded into the basal plate (Prakash and Wurst, 2004). *Shh* expression seems to be crucial for several neuronal populations in the ventral MHR (Hynes et al., 1995; Hynes et al., 2000; Lam et al., 2003; Ye et al., 1998). *Wnt1* is expressed along the midline of the dorsal and in two parallel stripes in the ventral midbrain and also as a ring in the caudal midbrain, immediately anterior to the mid-/hindbrain boundary and has been shown to be essential for development of tissues and neuronal cell populations in the MHR (McMahon et al., 1992; Prakash et al., 2006). *Fgf8* is expressed directly posterior to the mid-/hindbrain boundary as an open ring in the most anterior r1. *Fgf8* expression is required for the morphogenesis of the MHR (Chi et al., 2003; Meyers et al., 1998). Furthermore, the expression of MHO genes and the formation of ectopic hindbrain and midbrain structures in the diencephalon and posterior hindbrain can be induced by ectopic application of FGF8 protein (Crossley et al., 1996; Liu et al., 1999; Martinez et al., 1999). Besides *Fgf8*, also other *Fgfs*, including *Fgf15*, *Fgf17* and *Fgf18*, are expressed in the developing MHR. FGF15 has

been shown to regulate proliferation and cell cycle progression and is not restricted to the MHR (Gimeno et al., 2002). FGF17 is involved in the development of the anterior cerebellum (Xu et al., 2000). For FGF18, a contribution to the regulation of proliferation in the MHR was suggested, but loss of FGF18 in the MHR does not lead to any obvious defects (Liu et al., 2003; Ohbayashi et al., 2002).

The *Fgfr* expression in the mouse MHR has been analysed in several studies (Blak et al., 2005; Ishibashi and McMahon, 2002; Liu et al., 2003; Trokovic et al., 2003). According to these reports, *Fgfr1-3* are expressed in the developing mouse MHR while *Fgfr4* is not. *Fgfr1* is expressed throughout the MHR from E8.5 to E12.5. *Fgfr2* shows a dynamic expression pattern in the MHR expanding from E9.5 onwards from ventral to dorsal tissue. The dynamic *Fgfr3* expression is restricted to the ventral MHR. Due to these descriptions of *Fgfr* expression in the MHR, *Fgfr1* was believed to be the major mediator of FGF signalling in the MHR during development. Conditional $Fgfr1^{l/l}$ $En1^{Cre/+}$ mouse mutants, in which the *Fgfr1* gene was inactivated in the MHR after E9, were used to analyse the function of FGFR1 in the MHB (Trokovic et al., 2003). These mutants were viable and fertile, although they showed an abnormal gait and had problems with balance. Furthermore, they displayed a loss of the IC and of the cerebellar vermis, but structures derived from further anterior or posterior tissue of the dorsal MHR (i.e., the superior collliculi and the hemispheres of the cerebellum) were intact. In the ventral MHR of conditional FGFR1 mutants only a subtle disorganization of the locus coeruleus could be detected (Trokovic et al., 2003). These described alterations in conditional FGFR1 mutants are less severe than the alterations found in conditional FGF8 mutants, which were generated using the same $En1^{Cre/+}$ line (Chi et al., 2003). FGF8 MHR conditional knockout mice lose the complete MHR, due to loss of MHO gene expression and subsequent cell death. The tissue loss includes the cerebellar hemispheres and the dorsal SC as well as the ventral MHR, containing the LC, the VTA and SN, and the 3rd and 4th cranial nerve (Chi et al., 2003). The discrepancy between the *Fgf8* and *Fgfr1* conditional MHR knockout mice suggests that FGF signalling in the developing MHR is not mediated by FGFR1 alone (Naserke, 2007). However, *Fgfr2* and *Fgfr3* conditional MHR knockout mice, which were both generated using the same $En1^{Cre/+}$ line, revealed that FGFR2 and FGFR3 are not required for patterning and maintenance of the MHR (Blak et al., 2007). In both mouse mutants, the patterning of the MHR is not altered and neuronal populations develop normally and are maintained into adulthood. These studies suggest that FGFR2 and FGFR3 could

probably compensate partly the loss of FGFR1, especially in ventral tissue, but FGFR1 is sufficient to mediate FGF signalling in the developing MHR.

Although conditional depletion of FGFR2 in the mouse MHR, using *En1*$^{Cre/+}$ mice, did not affect the gross patterning and maintenance of the cerebellum, several studies showed an important function of FGFR2 in radial glia maintenance and in regulating migration and morphogenesis of glial cells. Retroviral delivery of a constitutively active form of FGFR2 to E9.5 brains resulted in increased number of radial glia cells (Yoon et al., 2004). In astroglia specific conditional FGFR2 mutants, using hGFAP-Cre mice, a slight reduction of cortical thickness and reduced number of astrocytes, especially in the upper cortical layers were observed in E18.5 brains (Smith et al., 2006). *In vitro* experiments showed that FGFR3 is involved in differentiation of oligodendrocyte progenitors, whereas FGF9 triggers process outgrowth via activation of FGFR2 in differentiated oligodendrocytes (Fortin et al., 2005). Additionally, FGFR2 seems to be involved in dopamine-dependent regulation of adult mouse behaviour since *Fgfr2*$^{l/l}$ *oligodendrocyte-specific 2, 3-cyclic nucleotide phosphodiesterase (Cnp1)* $^{Cre/Cre}$ mice display dramatic hyperactivity (Kaga et al., 2006). Interestingly, in *Fgfr2*$^{l/l}$ *Cnp1*$^{+/Cre}$ mice no altered behaviour was observed and increased locomotion in *Fgfr2*$^{l/l}$ *Cnp1*$^{Cre/Cre}$ mice was abolished by administration of dopamine receptor antagonists.

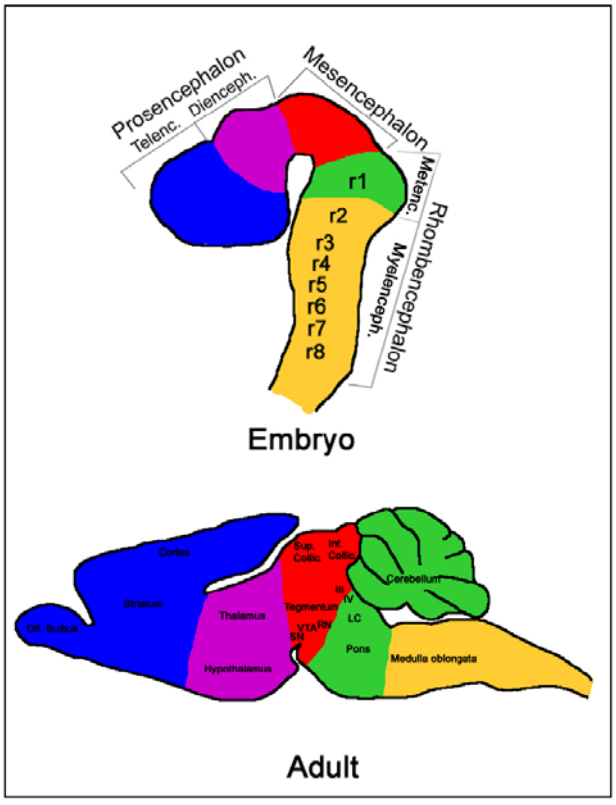

Figure 2. Relationship of adult and embryonic brain regions.
During embryogenesis (E8 – E10) the anterior neural tube is divided into Prosencephalon, Mesencephalon and Rhombencephalon. From E11 on Prosencephalon is further subdivided in Tel- and Diencephalon, and the Rhombencephalon is subdivided into Met- and Myelencephalon (with Rhombomeres 1 – 8 (r1 – r8)). Colour code is indicating the corresponding adult brain regions. LC: locus coeruleus; RN: raphe nucleus; SN: Substantia nigra; VTA: ventral tegmental area; III and IV: 3rd and 4th cranial nerve. (From Alexandra Blak Diss. 2007)

The cerebellum comprises a large proportion of the adult mouse brain and is thought to coordinate motor-neuron movement, learning and reflex adaptation. Genetically manipulated mouse models have determined a role of the cerebellum and distinct cerebellar cell populations in motor-coordination (Aruga et al., 2004; Barski et al., 2003). The adult mouse cerebellar cortex is organised in lobes and lobules with well defined layered cellular architecture (Fig. 3) (Inouye and Oda, 1980). The Purkinje cell layer (PCL) is separating the outer molecular layer (ML) from the inner granular layer (GL). The ML consists of basket cells and stellate cells, both inhibitory interneurons, which are embedded in a dense network of neurites and glial fibres. The GL contains the most abundant cerebellar neurons, the Granule neurons. The PCL is composed of Purkinje neurons, the only cerebellar output neurons, which are surrounded by the smaller Bergmann glia cells. Purkinje cells send axons to deep cerebellar nuclei neurons, which provide the primary output from the cerebellar cortex (Saab and Willis, 2003; Wang and Zoghbi, 2001). The radial Bergmann glia fibres are attached to the basal lamina at the surface of the cerebellum and are involved in both cerebellar developmental and modulation of cerebellar cortical activity in the adult (Delaney et al., 1996; Lordkipanidze and Dunaevsky, 2005; Yacubova and Komuro, 2003; Yue et al., 2005).

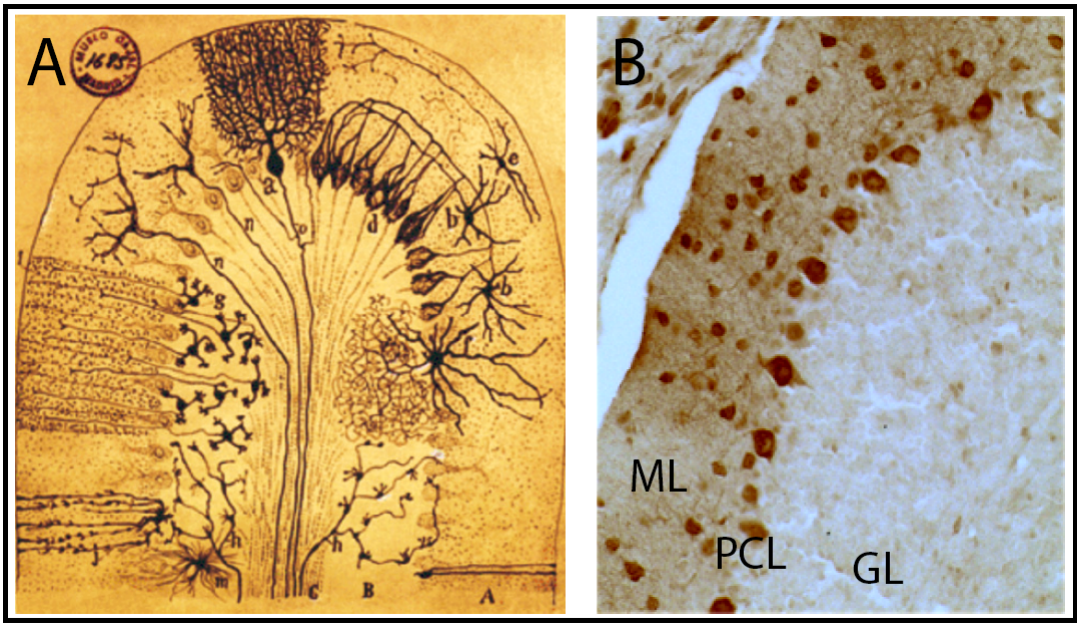

Figure 3. Cell morphology and location in the adult cerebellar cortex.
A: The outer molecular layer (A) contains the GABAergic stellate (e) and basket cells (b). Below the molecular layer is a single cell layer with Purkinje neurons (a) and Bergmann glia cells (j). The internal granular layer (B) consists of Granule neurons (g). Within the white matter tract(C) Oligodendrocytes (m) are found. Drawing from: S. Ramon y Cajal, Hisologie du Systeme Nerveux de l`Homme et des Vertebres (Maloine, Paris, 1911).
B: The immunohistochemical staining of the adult mouse cerebellum using Parvalbumin specific antibody shows labelled stellate and basket cells in the molecular layer (ML) and larger Purkinje cells in the Purkinje cell layer (PCL). GL: granular layer.

During embryonic development granule neuronal precursors populate the entire surface of the cerebellum. While post-mitotic, the Granule neurons leave this external granular layer and migrate along the Bergmann glia fibres through the ML and PCL inwards to establish the internal granular layer (Hatten and Heintz, 1995; Sgaier et al., 2005). Morphogenetic and cellular movements during embryonic and early postnatal stages are tightly regulated by several factors. Important insights into cerebellar development came from mice harbouring spontaneous mutations. *Weaver* mice harbour a single amino acid mutation in a G-protein coupled, inwardly rectifying K+ channel, GIRK2 (Mjaatvedt et al., 1995). This mutation acts cell-autonomous and leads to granule cell death and impairs postnatal granule cell migration across the ML (Hatten et al., 1986; Rakic and Sidman, 1973). The *Reeler* mouse contains a recessive mutation in the *Reelin (rl)* gene (Hamburgh, 1963). Reelin, an extracellular matrix protein is involved in glia-guided neuronal migration and Reeler mice display severe Purkinje cell ectopia and granule cell reduction (D'Arcangelo and Curran, 1998). The mutation in the *Disabled-1 (Dab1)* gene in *scrambler* mice leads to similar cerebellar abnormalities in neuronal positioning and migration (Sanada et al., 2004). Reelin regulates via the two surface receptors *very low density lipoprotein receptor (Vldlr)* and *apolipoprotein E receptor 2 (ApoER2*; also known as *Lrp8*) Dab1 activity (Hack et al., 2007). The defect in neuronal migration in *scrambler* mice are caused by *integrin alpha3 (Itga3)* mediated abnormal adhesion between newly generated neurons and radial glia fibres (Sanada et al., 2004). Members of the integrin family are cell surface receptors mediating cell-extracellular matrix and cell-cell interactions with important roles in cerebellum development and in differentiation of granule cells and Bergmann glia. Conditional *integrin beta1 (Itgb1)* CNS mutants, generated using *Nestin-Cre* transgenic mice, display a reduction in cerebellar size, reduced granule cell proliferation and ectopically positioned granule cells (Blaess et al., 2004). These cerebellar defects were largely recapitulated in conditional *integrin-linked kinase (Ilk)* CNS mutants, generated using the same *Nestin-Cre* transgenic mice (Belvindrah et al., 2006). *Ilk* is expressed in Bergmann glia cells and ILK depletion results in defects of Itgb1 dependent Glial process outgrowth and in reduced granule cell proliferation, as a secondary effect. The immense importance of Bergmann glia cells for cerebellar development is also demonstrated by postnatal ablation of astrocytes and by inducing premature Bergmann glia differentiation, respectively. Ablation of astrocytes, including Bergmann glia cells, in the first postnatal week, using transgenic mice containing the herpes simplex virus-thymidine kinase (HSV-TK) under the control of the human glial fibrillary acidic protein (hGFAP) gene promoter, resulted in disruption of the well defined layered cerebellar structure, reduced

cerebellar size, ectopic distribution of Purkinje cells and granule cells, and reduced number of granule cells (Delaney et al., 1996). Conditional *PTEN* (for *phosphatases and tensin homolog, deleted on chromosome 10*) astroglia mutants, generated using hGFAP-Cre mice, display premature differentiation of Bergmann glia cells (Yue et al., 2005). The premature Bergmann glia differentiation resulted in severe granule cell migration defects and abnormal laminar formation. Above all, the Notch signalling pathway plays an instructive role in promoting glial development (Gaiano and Fishell, 2002; Gaiano et al., 2000; Tanaka et al., 1999). In the strict sense the development and monolayer formation of Bergmann glia cells is regulated by Notch signalling. The conditional *Notch1/2* double mutants, generated using hGFAP-Cre mice, displayed disorganisation of Bergmann glia fibres, irregularities of Bergmann glia lining and ectopic localisation of Bergmann glia in the ML (Komine et al., 2007). Furthermore, the conditional RBP-J mutants, generated using the same hGFAP-Cre mice, showed the same Bergmann glia defects (Komine et al., 2007). RBP-J is a DNA binding protein, which mediates the transcription of Notch signalling target genes (Kato et al., 1996; Mumm and Kopan, 2000). An important Notch ligand, the Delta/Notch-like EGF-related receptor (DNER) is expressed by Purkinje cells and binds notch1 receptors expressed by Bergmann glia cells (Eiraku et al., 2005). Deficiency of DNER retards the formation of radial glia fibres and results in abnormal arrangement of Bergmann glia cells (Eiraku et al., 2005). Furthermore, the inactivation of *Jagged1 (Jag1)*, another notch ligand, in the cerebellar primordium at mid-embryogenesis, generated using *Engrailed2-Cre*, resulted in defects of Bergmann glia fibres formation, aberrant granule cell migration and ectopic differentiation and in the external germinal layer and molecular layer of the early postnatal cerebellum (Weller et al., 2006). Another signalling pathway, which has been shown to be involved in cerebellum development, is the *sonic hedgehog (Shh)* signalling pathway. Overexpression of *Shh* in the normal domain does not grossly alter the basic cerebellar foliation pattern, but does lead to prolonged proliferation of GCPs and an increase in the overall size of the cerebellum (Corrales et al., 2004). Furthermore, *Shh* null mutants and conditional *Shh* mutants, generated using *En1-Cre* or *Nestin-Cre* mice, display besides other defects in the MHR reduced cerebellar size (Blaess et al., 2006).

3.3 FGF signalling in Depression

Depression is one of the most common disorders in developed countries and one of the leading causes of disability worldwide (Lopez et al., 2006). Mood bias toward negative emotions, anhedonia, and psychomotor symptoms best characterise major depressive disorder (MDD) (Nelson and Charney, 1981). Imaging studies revealed many affected brain regions with altered size or morphology in depressive patients (Soares and Mann, 1997; Strakowski et al., 2005). However, the results concerning the size of certain brain areas among the different reports are mostly inconsistent depending on the homogeneity, classification, and age of analysed patients and the used imaging technique. Nevertheless, the size of the prefrontal cortex, the cingulate cortex, and the hippocampus seems to be reduced in depressed patients. Furthermore, the hypothalamic-pituitary-adrenal axis (HPA axis) is one of the intensively studied systems, which are functionally involved in depression (Deussing and Wurst, 2005; Holsboer et al., 1995; Muller and Wurst, 2004; Papiol et al., 2007). The heterogeneity of depression suggests involvement of a broad range of both, genetic and environmental factors. To study genetics of depression and antidepressant drugs in rodents behavioural tests like the forced swim test (FST) and the tail suspension test (TST) are used (Cryan et al., 2005; Detke et al., 1995; Lucki, 1997; Porsolt et al., 1978; Porsolt et al., 1977; Trullas et al., 1989). The most commonly used antidepressant drugs are acting on the noradrenergic or serotonergic neurotransmitter system by increasing the level of the monoamines Serotonin (5-hydroxytryptamine or 5-HT) and Noradrenalin (Meyer et al., 2006; Wong and Licinio, 2001). This strongly suggests the involvement of these systems in depression. In mice activation of the serotonin receptor 5-HT_6 using synthetic agonists leads to reduced immobility in the tail suspension test (TST), suggesting an antidepressant effect (Svenningsson et al., 2007). Additionally the use of a 5-HT_6 antagonist counteracts fluoxetine-induced biochemical and behavioural responses in mice (Svenningsson et al., 2007). Furthermore, the non-selective glycogen synthase kinase 3 (GSK3) inhibitor lithium chloride is used to treat depressive patients, suggesting strongly the involvement of GSK3 in depression (Benedetti et al., 2005; Jope and Roh, 2006; Leonardo and Hen, 2006). Rats treated with AR-A014418, a selective inhibitor of GSK3beta, showed less depression-like behaviour in the FST (Gould et al., 2004). Additionally many other proteins like the transcription factor cAMP responsive element binding protein 1 (CREB1), the neurotrophin brain-derived neurotrophic factor (BDNF), the corticotropin releasing hormone (CRH), the estrogen receptors alpha and beta (ERalpha and ERbeta), and the cannabinoid type 1 receptor (CB1R) are discussed to be involved in

depression. Linkage studies revealed that the occurrence of polymorphisms in the *Creb1* gene and *Creb1* related genes correlate with early-onset depression in humans (Zubenko et al., 2003a; Zubenko et al., 2003b). However, this correlation between CREB1 and early-onset depression could not be reproduced in another study (Burcescu et al., 2005). The levels of BDNF and its receptor tropomyosin-related kinase B (TrkB) are increased in the hippocampus of depressed patients upon antidepressant medication (Chen et al., 2001; Kozisek et al., 2008). Furthermore, in rats the infusion of BDNF into the hippocampus had antidepressant-like effects and the genetic mouse model harbouring the Val66Met BDNF gene mutation displayed increased anxiety-related behaviour (Chen et al., 2006; Shirayama et al., 2002). The involvement of the HPA-axis and the CRH system in depression is indicated by elevated CRH levels in the cerebrospinal fluid (CSF), increased number of CRH secreting neurons in limbic brain regions, and decreased number of CRH receptors in the frontal cortex in depressed patients (Holsboer, 2000; Muller and Wurst, 2004; Nemeroff et al., 1988; Nemeroff et al., 1984; Raadsheer et al., 1994). For ERalpha a positive correlation between polymorphisms and depressive disorders in females was shown whereas for ERbeta no clear correlation between gene polymorphisms and depression was found (Kealey et al., 2001; Tsai et al., 2003). However, in rats treatment with specific ERbeta agonists, but not specific ERalpha agonists, had antidepressant-like effects (Walf et al., 2004). Also the cannabinoid signalling via the cannabinoid receptors (CB) is thought to be involved in depression since cannabinoids have positive and antidepressant effects on depressed patients (Ashton et al., 2006). Furthermore, in rats the CB1R agonist WIN55,212-2 activates serotonergic neurons and exerts potent antidepressant-like properties in the FST (Bambico et al., 2007). However, the genetics of complex behaviour and especially a possible genetic predisposition for mood disorders such as depression are poorly understood. Probably a combination of genetic modifications and environmental factors are needed to model complex disorders like depression in mice (see Fig 4).

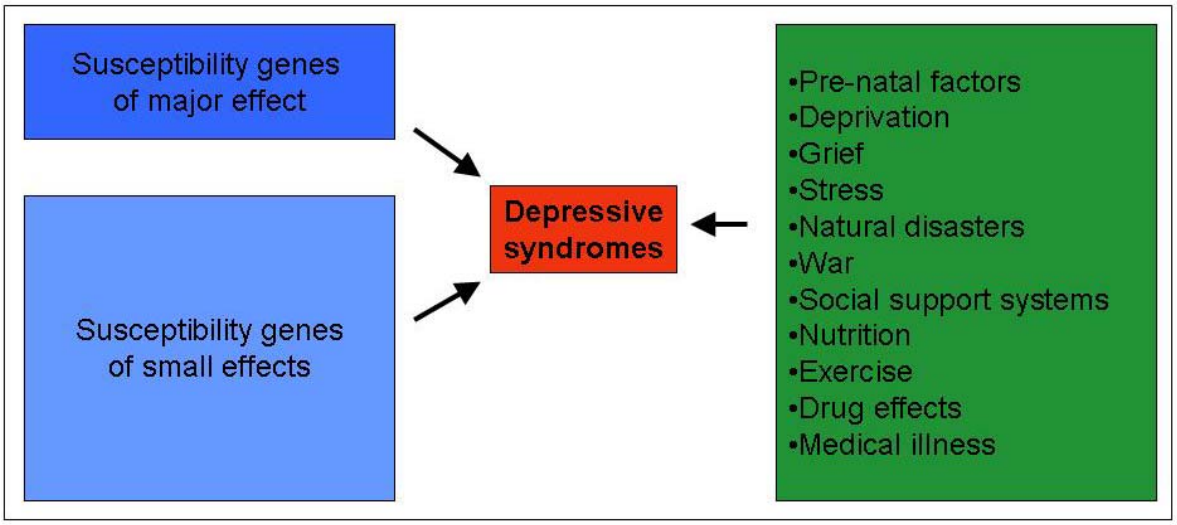

Figure 4. A conceptional approach to depression.
Available evidences suggest that neurobiological substrates underlying depression phenotypes are the outcome of a combination of genetic and environmental factors. Modified from: Wong and Licinio 2001.

Besides these candidate genes the capability of the adult brain to generate new neurons (adult neurogenesis), especially in the hippocampus, is thought to play a role in depression or at least in mediating antidepressant effects of therapeutic drugs (Sahay and Hen, 2007). Fluoxetine administration leads in adult mice to increased symmetric division of progenitor cells in the hippocampus (Encinas et al., 2006). In mice with a 129SvEvTac genetic background it has been shown that antidepressant effects of the SSRI fluoxetine depend on adult neurogenesis (Santarelli et al., 2003). However, the need of adult neurogenesis was found to be strain specific since fluoxetine has antidepressant effects in mice with BALB/cJ genetic background independently of adult neurogenesis (Holick et al., 2008). A further important aspect is the proper integration of newborn neurons in the adult neuronal network. It is not clear if and how antidepressants and candidate genes, which were shown to play a role in depression, influence this integration. A few studies reported that fluoxetine, Serotonin and BDNF, respectively, positively affect dendritic outgrowth (Chen et al., 2007; Kumamaru et al., 2008; Norrholm and Ouimet, 2001).

Several studies implicated the involvement of members of the FGF signalling system in neurological disorders and especially in mood disorders like major depression (Turner et al., 2006). Both, studies with rodents and post mortem analysis of brains from depressed patients, suggest a functional involvement of FGF signalling in depression. In mice with conditional FGFR1 ablation in radial glia cells, generated using hGFAP-Cre mice, a reduced hippocampal

size was found (Ohkubo et al., 2004). Interestingly, reduced hippocampal size is often found in depressed patients (Bremner et al., 2000; Mervaala et al., 2000; Sheline et al., 1999). Furthermore, in adult rats administration of the three antidepressants desipramine, fluoxetine, and mianserin, respectively, induced *Fgf2* expression, especially in cerebral cortex and hippocampus (Mallei et al., 2002). Similar results were obtained in rats treated with fluoxetine together with the antipsychotic drug olanzapine (Maragnoli et al., 2004). Fluoxetine and olanzapine co-administration lead to increased *Fgfr2* expression in the three brain regions hippocampus, prefrontal cortex and striatum. In humans suffering from depression post mortem brain analysis revealed increased expression of *Fgfr1* and decreased expression of *Fgf2* in the hippocampus (Gaughran et al., 2006). Furthermore, a gene expression analysis using post mortem material from depressed and nonpsychiatric control subjects revealed deregulation of FGF family members (Evans et al., 2004). In the dorsolateral prefrontal cortex of depressed patients *Fgf1, Fgfr2*, and *Fgfr3* expression was reduced. However, an open question in this kind of studies is always if the altered expression is causing depression or if it is a consequence of the disease.

3.4 RNA interference

Silencing of gene expression by RNA interference (RNAi) has become a powerful tool for functional genomics in mammalian cells. RNAi is a sequence specific gene silencing process that occurs at the messenger RNA (mRNA) level. In invertebrate cells, long double stranded RNAs (dsRNA), which are processed into short interfering RNAs (siRNA) by the ribonuclease Dicer, induce efficient and specific gene silencing. In this sequence guided process the siRNA antisense strand serves as a template for the RNA-induced silencing complex (RISC). RISC recognises and cleaves the complementary mRNA, which is then rapidly degraded (Elbashir et al., 2001). In mammalian cells, long dsRNAs (> 30 bp) elicit an interferon response resulting in the global inhibition of protein synthesis and non-specific mRNA degradation. However, it has been shown that short synthetic dsRNAs trigger the specific knockdown of mRNAs in mammalian cells without interferon activation, if their length is below 30 bp (Elbashir et al., 2001). Such synthetic siRNAs can be easily introduced into cultured cells and induce a transient knockdown that enables the study of mammalian gene function within a short time frame. Due to advances in the delivery and design of

siRNAs, gene silencing developed by now into a routine method for *in vitro* use. Shortly after the establishment of siRNA mediated transient gene silencing, DNA based expression vectors were developed that allow the endogenous production of small dsRNAs in mammalian cells (Brummelkamp et al., 2002; Lee et al., 2002; Paddison et al., 2002). The vector derived transcripts are designed to contain a sense and an antisense region that is complementary to a selected mRNA segment. These transcripts can fold back into a stem-loop structure and form short hairpin RNAs (shRNAs) that are processed by Dicer in a similar way as the siRNAs. Since shRNA expression vectors can be stably integrated into the genome, they allow permanent, long lasting gene silencing in cell lines and organisms (Fig. 5).

Soon after these technologies were introduced for use in cultured cells it became an obvious task to explore RNAi mediated gene silencing also in mice. The number of reports on RNAi in transgenic mice has increased to more than 20, representing all standard methods to generate transgenic mice (Kuhn et al., 2007). ShRNA transgenic mice were produced by pronuclear DNA injection (Hasuwa et al., 2002), by infection of zygotes or ES cells with lentiviral vectors (Rubinson et al., 2003), by random integration into ES cells (Lickert et al., 2004) and targeted transgenesis (knock-in) of single vector copies into ES cells through recombinase mediated cassette exchange or homologous recombination (Hitz et al., 2007; Oberdoerffer et al., 2005). The phenotypes of knockdown and the corresponding knockout mice were compared and found to be identical or very similar during embryogenesis (Kunath et al., 2003).

By comparison of heterozygous and homozygous knockout mice, it is well known that 50% reduction in gene expression in heterozygous mutants rarely results in a detectable phenotype. However, little is known about intermediate phenotypes with 70%-80% reduced expression of a certain gene. In many cases this could reflect the situation in diseases which are often caused by point mutations in one specific gene. Depending on the efficiency of the used shRNA, RNAi could be used to generate knockdown mice with various preselected knockdown levels. Together with the fast and easy application, this opportunity to gradually regulate gene activity is one of the main advantages of RNAi compared to conventional knockout mice.

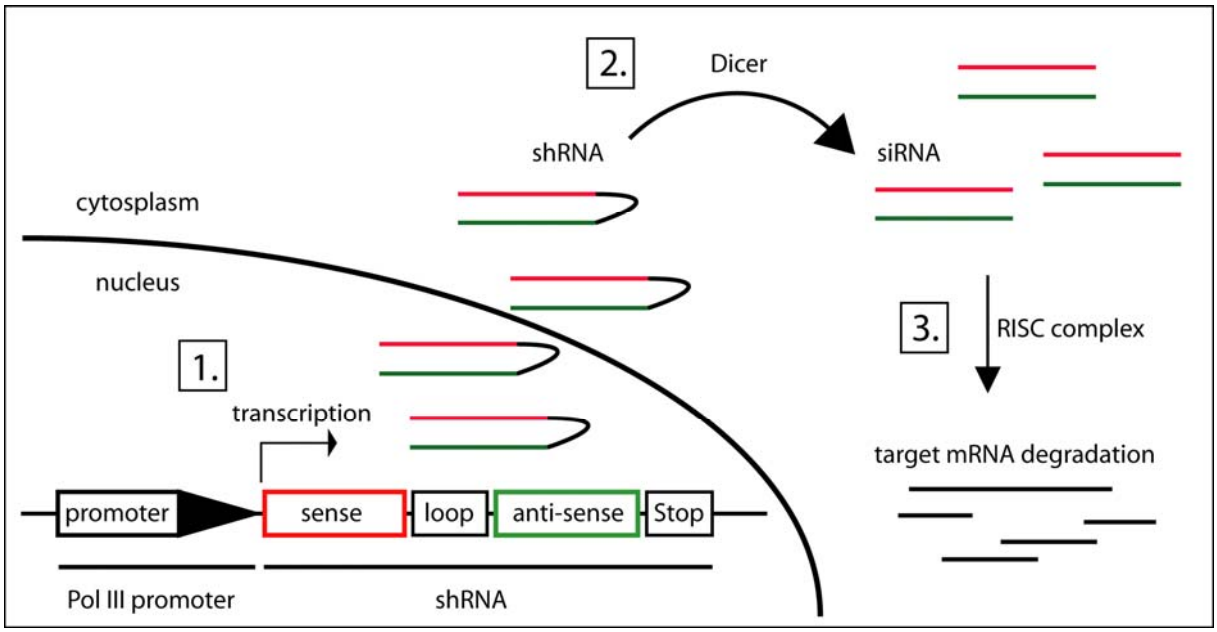

Figure 5. Schematic drawing of vector-based RNAi.

The small hairpin (sh) RNA contains a sense (18 to 23 nucleotides identical to a sequence of the targeted mRNA), a loop and an anti-sense sequence (complementary to the sense sequence) and is coded on a plasmid or virus. RNA Polymerase III (Pol III) mediated transcription results in a small RNA molecule that forms a hairpin structure (1.). The shRNA is translocated into the cytoplasm and processed by the enzyme Dicer, resulting in double-stranded siRNA (2.). The siRNA is incorporated into the RNA-induced silencing complex (RISC) and leads to degradation of targeted mRNAs (3.).

In order to generate mouse models for depression we applied the RNAi technology to silence the expression of *P2rx7* in adult mice. P2RX7 is an ATP gated membrane ion channel and is expressed in several tissues in adult rodents, including the brain (Chessell et al., 1998; Robertson et al., 2001; Sim et al., 2004; Yu et al., 2008). P2RX7 plays an important role in extracellular ATP induced cell death and is linked to several human diseases (Bulanova et al., 2005; Kawamura et al., 2005; Khakh and North, 2006). The importance of P2RX7 for the immune system is demonstrated by its ability to regulate Leukocyte function and inflammatory response (Labasi et al., 2002). Absence of the P2RX7 leads to an inability of peritoneal macrophages to release IL-1 in response to ATP (Solle et al., 2001). In the adult brain activation of P2RX7 leads to the production and release of Tumor Necrosis Factor (TNF) in activated microglia and thereby protects neurons against glutamate toxicity (Suzuki et al., 2004). Due to the role of P2RX7 in the immune system and in microglia, so far the role of P2RX7 in the adult brain was mainly studied in respect to microglia activation (Choi et al., 2007; Skaper et al., 2006). However, it was also shown that P2RX7 is expressed in neurons of

the CNS and the peripheral nervous system. P2RX7 seems to be located at the synapses, but its role there is not clearly identified (Anderson and Nedergaard, 2006). P2RX7 is targeted to presynaptic terminals and enhances excitatory synaptic transmission at central synapses (Deuchars et al., 2001; Ireland et al., 2004). In the peripheral nervous system P2RX7 seems to be involved in vesicle release at neuromuscular junctions (Moores et al., 2005). *P2rx7* is the mouse homologue to the human *P2x7*. Recently, linkage studies showed a positive correlation between point mutations in the *P2x7* gene and the appearance of depressive disorder in humans (Barden et al., 2006; Erhardt et al., 2007; Lucae et al., 2006).

4 RESULTS

4.1 FGFR2 is necessary for proper cerebellum development

4.1.1 The *Fgfr2$^{lox/lox}$; Nestin-Cre* mouse mutant

To investigate the role of FGFR2 during brain development, FGFR2 was inactivated in all cells of the central nervous system (CNS) from embryonic day 11.5 (E11.5) onwards, using *Nestin-Cre* mice. The mice carrying a loxP-site flanked exon5 of the *Fgfr2* gene (floxed FGFR2) were generated by Prof. Dr. Michael Sendtner (Blak et al., 2007). Cre recombinase mediated deletion of exon5 causes a frame shift resulting in a stop codon in exon6 and therefore leads to an inactive truncated FGFR2 protein. To determine whether the mice carry floxed alleles or not I screened the genomic DNA extracted from the tail tips from all obtained mice by PCR with specific primers. Floxed alleles gave PCR products of 800bp whereas the amplification of the WT alleles resulted in a PCR product of 800bp (Fig. 6, C). The mice used in this study were on a mixed genomic background with fractions from *SV129* and *C57/Bl6* inbred strains.

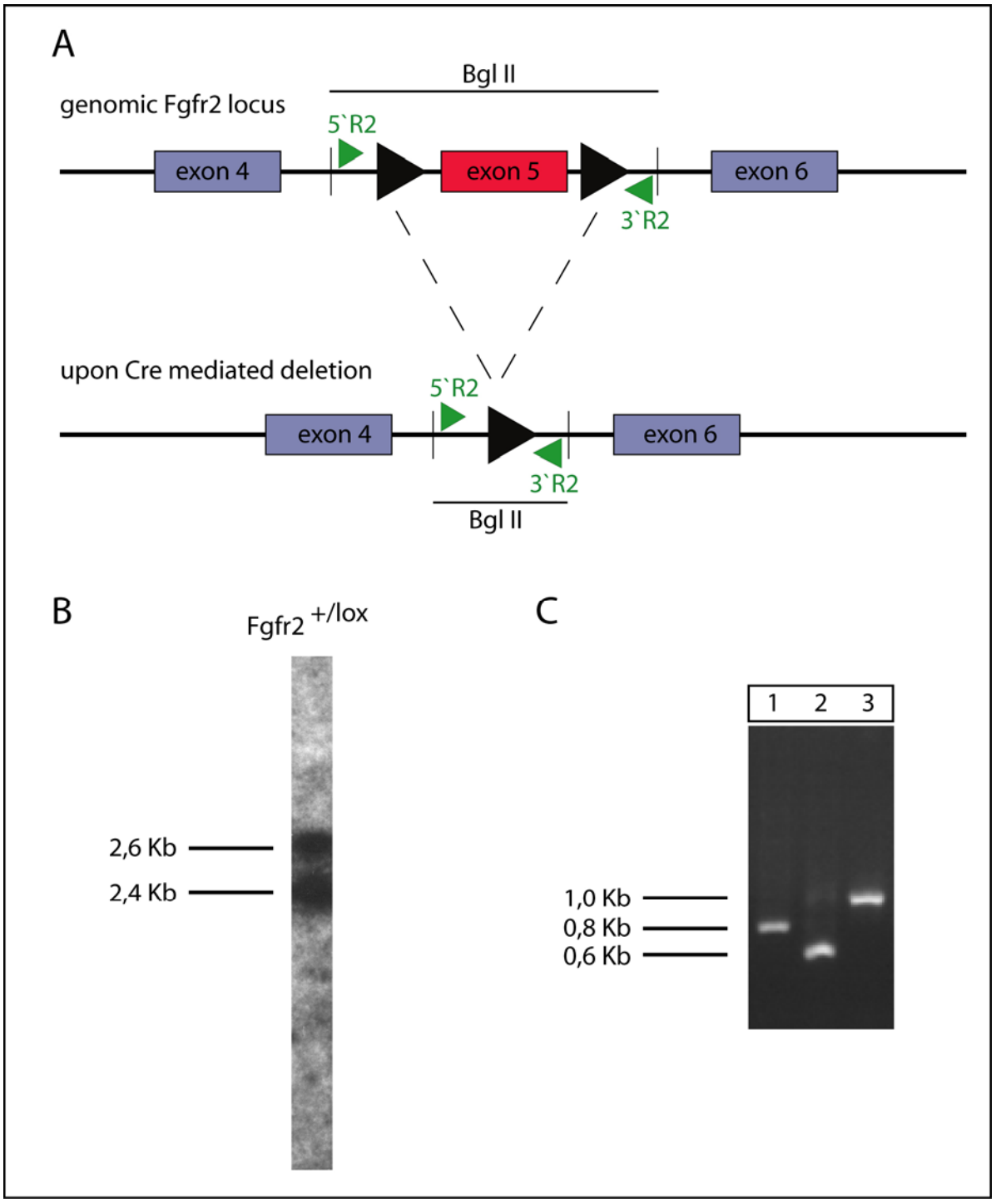

Figure 6. Structure of the conditional *Fgfr2* gene

A: Schematic drawing of genomic *Fgfr2* locus. Exon5 is flanked by loxP sites and can be deleted by Cre mediated excision. The primer pair 5`R2 and 3`R2 was used for PCR genotyping and BglII digested genomic DNA was used for Southern blot genotyping. B: Southern blot analysis of BglII digested genomic tail DNA from heterozygous mice shows the 2.6 Kb band of the loxP flanked allele and the 2.4 Kb wt band. C: PCR, using the primers 5`R2 (R2 forward) and 3`R2 (R2 reverse), of DNA from wt mice (1) and homozygous floxed mice with (2) and without Cre deletion (3).

The floxed FGFR2 mice were crossed to the transgenic *Nestin-Cre* mice (Tronche et al., 1999) which were on a pure C57/Bl6 background. The *Nestin-Cre* mice carry a Cre recombinase gene under the control of the rat Nestin promoter and express the Cre recombinase throughout the entire nervous system. The Cre recombinase expression starts at around E11.5 in all glial and neuronal precursors (Tronche et al., 1999; Zimmerman et al., 1994). The obtained heterozygous floxed FGFR2 mice containing one Cre allele (F1 generation) were then used for intercrossings. The analysis of the offspring (F2) showed that the ratio between males and females as well as the ratio between the different genotypes was according to Mendel's laws. The homozygous mutants *(Fgfr2* $^{lox/lox}$*; Nestin-Cre)* were viable and fertile and displayed no obvious behavioural phenotype. Nevertheless, the mutant mice had significantly less weight compared to their WT littermates (Fig. 7, C). Some of the homozygous mutants were used for a first histological analysis. The rest of the F2 homozygous mutants were crossed to *Fgfr2* $^{lox/lox}$ mice and also here I got Mendelian ratios of the two possible genotypes (*Fgfr2* $^{lox/lox}$ with or without *Nestin-Cre*). The comparison between the offspring from these heterozygous-heterozygous breedings with the offspring from later homozygous-homozygous breedings showed no obvious difference. Therefore, I used routinely the *Fgfr2* $^{lox/lox}$ mice and crossed them to *Fgfr2* $^{lox/lox}$*; Nestin-Cre* mice to increase the number of mutant pups. To determine the efficiency of Cre mediated recombination brains from adult mice were analysed by ISH with an *Fgfr2* exon5 specific probe and by Western blot using an antibody directed against the FGFR2 C-terminus. These analysis showed, as expected, the absence of exon5 in the *Fgfr2 mRNA* (Fig. 7, A) and a dramatic decrease in FGFR2 protein level (Fig. 7, B) in homozygous mutants. Probably due to the maintained expression of *Fgfr2* in the choroid plexus (Fig7, A) a small amount of one FGFR2 isoform is still present in the mutant brains (Fig. 7, B).

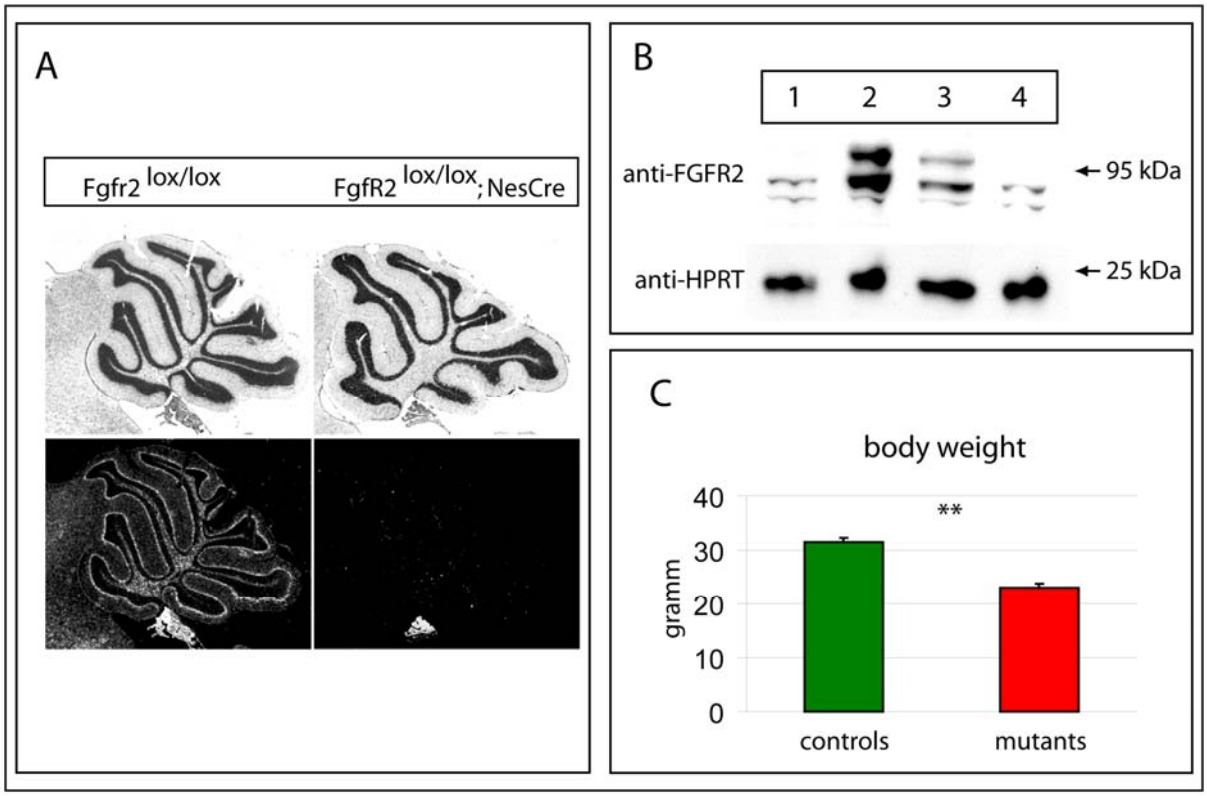

Figure 7. Characterisation of Cre mediated FGFR2 inactivation in *Fgfr2* $^{lox/lox}$*; Nestin-Cre* mice.

A: Brightfield (upper panels) and darkfield (lower panels) of saggital sections from FGFR2 $^{lox/lox}$ (left) and *Fgfr2* $^{lox/lox}$*; Nestin-Cre* mice (right). In situ hybridisation, using an *Fgfr2* exon5 specific probe, reveales efficient deletion of exon5 upon Cre mediated excision. B: Western blot of total brain protein extracts from *Fgfr2* $^{lox/lox}$*; Nestin-Cre* (1 and 4), wt (2), and *Fgfr2* $^{lox/lox}$*; Nestin-Cre* mice (3) demonstrates efficiency of Cre deletion on protein level. HPRT was used as loading control. C: At the age of 16 weeks *Fgfr2* $^{lox/lox}$*; Nestin-Cre* mice have significantly less weight than wt mice (n = 24 for each group; * $p < 0.01$).

4.1.2 Analysis of adult *Fgfr2* $^{lox/lox}$; *Nestin-Cre* mice

4.1.2.1 Nissl staining

The focus of this study was to explore the nonredundant function of FGFR2 in the adult mouse brain. Since it was already shown that FGFR2 inactivation in the MHR did not lead to any alterations, nether in embryos nor in adults (Blak et al., 2007), I expected only a marginal role of FGFR2 during brain development. The comparison of adult brains from WT mice and

homozygous mutant mice (*Fgfr2 $^{lox/lox}$; Nestin-Cre*) after Nissl staining showed no obvious alterations in the gross morphology or size. All brain regions were present in the mutants and seemed to be unaltered when compared with their WT littermates (Fig. 8).

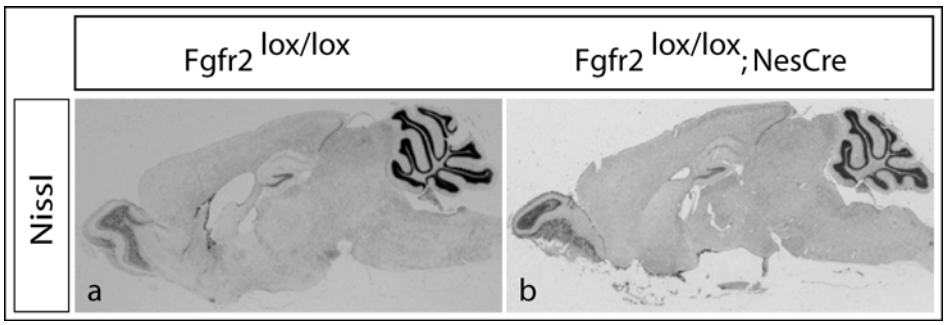

Figure 8. No gross morphological alterations in brains from *Fgfr2 $^{lox/lox}$; Nestin-Cre* mice.
Nissl staining of saggital sections from adult brains revealed no obvious differences between wt (a) and mutant (b) mice.

4.1.2.2 **Standard Neurotransmitter - TH, SERT and VAChT**

To get a first overview of the effects of FGFR2 deletion on specific cell populations in the adult brain the dopaminergic, the serotonergic, and the cholinergic systems were analysed by ISH. As markers I used probes against *tyrosine hydroxylase (TH)*, *serotonin transporter (SERT)* and vesicular *acetylcholine transporter (VAChT)*, respectively. I did not see alterations in any of the mentioned systems. The localization and distribution of positive cells for the used markers seemed to be identical in WTs, heterozygous mutants, and homozygous mutants (Fig. 9).

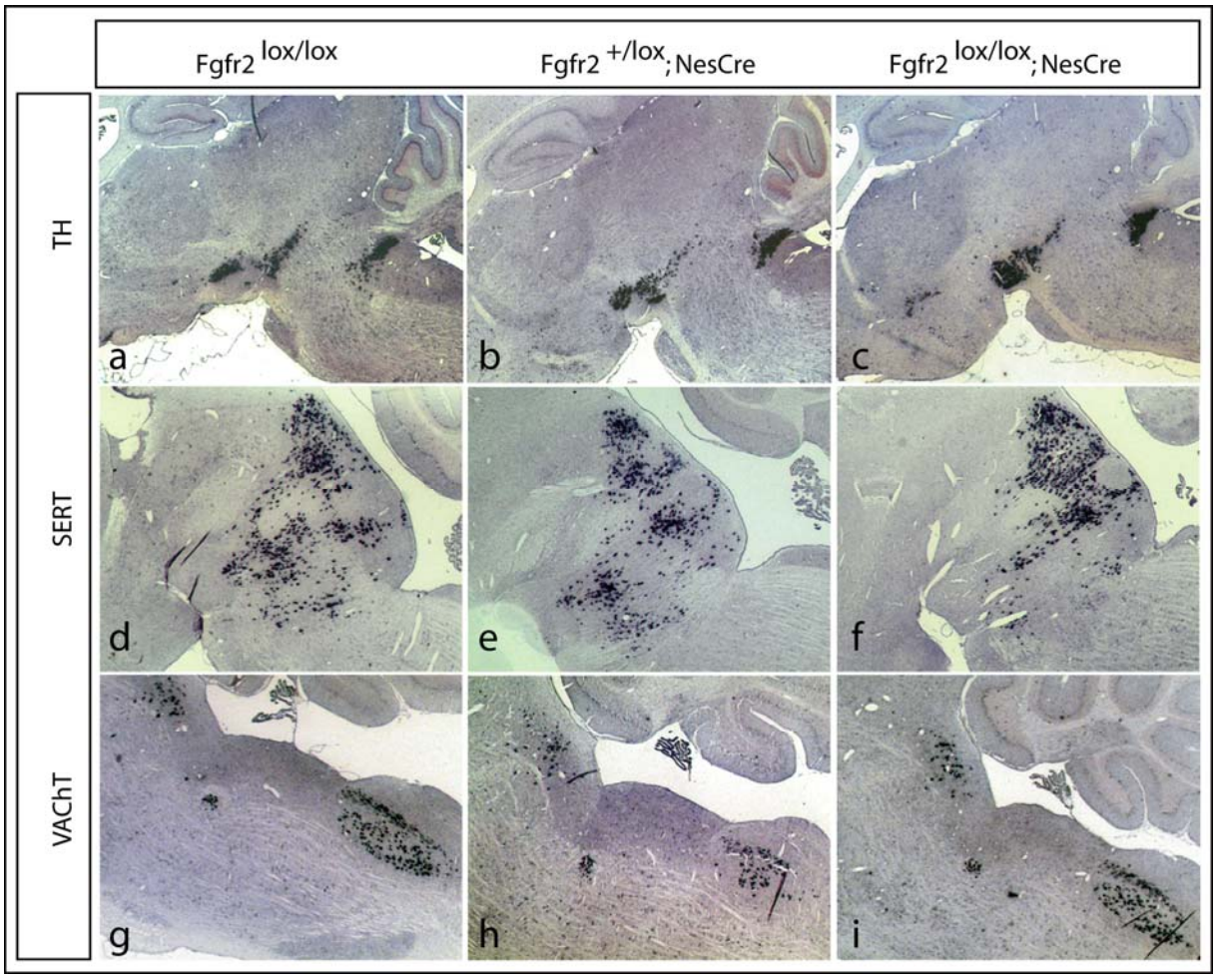

Figure 9. FGFR2 deletion did not affect expression of dopaminergic, serotonergic or acetylcholinergic markers in the adult brain.

Adult brain saggital sections from *Fgfr2* $^{lox/lox}$ (a, d, g), *Fgfr2* $^{lox/lox}$*; Nestin-Cre* (b, e, h), and *Fgfr2* $^{lox/lox}$*; Nestin-Cre* mice (c, f, i) upon *in situ* hybridization were compared. No significant effect of FGFR2 deletion on TH (for dopaminergic neurons; a, b, c), SERT (for serotonergic neurons; d, e, f), and VAChT (for acetylcholinergic neurons; g, h, i) expression was observed.

4.1.2.3 **GAD65**

To analyse the gabaergic system in the adult mouse brain I used an ISH probe against *glutamic acid decarboxylase 65 (GAD65)*. There were no alterations in most of the brain regions. The only difference between brains from WT mice and their mutant littermates can be observed in the cerebellum. First of all, cerebella of some mutant brains were slightly smaller than the cerebella from their WT littermates. The second alteration concerns the

position of the GAD65 positive cells. The cells of the cerebellum of WT brains are organized in distinct layers. This well structured organization is disturbed in the anterior (rostral) part of the cerebellum in mutant brains (Fig. 10; c). There was a great variability in the intensity of the observed alteration of the cerebellar structure between the analysed mutants. In some cases no changes in the organization of GAD65 positive cells were detectable (mild phenotype; Fig. 10, e), whereas in others the lobules II and III were not any more recognizable (severe phenotype; Fig. 10; c). In total I performed histological analysis on 20 mutant mice. In six of them (= 30%) I found a mild phenotype and 14 mutants (= 70%) showed a severe phenotype (Fig. 10; f). The altered structure of the anterior cerebellum was only detectable in homozygous mutants (*Fgfr2* $^{lox/lox}$*; Nestin-Cre*) and never in heterozygous mutants (*Fgfr2* $^{+/lox}$*; Nestin-Cre*) (Fig. 10, b). Therefore I name from here on only homozygous mutant (*Fgfr2* $^{lox/lox}$*; Nestin-Cre*) as mutants and floxed FGFR2 mice without *Nestin-Cre* (*Fgfr2* $^{lox/lox}$) as WT or control.

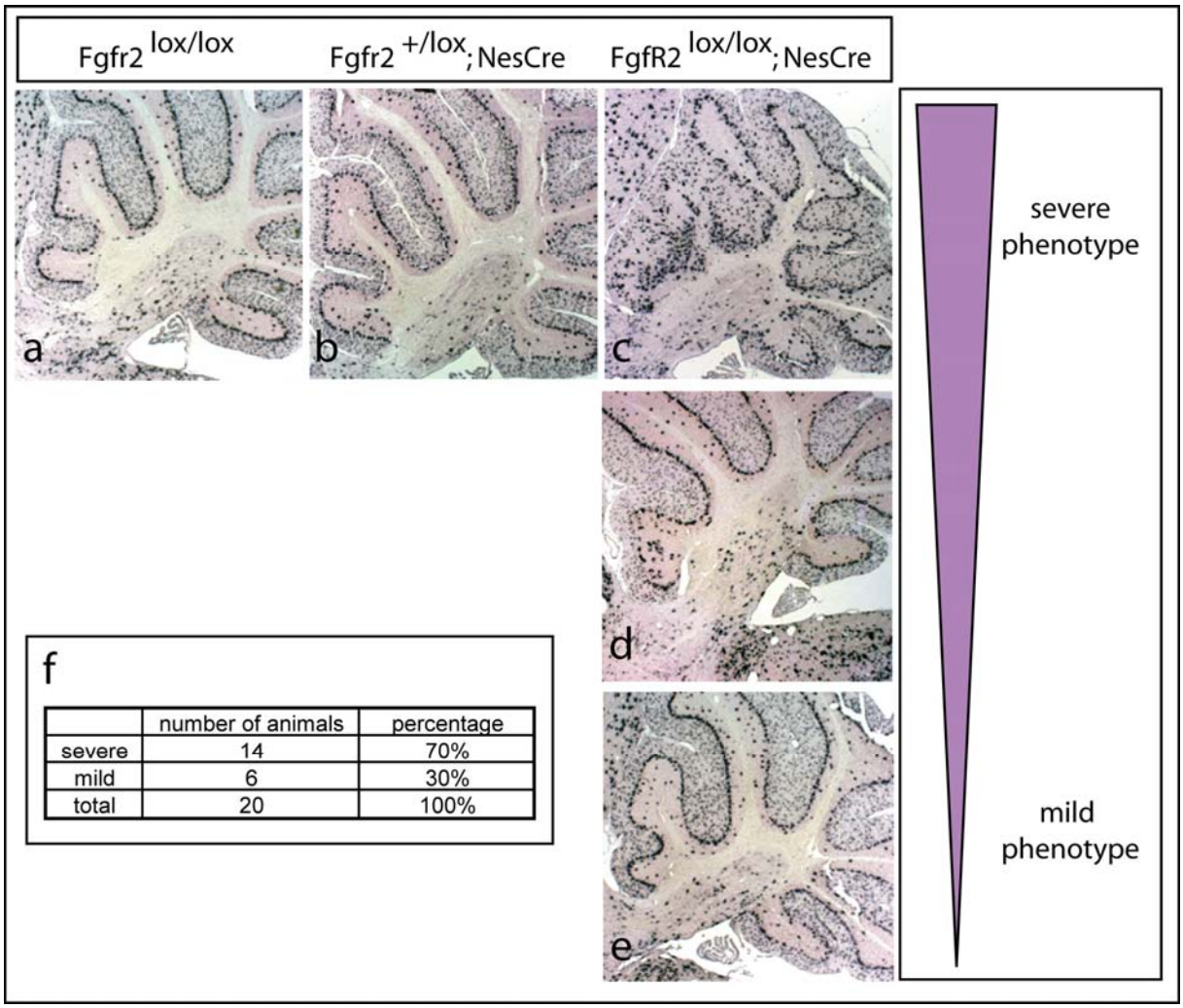

Figure 10. Morphological defects in *Fgfr2$^{lox/lox}$; Nestin-Cre* cerebella.
Expression of *GAD65* mRNA in saggital sections from WT mice (*Fgfr2$^{lox/lox}$*; a), heterozygous mutants (*Fgfr2$^{+/lox}$; Nestin-Cre*; b), and homozygous mutants (*Fgfr2$^{lox/lox}$; Nestin-Cre*; c, d, e). No differences are found between WT (a) and heterozygous mutant (b) cerebella. Cytoarchitectural alterations are present at different levels in the anterior part of the cerebellum in homozygous mutants (*Fgfr2$^{lox/lox}$; Nestin-Cre*; c, d, e). The ratio of mildly and severely affected mutants is shown in f.

4.1.2.4 **Purkinje cells and Granule neurons**

To be able to draw a more detailed picture of the observed alterations in the anterior cerebellum of mutant mice I performed IHC using antibodies against proteins that are at least to some extend specifically expressed by the two major neuronal populations within the cerebellum, the Purkinje cells and the Granule neurons. For the Purkinje cells, which are also *GAD65* positive, I used as markers Parvalbumin and the more specific Calbindin. An antibody directed against Calretinin was used to label the Granule neurons. In mutant mice with mild phenotype the Purkinje cells are not evenly distributed in a chain-like structure within the Purkinje cell layer (Fig. 11, c). Instead they formed small groups of cells within the Purkinje cell layer flanked by gaps lacking Parvalbumin-positive Purkinje cells. These gaps appear because the space seems to be occupied by Calretinin positive Granule neurons (Fig. 11, g). Since in mutants Granule neurons can be found within the molecular layer in radial chains the incorrect positioning of Granule neurons seems to be a consequence of incomplete migration during postnatal development from the surface of the cerebellum, the external granular layer, to the internal granular layer (Fig. 11, i, j, k).

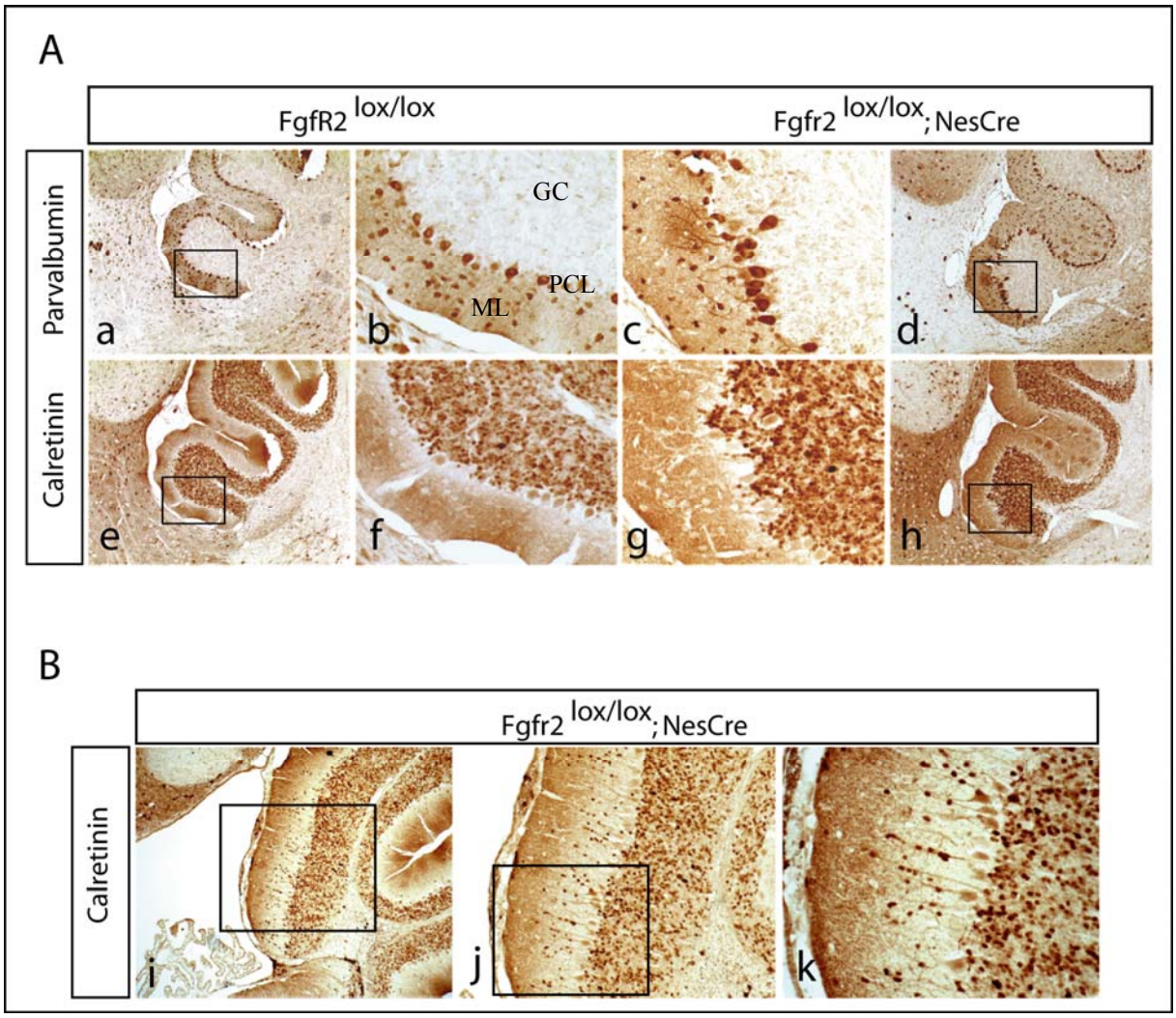

Figure 11. Mispositioned neurons in mildly affected *Fgfr2*$^{lox/lox}$*; Nestin-Cre* cerebella.

Sagittal sections of the cerebellum from *Fgfr2*$^{lox/lox}$ (a, b, e, f) and *Fgfr2*$^{lox/lox}$*; Nestin-Cre* (c, d, g, h, I, j, k) mice. A: Immunostaining for Parvalbumin shows regulary organised Purkinje cells within the Purkinje cell layer in the *Fgfr2*$^{lox/lox}$ cerebellum (b) and irregular arranged Purkinje cells in *Fgfr2*$^{lox/lox}$*; Nestin-Cre* cerebellum (c) including gaps within the PCL without Purkinje cells and one Purkinje cell within the granular layer. Consecutive sections of a, b, and c, d were immunostained for Calretinin (e, f, g, h). Calretinin positive Granule neurons are located within the granule layer in FGFR2$^{lox/lox}$ cerebellum (f). In the *Fgfr2*$^{lox/lox}$*; Nestin-Cre* cerebellum the PCL is interrupted by groups of granule neurons (g). B: In sagittal section from another *Fgfr2*$^{lox/lox}$*; Nestin-Cre* cerebellum Calretinin positive Granule neurons are found in a chain-like organisation within the molecular layer (i, j, k). GC: granular layer; PCL: Purkinje cell layer; ML: molecular layer.

In mutants with a strong phenotype the Calbindin positive Purkinje cells were, at least in the anterior part of the cerebellum, not any more organized in a chain-like structure within the Purkinje cell layer as found in WT cerebella (Fig. 12). Rather the Purkinje cell layer does not

exist any more because the Purkinje cells and also the Granule neurons are distributed in a random manner throughout the cerebellum (Fig. 12, d). Like in mutants with a milder phenotype also here in severely affected mutants the structure in the anterior (rostral) part of the cerebellum is less elaborated and recognisable than in posterior (caudal) parts.

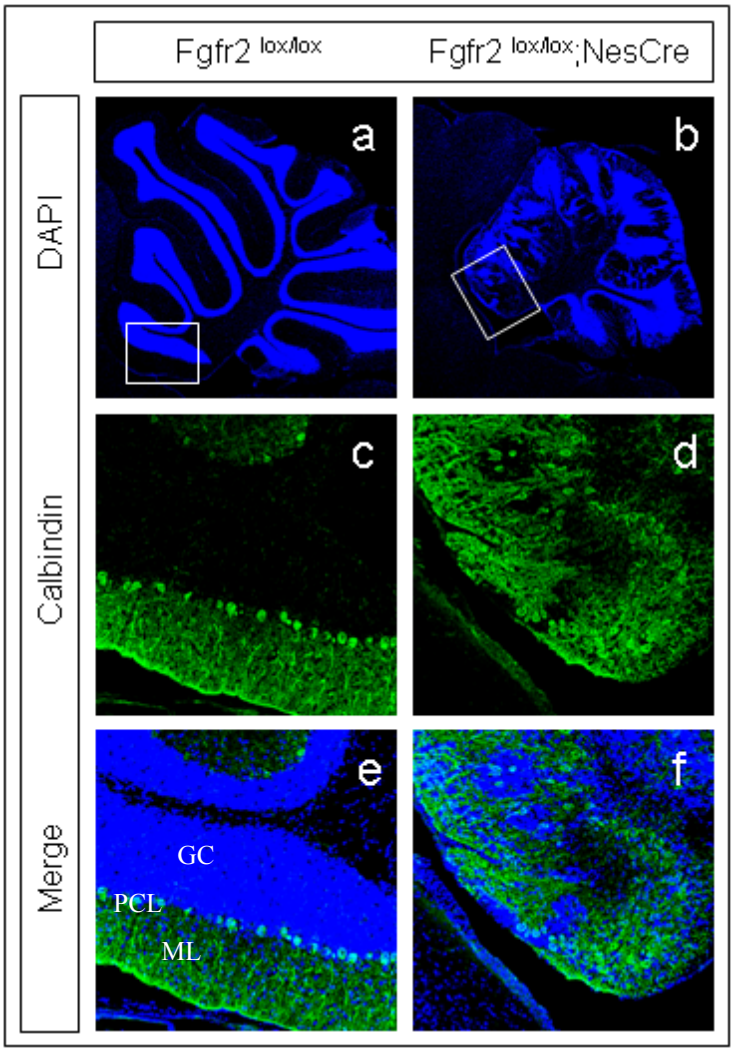

Figure 12. The layered structure is lost in severely affected *Fgfr2*$^{lox/lox}$*; Nestin-Cre* cerebella

Dapi staining (blue; a, b, e, f) and fluorescence-immunostaining for Calbindin (green; c, d, e, f) on saggital sections of an *Fgfr2*$^{lox/lox}$ cerebellum (a, c, e) and a severely affected *Fgfr2*$^{lox/lox}$*; Nestin-Cre* cerebellum (b, d, f). GC: granular layer; PCL: Purkinje cell layer; ML: molecular layer.

4.1.2.5 **Bergmann Glia markers**

The Purkinje cell layer is not composed only of Purkinje cells but contains also specific glia cells, the Bergmann glia cells. These Bergmann glia cells are surrounding the Purkinje cells. Their cell bodies are located within the Purkinje cell layer but their long extensions pass the molecular layer and reach the surface of the cerebellum. These glial processes are crucial for the migration of Granule neurons from the external to the internal granular layer during the first three postnatal weeks and they are also important for the correct organization of Purkinje cell dendrites within the molecular layer (Hatten and Heintz, 1995; Lordkipanidze and Dunaevsky, 2005). To investigate the status of the Bergmann glia cells in the mutants I performed IHC with antibodies directed against S100beta, a Calcium binding protein primarily present in Bergmann glia cell bodies, or GFAP, a protein that is mostly localized in the Bergmann glia fibres.

The position of Bergmann glia cell bodies was especially in the anterior parts of the cerebellum from mutant brains clearly altered. In Wt cerebella all Bergmann glia cells lie within the Purkinje cell layer (Fig. 13, a). In contrast to this well-defined organization in the WT cerebellum the Bergmann glia cell bodies in the mutant cerebellum are also found outside the Purkinje cell layer within the molecular layer (Fig. 13, b). Even more striking differences can be found with regard to the Bergmann glia fibres. In the WT cerebellum these fibres cross the molecular layer and adhere to the pial surface (Fig. 13, c, e). In some regions of the anterior part of the mutant cerebellum only a few if any processes can be found that reach the surface (Fig. 13, d, f). The cell bodies and processes of Bergmann glia cells in the posterior part of the mutant cerebellum were basically unaltered.

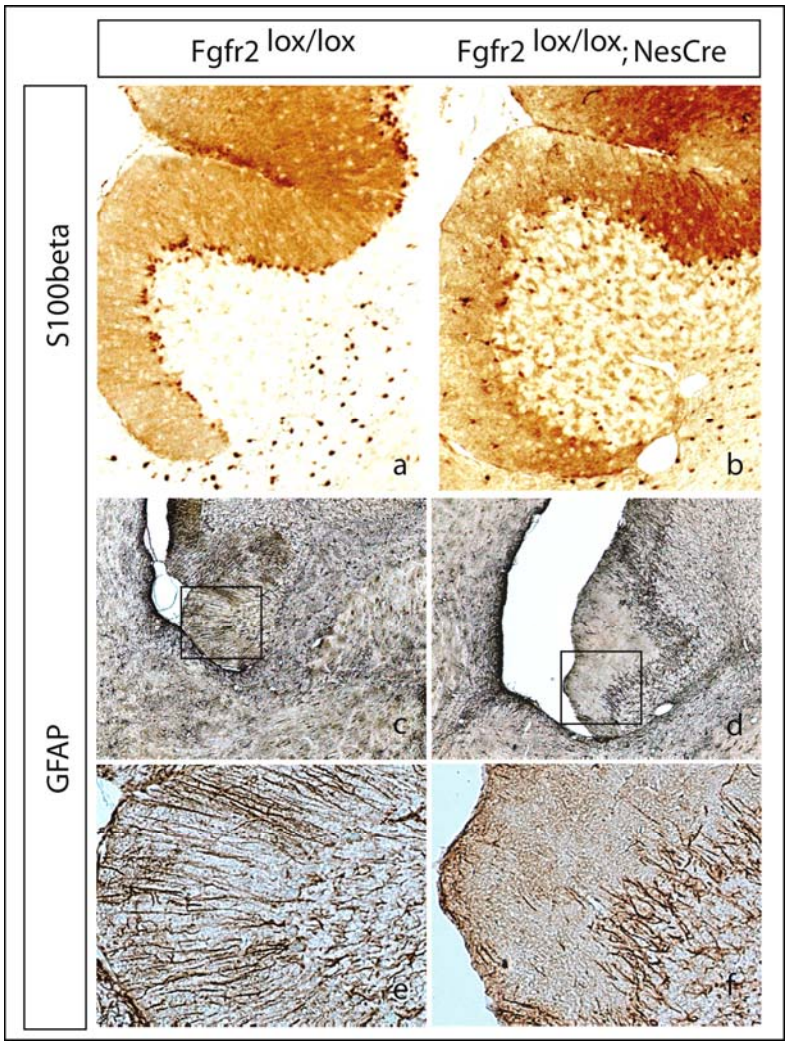

Figure 13. Alterations in positioning and morphology of Bergmann glia in *Fgfr2*$^{lox/lox}$*; Nestin-Cre* cerebella.

Immunostaining for S100ß on sagittal sections shows S100ß positive Bergmann glia cells in *Fgfr2*$^{lox/lox}$ cerebellum arranged within the Purkinje cell layer (**a**). In *Fgfr2*$^{lox/lox}$*; Nestin-Cre* cerebellum mis-positioned Bergmann glia cells are also found in the molecular layer (**b**). GFAP immunostained Bergmann glia fibers are crossing the ML in *Fgfr2*$^{lox/lox}$ cerebellum (**c, e**). Bergmann glia fibers in *Fgfr2*$^{lox/lox}$*; Nestin-Cre* cerebellum are shorter and do not reach the cerebellar surface (d, f).

4.1.2.6 Analysis of Bergmann Glia in *Fgfr2*$^{lox/lox}$*; En1Cre* mice

The finding that mice lacking FGFR2 in the nervous system have altered cerebellar structures does not fit with earlier findings. No alterations in cerebellar organization and patterning were found in mice lacking FGFR2 in the MHR from embryonic day E8.5 on (Blak et al., 2007). In the mentioned study the loxP flanked exon5 of the *Fgfr2* gene was deleted using a mouse line with Cre recombinase expression under the control of the *Engrailed1 (En1)* promoter (*Fgfr2*

lox/lox;En1Cre). To clarify this discrepancy between the *Fgfr2 lox/lox; En1Cre* mutants and my results I re-analysed the *Fgfr2 lox/lox; En1Cre* mutants by IHC focusing on the Bergmann glia cells. Therefore I performed IHC using the same antibodies (S100beta and GFAP) as I used to analyse Bergmann glia in *Fgfr2lox/lox; Nestin-Cre* mutants. I found with both, S100beta and GFAP, differences between *Fgfr2 lox/lox; En1Cre* mice and their WT littermates (Fig. 14). The observed alterations in these *Fgfr2 lox/lox; En1Cre* mutants were very similar to what can be found in *Fgfr2lox/lox; Nestin-Cre* mutants. Some of the Bergmann glia cell bodies are within the molecular layer (Fig. 14, b, c) and not all Bergmann glia processes are able to cross the molecular layer and reach the surface of the cerebellum (Fig. 14, e, g).

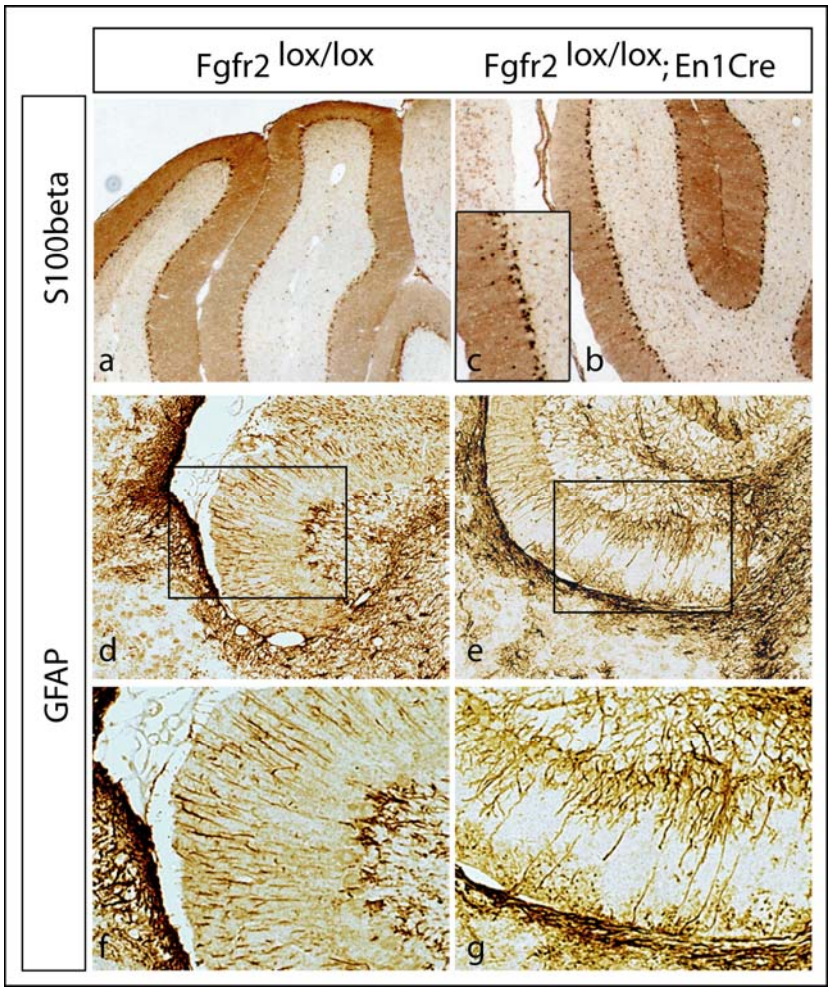

Figure 14. Alterations in morphology and positioning of Bergmann glia in *Fgfr2lox/lox; En1Cre* cerebella.

Sagittal sections of *Fgfr2lox/lox* control brains were immunostained for S100ß (a) and GFAP (d, f). Similar to the Bergmann glia defects in *Fgfr2lox/lox; Nestin-Cre* (see Figure 13) the position of S100ß positive Bergmann glia cells is altered in *Fgfr2lox/lox; En1Cre* cerebella (b) and some Bergmann glia fibers in *Fgfr2lox/lox; En1Cre* cerebella fail to reach the cerebellar surface (e, f).

4.1.2.7 Expression of FGF signalling downstream targets – *Sef1, Sprouty1* and *Mkp3*

To determine whether the observed changes in the anterior part of the cerebellum is due to a complete loss of FGF signalling I analysed the expression of three downstream targets in the adult brain by ISH (Fig. 15; for expression of Fgfrs see Fig. 23). It is known that active FGF signalling leads to the expression of *Sef1, Sprouty1*, and *Mkp3* (Echevarria et al., 2005; Furthauer et al., 2002; Hanafusa et al., 2002; Kawakami et al., 2003). All three proteins are involved in negative feedback loops and therefore in regulating the intensity and duration of the intracellular FGF signal. Their expression is used in embryos to determine the status of FGF signalling (Blak et al., 2007), but there are no studies about their expression pattern in the adult mouse brain.

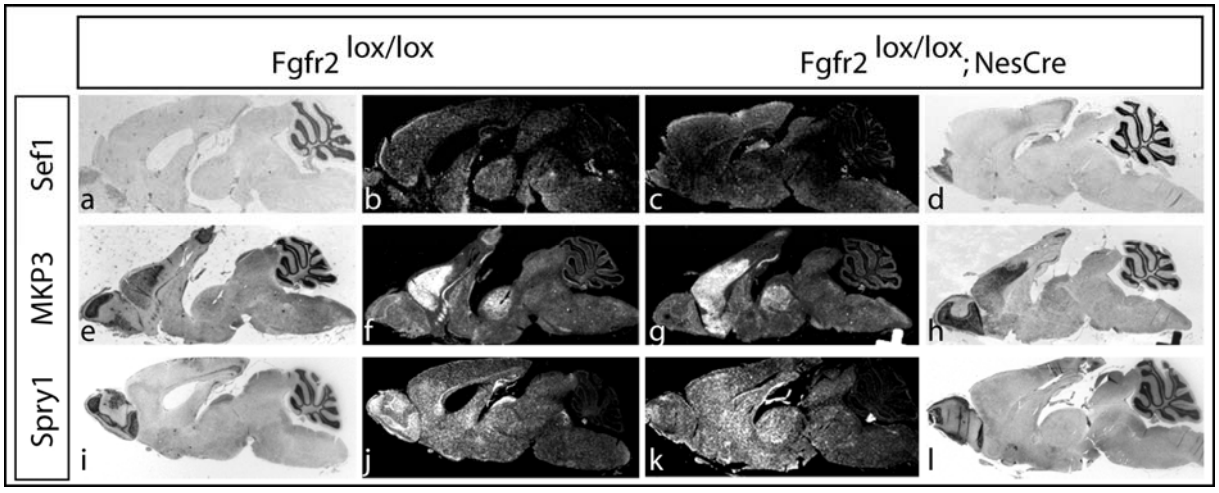

Figure 15. Expression of FGF signalling downstream targets in adult brain - overview.
In situ hybridisations (ISH) for *Sef1* (a, b, c, d), *Mkp3* (e, f, g, h), and *Spry1* (i, j, k, l) were performed on midsaggital sections of adult brains. A, d, e, h, i, and l are brightfield pictures. B, c, f, g, j, and k are darkfield pictures. ISH signals for *Sef1* were very weak (b, c). *Mkp3* and *Spry1* expression was detected in most brain regions showing no obvious difference between wt and mutant mice (f, g for *Sef1* and j, k for *Spry1*).

Unfortunately the signal intensity in the ISH using a probe against *Sef1* was very faint. A weak *in situ* signal is detectable in several regions like in some cortical layers, the corpus callosum, the thalamus, the choroide plexus or the Purkinje cell layer (Fig. 15, b, c and Fig. 16, b, c). Due to the low signal intensity, which was just slightly stronger than the unspecific background signal, the interpretation of these data was not reliable. It is not clear if the

weakness of the signal is due to the low expression level of *Sef1* or if *Sef1* is not expressed at all in the adult brain. Therefore I concentrated on the expression of *Mkp3* and *Sprouty1*.

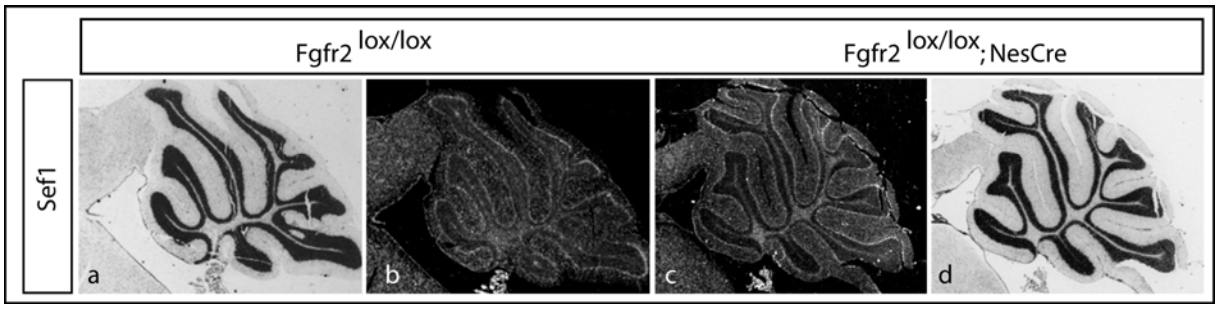

Figure 16. Expression of *Sef1* in adult *Fgfr2*$^{lox/lox}$*; Nestin-Cre* cerebellum.

ISH on saggital section revealed weak *Sef1* hybridisation signals in the Purkinje cell layer and white matter tract in both, wt mice (b) and mutants (c).

A very strong expression of *Mkp3* was detected in the cingulate cortex, the hippocampus, the thalamus, and the Purkinje cell layer. However, the expression pattern within the cortex was very dynamic along the medio-lateral and anterior-posterior axis. But also in all other regions of the adult brain I found *Mkp3* expression at variable expression levels (Fig. 15, f, g). The expression pattern within the cerebellum was distinct. The Purkinje cell layer showed very strong *Mkp3* expression whereas only a few *Mkp3* positive cells can be found in the molecular layer and almost none within the granular layer (Fig. 17, b, c). Interestingly, the expression pattern of *Mkp3* in the anterior part of the mutant cerebellum becomes more diffuse and the intensity within the Purkinje cell layer decreases (Fig. 17, e, f). Indicating, that the *Mkp3* positive cells are still present but they left the Purkinje cell layer and end up within the molecular layer.

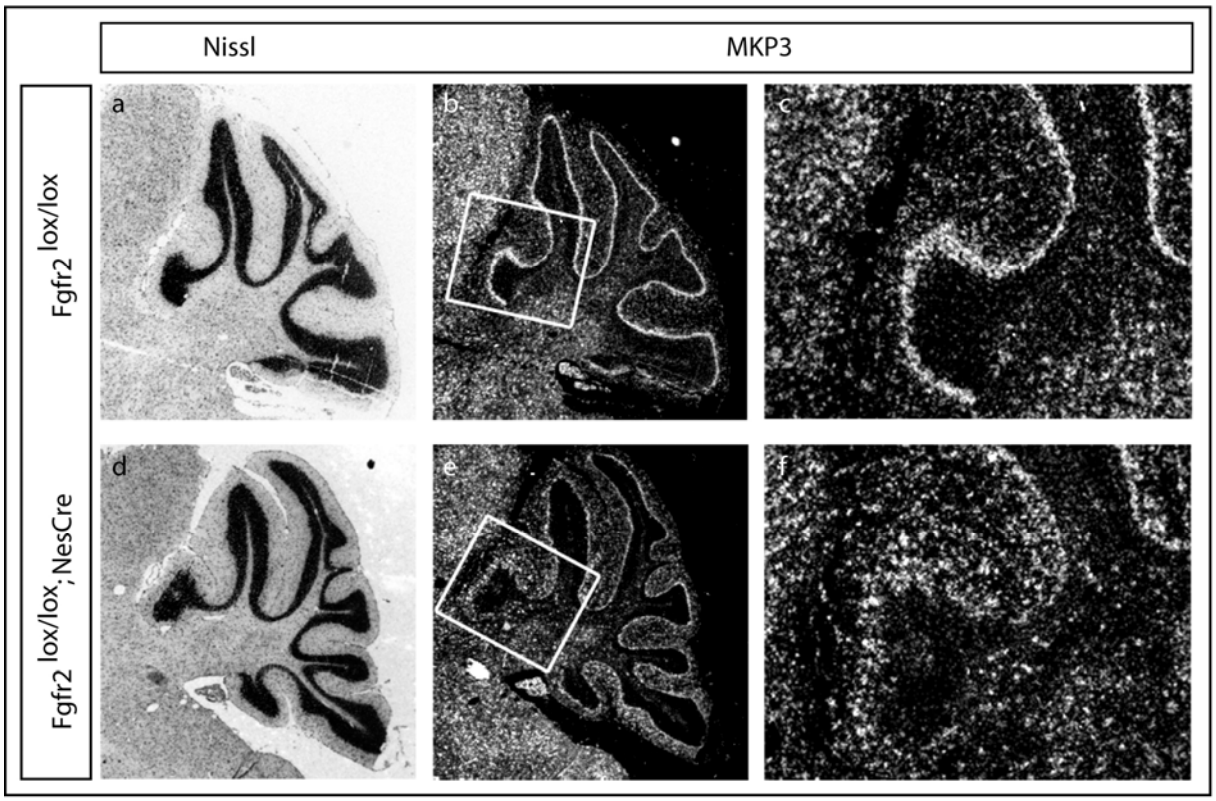

Figure 17. Expression of *Mkp3* in adult *Fgfr2*$^{lox/lox}$*; Nestin-Cre* cerebellum.

Saggital sections were used to for ISH. Strong *Mkp3* ISH signals are found in the Purkinje cell layer. In wt cerebellum *Mkp3* positive cells are densly packed within the Purkinje cells layer (b, c). In the anterior part of mildly affected mutant cerebellum distribution of *Mkp3* positive cells is broader and many *Mkp3* positive cells are in the molecular layer (e, f). a and d are brightfield images. b, c, e, and f are darkfield images.

In general, *Sprouty1* seems to be ubiquitously expressed throughout the brain with highest expression levels in forebrain regions (Fig. 15, j, and k). The expression pattern of *Sprouty1* in the anterior part of the cerebellum is similar to the one of *Mkp3* (Fig. 18, b, f). However, the expression intensity seems to be weaker as compared to the *Mkp3* expression. In the cerebellum from WT mice *Sprouty1* expression is very intense within the Purkinje cell layer and weak in the molecular layer. Almost no *Sprouty1* positive cells can be found within the granular layer. In the lateral anterior part of the mutant cerebellar vermis the distinct expression of *Sprouty1* in the Purkinje cell layer becomes weaker and more diffuse (Fig. 18, c), similar to *Mkp3* expression.

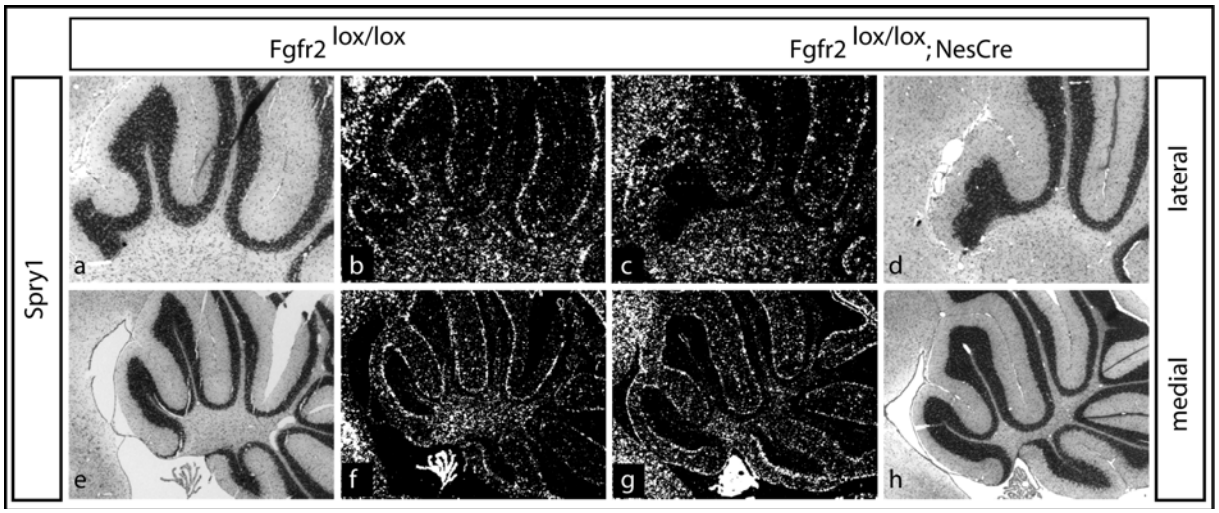

Figure 18. Expression of *Spry1* in adult *Fgfr2$^{lox/lox}$; Nestin-Cre* cerebellum.

Lateral (a, b, c, d) and medial (e, f, g, h) saggital sections were used for ISH to analyse *Spry1* expression. In wt cerebellum *Spry1* positive cells are found in the Purkinje cell layer and within the white matter tract (b, f). *Spry1* ISH signal in the anterior part of the Purkinje cell layer in lateral section of mutant cerebellum (c) is weaker than in wt cerebellum (b). *Spry1* expression in lateral section of mutant cerebellum (g) shows no obvious alteration as compared to the lateral section of wt cerebellum (f). a, d, e, and h are brightfield pictures. b, c, f, and g are darkfield pictures.

4.1.2.8 Down regulation of *Fgfr2* mRNA in *Fgfr2$^{lox/lox}$; Nestin-Cre* mice

The altered expression of downstream targets of FGF signalling indicated rather a positioning defect of cells in the anterior part of the mutant cerebellum than a loss of cells. To determine if all initially *Fgfr2* positive cells are still present and some of them failed to find their exact position within the cerebellar structure I performed ISH with a probe directed against exon 9 and 10 of the *Fgfr2* mRNA. This probe should detect the *Fgfr2* transcript also in those cells that have lost the exon5 of the *Fgfr2* mRNA and therefore do not contain the functional FGFR2 protein. This is possible because the resulting stop codon in exon6, after Cre recombinase mediated deletion of exon5, should not alter the *Fgfr2* promoter activity or the transcription of *Fgfr2* mRNA but only the translation of *Fgfr2* mRNA.

In general, the expression pattern of *Fgfr2* in brains from mutant mice recapitulated the expression pattern seen in WT mice with the important exception that the *Fgfr2* expression in

the mutant cerebellum was severely altered when compared to the WT cerebellum (Fig. 19). In mutants with a severe phenotype the expression of *Fgfr2* mRNA was almost completely abolished in the Purkinje cell layer. Solely in the most posterior parts of the mutant cerebellum a few *Fgfr2* positive cells within the Purkinje cell layer can be found (Fig. 19, g, h).

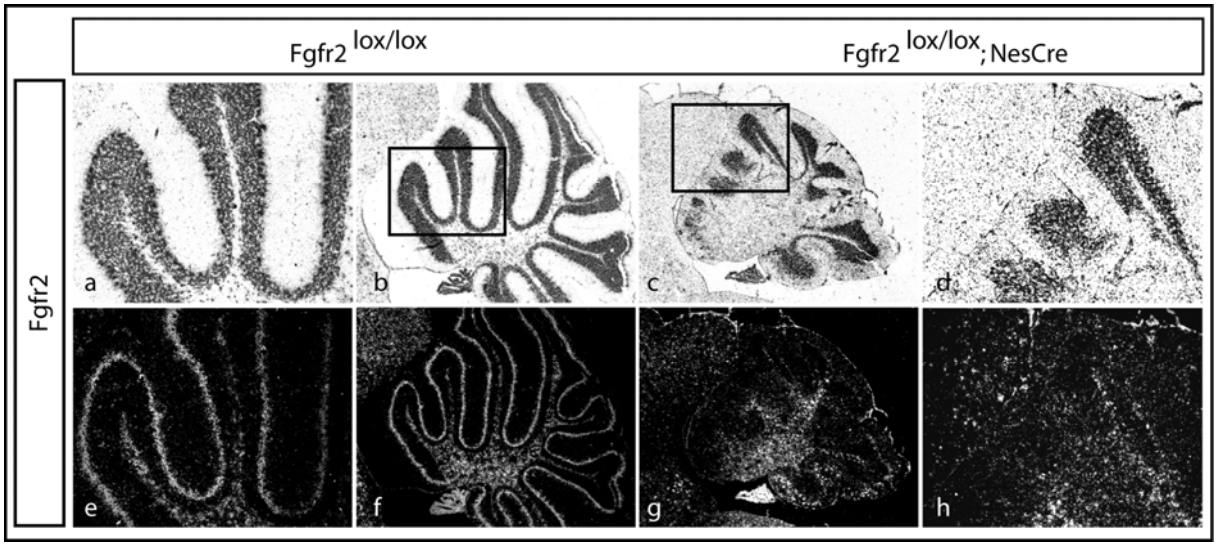

Figure 19. Expression of *Fgfr2* in adult severely affected *Fgfr2*$^{lox/lox}$*; Nestin-Cre* cerebellum. Saggital sections were hybridised with a specific *in situ* probe for FGFR2 exon 9/10. The *Fgfr2* exon 9/10 specific probe detects the *Fgfr2* mRNA in both, wt and mutant cerebellum. Strong *Fgfr2* ISH signal is detected in wt cerebellum in Purkinje cell layer and within the white matter tract (e, f). In severely affected mutant cerebellum *Fgfr2* mRNA is still detected in the white matter tract but seems to be absent in the Purkinje cell layer (g, h).

Using consecutive sections from a mutant mouse with a mild phenotype, the negative correlation between *Fgfr2* positive cells and the described alterations in Bergmann glia cells becomes obvious (Fig. 20). In the posterior parts of the cerebellum, where I do not find any morphological alterations, the *Fgfr2* mRNA is present within the Purkinje cell layer (Fig. 20, a). In the anterior part of the mutant cerebellum the amount of *Fgfr2* mRNA within the Purkinje cell layer is dramatically reduced or completely absent (Fig. 20, b). ISH with a probe against *Gad65*, labelling gabaergic neurons including Purkinje cells, and IHC with antibodies directed against S100beta or GFAP, labelling the Bergmann glia cells, revealed that both cell

types of the Purkinje cell layer, the GABAergic Purkinje cells and the S100beta positive Bergmann glia cells, are still present (Fig. 20, d, e, f). Even though, the S100beta staining in the anterior part of the mutant cerebellum was very weak. Nevertheless, the lack of the *Fgfr2 in situ* signal within this region of the mutant cerebellum indicates rather a silenced *Fgfr2* promoter than a loss of cells.

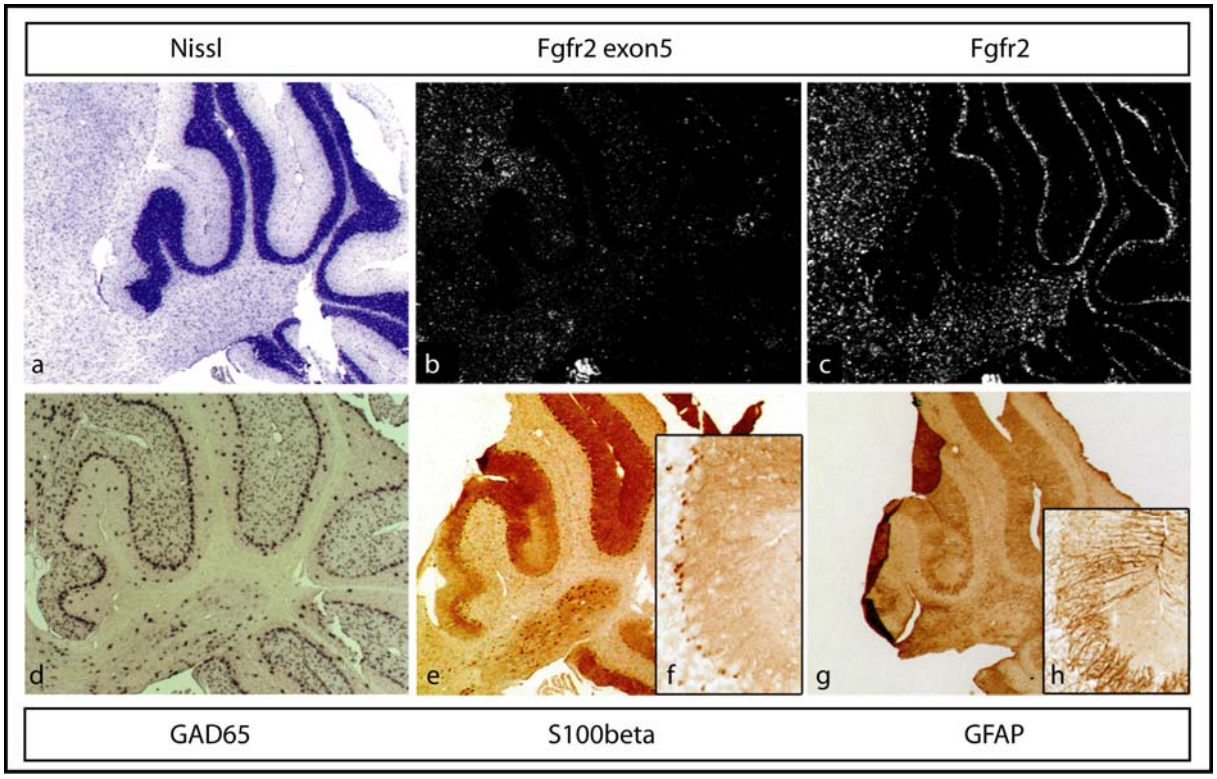

Figure 20. Correlation of Bergmann glia defects and *Fgfr2* mRNA expression in mildly affected *Fgfr2*$^{lox/lox}$*; Nestin-Cre* cerebellum.

Consecutive saggital sections were used for Nissl staining (a), ISH (*Fgfr2* exon5 probe in b, *Fgfr2* exon 9/10 probe in c, *Gad65* probe in d), and immunohistochemistry (S100ß in e and f, GFAP in g and h). The cerebellar structure appears normal after Nissl staining (a) and ISH using *Fgfr2* exon5 specific riboprobe revealed the deletion of this exon in almost all cells within the cerebellum (b). FGFR2 exon9/10 expression was abolished in cells of the PCL in lobules II and III whereas the expression in cells in the posterior lobes was still present (c). *Gad65* positive gabaergic neurons (d) and and S100ß positive Bergmann glia cells (e, f) were still present in the entire PCl. Many of the GFAP labelled processes of the Bergmann glia cells failed to reach the cerebellar surface in lobules II and III (g, h).

4.1.2.9 Expression of *Fgfr1* and *Fgfr3* in *Fgfr2*$^{lox/lox}$; *Nestin-Cre* mice

Since the downstream targets of FGF signalling are still expressed other *Fgfrs* than *Fgfr2* should be expressed and active in the affected areas of the cerebellum. To define which *Fgfrs* are expressed in the adult cerebellum I performed ISH on WT brains for all four known *Fgfrs* and compared their expression pattern. It is known that a strong activation of FGFR1 by FGF8b can lead to a silencing of the *Fgfr2* and *Fgfr3* promoter in embryonic tissue from the MHR (Liu et al., 2003). So far there is no evidence that this silencing occurs also in adults and *in vivo*. To figure out if the absent *Fgfr2* mRNA in the anterior part of the mutant cerebellum is caused by FGFR1 mediated silencing of the *Fgfr2* promoter I performed ISH for *Fgfr1* and *Fgfr3* on mutant brains.

First, I compared the expression of all four FGF receptors in brains from WT mice. All receptors, except *Fgfr4*, showed a clear and strong ISH signal (Fig. 21). A more detailed analysis of the *Fgfr4* ISH revealed that *Fgfr4* expression in the adult brain is not detectable (Fig. 22, b, c). Therefore *Fgfr4* was excluded from further analysis.

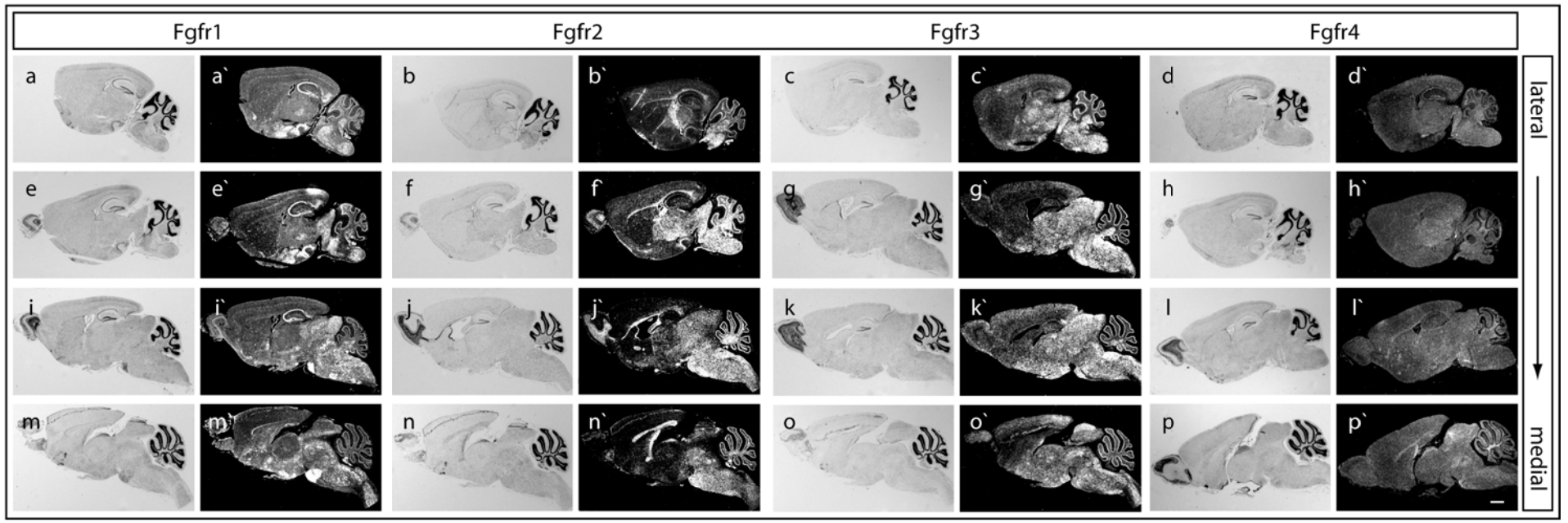

Figure 21. Expression of *Fgfrs* in adult wt brains.

Saggital sections were used to for ISH. *Fgfr1* (a, e, i, m), *Fgfr2* (b, f, j, n), and *Fgfr3* (c, g, k, o) are expressed throughout the entire brain whereas ISH for *Fgfr4* (d, h, l, p) showed no specific hybridisation signal. For *Fgfr1* strongest ISH signal is found in Pons and hippocampus. *Fgfr2* ISH revealed high expression levels in corpus callosum and caudal brain regions like thalamus, cerebellum and brain stem. *Fgfr3* seems to be evenly expressed throughout the brain with slightly stronger ISH signal in posterior brain regions. Brightfield and corresponding darkfield pictures are shown. Scale bar: 1mm.

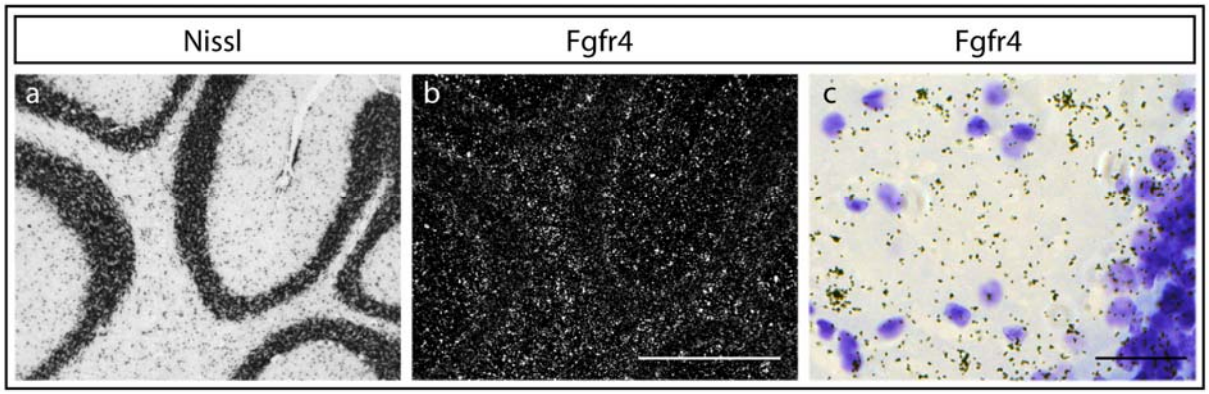

Figure 22. *Fgfr4* expression is not detectable in adult wt brain.

ISH was performed on saggital sections of wt brains. No specific hybridisation signal in any brain region was detected. As an example a part of the cerebellum is shown (b). Higher magnification picture (c) of the same region reveals that observed weak signal highly likely represents background signal (c). a and c, brightfield; b, darkfield; Scale bars: 500µm in b and 25 µm in c.

All three analysed *Fgfrs*, *Fgfr1, Fgfr2*, and *Fgfr3*, are expressed in the adult cerebellum (Fig. 23). *Fgfr1* is expressed in the Purkinje cell (PC) layer and in granular cells (GC) (Fig. 23, b, f). The expression of *Fgfr2* was found within the PC layer and the GC layer (Fig. 23, c, and g). But in contrast to the *Fgfr1* expression, *Fgfr2* has a more distinct expression pattern within the GC layer. These *Fgfr2* positive cells within the GC layer are probably oligodendrocytes. The expression of *Fgfr3* is restricted to the PC layer (Fig. 23, d, h).

Since all three analysed *FGF receptors* are expressed in the PC layer I analysed this structure more in detail (Fig. 23, i, j, k). The expression of all three *FGF receptors* seems to be concentrated in the smaller Bergmann glia (BG) cells. The expression of the three *FGF receptors* in the larger PC seems to be very weak or absent.

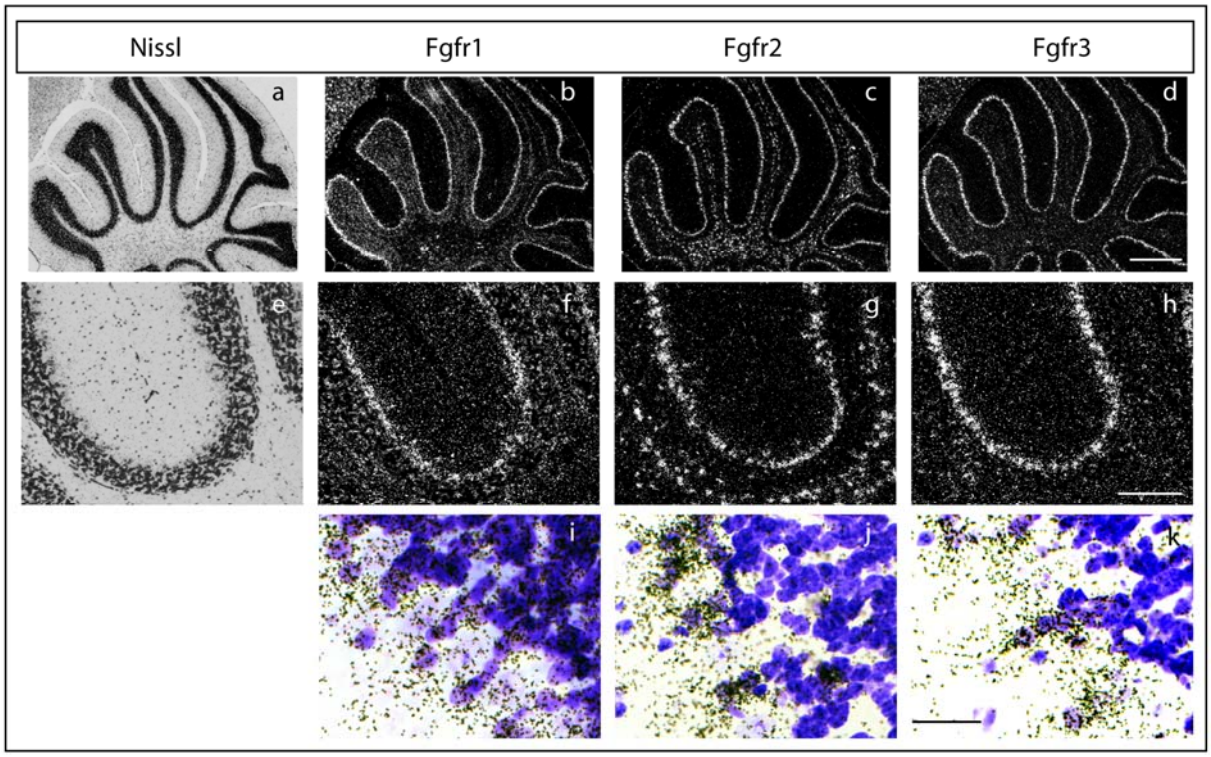

Figure 23. *Fgfr1*, *Fgfr2*, and *Fgfr3* expression in adult wt cerebellum.

Consecutive saggital sections were used to compare expression of the three *Fgfrs*. All of them are expressed strongly by Bergmann glia cells in the Purkinje cell layer (b, c, d and i, j, k). In addition *Fgfr1* is expressed in Granule neurons (f) and *Fgfr2* is expressed by oligodendrocytes within the white matter tract (h). a, e, i, j, and k: brightfield; b, c, d, f, g, and h: darkfield; Scale bars: 500µm in d, 250µm in h, 25µm in k.

Surprisingly, the expression level of *Fgfr1* specifically within the PC layer seems to be reduced in mutants (Fig. 24). The Bergmann Glia cells from mutant mice did not express *Fgfr1* at such a strong level as the Bergmann Glia cells from their WT littermates (Fig. 25). The *Fgfr1* expression in other regions, e.g. within the cuneiform nucleus (Fig. 24) or the granular layer (Fig. 25) were not affected in mutant cerebella.

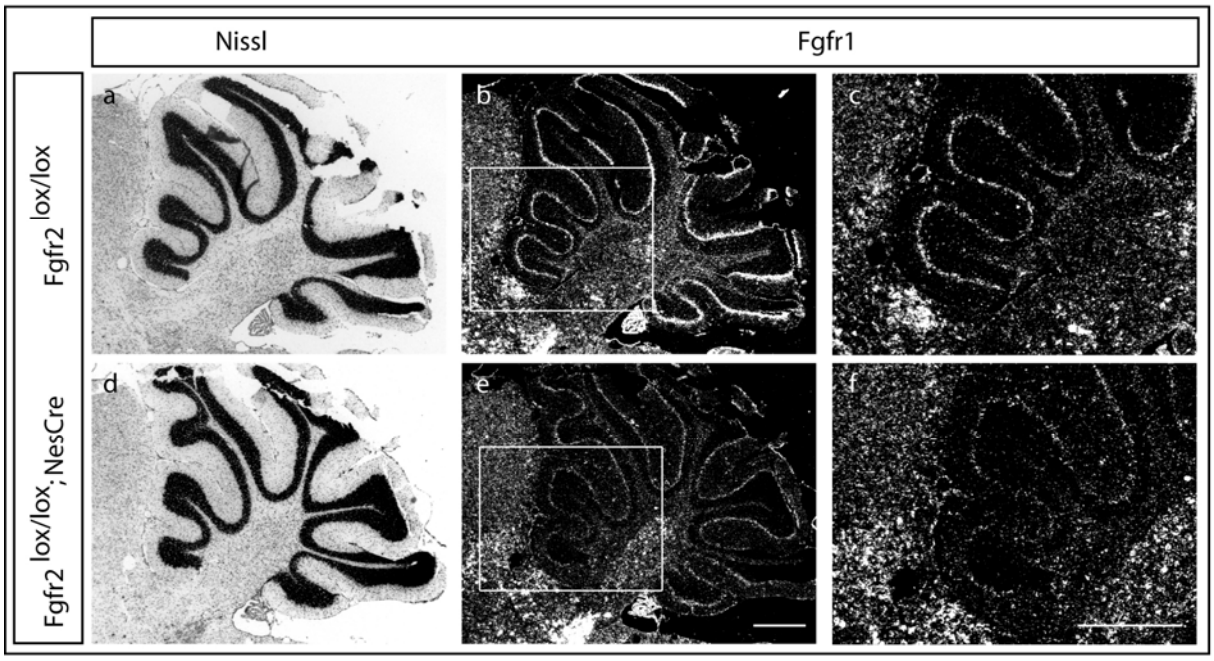

Figure 24. *Fgfr1* expression in mildly affected *Fgfr2* $^{lox/lox}$*; Nestin-Cre* cerebellum.

ISH were performed on saggital sections. *Fgfr1* expression pattern in *FGFR2* $^{lox/lox}$*; Nestin-Cre* cerebellum (e, f) is not altered as compared to wt cerebellum (b, c). However, intensity of the ISH signal seems to be weaker in the Purkinje cell layer of mutant mice (compare c and f). Scale bar 500µm.

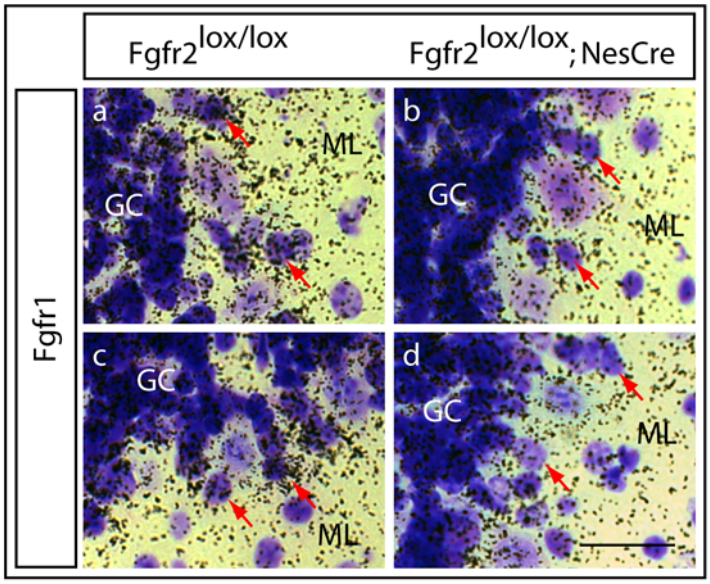

Figure 25. *Fgfr1* expression in Purkinje cell layer of *Fgfr2* $^{lox/lox}$*; Nestin-Cre* mice.

Saggital sections from adult mice were used for ISH. In wt cerebellum strong *Fgfr1* expression is found in granule cells (GC) in the granular layer and in Bergmann glia (red arrows in a and c). In mutant cerebellum (b, d) *Fgfr1* expression in GC unaltered whereas Bergmann glia cells seem to express less or no *Fgfr1* (red arrows in b, d) as compared to wt. Scale bar 25µm.

Fgfr3 is still expressed within the PC layer of mutant mice (Fig. 26, c, and f) but the distribution of *Fgfr3* positive cells was altered. Many *Fgfr3* positive cells are found within the molecular layer. The expression pattern of *Fgfr3* is reflecting the expression pattern of *Mkp3* (Fig. 26, f, red arrows). Therefore *Fgfr3* seems to be responsible for an active FGF signalling in the adult cerebellum of mutant mice which was indicated by *Mkp3* ISH (Fig. 17).

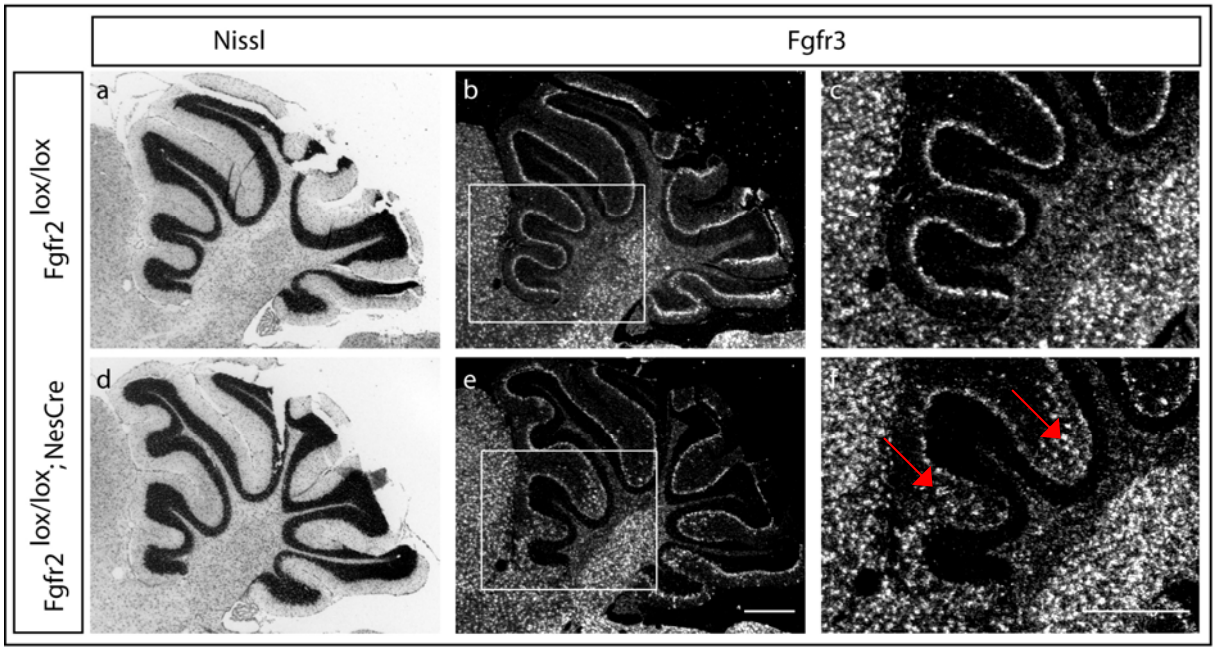

Figure 26. *Fgfr3* expression in *FGFR2* $^{lox/lox}$*; Nestin-Cre* cerebellum.

Fgfr3 ISH was performed on saggital sections of adult wt (a, b, c) and mutant (d, e, f) brains. In wt cerebellum strong *Fgfr3* expression is found within the Purkinje cell layer and no *Fgfr3* positive cells are present within the molecular layer (b, c). In FGFR2 mutants *Fgfr3* positive cells are found in the molecular layer of the anterior part of the cerebellum (arrows in f). Scale bars: 500µm.

4.1.3 Analysis of *Fgfr2 $^{lox/lox}$; Nestin-Cre* embryos and young mice

To explain the alterations found in the cerebellum from mutant mice it is necessary to analyse the cerebellar structure in young animals. Therefore I analysed young mice (P4 and P6) and embryos (E17 and E18).

The general cerebellar structure and the expression of the Purkinje cell marker Calbindin were unaltered in E17.0 Embryos. In E18 embryos the altered structure of the cerebellum of mutant mice became obvious (Fig. 27). Even though the cerebellar structure is still developing at this stage there are clear differences. The beginning of foliation, which is clearly recognizable in the cerebellum from WT mice, is not yet well defined in the mutant cerebellum. Nevertheless, the layered structure, with the external granular layer at the surface and the Purkinje cell layer below, is established in the WT cerebellum as well as in the mutant cerebellum.

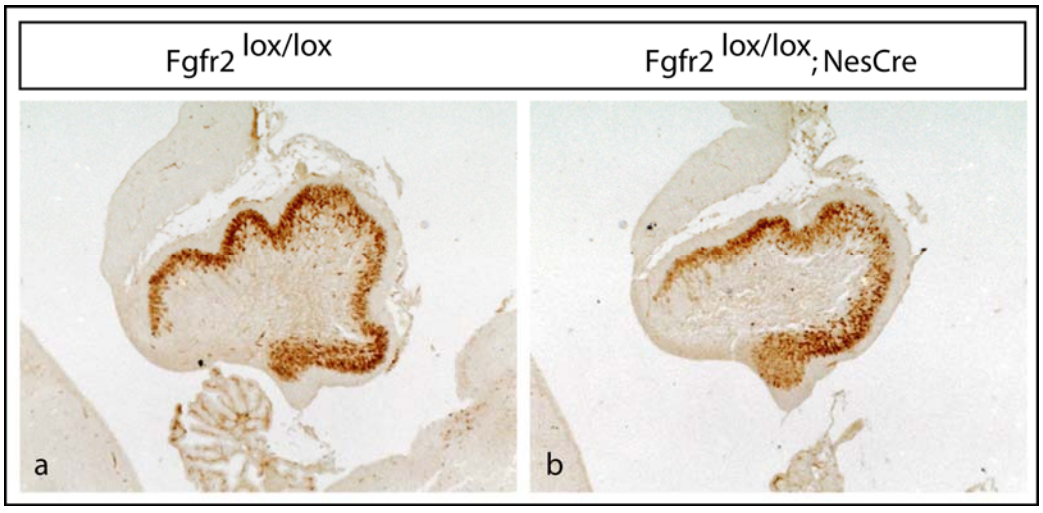

Figure 27. Alterations in the embryonic cerebellum of *Fgfr2 $^{lox/lox}$; Nestin-Cre* mice.
Saggital sections of E18 brains from wt (a) and mutant mice (b) were used for IHC. Calbindin staining (specific marker for Purkinje cells) revealed underdeveloped foliation of the mutant cerebellum.

Similar differences between mutant and WT cerebella were found in young animals (Fig. 28). The foliation process in the cerebellum from mutant mice seems to be disturbed. At these developmental stages the Granule neurons are migrating in the wt cerebellum from the

external granular layer through the Purkinje cell layer to form the internal granular layer (Fig. 28, c, e; red arrows). An internal granular layer is not visible in mutant cerebellum (Fig. 28, d, f; red arrows). Nevertheless, the Purkinje cell layer in the mutant cerebellum is broader, and there are many Purkinje cells, and even groups of Purkinje cells, outside of the Purkinje cell layer.

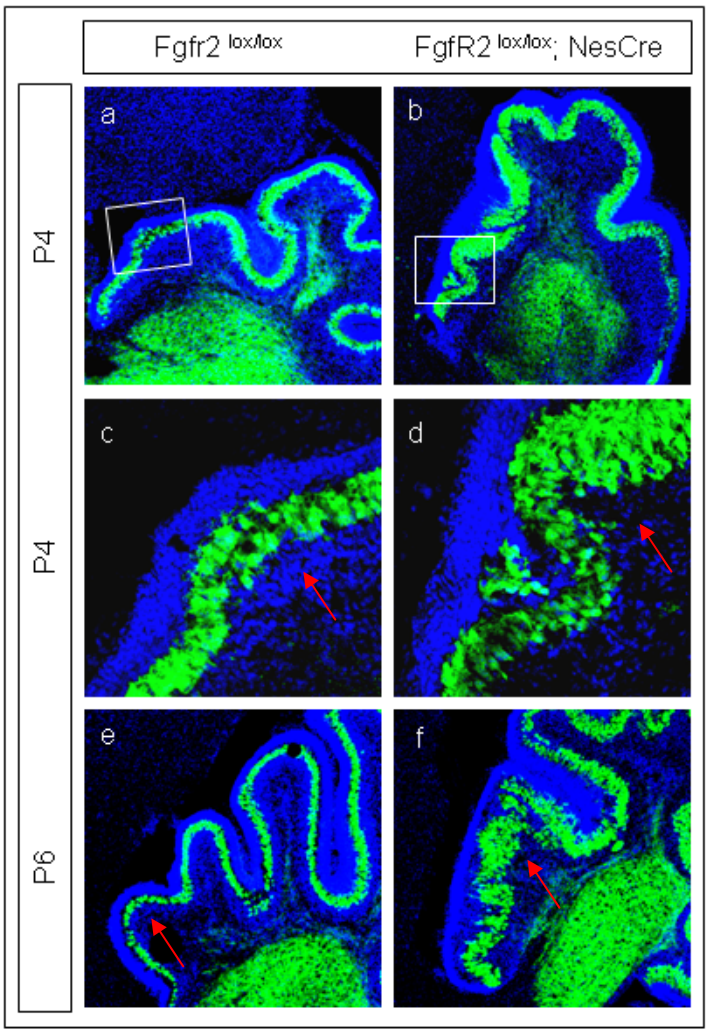

Figure 28. Cerebellar defects in *Fgfr2* $^{lox/lox}$*; Nestin-Cre* mice during postnatal development.

Brains from 4 days old (P4; a, b, c, d) and 6 days old animals (e, f) were used for fluorescence-IHC. Dapi staining (blue) and fluorescence-immunostaining for Calbindin (green) on saggital sections of *Fgfr2*$^{lox/lox}$ cerebellum (a, c, e) and severely affected *Fgfr2*$^{lox/lox}$*; Nestin-Cre* cerebellum (b, d, f). Regions with high cellular density represent the developing internal granular layer (red arrows in c and e). In mutants the internal granular layer is underdeveloped (red arrows in d and f).

4.1.4 Behaviour of *Fgfr2 $^{lox/lox}$; Nestin-Cre* mice

To find out if the alterations in the mutant cerebellum have behavioural consequences I used three different behaviour tests. The modified Hole Board (mHB) gives a general overview about several behavioural parameters. The forced swim test (FST) is used to analyse depression-like behaviour. There are studies linking FGFR2 to depressive disease in humans (Evans et al., 2004; Turner et al., 2006). Since it is known that the cerebellum is important for the control of movements (Manni and Petrosini, 2004) we were in particular interested in investigating the motor coordination of mutant mice, which was tested on the Rotarod.

4.1.4.1 **Modified Hole Board (mHB)**

Even though the mutants did not display any obvious behavioural deficits, in the mHB they showed significant differences in several measured parameters when compared with WT mice. The parameters differing between mutant and WT mice can be separated into two groups, horizontal locomotion and vertical locomotion. The mutants showed less activity in both parameter groups. Regarding horizontal locomotion a significant decrease in the number of line crossings, in the traveled distance, in mean velocity and in maximum velocity was found (Fig. 29, A, B, C, D). Concerning the vertical locomotion I found a significant decrease in the rearing behaviour on board of mutants compared to WT mice (Fig. 29, E). Mutants needed also more time before they performed the first rearing on board (Fig. 29, F). Interestingly, in mutant mice the latency to the first rearing outside of the board was significantly lower than observed in WT mice (Fig. 29, I). This indicates an inhibition of vertical behaviour in mutant mice on board whereas the vertical behaviour was in general unchanged or even enhanced as compared to WT mice (see latency to first rearing in box; Fig. 29, I).

In male mutants I found a significantly decreased distance to the wall and therefore an increased distance to the board as compared to the WT mice (Fig. 29, G, and H). Here, the average position of the mice between the wall on one side and the board on the other side was measured.

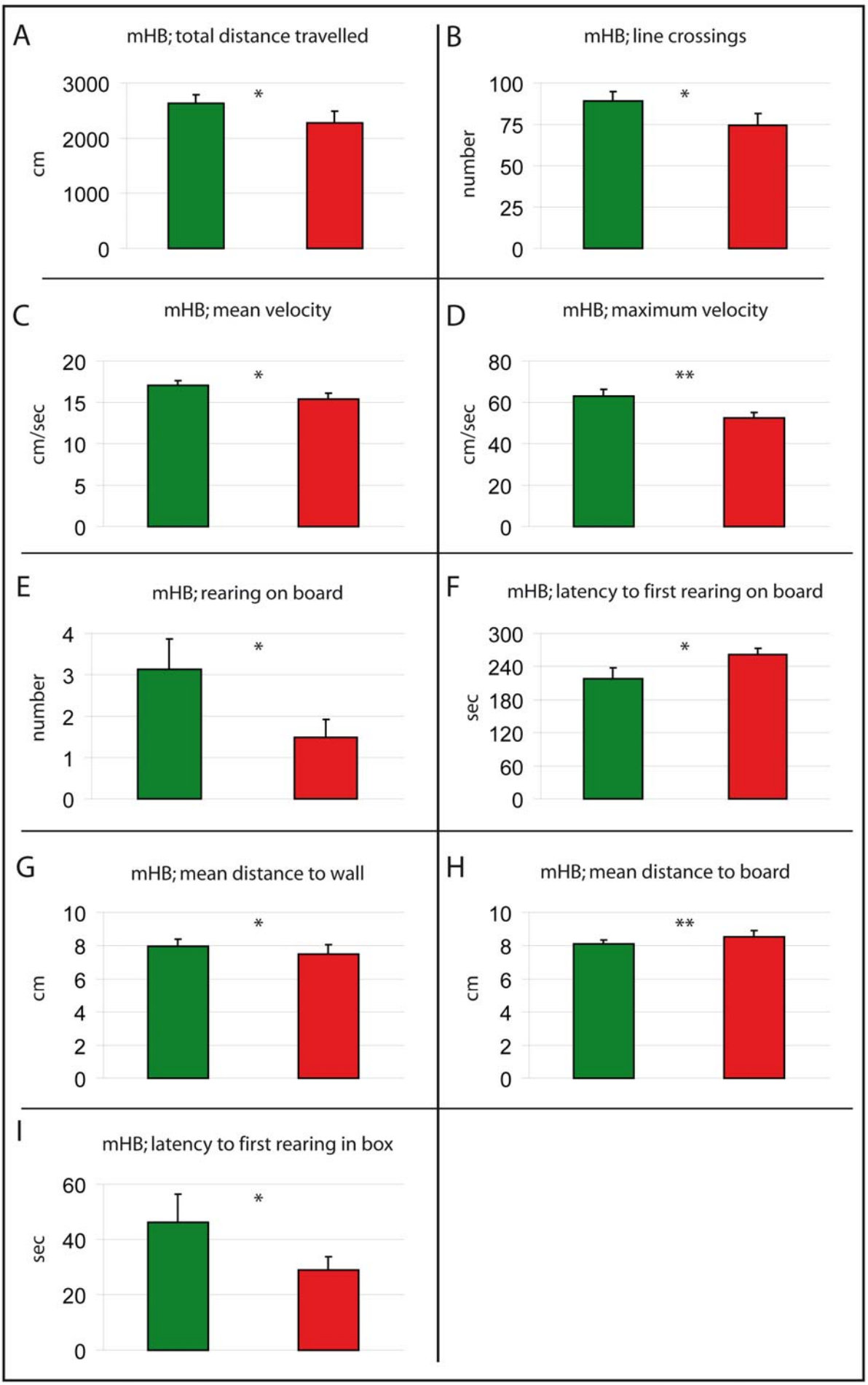
A
mHB; total distance travelled
cm
3000
2000
1000
0
*
B
mHB; line crossings
number
100
75
50
25
0
*
C
mHB; mean velocity
cm/sec
20
15
10
5
0
*
D
mHB; maximum velocity
cm/sec
80
60
40
20
0
**
E
mHB; rearing on board
number
4
3
2
1
0
*
F
mHB; latency to first rearing on board
sec
300
240
180
120
60
0
*
G
mHB; mean distance to wall
cm
10
8
6
4
2
0
*
H
mHB; mean distance to board
cm
10
8
6
4
2
0
**
I
mHB; latency to first rearing in box
sec
60
40
20
0
*

Figure 29. Impact of CNS specific FGFR2 inactivation on unconditioned behaviour of mice in the modified Hole Board paradigm (mHB) at the age of 10 weeks.
Significant alteration were found in horizontal (A, B, C, D, G, H) and vertical (E, F, I) locomotor activity. Data are expressed as means + S.E.M. There were no significant interaction between sex and genotype. Significant differences between mutant and control mice are indicated by asterisks: ** $p < 0.01$; * $p < 0.05$. green bars: control animals; red bars: mutants.

4.1.4.2 **Forced Swim Test (FST)**

In the FST I found an increased struggling behaviour in mutant mice when compared with WT mice (Fig. 30, C). The FST is often used to determine depression-like behaviour in mice. Increased struggling behaviour is usually interpreted as decreased depression-like behaviour. The other two measured parameters, floating and swimming, were not significantly altered in mutant mice (Fig. 30, A, B).

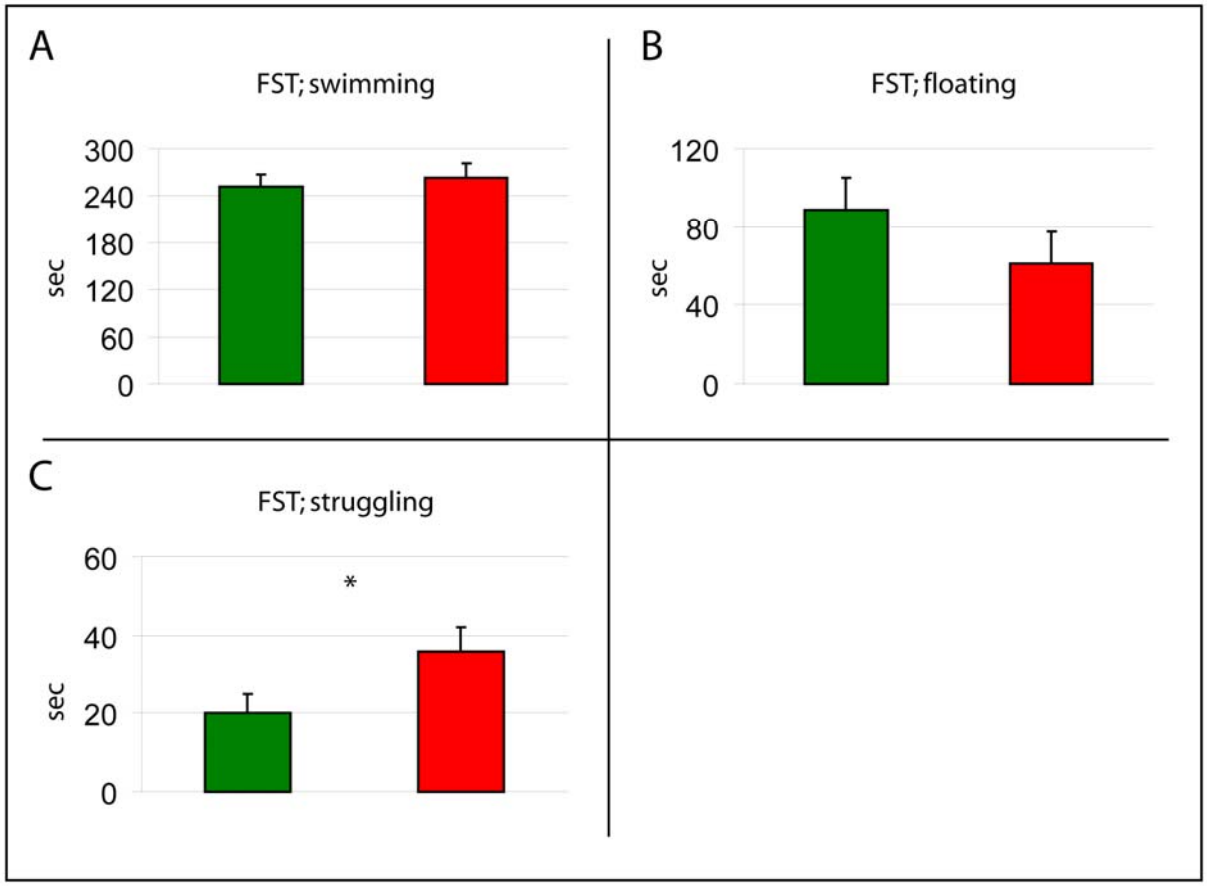

Figure 30. Behaviour of *Fgfr2* $^{lox/lox}$*; Nestin-Cre* mice in the forced swim test (FST).
There were no significant differences between mutants (red bars) and control animals (green bars) in swimming and floating behaviour (A, B). Mutant mice spent significantly more time with struggling (C) than wt mice. Data are expressed as means + S.E.M. There were no significant interaction between sex and genotype. Significant differences between mutant and control mice are indicated by asterisks: ** $p < 0.01$; n.s.: not significant.

4.1.4.3 **Rotarod**

Mutants and WT mice did not show any significant differences in the performance on the Rotarod, a test for motor-coordination (Fig. 31). This result is surprising, because the involvement of the cerebellum in the coordination of movements is well established (Manni and Petrosini, 2004).

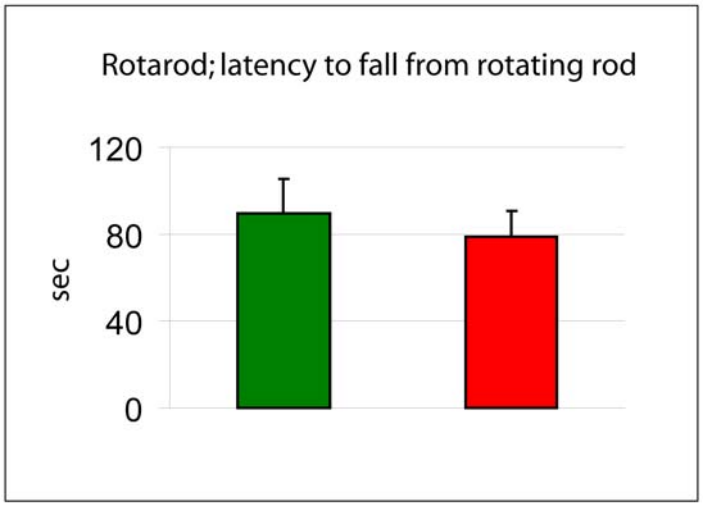

Figure 31. Behaviour of *Fgfr2* $^{lox/lox}$*; Nestin-Cre* mice on the rotating rod (Rotarod).
There was no significant difference between mutants (red bar) and control animals (green bar) in Rotarod performance and no significant interaction between sex and genotype. Data are expressed as means + S.E.M. n.s.: not significant.

As shown in the histological analysis in 3.1, mutants display varying levels of malformations of the cerebellum. In some cases, I saw only a few mispositioned Purkinje cells and Bergmann glia fibers that did not reach the cerebellar surface. On the other hand, I found also mutants with severely disturbed cerebella and a complete loss of the distinctly layered

structure in the anterior part of the cerebellum. A detailed analysis of the Rotarod results revealed that there was one male mutant (No. 30064156), which performed the rotarod extremely good (Fig. 32). This mutant stayed 140 seconds on the rotating rod whereas all other mutants spent less than 80 seconds on the Rotarod.

Performance on Rotarod (males)

	Fgfr2 lox/lox			Fgfr2 lox/lox; NesCre	
	ID No.	sec		ID No.	sec
1	30064150	98	1	30064149	72
2	30064151	54	2	30064152	50
3	30064153	119	3	30064155	45
4	30064154	16	4	30064156	140
5	30064158	58	5	30064157	47
6	30064159	56	6	30064162	32
7	30064160	131	7	30064163	77
8	30064161	109	8	30064164	25
9	30064166	42	9	30064165	80
10	30064168	36	10	30064167	59
11	30064170	108	11	30064169	67
12	30064171	43	12	30064174	66
13	30064172	230			
14	30064173	51			
15	30064175	82			

Figure 32. Rotarod performance of *Fgfr2* $^{lox/lox}$ and *Fgfr2* $^{lox/lox}$*; Nestin-Cre* males.
15 wt males (FGFR2 $^{lox/lox}$) and 12 mutant males (FGFR2 $^{lox/lox}$; Nestin-Cre) were analysed on the Rotarod (see also Figure 31). Great differences between the performance of individual males were observed. In control males performance ranged from 16 seconds (sec) to 230 seconds and in the mutant group from 25 to 140 seconds. The three indicated animals (ID No. 30064154; ID No. 30064156; ID No. 30064164) were used for further analysis (see Figure 33).

I analysed the mice marked in Fig. 32 concerning the histological phenotype. As controls I used one mutant with low performance on the Rotarod (No. 30064164) and one WT mouse (No. 30064154). The results showed, as expected, that the mutant with a good performance on the Rotarod (No. 30064156) had no obvious alterations in the cerebellar structure and appeared similar to the WT cerebellum (No. 30064154) (Fig. 33, b, e). In contrast to these two mice, the mutant with the low performance on the Rotarod (No. 30064164) showed a dramatically disturbed organisation of the cerebellum (Fig. 33, c, f).

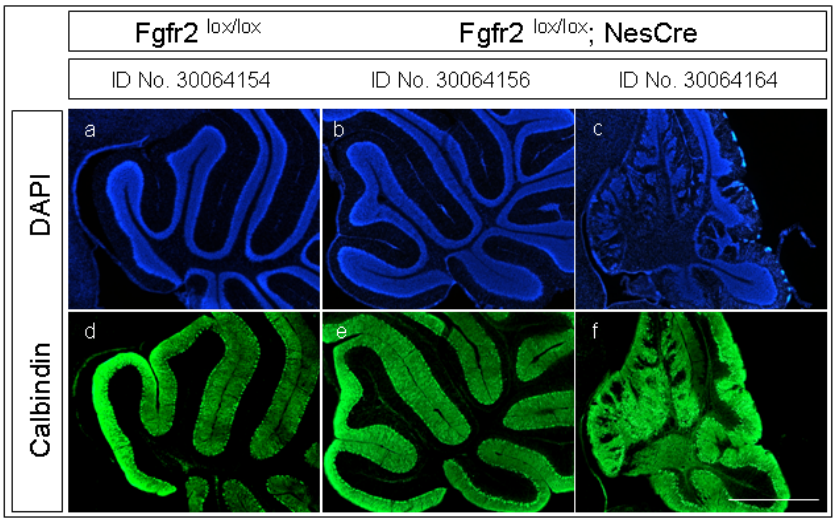

Figure 33. Cerebellum histology of males used previously in the Rotarod test.
Saggital sections from one *Fgfr2* $^{lox/lox}$ (a, d) and two mutants (*FGFR2* $^{lox/lox}$*; Nestin-Cre*; b, c, e, f) were analysed. DAPI staining (blue in a, b, c) and Calbindin F-IHC (green in d, e, f) revealed normal cerebellar morphology in one mutant (ID No. 30064156) and severely altered cerebellar morphology in the other mutant (ID No. 30064164). Scale bar: 1mm.

The histological analysis indicates a negative correlation between the level of cerebellar malformation and the performance on the Rotarod and motor-coordination abilities. Interestingly, the analysis of the Rotarod results without the mutant with the mild phenotype and good Rotarod performance (No. 30064156), even leads to a significant difference ($p < 0.05$) between the male mutants and the male WT mice (Fig. 34).

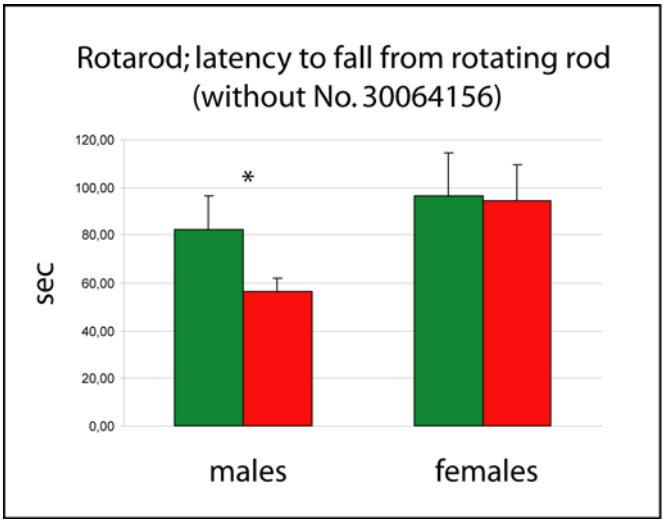

Figure 34. Re-calculated Rotarod performance of *FGFR2* $^{lox/lox}$*; Nestin-Cre* males.
Statistical analysis of Rotarod performance excluding the mutant shown to have mildly affected cerebellum (Figure 33; ID No. 30064156) revealed a significant difference between control and mutant males. Data are expressed as means + S.E.M. Significance is indicated by asterisk; * $p < 0.05$.

4.2 Loss of FGFR2 in mature forebrain neurons leads to increased depression-like behaviour

As already mentioned, there are studies showing a possible involvement of FGFR2 in depressive disorders in humans (Evans et al., 2004; Turner et al., 2006). First of all I analysed the expression of the four *Fgfrs* in the adult mouse brain in regions, which are known to be involved in depressive diseases in humans. To investigate the role of FGFR2 in depression-like behaviour in mice I generated a conditional *Fgfr2* knockout mouse, in which exon5 of *Fgfr2* is deleted in forebrain neurons. These mice were analysed in several behavioural tests to examine the effect of loss of FGFR2 on the general behaviour and in particular on depression-like behaviour.

4.2.1 Expression of FGFRs in "depressive" brain regions

To ensure a meaningful analysis of the involvement of FGFR2 in depressive disorders using mouse models, I first analysed the *Fgfr2* expression in Wt mice by ISH. To get a more complete overview of the situation I included also *Fgfr1* and *Fgfr3* in this analysis. *Fgfr4* was excluded from the expression analysis because of the extremely weak ISH signal shown in Fig. 22. I especially concentrated on those brain regions which were already described in former studies to be important in depressive diseases in humans (Soares and Mann, 1997; Strakowski et al., 2005). Based on findings from other studies which implicated FGF signalling in depressive diseases I first analysed the expression of the three *Fgfrs* in the prefrontal cortex, the cingulate cortex and the hippocampus (Evans et al., 2004; Mallei et al., 2002). Furthermore, I looked also in detail at *Fgfr* expression in the amygdala and the striatum, two regions which are thought to be involved in depression. The cerebellar Vermis is one of the brain regions which were linked to major depression (Konarski et al., 2005). The expression of the three *Fgfrs* in the cerebellar Vermis is already described in section 3.1 (Fig. 23).

All three analysed *Fgfrs* are expressed throughout the prefrontal cortex and the cingulate cortex (Fig. 35 and Fig. 36). *Fgfr3* is expressed equally in the whole prefrontal cortex whereas for *Fgfr1* the strongest expression has been detected in the 5th cortical layer (Fig. 35, b, f).

Fgfr2 is expressed strongly in ventral part of the prefrontal cortex (Fig. 35, c, g). Similar results come from the expression of the three *Fgfrs* in the cingulate cortex, where *Fgfr1* expression is stronger in the ventral parts and *Fgfr2* and *Fgfr3* are ubiquitously expressed (Fig. 36).

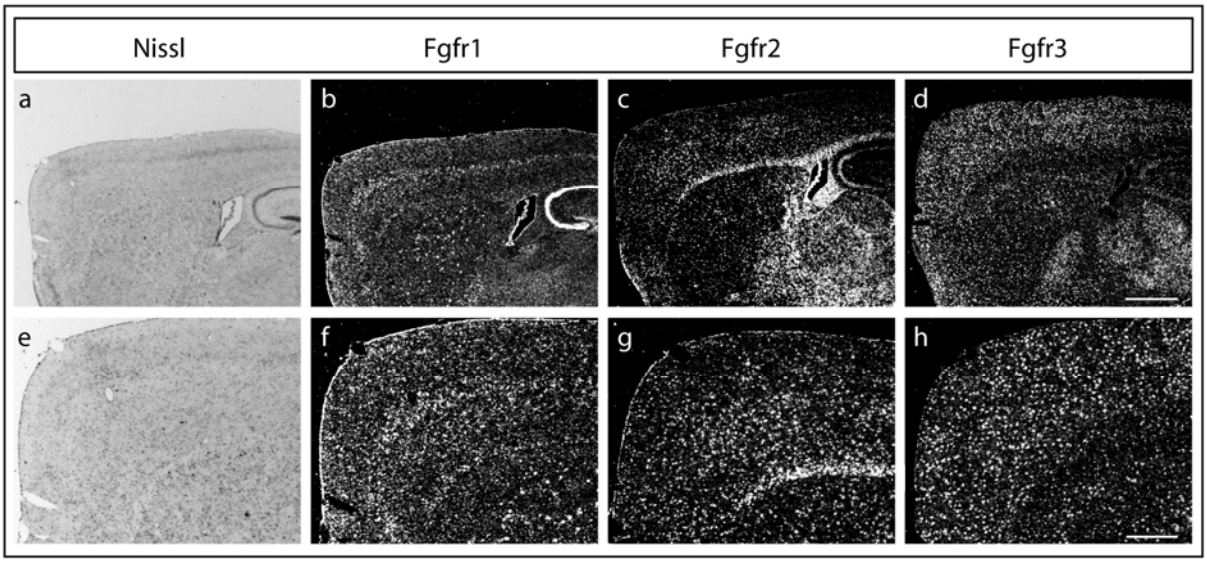

Figure 35. Expression of *Fgfrs* in the prefrontal cortex of adult wt mice.

Fgfr1, Fgfr2, and *Fgfr3*, respectively, are expressed in the prefrontal cortex. Strongest *Fgfr1* expression is found in the 5th cortical layer (b, f). *Fgfr2* is expressed mainly in the ventral part of the prefrontal cortex (c, g) whereas *Fgfr3* expression is present throughout the entire region (d, h). Scale bars: 1mm in d; 500µm in h.

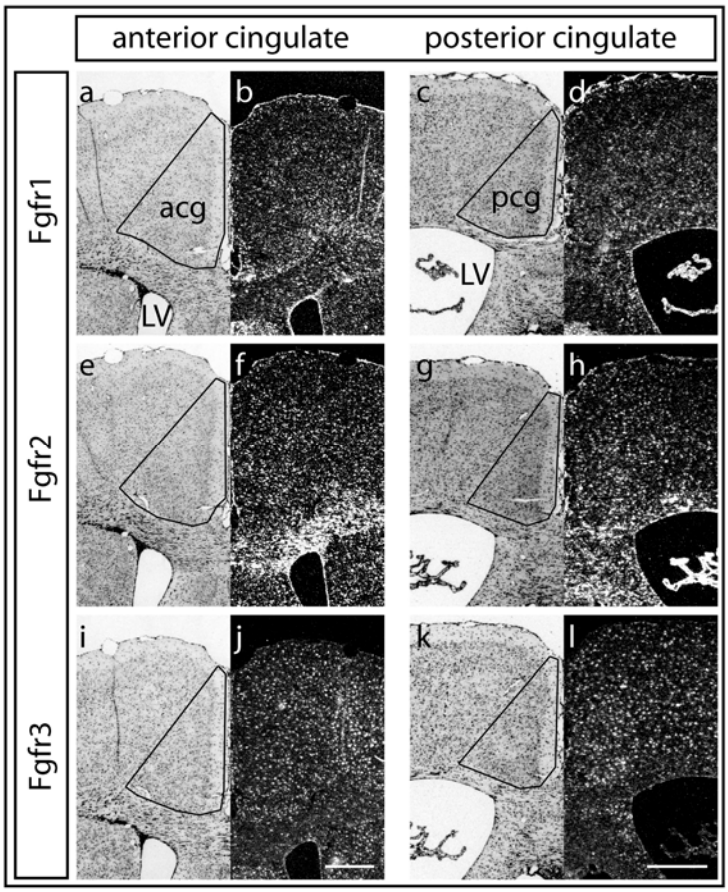

Figure 36. Expression of *Fgfrs* in the cingulate cortex of adult wt mice.

Coronal sections were used for ISH. *Fgfr1, Fgfr2*, and *Fgfr3*, respectively, are expressed in the cingulate cortex. Weak *Fgfr1* expression is found mainly in the ventral part of the cingulate cortex (b, d). *Fgfr2* (f, h) is expressed evenly throughout the entire region whereas *Fgfr3* (j, l) seems to reach higher expression levels in the posterior cingulate cortex. Acg: anterior cingulate cortex; pcg: posterior cingulate cortex; LV: lateral ventricle; Scale bars: 500µm.

Several studies suggest the involvement of the hippocampus in depressive diseases. There are hints for functional as well as structural or size alterations of the hippocampus in patients with major depression (Posener et al., 2003; Strakowski et al., 2005). Recently also the hippocampal adult neurogenesis has been linked to Depression (Sahay and Hen, 2007). The new neurons are generated in the subgranular zone (SGZ) of the dentate gyrus (DG). The expression of the three analysed *Fgfrs* in the hippocampus is shown in Fig. 37.

In the pyramidal cells of the cornu ammonis (CA) the expression of *Fgfr1* is very strong (Fig. 37, b) whereas *Fgfr2* and *Fgfr3* seem not to be expressed in these cells (Fig. 37, c, d). A few positive cells within the Hillus can be found for all three *Fgfrs* but expression seems to be completely absent in the granular layer of the DG (Fig. 37, f, g, h). Higher magnification

images of the SGZ, where new neurons are generated, are shown in Fig. 37, i, j, and k. Many *Fgfr1* positive cells and some *Fgfr2* positive cells are present in the SGZ (Fig. 37, i, j), whereas *Fgfr3* seems to be expressed only in a few cells (Fig. 37, k). These results indicate a possible role of *Fgfr1* and maybe also *Fgfr2* and *Fgfr3* in generation or differentiation of new neurons in the adult hippocampus.

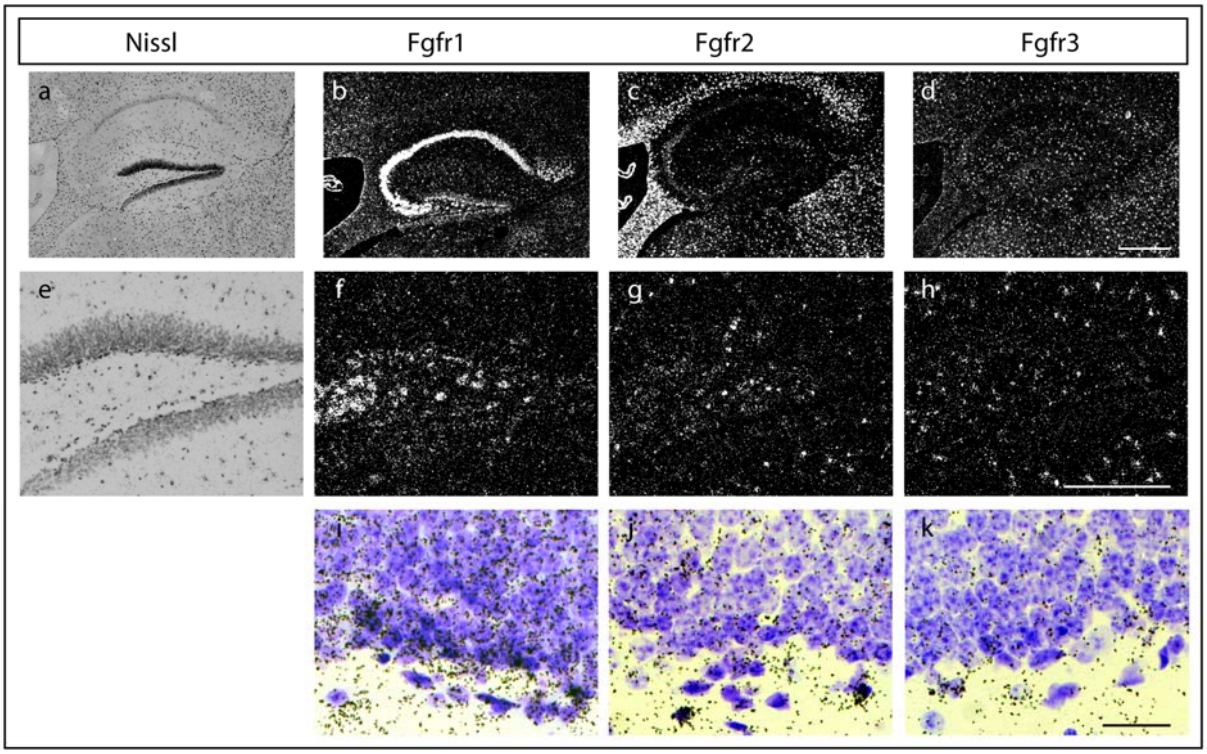

Figure 37. Expression of *Fgfrs* in the hippocampus of adult wt mice.

ISH was performed on saggital sections and revealed strong *Fgfr1* (b), weak *Fgfr2* (c), and no *Fgfr3* (d) expression in the hippocampal cornum ammonis (CA) region. Many *Fgfr1* positive cells are present within the Hillus (f) and the subgranular zone of the dentate gyrus (i). Only a few *Fgfr2* expressing cells (g, j), and even less *Fgfr3* positive cells (h, k), are found within the Hillus and the subgranular zone of the DG. Scale bars: 500µm in d; 250µm in h; 25µm in k.

For a complete picture about the involvement of the three *Fgfrs* in adult neurogenesis, I analysed also the subventricular zone (SVZ) and the rostral migratory stream (RMS) (Fig. 38 and Fig. 39.). The SVZ is the second region of the adult mouse brain where new neurons are generated (Doetsch et al., 1997). These neurons migrate along the RMS and end up in the olfactory bulbs (Hack et al., 2005).

Surprisingly, in this neurogenic region *Fgfr1* expression seems to be very weak or absent (Fig. 38, b, f). Instead *Fgfr2* expression is found in the SVZ (Fig. 38, c, g) and even more intense in the RMS (Fig. 39, c, g). *Fgfr3* is expressed weakly in the SVZ (Fig. 38, d, h) but not in the RMS (Fig. 39, d, h). Taken together, this expression data suggest a dominant role of *Fgfr1* in the hippocampal and of *Fgfr2* in the subventricular adult neurogenesis.

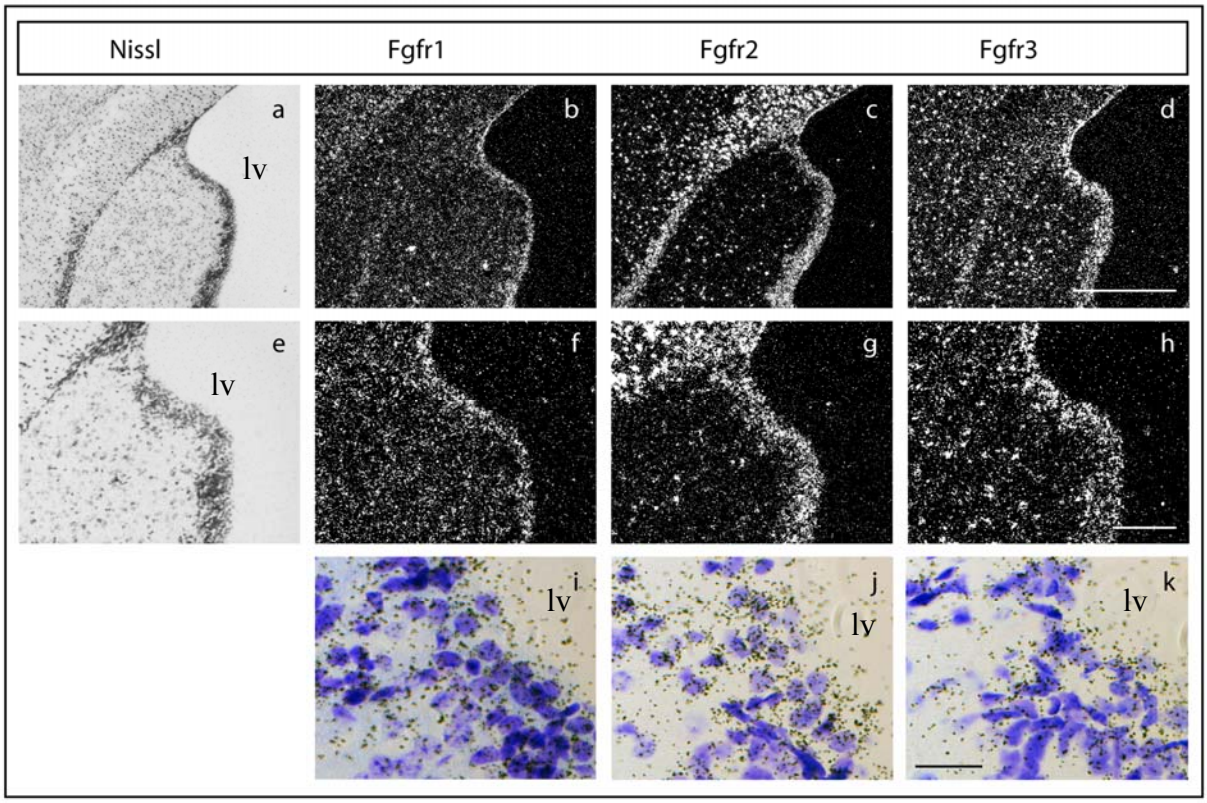

Figure 38. Expression of *Fgfrs* in the subventricular zone (SVZ) of adult wt mice.

ISH was performed on saggital sections and revealed no *Fgfr1* (b, f, i), moderate *Fgfr2* (c, g, j), and weak *Fgfr3* (d, h, k) expression in the SVZ region. Lv: lateral ventricle. Scale bars: 500µm in d; 250µm in h; 25µm in k.

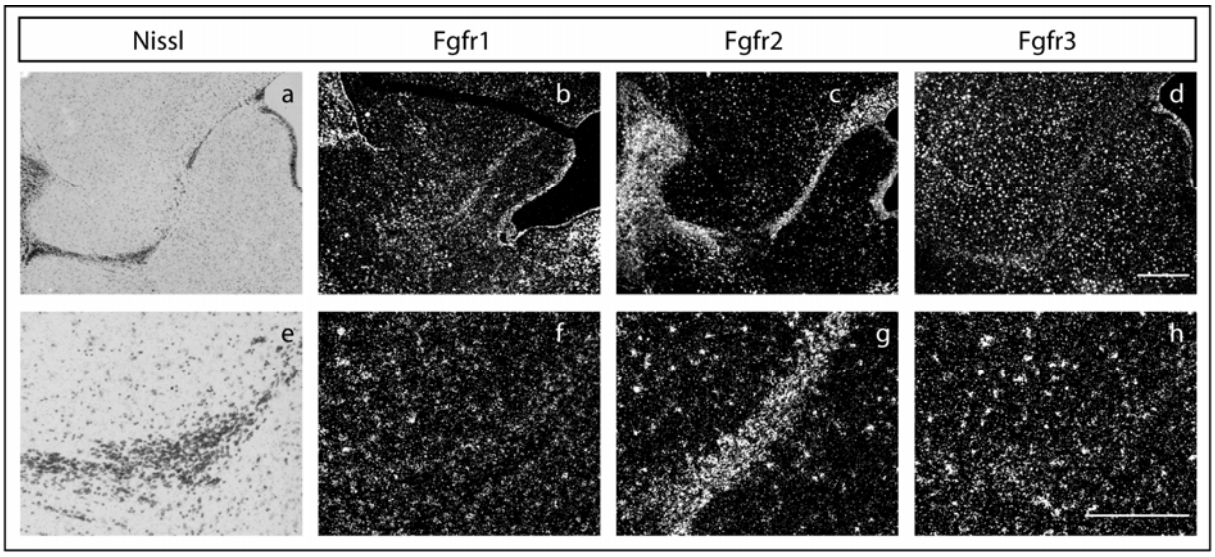

Figure 39. Expression of *Fgfrs* in the rostral migratory stream (RMS) of adult wt mice.
ISH was performed on saggital sections and revealed weak *Fgfr1* (b, f), strong *Fgfr2* (c, g), and weak *Fgfr3* (d, h) expression in the RMS. Scale bars: 500µm in d; 250µm in h.

The amygdala is one of the most important brain areas for the control of emotions and is probably also involved in depressive disorders (Phelps and LeDoux, 2005; Strakowski et al., 2005). I concentrated on the central and lateral parts of amygdala since these are the regions which are mostly considered as responsible for processing emotional input (lateral amygdala) and output (central amygdala). All three *Fgfrs* are expressed in the central amygdala (Fig. 40, d, e, and f). However, *Fgfr2* and *Fgfr3* were strongly expressed in the lateral amygdaloid nuclei (Fig. 40, e, f, k, l) whereas almost no *Fgfr1* ISH signal has been detected in the lateral amygdala (Fig. 40, d, j).

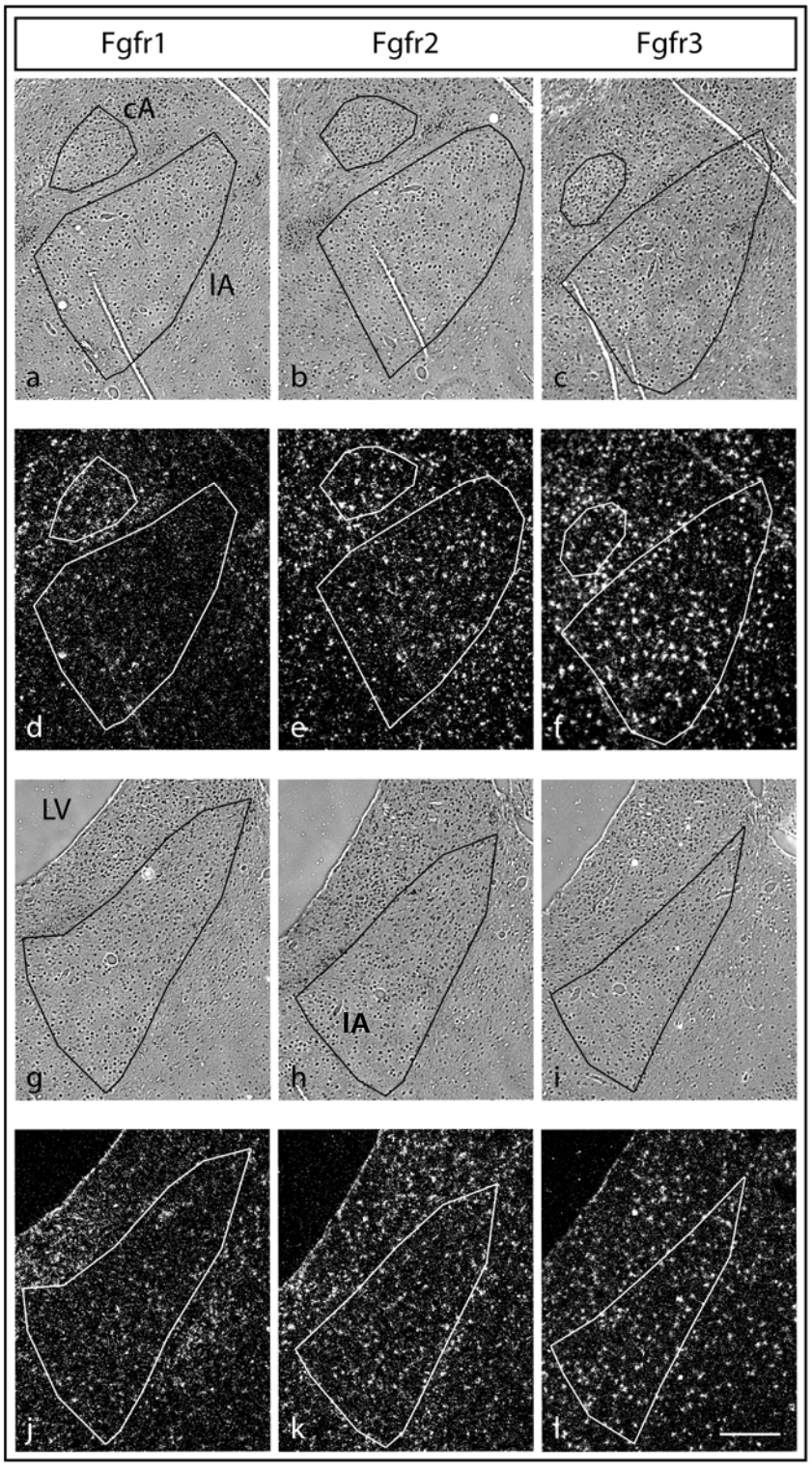

Figure 40. Expression of *Fgfrs* in the central (cA) and lateral amygdala (lA) of adult wt mice.

ISH was performed on coronal sections from anterior (a, b, c, d, e, f) and posterior (g, h, I, j, k, l) regions. *Fgfr1* (d), *Fgfr2* (e) and *Fgfr3* (f) are all expressed in the cA. *Fgfr1* is absent in the anterior part of the lA (d) and weakly expressed in the posterior part of the lA (j). *Fgfr2* (e, k) and *Fgfr3* (f, l) are both moderately expressed in the lA. Areas of central amygdala (cA) and lateral amygdala (lA) are indicated. LV: lateral ventricle; Scale bars: 250µm

The last analysed brain region is the striatum. The striatum is involved in the control of emotions like motivation and there are hints for an involvement in drug addiction and depressive diseases (Fasano and Brambilla, 2002; Nestler and Carlezon, 2006; Schultz, 2006). As shown in Figure 41 all three *Fgfrs* are expressed in this brain region. *Fgfr1* is expressed strongly in only a few cells (Fig. 41, b, d) whereas *Fgfr2* is expressed in many cells throughout the striatum (Fig. 41, f, h). The expression of FGFR2 seems to be stronger in the dorso-medial part of the striatum. *Fgfr3* is expressed like FGFR2 in many cells of the striatum but the distribution of the *Fgfr3* positive cells is complementary (Fig. 41, j, l). Most of *Fgfr3* positive cells are in the ventral and lateral part of the striatum (Fig. 41, l).

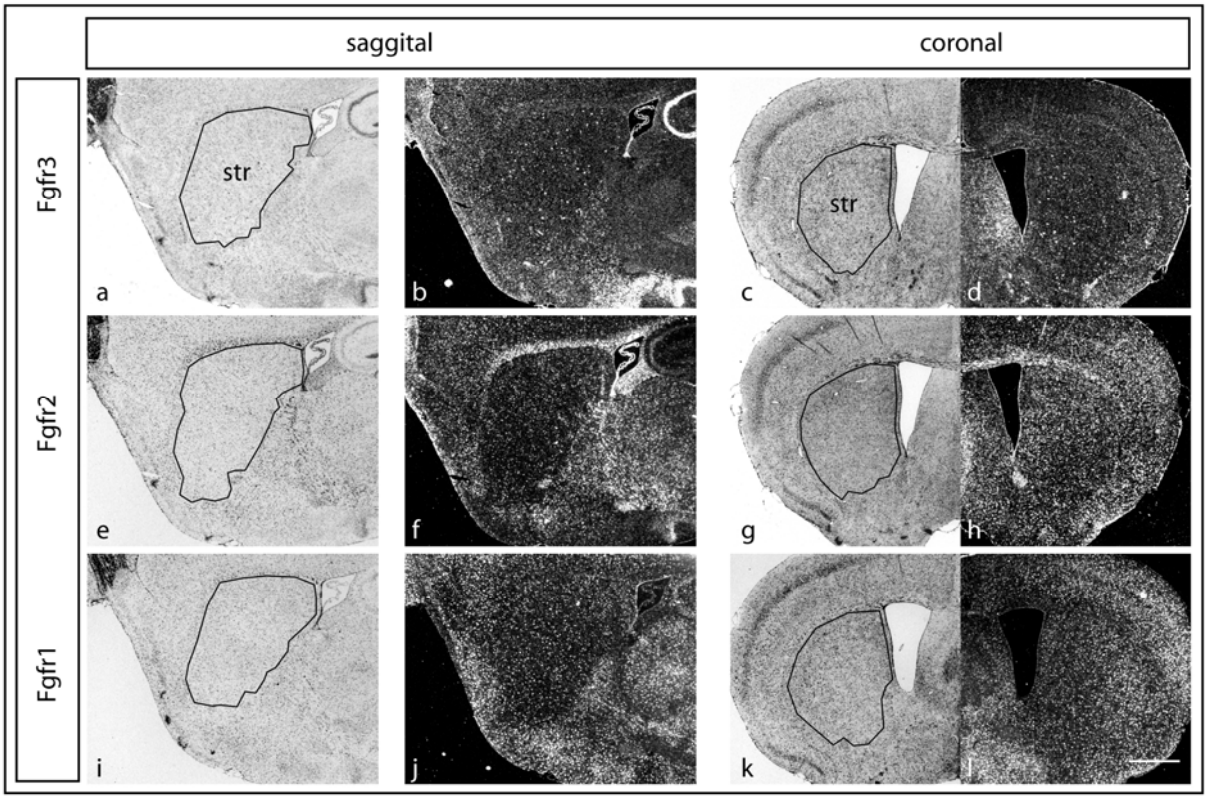

Figure 41. Expression of *Fgfrs* in the striatum of adult wt mice.

ISH was performed on saggital (a, b, e, f, I, j) and coronal (c, d, g, h, k, l) sections. *Fgfr1* is strongly expressed in a few big cells distributed throughout the striatum (b, d). Many *Fgfr2* positive cells are found among the entire striatum (f, h). The same holds true for *Fgfr3* (j, l). However, *Fgfr2* expression is strongest in the dorsal part, wheras *Fgfr3* is highly expressed in the lateral part of the striatum. Scale bar: 1mm.

4.2.2 The *Fgfr2$^{lox/lox}$; CamKII-Cre* mouse mutant

I generated a mouse model with specific deletion of FGFR2 in forebrain neurons, to test the hypothesis that a loss of FGFR2 function in specific brain areas leads to increased depression-like behaviour in mice. To disrupt *Fgfr2* in the adult mouse brain the conditional knockout (cko) strategy was applied, using a mouse line expressing the Cre recombinase (Cre) under the control of the *calcium/calmodulin-dependent protein kinase II α subunit (CamKIIα)* promoter and the already described *Fgfr2 $^{lox/lox}$* mice (Fig. 6) (Blak et al., 2007; Minichiello et al., 1999). The resulting mice harboured a disrupted *Fgfr2* gene in all mature forebrain neurons. The used *CamKII-Cre* mice were backcrossed at least in the fifth generation on a C57/Bl6 background. The *CamKII* promoter activity should start at P20 in mature forebrain neurons. In the resulting offspring, the pups containing homozygous *Fgfr2* floxed alleles and one *CamKII-Cre* allele should have postnatal FGFR2 deficient forebrain neurons. These mice are named here in this study "forebrain mutants". These forebrain mutants were viable and fertile and did not display any obvious alterations in their behaviour.

In the histological analysis of the forebrain mutants, I did not find any morphological alterations (Fig. 42). As expected, deletion of *Fgfr2* exon5 in postnatal mature forebrain neurons did not affect the general structure or the organization of the adult mouse brain. Using the *Fgfr2* exon5 specific probe, I saw just a faint reduction of the signal intensity in the forebrain (Fig. 42, d). This could be due to the fact, that *Fgfr2* is also expressed in glia cells, which do not express Cre and therefore still express the *Fgfr2* mRNA including the exon5.

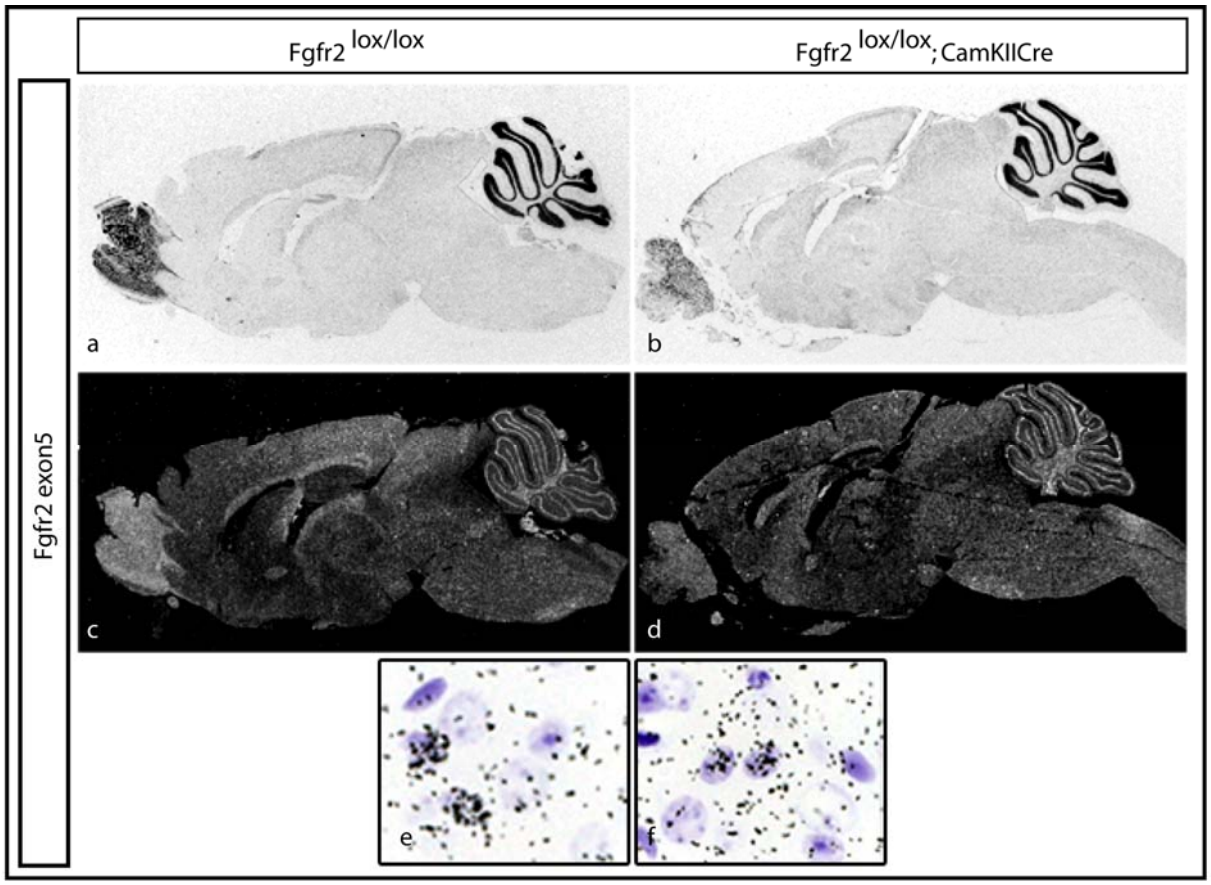

Figure 42. Brain anatomy and Cre mediated deletion of *Fgfr2* exon5 in adult *Fgfr2* $^{lox/lox}$*; CamKII-Cre* mice.

ISH, using an *Fgfr2* exon5 specific probe, was performed on saggital sections of adult brains from control (*Fgfr2* $^{lox/lox}$; a, c, e) and mutant animals (*Fgfr2* $^{lox/lox}$*; CamKII-Cre*; b, d, f). Nissl staining revealed no obvious differences between control (a) and mutant brain (b). *Fgfr2* exon5 expression level seems to be slightly reduced in the cortex of mutant brain (d) as compared to the control brain (c). Higher magnification of cortical areas revealed specific ISH signals in both, control (e) and mutant (f).

Since it was not yet clear, to which extend the *Fgfr2* expression was diminished in forebrain mutants I performed a Western blot to analyse *Fgfr2* expression at the protein level. Surprisingly, I found a significant reduction in FGFR2 protein levels in all analysed brain regions and not only in the regions belonging to the forebrain (Fig. 43). The reduction of FGFR2 protein levels differed among the regions but still indicates the expression of Cre recombinase in all analysed brain regions. Nevertheless, there is also a strong reduction of FGFR2 in the forebrain.

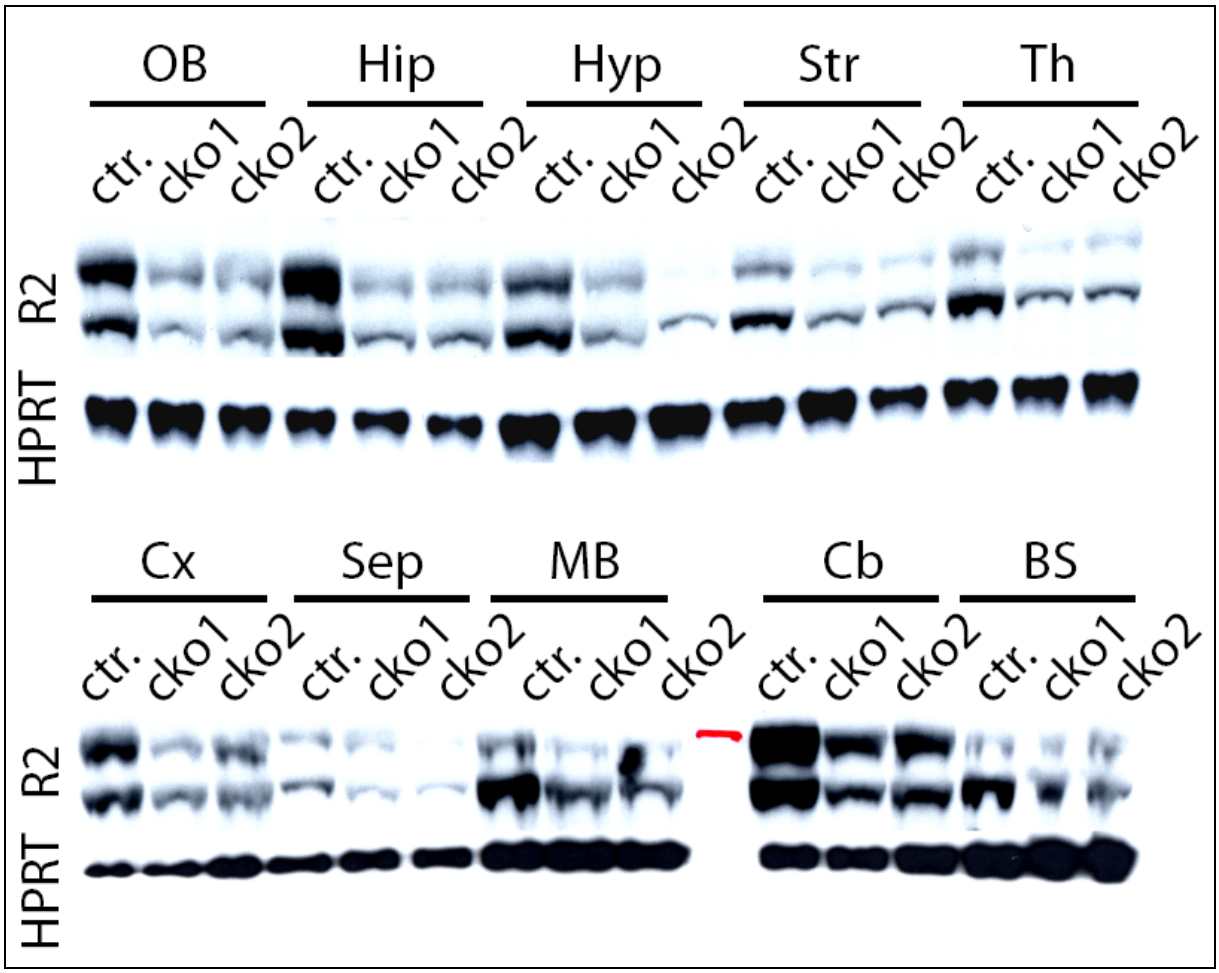

Figure 43. FGFR2 protein levels are reduced in all brain regions of adult *Fgfr2* $^{lox/lox}$*; CamKII-Cre* mice.

Western blot analysis of protein extracts from different brain regions of control animal (ctr.; *Fgfr2* $^{lox/lox}$) and two forebrain mutants (cko1 and cko2; *Fgfr2* $^{lox/lox}$*; CamKII-Cre*). Two FGFR2 bands are present since the used FGFR2 antibody recocnises both FGFR2 isoforms. FGFR2 (R2) protein levels were reduced in all brain regions in both forebrain mutants. HPRT was used as loading control. OB: olfactory bulbs; Hip: hippocampus; Hyp: hypothalamus; Str: striatum; Th: thalamus; Cx: cortex; Sep: septum; MB: midbrain; Cb: cerebellum: BS: brain stem.

The reduction of the FGFR2 protein level in the cerebellum lead to the idea, that also in these forebrain mutants the cerebellar structure is altered, as already described for the *Fgfr2* $^{lox/lox}$*; Nestin-Cre* mice (part 3.1). Since the forebrain mutants were generated to analyse the role of FGFR2 in depression-like behaviour of mice, a generally altered behaviour due to cerebellar malformations would make the interpretation of behaviour tests more complicated. Therefore I determined the organization of the cerebellum in forebrain mutants using IHC. I did not see any differences between the cerebella of forebrain mutants and WT mice (Fig. 44). The reduced amount of FGFR2 protein in the cerebellum in forebrain mutants seen in the Western blot analysis (Fig. 43; Cb) had no effect on the Bergmann glia fibres.

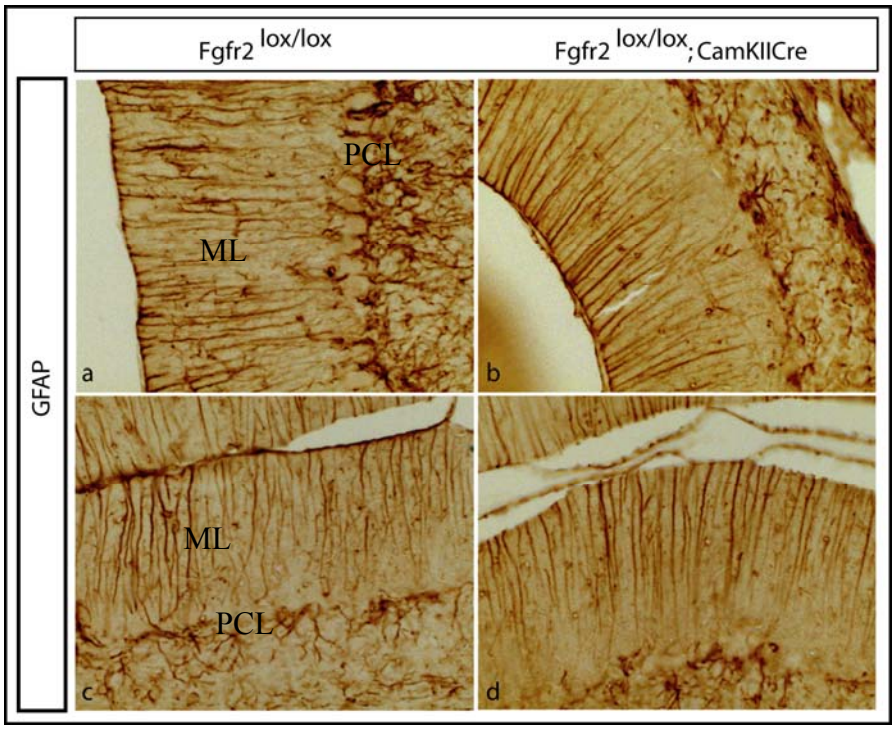

Figure 44. Cerebellum of adult *Fgfr2 lox/lox; CamKII-Cre* mice is histologically normal.

Saggital brain sections from two control (a, c) and two forebrain mutant mice (b, d) were used for GFAP IHC. No differences between wt and mutant mice were observed. ML: molecular layer; PCL: Purkinje cell layer.

4.2.3 Behaviour of *Fgfr2lox/lox; CamKII-Cre* mice

The main reason to generate the forebrain mutants was to analyse their behaviour in respect to altered depression-like behaviour. To get a complete overview about the behavioural changes, caused by the lack of FGFR2 in certain cell populations of the adult brain, these mice were analysed in eight different behaviour tests.

4.2.3.1 Modified Hole Board (mHB)

The mHB is used to get a broad overview of mouse behaviour. More than 30 different parameters regarding locomotion, anxiety, exploration and others are calculated and analysed. Only in one parameter significant differences between the forebrain mutants and the WT mice

could be detected, indicating a very faint behavioural effect of FGFR2 loss. Forebrain mutants showed less rearing behaviour on board than WT mice (Fig. 45, A). A decreased rearing behaviour on board was also observed in *Fgfr2* $^{lox/lox}$*; Nestin-Cre* mutants, that were also tested in the mHB (Fig. 29). Therefore, the observed alteration in rearing behaviour in *Fgfr2* $^{lox/lox}$*; Nestin-Cre* mutants could also be caused by the lack of FGFR2 in other brain regions than by the described cerebellar malformations in *Fgfr2* $^{lox/lox}$*; Nestin-Cre* mutants.

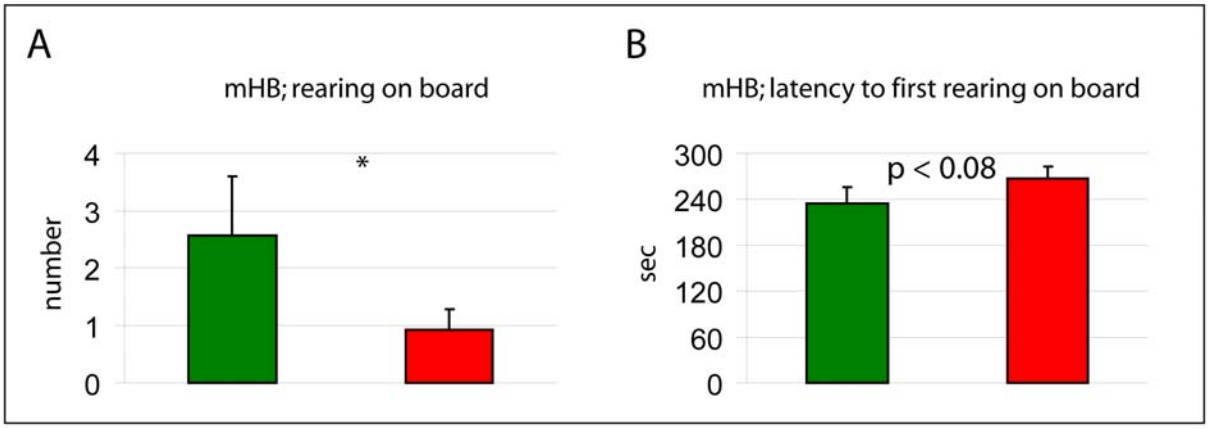

Figure 45. Impact of forebrain specific FGFR2 inactivation on unconditioned behaviour in mice in the modified Hole Board paradigm (mHB) at the age of 10 weeks.
The only significant alteration is found in the number of rearings on board (A). In addition there was a tendency ($p < 0.08$) that forebrain mutants need more time before first rearing on board (B). Data are expressed as means + S.E.M. There were no significant interaction between sex and genotype. Significant differences between mutant and control mice are indicated with asterisk: * $p < 0.05$. green bars: control animals; red bars: mutants.

4.2.3.2 **Rotarod**

The average time that the mice spent on the rotating rod was not altered in forebrain mutants compared to WT mice (Fig. 46, A). The forebrain mutants seem to be capable of coordinating their movements in a proper way. Nevertheless, the number of passive rotations, where the mice stopped running and were turned around on the rod, was significantly increased in forebrain mutants compared to WT mice (Fig. 46, B). Running on the rotating rod is a stressful situation for the tested mice. Therefore the enhanced number of passive rotation observed in forebrain mutants could display a kind of altered passive coping behaviour under stress.

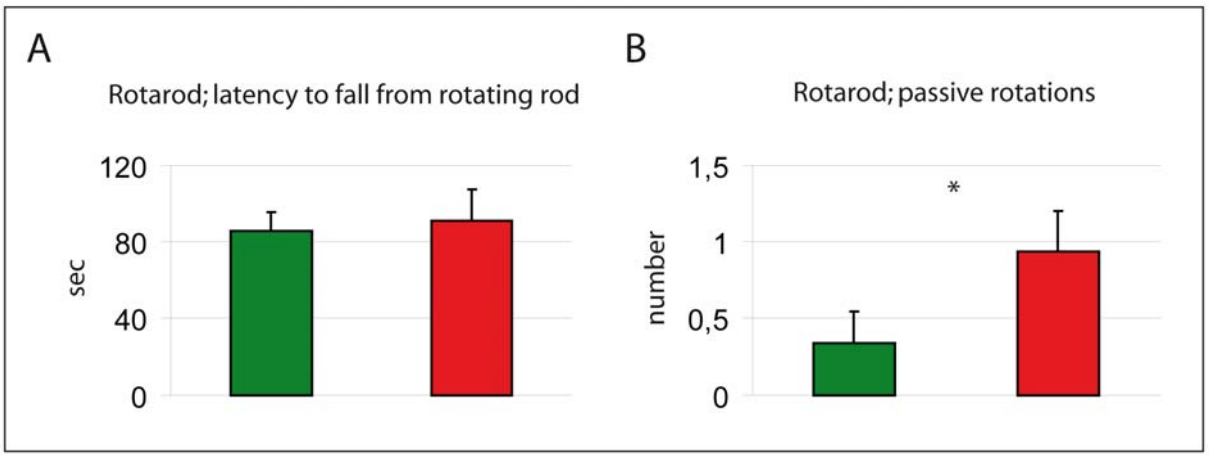

Figure 46. Behaviour of *Fgfr2* $^{lox/lox}$*; CamKII-Cre* mice on the rotating rod (Rotarod).
There was no significant difference between mutants (red bar) and control animals (green bar) in latency to fall from the rotating rod (A). However, the number of passive rotations was increased in forebrain mutants (B). There was no significant interaction between sex and genotype. Data are expressed as means + S.E.M. Significant differences between mutant and control mice are indicated with asterisk: * $p < 0.05$; n.s.: not significant. green bars: control animals; red bars: mutants.

4.2.3.3 **Light/dark box (LD) and Elevated plus maze (EPM)**

Another indication for an altered coping behaviour comes from the light-dark box (LD) test. This test is mainly used to determine the anxiety-related behaviour in mice (Belzung and Griebel, 2001; Bourin and Hascoet, 2003). The main parameters regarding anxiety, time spent in the lit compartment and the dark compartment, respectively, did not differ between forebrain mutants and WT mice (Fig. 47, A, B). However, forebrain mutants moved faster in the lit compartment and showed also altered values for the mean turn angles and meander in the aversive light compartment (Fig. 47, C, E, and F). The observed differences could be explained by the stressful situation when the mice are moving under bright light conditions through the lit compartment. In this case the increased velocity of forebrain mutants could rather be interpreted as active coping behaviour.

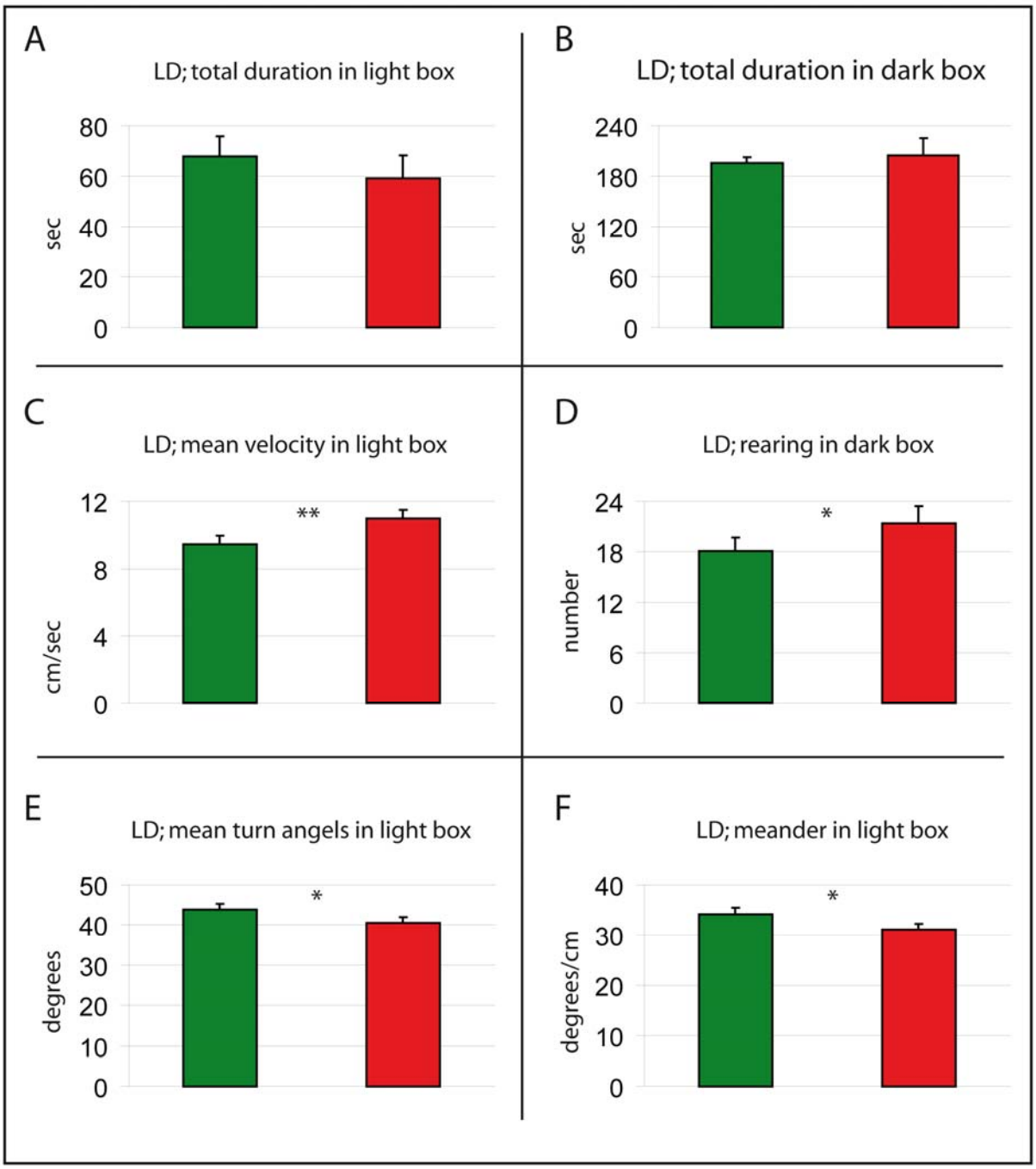

Figure 47. Behaviour of *Fgfr2* $^{lox/lox}$*; CamKII-Cre* mice in the light/dark box (LD).
There was no significant difference between mutants and control animals in the time the mice spent in lit or dark compartment (A, B). However, forebrain mutants showed significantly increased mean velocity in the lit compartment (C) and the number of rearings in dark compartment (D). Additionally mean turn angles (E) and meander (F) in lit compartment were significantly lower in forebrain mutants. There was no significant interaction between sex and genotype. Data are expressed as means + S.E.M. Significant differences between mutant and control mice are indicated with asterisk: ** $p < 0.01$; * $p < 0.05$; n.s.: not significant. green bars: control animals; red bars: mutants.

The second task for analysing anxiety-related behaviour is the elevated plus-maze (EPM) (Belzung and Griebel, 2001). Also here the forebrain mutants showed in some parameters significant differences (Fig. 48). Like in the LD the main parameters for anxiety-related behaviour were not altered in forebrain mutants (Fig. 48, A, B, C). Nevertheless, the forebrain mutants moved faster within the closed arms (Fig. 48, E, and F). Again this difference between forebrain mutants and WT mice could be explained by an active coping behaviour. The forebrain mutants run faster within the closed arms to escape from the frightening situation on the elevated maze.

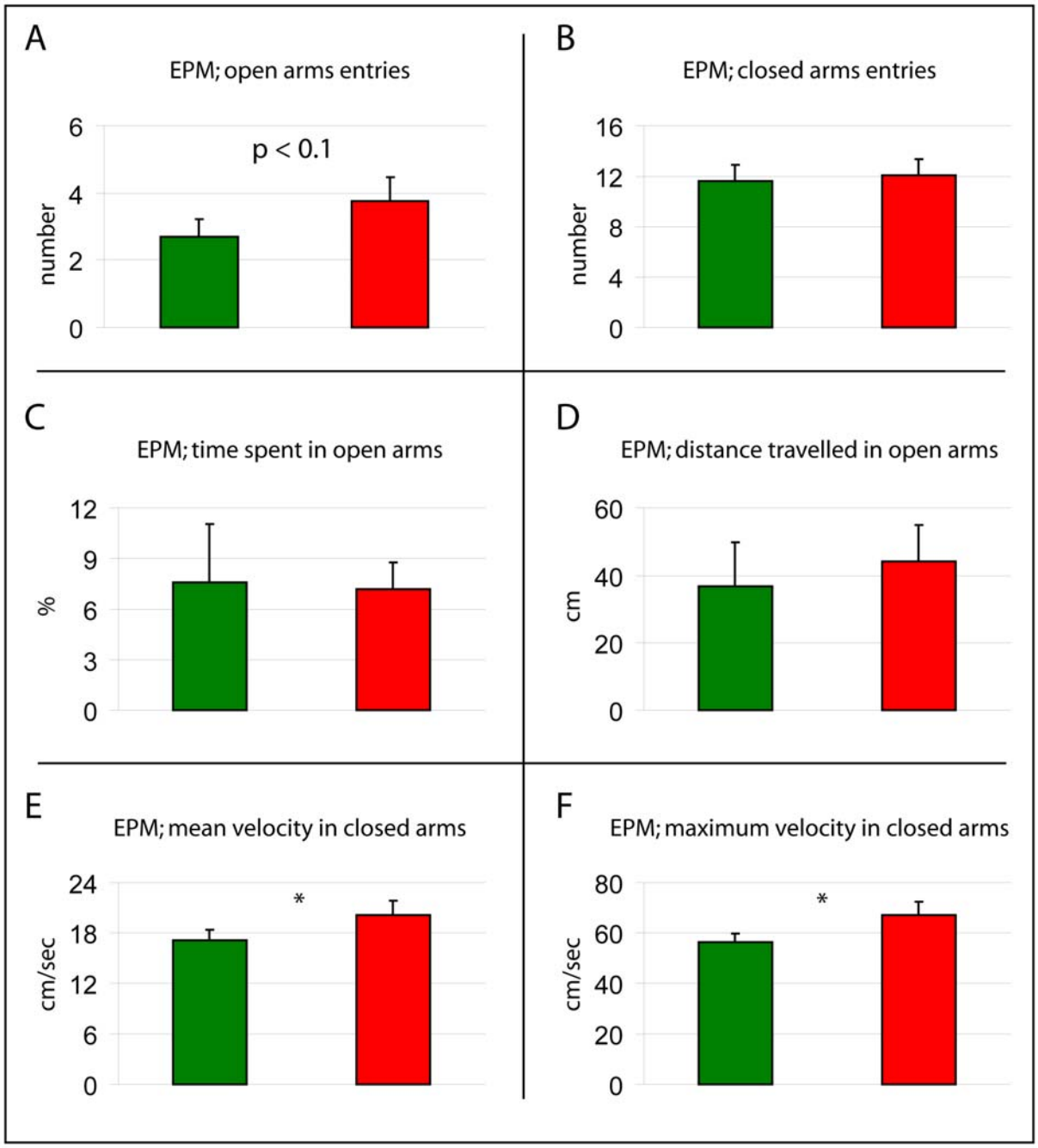

Figure 48. Behaviour of *Fgfr2* $^{lox/lox}$*; CamKII-Cre* mice in the elevated plus maze (EPM). There was a tendency of forebrain mutants to more open arm entries (A) and no significant difference between mutants and control animals in the number of closed arm entries (B). There was also no significant difference in time spent in open arms (C) or in the distance travelled in open arms (D). Forebrain mutants displayed significantly higher mean and maximum velocity in closed arms than control mice (E, F). There was no significant interaction between sex and genotype. Data are expressed as means + S.E.M. Significant differences between mutant and control mice are indicated with asterisks: * $p < 0.05$; n.s.: not significant. green bars: control animals; red bars: mutants.

4.2.3.4 Social interaction (SI) and Social discrimination (SD)

To determine their social behaviour mice were tested for social interaction (SI) and in social discrimination (SD). The results from the LD and EPM tasks suggested an altered coping behaviour in forebrain mutants compared to WT mice. Due to this observed alterations one could expect a decrease in the time forebrain mutants interact with unfamiliar animals. Indeed female forebrain mutants spent significantly more time without any interaction ($p < 0.05$ one-tailed t-test) and spent significantly less time with active ($p < 0.05$ one-tailed t-test) or passive ($p < 0.05$ one-tailed t-test) interaction (Fig. 48). However, no statistically significant alterations between male forebrain mutants and male WT mice were observed. The male forebrain mutants showed even a statistically not significant tendency to interact more with the unfamiliar animal than the male WT mice.

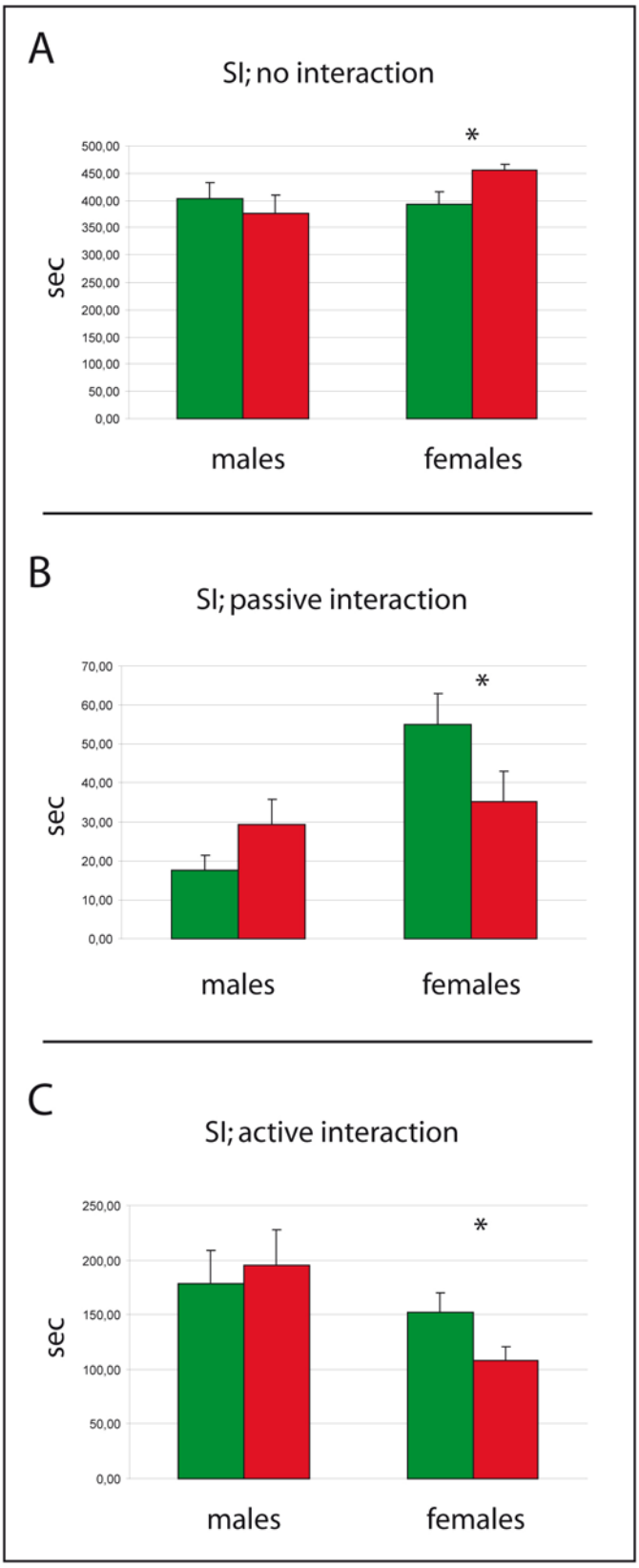

Figure 48. Social interaction (SI) of *Fgfr2* $^{lox/lox}$*; CamKII-Cre* mice.
There were no significant differences between the pooled groups of control animals and forebrain mutants (A, B, C). However, seperate analysis of the females revealed significant alteration in all three parameters between wt females and forebrain mutant females (A, B, C). There was no significant interaction between sex and genotype. Data are expressed as means + S.E.M. Significant differences between mutant and control mice are indicated with asterisks: * $p < 0.05$; n.s.: not significant. green bars: control animals; red bars: mutants.

According to the SI task and the tasks for anxiety-related behaviour, LD and EPM, we expected either no alteration between the forebrain mutants and the WT mice in the SD task or a decreased preference of the forebrain mutants for interacting with the unfamiliar animal.

Indeed I did not found any differences between forebrain mutants and WT mice in this task. All four groups, male forebrain mutants and WT mice and female forebrain mutants and WT mice, showed the expected preference to interact with the unfamiliar animal (Fig. 50). This shows that all analysed groups can distinguish between familiar and unfamiliar mice.

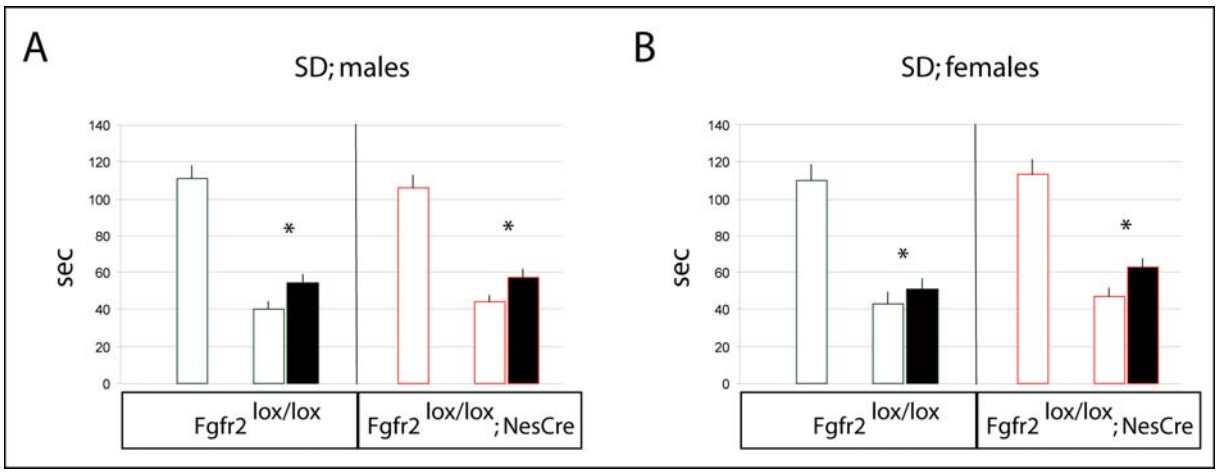

Figure 50. Behaviour of *Fgfr2* $^{lox/lox}$*; CamKII-Cre* mice in the social discrimination (SD) task. All analysed groups (male controls, male mutants, female controls, and female mutants) showed a significant preference for the unfamiliar subject (A, B). There was no significant interaction between sex and genotype. Data are expressed as means + S.E.M. Significant differences between mutant and control mice are indicated with asterisks: * $p < 0.05$. Open green bars: interaction of wt animals with familiar subject; open red bars: interaction of forebrain mutants with familiar subject; black bars: interaction with unfamiliar subject.

4.2.3.5 **Tail suspension test (TST) and Forced swim test (FST)**

The two principal behavioural paradigms to assess depression-like behaviour in mice are the tail suspension test (TST) and forced swim test (FST) (Gottesman and Gould, 2003). In the TST the time the mouse spent immobile can be used as a parameter to appreciate depression-like behaviour. In general this duration of immobility was not significantly altered in the forebrain mutants compared to WT mice (Fig. 51).

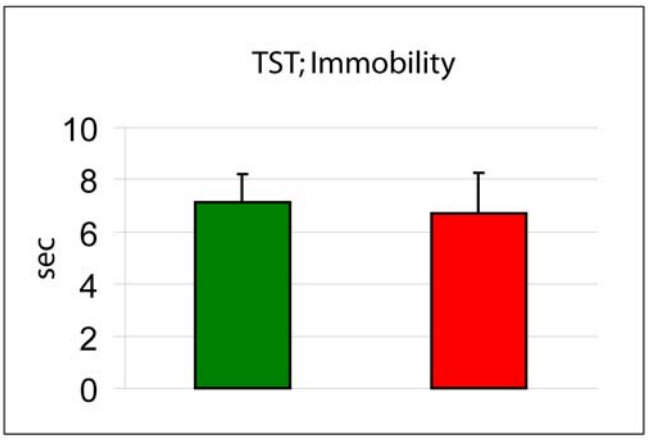

Figure 51. Behaviour of *Fgfr2* $^{lox/lox}$*; CamKII-Cre* mice in the tail suspension test (TST).
There was no significant difference between mutants and control mice and no significant interaction between sex and genotype. Data are expressed as means + S.E.M. n.s.: not significant. green bars: control animals; red bars: mutants.

The second task used to analyse the behaviour related to depression, the FST, revealed significant alterations between forebrain mutants and WT mice. The time spent with struggling (or climbing) was significantly decreased ($p < 0.05$) in forebrain mutants over the whole test period (Fig. 52, A, climbing, overall). Also a tendency ($p < 0.1$) to increased swimming behaviour was seen in forebrain mutants whereas the time spent with floating was not altered over the whole test period (Fig. 52, A, floating and swimming, overall).

A more detailed analysis was done by dividing the FST into two parts. We analysed the first three minutes and the last three minutes separately because the struggling behaviour is mostly present in the first half of the test while the floating behaviour was more in the second half. This detailed analysis revealed a significant difference between forebrain mutants and controls in struggling in the first half ($p < 0.05$) (Fig. 52, A, climbing, 1st – 3rd min) and additionally a tendency that forebrain mutants spent less time with floating ($p = 0.06$) and significantly more time with swimming ($p < 0.05$) (Fig. 52, A, floating and swimming, 1st – 3rd min). To determine if this subtle alteration in struggling is related to depressive behaviour we analysed the acute response to the commonly used antidepressant drug fluoxetine in forebrain mutants and control animals in the FST (Fig. 52, B). New groups of forebrain mutants and wt mice were tested 30 minutes after fluoxetine administration (20 mg/kg body weight; intraperitoneal (ip) injections). There was no difference in struggling behaviour

between control and forebrain mutant mice after sodium chloride (NaCl) injection (Fig. 52, B, climbing, overall). However, in control animals administration of fluoxetine increased the time spent with struggling whereas in forebrain mutants the time spent with struggling was reduced. This fluoxetine dependent change in struggling lead to significant differences between forebrain mutants and control animals in time spent with struggling over the whole test period ($p < 0.05$) (Fig. 52, B, climbing, overall). Analysis of the first half of the test period revealed a significant interaction of genotype and treatment in time spent with struggling (genotype x treatment $F(1, 38) = 5.6$; $p < 0.05$) and post hoc analysis showed a significant reduction of the time spent with struggling in forebrain mutants after fluoxetine injection as compared to NaCl injection ($p < 0.05$) (Fig. 52, B, climbing, $1^{st} – 3^{rd}$ min). In the second test half there was no interaction between genotype and treatment in struggling behaviour although the time spent with struggling was reduced in forebrain mutants after fluoxetine injection as compared to NaCl injection ($p < 0.05$) (Fig. 52, B, climbing, $4^{th} – 6^{th}$ min). There was no interaction between genotype and treatment in time spent with floating or with swimming, respectively, neither in the whole FST nor in one of the separately analysed periods. However, both values, floating and swimming, were altered in the second half in forebrain mutants treated with fluoxetine as compared with forebrain mutants treated with NaCl (second half floating, $p < 0.05$; second half swimming, $p < 0.05$) (Fig. 52, B, floating and swimming, $4^{th} – 6^{th}$ min).

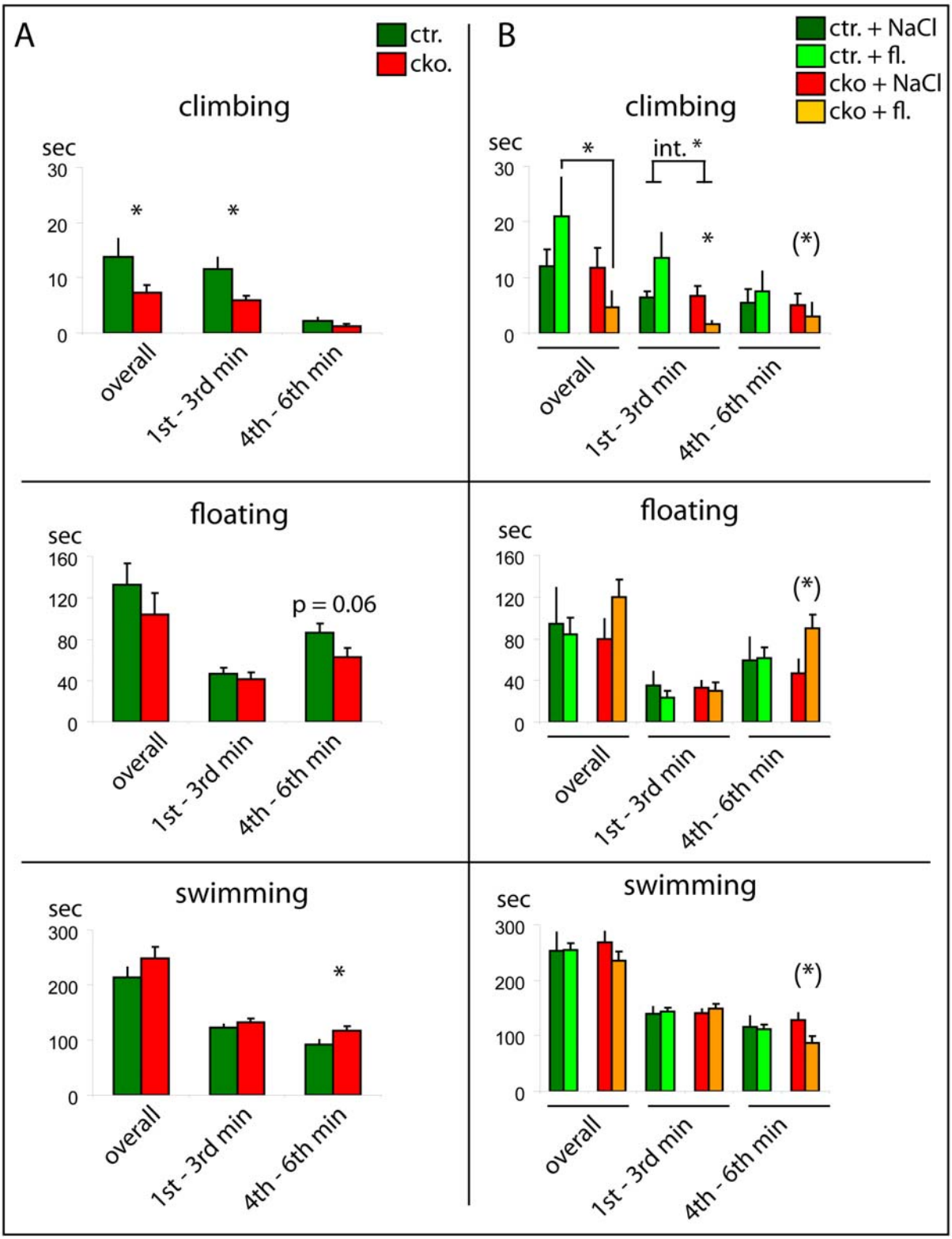
A
ctr.
cko.
climbing
sec
30
20
10
0
*
*
overall
1st - 3rd min
4th - 6th min
B
ctr. + NaCl
ctr. + fl.
cko + NaCl
cko + fl.
climbing
sec
*
int. *
*
(*)
floating
sec
160
120
80
40
0
p = 0.06
floating
sec
(*)
swimming
sec
300
200
100
0
*
swimming
sec
(*)

Figure 52. Behaviour of *Fgfr2* $^{lox/lox}$*; CamKII-Cre* mice in the forced swim test (FST).
Naïve mice were tested directly (A) or 30 minutes after ip injection of NaCL or fluoxetine (B) in the FST. A: Without previous treatment forebrain mutants spent significantly less time with climbing (also called struggling) in the first test period (1^{st} – 3^{rd} min) and during the whole test (overall). Furthermore, in the second test period (4^{th} – 6^{th} min) forebrain mutants showed a tendency to spend less time with floating and more time with swimming. There was no significant interaction between sex and genotype. Therefore the pooled results from both sexes are shown. B: Fluoxetine treatment had opposite effects on wt and mutant animals resulting in significantly different climbing durations over the whole test period (overall) and even significant interaction between treatment and genotype for the first test period (1^{st} – 3^{rd} min). Furthermore, fluoxetine treatment reduced significantly the time forebrain mutants spent with climbing in the first and second test period as compared to NaCl treated forebrain mutants. In addition fluoxetine treated forebrain mutants spent more time with floating and less time with swimming during the second test period as NaCl treated forebrain mutants. Data are expressed as means + S.E.M. Significant differences between mutant and control mice are indicated with asterisks: * $p < 0.05$. Significant differences between mutant and control mice without significant interaction between control and mutant groups are indicated with (*).Ctr: control; cko: conditional knockout mice (forebrain mutants; *Fgfr2* $^{lox/lox}$*; CamKII-Cre*) fl: fluoxetine; NaCl: Sodium chloride; int: interaction.

4.2.4 Evaluation and application of the RNA knockdown strategy

Beside FGFR2 we wanted also to analyse the role a P2RX7 in depression (Lucae et al., 2006). In order to generate a mouse model for studying P2RX7 functions in depressive disorders we decided to apply the RNAi technology. Using RNAi technology to generate mutant mice is a fast alternative to the conventional knockout strategy. Since RNAi occurs at the post-transcriptional level there is no need to manipulate the genomic locus of the targeted gene. A construct containing a polymerase III promoter driven small hairpin RNA (shRNA) can be integrated at any transcriptionally active genomic locus. To achieve fast production of shRNA mutants I used a Phi C31 Integrase based system (Hitz, 2007). To this end I inserted into the *Rosa26* locus a construct containing a pgk promoter driven and attP flanked hygromycin resistance gene (Fig. 56). In a second step I exchanged the hygromycin resistance gene against a neomycin resistance gene followed by the shRNAs against various genes driven by a polymerase III promoter (U6 promoter) (Fig. 56). To evaluate the functional capability of the system I first used shRNAs against *Wnt1*.

4.2.4.1 Generation of Wnt1 knockdown mice

Since the generation of RNAi mutants using a shRNA vector in a defined genomic locus was rather new I first planed to validate that the system is functional. As target gene for this validation I chose *Wnt1*. The *Wnt1* knockout phenotype is known and efficient knockdown of *Wnt1* should lead to the same or at least to a similar phenotype (McMahon and Bradley, 1990; Thomas and Capecchi, 1990).

4.2.4.2 In vitro test of shRNA constructs against *Wnt1*

I selected three different target sequences against *Wnt1* based on the prediction of public shRNA design programs and cloned them into the human U6 promoter containing pShag plasmid (Paddison et al., 2004) (Fig. 54, A). To test the selected shRNA sequences against *Wnt1* I cloned the *Wnt1* cDNA in frame with the ORF of the *lacZ* gene. This should lead to a fusion *lacZ-Wnt1* mRNA and also to a fusion Protein containing a functional ß-Galactosidase. Targeting the Wnt1 fraction of the fusion mRNA using a specific shRNA reduces the amount of this fusion mRNA and consequently leads to a decreased ß-Galactosidase activity (Fig. 53).

The ß-Galactosidase activity was used in an assay to quantify the knockdown efficiency of the used shRNA.

The plasmid containing the *lacZ-Wnt1* fusion mRNA and a second plasmid containing the U6 promoter driven specific shRNA against *Wnt1* were co-transfected. The ß-Galactosidase assay revealed a dramatically reduced ß-Galactosidase activity and therefore a strong knockdown for all three tested shWnt1 constructs (Fig. 53).

Construct No.1 (pBS-U6-shWnt1/1) (Fig. 54, A) was then subcloned into an attB sites containing plasmid, which afterwards can be used for the Phi31 Integrase mediated exchange in ES cells (Fig. 54, B). This allows the subsequent insertion of a single shRNA into a certain genomic locus (Fig. 56). The sequences of all generated RNAi plasmids were verified by sequencing from both sides to exclude mutations and ensure correct integration of cloned fragments.

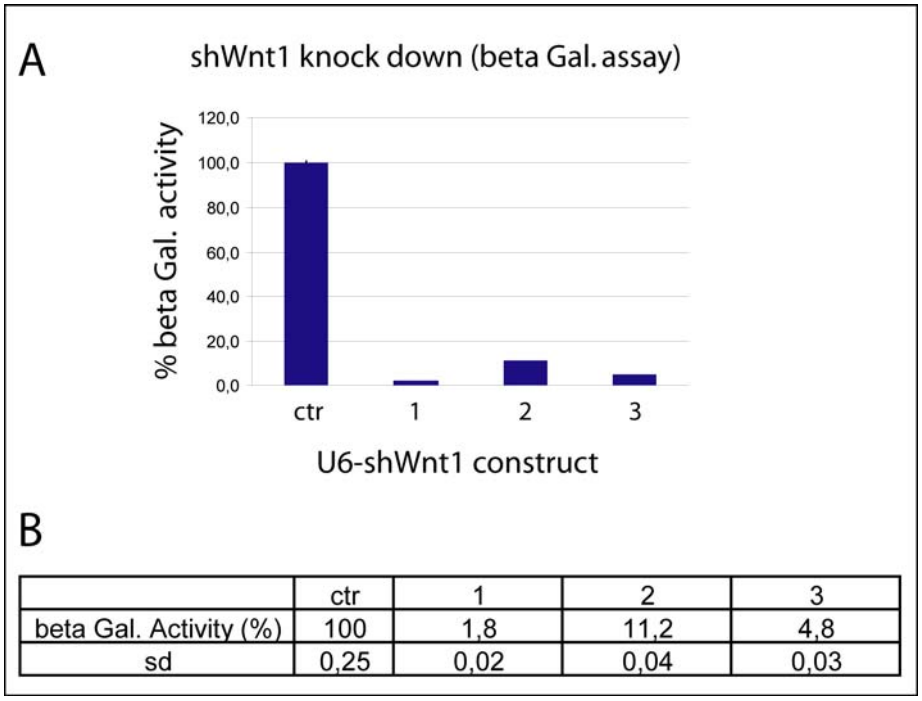

B

	ctr	1	2	3
beta Gal. Activity (%)	100	1,8	11,2	4,8
sd	0,25	0,02	0,04	0,03

Figure 53. ß-Galactosidase (ß-Gal.) activity of Wnt1-lacZ fusion protein.

A: ES cells were co-transfected with an expression vector for Wnt1-lacZ fusion protein and three different shWnt1 plasmids. Two days after transfection cells were lysed and RNA was used for ß-Gal. activity assay. All three shWnt1 plasmids efficiently reduced ß-Gal. activity. B: Relative ß-Gal. activity values and standard deviations (sd). Ctr: control (Wnt1-lacZ vector alone); 1, 2, 3: shWnt1 plasmids shWnt1-1, shWnt1-2 and shWnt1-3.

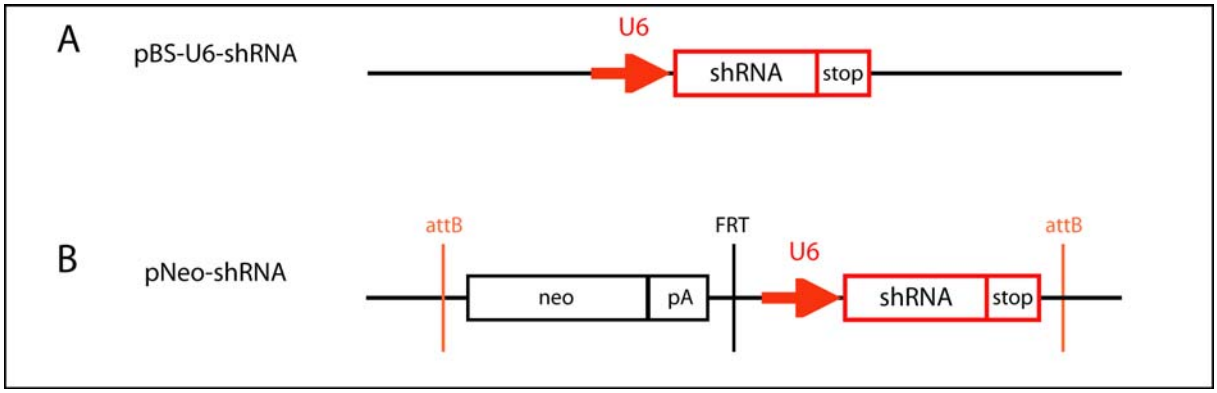

Figure 54. Schematic drawing of used shRNA expression vectors.

A: The plasmid pBS-U6-shRNA was used for transient transfections and *in vitro* analysis of knockdown efficiencies of the different hairpin sequences. B: The DNA fragment containing the U6 promoter, the shRNA, and the stop signal was sub-cloned from pBS-U6-shRNA into pNeo-shRNA for RMCE based stable integration within the genomic Rosa26 locus. U6: human U6 promoter; neo: neomycin resistance; pA: poly adenylation signal; attB: recognition site for C31 integrase; FRT: recognition site for Flp recombinase.

The subcloned shWnt1/1 construct was again used in the ß-Galactosidase assay to check the functionality. Also after co-transfections using the new attB flanked shWnt1/1 the ß-Galactosidase activity was clearly reduced (Fig. 55). Therefore I concluded that the new environment had no effect on the knockdown efficiency of the shRNA. The shWnt1/1 containing plasmid was used to generate stable ES cell clones and subsequently to generate also transgenic mice.

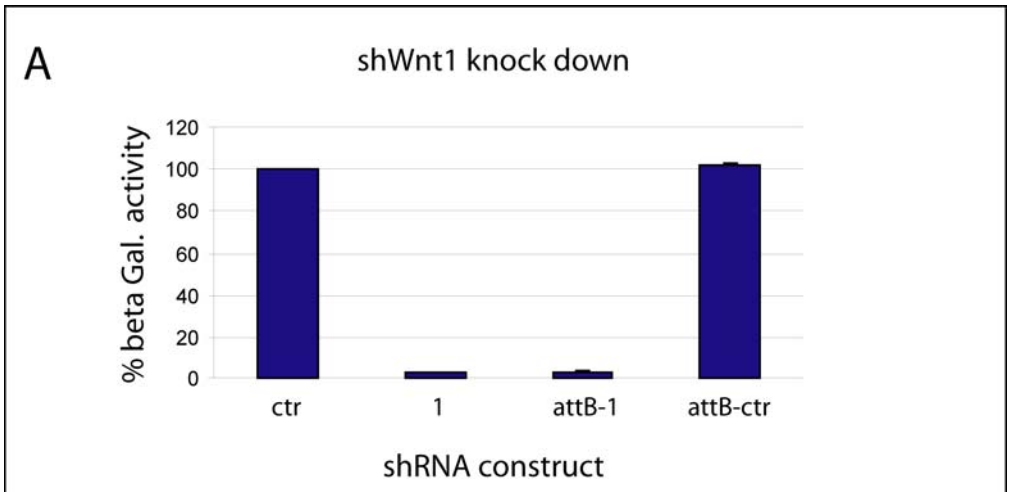

B

	ctr	1	attB-1	attB-ctr
beta Gal. Activity (%)	100	2,9	3,2	102,4
sd	0,09	0,01	0,01	0,09

Figure 55. ß-Galactosidase (ß-Gal.) activity of Wnt1-lacZ fusion protein.

A: ES cells were co-transfected with an expression vector for Wnt1-lacZ fusion protein and pBS-U6-shWnt1-1 (1) or pNeo-shWnt1-1 (attB-1). Two days after transfection cells were lysed and RNA was used for ß-Gal. activity assay. Both shWnt1 containing plasmids efficiently reduced ß-Gal. B: Relative ß-Gal. activity values and standard deviations (sd). Ctr: control (Wnt1-lacZ vector alone); 1: Wnt1-lacZ vector + pBS-U6-shWnt1-1; attB-1: Wnt1-lacZ vector + pNeo-shWnt1-1; attB-ctr: Wnt1-lacZ vector + empty pNeo plasmid.

4.2.4.3 **Generation of the PhiC31 integrase based exchange system**

For the generation of RNAi transgenic mice we developed a Phi C31 Integrase based exchange system (Fig. 56). The first step was to integrate a landing platform containing an attP site flanked hygromycin resistance gene into the genomic *Rosa26* locus. The resulting stable ES cell clone (Fig. 56, B) can than be used to insert a U6 promoter driven shRNA construct at the same genomic locus via a Phi C31 Integrase mediated cassette exchange (RMCE) (Fig. 56, C). To ensure the capability of pluripotency of the generated ES cell clone I used this clone for the generation of chimeric mice. The breeding of the chimeras revealed a transmission of the targeted *Rosa26* locus containing the pgk promoter and the hygromycin resistance gene to their progenies (Fig. 56, F).

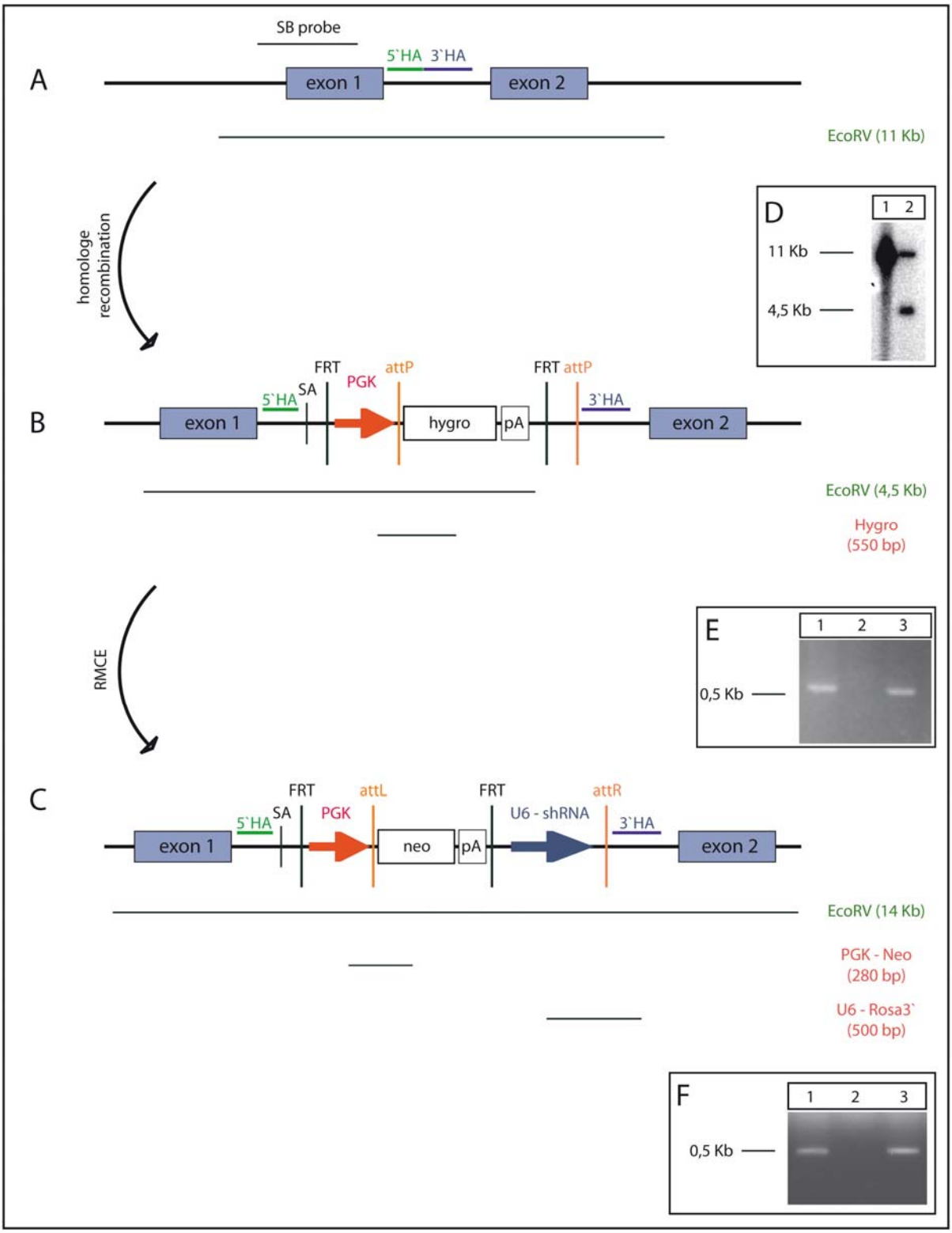
SB probe
A
5`HA
3`HA
exon 1
exon 2
EcoRV (11 Kb)
homologe recombination
D
1 2
11 Kb
4,5 Kb
B
FRT
PGK
attP
FRT attP
5`HA
SA
hygro
pA
3`HA
exon 1
exon 2
EcoRV (4,5 Kb)
Hygro (550 bp)
RMCE
E
1 2 3
0,5 Kb
C
FRT
attL
FRT
attR
5`HA
SA
PGK
neo
pA
U6 - shRNA
3`HA
exon 1
exon 2
EcoRV (14 Kb)
PGK - Neo (280 bp)
U6 - Rosa3` (500 bp)
F
1 2 3
0,5 Kb

Figure 56. Strategy for generation of shRNA transgenic mice.

A: The genomic *Rosa26* locus is used for RMCE mediated insertion of shRNAs. The intron between the first and second exon is used for homologous recombination. Succesful recombination events were verified by Southern blot. The Southern blot probe is indicated above (SB). B: The so called acceptor ES cells harbor a *Rosa26* locus modified by a pair of attP sites and a pgk-promoter driven hygromycin resistance gene. C: Upon C31 Integrase mediated recombination (RMCE) between the modified *Rosa26* locus and the pNeo-shRNA donor vector, containing a pair of C31 Integrase attB sites, the hygromycin coding region becomes replaced by a neomycin resistance coding region and the U6-promoter driven shRNA unit. Genomic EcoRV DNA fragments for Southern blotting (recognized by Rosa 5`probe) and the corresponding size of the fragment are indicated (green) in A, B, and C. PCR genotyping opportunities are indicated below and the size of amplificated fragments are written in red. D: Southern blot analysis of a wt ES cell clone (1) and an ES cell clone underwent succesfull homologous recombination (2). Genomic DNA was digested with EcoRV. The wild type *Rosa26* locus appears as 11 kb band and acceptor ES cells harboring the hygromycin resistance gene show an additional 4.5 kb band. E: Hygro PCR genotyping of mouse tail DNA results in a 550bp band. F: Upon RMCE the correct ES cell clones, containing a neomycin resistance gene and the U6-shRNA construct (shWnt1), is identified by U6-Rosa3` PCR genotyping and results in a 500bp band (1 and 3).

4.2.4.4 **Generation of stable shWnt1 ES cell clones**

An ES cell clone containing the pgk promoter driven and attP site flanked hygromycin resistance gene (Fig. 56, B) was used to generate shWnt1 transgenic ES cells. I co-transfected these cells with a Phi31 Integrase expression plasmid together with a plasmid containing an attB flanked neomycin resistance gene and the U6 promoter driven shWnt1/1 construct (Fig. 54, B). From 24 tested neomycin resistant clones 6 clones harboured the shWnt1/1 construct at the correct genomic position. Therefore the efficiency of the used Phi C31 Integrase mediated cassette exchange was 25%. The results of the PCR genotyping using specific primers (U6-Rosa3` PCR) are shown in Fig.55, E.

4.2.4.5 **shWnt1 in vivo results**

Since the goal of establishing the RMCE system was to have a tool for the rapid generation of shRNA transgenic mice I analysed the effect of the *Wnt1* knockdown in vivo. Therefore, I used a shWnt1/1 Es cell clone to generate shWnt1/1 transgenic mouse embryos via tetraploid aggregation. The tetraploid aggregation technology allows the generation of completely ES cell derived embryos and mice (Nagy et al., 1993). The resulting shWnt1/1 transgenic E10.5 embryos had normal mid- hindbrain regions (Fig. 57, A). Resulting shWnt1/1 transgenic mice from such tetraploid aggregation even survived until adulthood and displayed no obvious phenotype. However, from knockout embryos it is known that the mid- hindbrain region is severely affected by the loss of Wnt1 and it is also known that the loss of Wnt1 leads to embryonic lethality (McMahon and Bradley, 1990; Thomas and Capecchi, 1990). Therefore the knockdown of *Wnt1* using the hairpin shWnt1/1 did not lead to a similar phenotype as known from knockout studies.

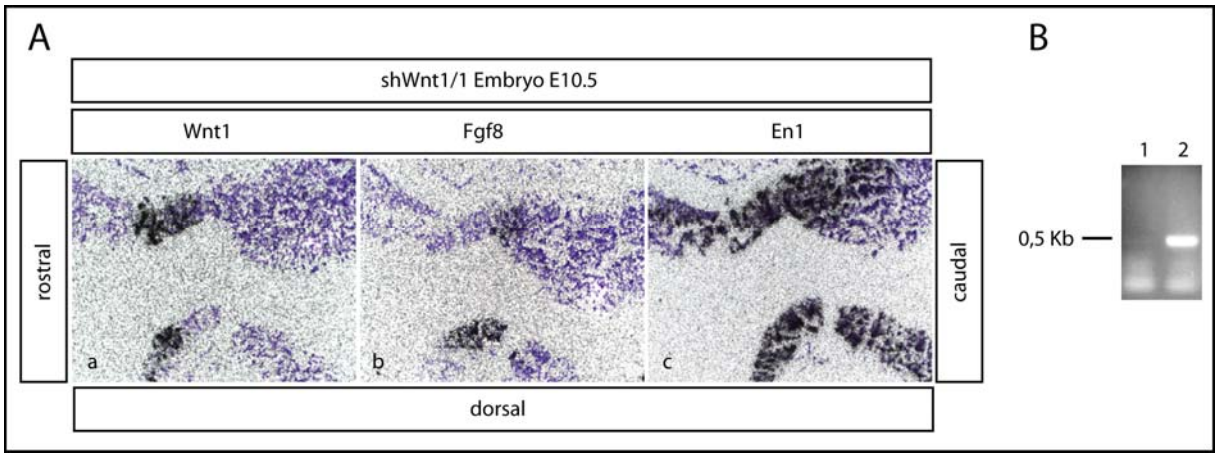

Figure 57. shWnt1 Embryos do not recapitulate Wnt1 knockout phenotype.
A: ISH on saggital sections from E10.5 Embryos, using *Wnt1* (a), FGF8 (b), and *En1* (c) specific probes, revealed normal expression of these MHR marker genes. Wnt1 expression is found rostraly and *Fgf8* caudaly from the MHB, whereas *En1* is expressed throughout the whole MHR. B: U6-Rosa3` PCR genotyping of Embryos. 1 = wt; 2 = shWnt1 transgenic Embryo (Histological analysis of embryo 2 is shown in A).

4.2.4.6 ***in vitro*** **re-analysis of Wnt1 hairpins using qReal Time-PCR**

To find out, why the used shWnt1 hairpin did not lead to the expected embryonic lethality, I repeated the transient transfection of ES cells with plasmids containing the U6 promoter driven shWnt1 hairpin constructs. The transfected ES cells were then used to measure the *Wnt1* mRNA level by quantitative Real Time PCR (Fig. 58). In contrast to the so far used indirect and artificial ß-Galactosidase assay this sensitive technique allows to determine the effect of the hairpins on the endogenous *Wnt1* mRNA. Surprisingly, this repeated analysis of the knockdown efficiencies revealed a different result than the ß-Galactosidase assay (Fig. 55). With this sensitive technique the hairpin shWnt1/3 showed the best knockdown efficiency. In shWnt1/1 transfected cells (the hairpin used for in vivo experiments in Fig. 57) the knockdown reached only about 26%. This weak knockdown level is probably the reason, why the knockout phenotype is not recapitulated in the shWnt1/1 embryos.

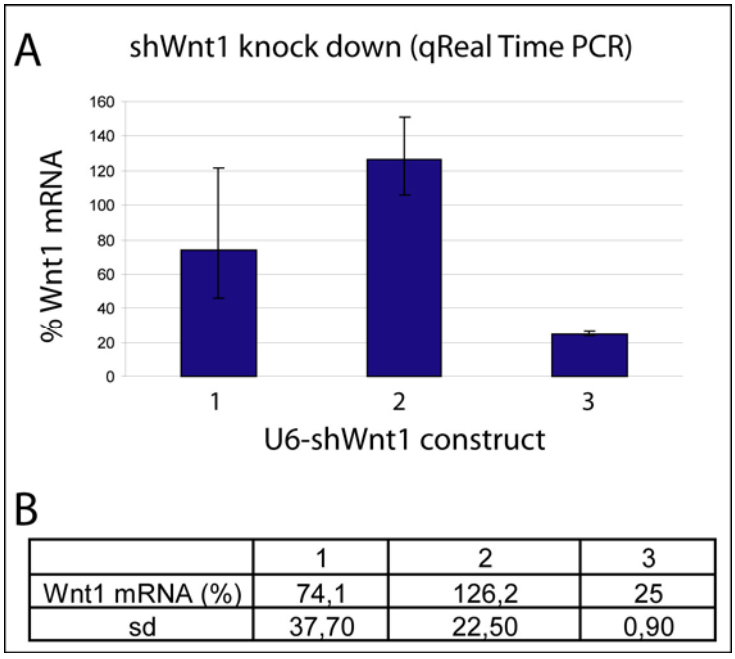

B

	1	2	3
Wnt1 mRNA (%)	74,1	126,2	25
sd	37,70	22,50	0,90

Figure 58. shWnt1 efficiencies determined by quantitative Real Time (qReal Time) PCR.

A: ES cells were transfected with pBS-U6-shWnt1-1 (1), pBS-U6-shWnt1-2 (2), or pBS-U6-shWnt1-3 (3). Two days after transfection cells were lysed and RNA was used for qReal Time PCR. shWnt1-3 is the only efficiently silencing construct. B: Relative *Wnt1* mRNA levels and standard deviations (sd).

4.2.5 Generation of *P2rx7* knockdown mice

Based on studies describing an involvement of the human ATP-gated ion channel P2X7 in depressive disorders, I decided to generate a shP2RX7 transgenic mouse (Barden et al., 2006). Therefore I used the already described Phi31 Integrase based RMCE and cloned and tested six different shRNA constructs against *P2rx7*. Finally, I generated the shP2RX7 transgenic mouse and determined the knockdown efficiency in different tissues in the adult animal.

4.2.5.1 Generation and in vitro test of *P2rx7* shRNA constructs

The results with the shWnt1/1 hairpin did not recapitulate the *Wnt1* knockout phenotype (Fig. 57, A) and therefore did not give the ultimate proof that our single hairpin strategy is functional. Nevertheless, this experiment showed that the RMCE system works and that the evaluation of the knockdown efficiency *in vitro* is crucial for the successful generation of shRNA transgenic mice. To target *P2rx7* I cloned six shRNA sequences against the ATP-gated ion channel P2RX7. The selection of the sequences was again based on the results of public shRNA design programs. But in contrast to the shWnt1 experiments I started with more shRNA sequences and determined from beginning on the effect of the shRNAs on the endogenous *P2rx7* mRNA level. Two similar techniques were used, the semiquantitative reverse transcriptase PCR (RT-PCR) and the quantitative Real Time PCR (qRealTime-PCR). Both strategies gave similar results regarding the relative knockdown efficiencies of the different shRNA constructs (Fig. 59). In both cases the construct shP2RX7/1 had the best knockdown efficiency with 66% as quantified by qReal Time PCR.

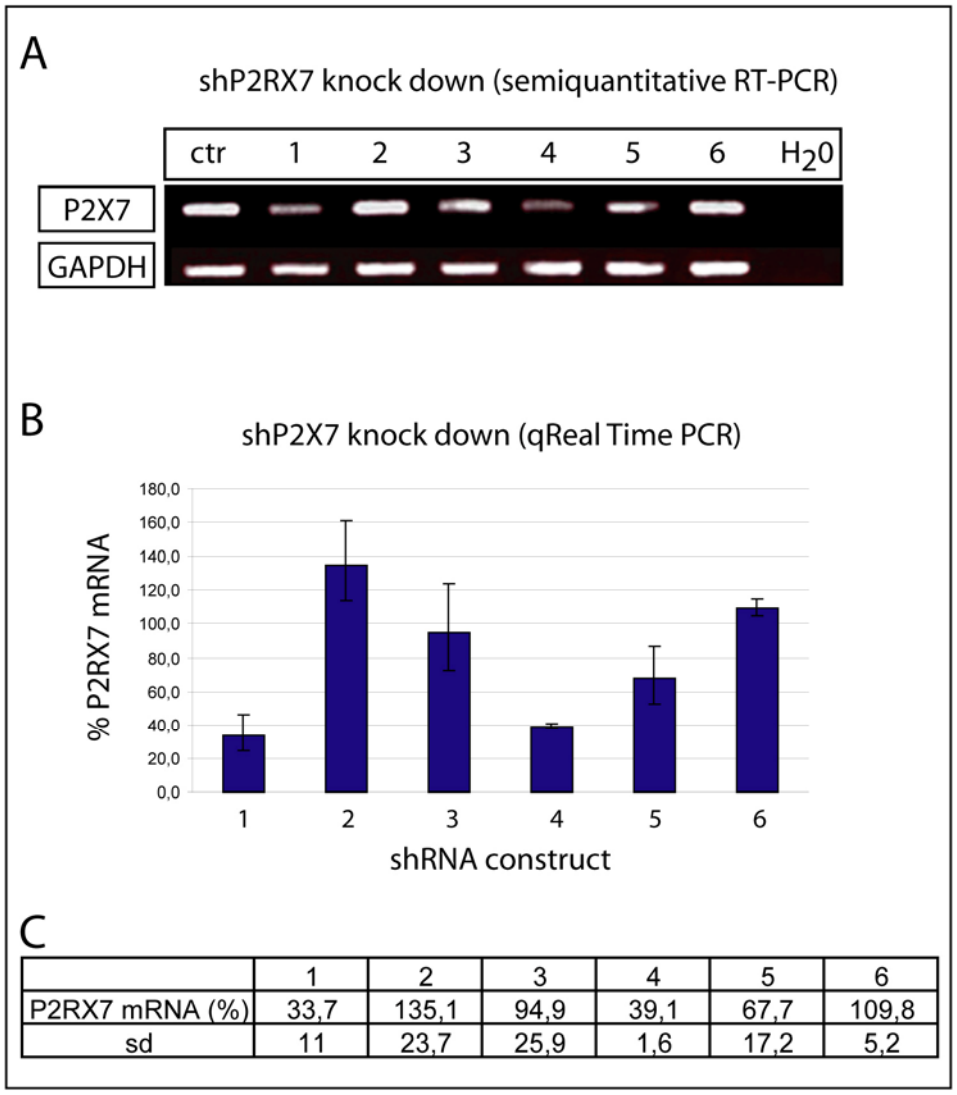

C

	1	2	3	4	5	6
P2RX7 mRNA (%)	33,7	135,1	94,9	39,1	67,7	109,8
sd	11	23,7	25,9	1,6	17,2	5,2

Figure 59. shP2RX7 efficiencies determined by PCR.

ES cells were transfected with pBS-U6-shP2RX7/1 (1), pBS-U6-shP2RX7/2 (2), pBS-U6-shP2RX7/3 (3), pBS-U6-shP2RX7/4 (4), pBS-U6-shP2RX7/5 (5), and pBS-U6-shP2RX7/6 (6). Two days after transfection cells were lysed and RNA was used for semiquantitative reverse transcription (RT) PCR (A) or qReal Time PCR (B, C). C: Relative *P2rx7* mRNA. levels and standard deviations (sd). *Gapdh* was used for normalisation in A. ctr: ES cells transfected with an empty pBS-U6 vector.

4.2.5.2 **Generation of stable shP2RX7 ES cell clones**

Based on the results of the semiquantitative RT-PCR and the qRealTime-PCR I used the shP2RX7/1 construct for subcloning into the exchange vector (Fig. 60). Stable ES cell clones harbouring the U6 promoter driven shP2RX7/1 construct within the genomic *Rosa26* locus were generated by co-transfection of the acceptor ES cell clone with the two plasmids pNeo-

shP2RX7/1 and the C31 integrase expression vector. The analysis of these ES cell clones via DNA sequencing, southern blot, and PCR genotyping using specific primers (PGK-U6 PCR) revealed that the U6 promoter and the shRNA sequence were not in the same orientation like the pgk-neomycin complex (Fig. 60, B). However, since the U6 promoter and the shRNA sequence are orientated in the same direction the shRNA should be transcribed and is therefore functional.

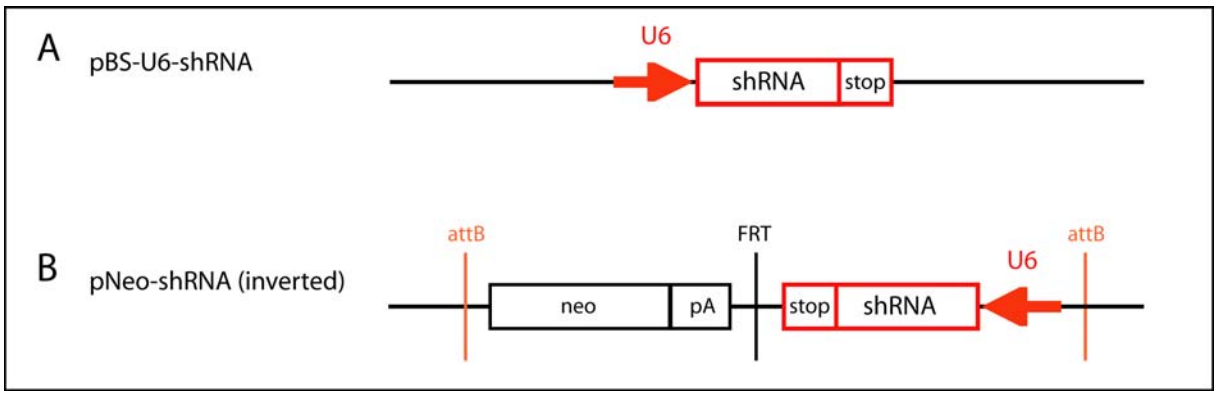

Figure 60. Schematic drawing of shP2RX7 expression vectors.

A: The plasmid pBS-U6-shRNA was used for transient transfections and *in vitro* analysis of knockdown efficiencies of the different hairpin sequences. B: The DNA fragment containing the U6 promoter, the shRNA, and the stop signal was sub-cloned from pBS-U6-shRNA into pNeo-shRNA for RMCE based stable integration within the genomic *Rosa26* locus. Since the U6-shRNA-stop construct is in the opposite direction to the *Rosa26* and neo transcription, this vector was named pNeo-shRNA (inverted). U6: human U6 promoter; neo: neomycin resistance; pA: poly adenylation signal; attB: recognition site for C31 integrase; FRT: recognition site for Flp recombinase.

The ES cell clone shP2RX7/1/5 was then used for the generation of transgenic mice to determine if the orientation of the U6 promoter and the following shRNA sequence, in respect to the pgk promoter and the neomycin resistance gene, is important for functionality. Furthermore, Southern blot analysis showed that the exchange in this clone was not complete. In fact the construct containing the neomycin resistance gene and the shRNA sequence was inserted downstream (3`) of the pgk promoter but the hygromycin resistance gene remained in the genome (Fig. 61).

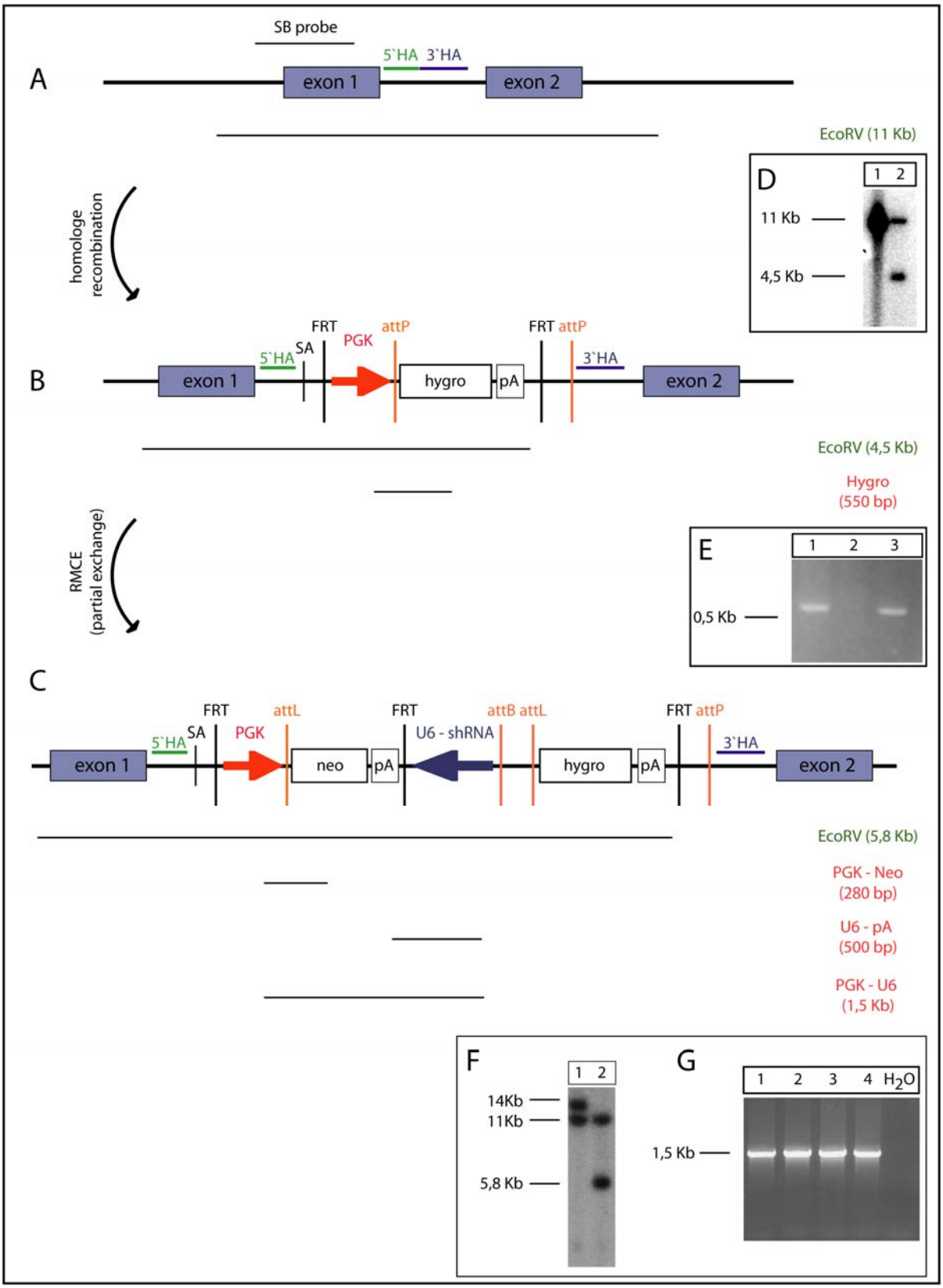
SB probe
A
5`HA 3`HA
exon 1
exon 2
EcoRV (11 Kb)
D
1 2
11 Kb
4,5 Kb
homologe recombination
B
FRT
PGK
attP
5`HA
SA
hygro
pA
FRT attP
3`HA
exon 1
exon 2
EcoRV (4,5 Kb)
Hygro (550 bp)
RMCE (partial exchange)
E
1 2 3
0,5 Kb
C
FRT
attL
FRT
attB attL
FRT attP
5`HA
SA
PGK
neo
pA
U6 - shRNA
hygro
pA
3`HA
exon 1
exon 2
EcoRV (5,8 Kb)
PGK - Neo (280 bp)
U6 - pA (500 bp)
PGK - U6 (1,5 Kb)
F
1 2
14Kb
11Kb
5,8 Kb
G
1 2 3 4 H2O
1,5 Kb

Figure 61. Strategy for generation of shP2RX7 transgenic mice.

A: The genomic *Rosa26* locus is used for RMCE mediated insertion of shRNAs. The intron between the first and second exon is used for homologous recombination. Succesful recombination events were verified by southern blot. The southern blot probe is indicated above (SB). B: The so called acceptor ES cells harbor a *Rosa26* locus modified by a pair of attP sites and a pgk-promoter driven hygromycin resistance gene. C: Upon C31 Integrase mediated partial recombination (RMCE) between the modified Rosa26 locus and the pNeo-shRNA (inverted) donor vector, containing a pair of C31 Integrase attB sites, the hygromycin coding region becomes displaced by a neomycin resistance coding region and the U6-promoter driven shRNA unit. Genomic EcoRV DNA fragments for Southern blotting (recognized by Rosa 5`probe) and the size of the fragment is indicated (green) in A, B, and C. PCR genotyping opportunities are indicated below and the size of amplificated fragments are written in red. D: Southern blot analysis of a wt ES cell clone (1) and an ES cell clone underwent succesfull homologous recombination (2). Genomic DNA was digested with EcoRV. The wild type *Rosa26* locus appears as 11 kb band and acceptor ES cells harboring the hygromycin resistance gene show an additional 4.5 kb band. E: Hygro PCR genotyping of mouse tail DNA results in a 550bp band. F: Upon partial RMCE the correct ES cell clone (2), containing a neomycin resistance gene and the inverted U6-shP2RX7 construct, is identified by southern blotting. In comparison the ES cell clone 1 underwent complete RMCE, with deleted hygromycin coding region. G: Upon partial RMCE the 4 correct ES cell clones, containing a neomycin resistance gene and the inverted U6-shP2RX7 construct, are identified by PGK-U6 PCR genotyping and results in a 1.5 Kb band.

4.2.5.3 **Characterization of P2rx7 knockdown mice**

The ES cell clone shP2RX7/1/5 was used to generate shP2RX7 transgenic mice via blastocyst injection. The resulting chimeras were bred to C57/Bl6 mice and the offspring were analysed regarding the transmission of the shRNA transgene by PCR and southern blot (Fig. 62, A, B). The pups which were positive for the shP2RX7 transgene did not display any obvious behavioural alterations and were used for breeding to expand the colony. Hereby, I realised that these mice did not breed well and within their offspring the ratio between transgenic shP2RX7 mice and Wt animals was not following the mendelian`s rules. About 20% of the offspring died before the third week after birth and were therefore not genotyped. Among the survivors I found too few transgenic animals and some of them even died between the third and the sixth week after birth.

I sacrificed five shP2RX7/1 transgenic animals and 5 littermates in the age of six to nine weeks to determine the *P2rx7* knockdown efficiency *in vivo*. The RNA from the brain, the heart, and the liver was extracted and used for qRealTime-PCR. The *P2rx7* mRNA level was

reduced in all analysed tissues (Fig. 62, C, and D). However, the strongest effect with a knockdown efficiency of 88% was seen in brain samples. Behavioural phenotyping of shP2RX7 mice will be done in collaboration with MPI of Psychiatry, Munich, and *Affectis Pharmaceuticals, Munich*.

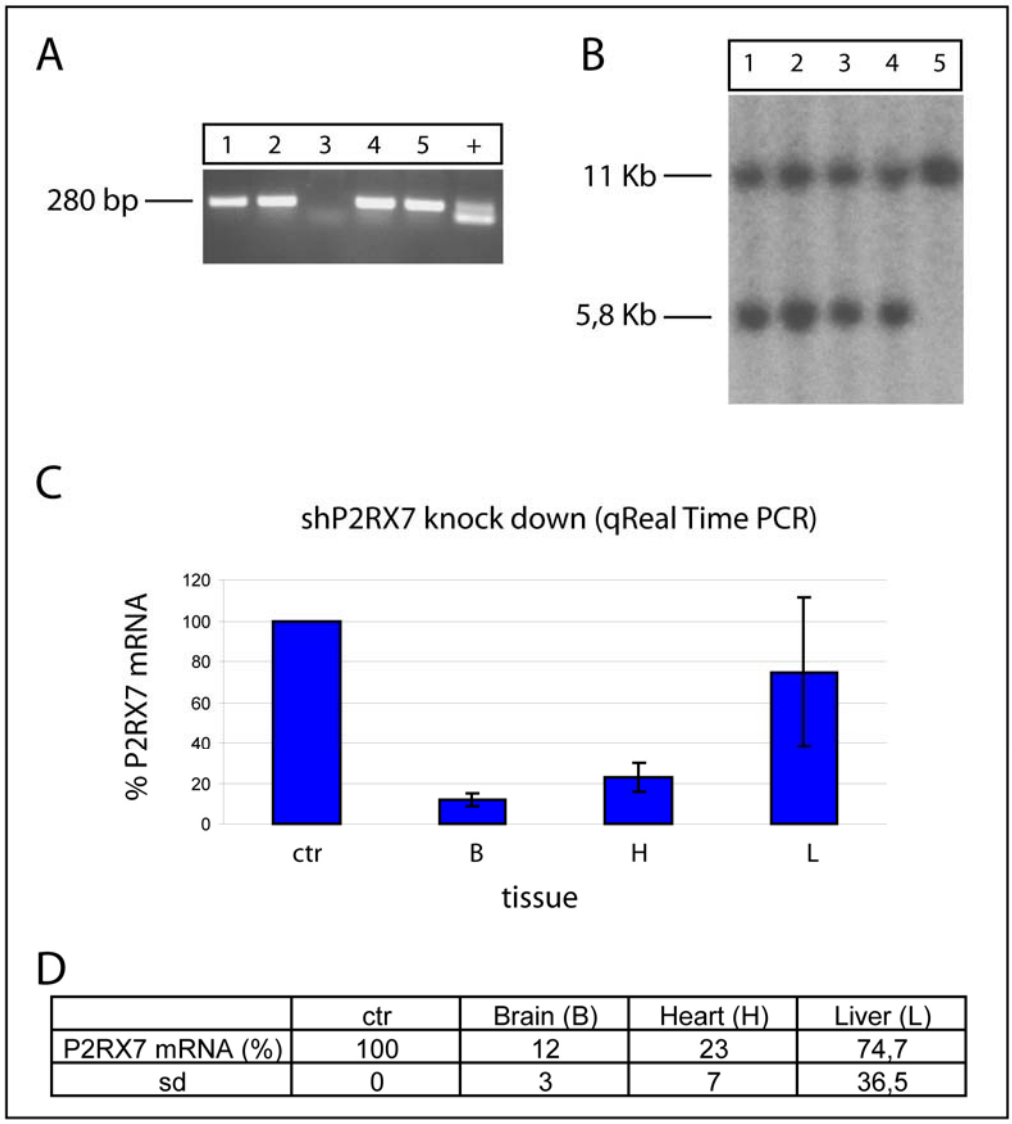

D

	ctr	Brain (B)	Heart (H)	Liver (L)
P2RX7 mRNA (%)	100	12	23	74,7
sd	0	3	7	36,5

Figure 62. Efficient silencing of *P2rx7* mRNA in the adult brain.

A: PGK-Neo PCR genotyping of tail DNA shows that 1, 2, 4, and 5 contains the shP2RX7 transgene. DNA from the ES cell clone, used for mouse generation by blastocyst injection, is used as a positive control (+). B: Sothern blot genotyping of EcoRV digested tail DNA from four shP2RX7 transgenic mice (1, 2, 3, and 4) and one wt mouse (5). C: Total RNA from brain (B), heart (H), and liver (L) were used for qReal Time PCR. In all three tissues *P2RX7* mRNA levels were reduced. However, in liver the reduction was quite inefficient. Ctr: *P2RX7* mRNA levels of non-transgenic littermates. B: Relative ß-Gal. activity values and standard deviations (sd).

4.2.6 Cloning and in vitro test of shRNAs against *Fgfr2* and *Fgfr3*

Driven by the convincing results from the shP2RX7 transgenic mice I started to generate also shRNAs against *Fgfr2* and *Fgfr3* to allow generation double transgenic mice with conditional shRNAs against both, *Fgfr2* and *Fgfr3*. The idea behind these experiments was to down regulate the two *Fgfrs* at the same time in the same brain regions and to analyse than these mice for altered depression-like behaviour. Since there are studies linking both *Fgfrs*, *Fgfr2* and *Fgfr3*, to depressive disorders (Evans et al., 2004; Turner et al., 2006), it would be very helpful to analyse the behaviour of those mice.

Based on the prediction of public shRNA design programs I selected four different target sequences against *Fgfr2* and *Fgfr3*, respectively. These shRNA constructs were cloned into the pShag plasmid (Paddison et al., 2004) to be expressed under the control of the human U6 promoter (Fig. 54, A). The shRNA containing plasmids were transfected into ES cells and the knockdown efficiency was estimated by measuring the endogenous *Fgfr2* and *Fgfr3*, mRNA levels using qRealTime-PCR (Fig. 63). The transfection of ES cells with the shFGFR2/3 construct leads to a 54% reduction of the *Fgfr2* mRNA level (Fig. 63, A, B). The *Fgfr3* mRNA level of the ES cells was reduced by 61% upon transfection with the shFGFR3/4 construct (Fig. 63, C, and D). The loop region of the shRNA constructs contains a HindIII restriction site for further cloning steps. Into the loop region of these shRNA constructs, FGFR2/3 and shFGFR3/4, a loxP site flanked stop cassette could be inserted and they could be subcloned together into one single plasmid. Finally, a conditional shFGFR2-shFGFR3 double knockdown mouse could be generated but was beyond the scope of the present work (Steuber-Buchberger et al., 2008).

A

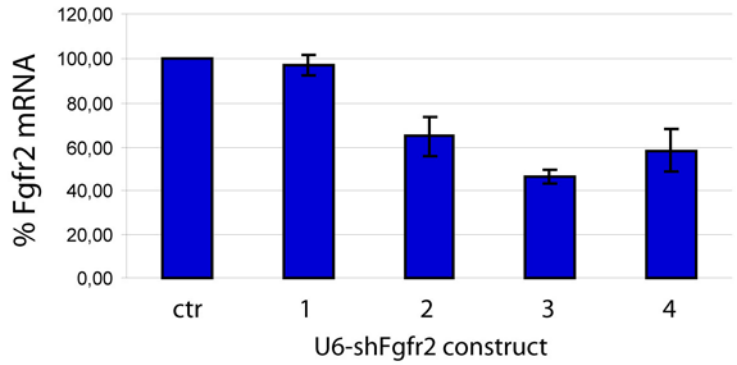

B

	ctr	1	2	3	4
Fgfr2 mRNA (%)	100	96,73	64,67	46,36	58,24
sd	0	4,7	9,1	3,3	9,8

C

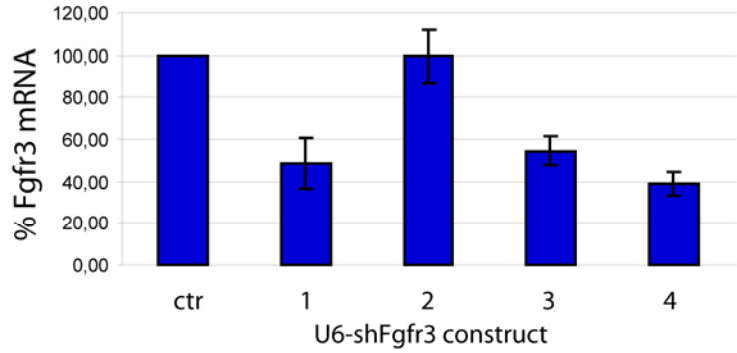

D

	ctr	1	2	3	4
Fgfr3 mRNA (%)	100	48,3	99,6	54,5	39,2
sd	0	12,2	12,4	7,1	5,7

Figure 63. shFGFR2 and shFGFR3 efficiencies determined by qReal Time PCR.

ES cells were transfected and two days later lysed. RNA was used for qReal Time PCR. A: Cells were transfected with pBS-U6-shFGFR2/1 (1), pBS-U6-shFGFR2/2 (2), pBS-U6-shFGFR2/3 (3), and pBS-U6-shFGFR2/4 (4). B: Relative *Fgfr2* mRNA levels and standard deviations (sd). C: Cells were transfected with pBS-U6-shFGFR3/1 (1), pBS-U6-shFGFR3/2 (2), pBS-U6-shFGFR3/3 (3), and pBS-U6-shFGFR3/4 (4). D: Relative *Fgfr3* mRNA levels and standard deviations (sd). ctr: ES cells transfected with pBS-U6-shWnt1-1 as negative control.

5 DISCUSSION

5.1 FGFR2 in cerebellum development

In this study, it was shown that CNS specific *Fgfr2* conditional knockout (cko) mice display cerebellar malformations with a broad range of severity. The anterior cerebellar lobules II and III seem to be most susceptible to FGFR2 dependent alterations. Severely affected FGFR2 cko cerebella did not show the typical layered organisation, especially in the anterior region. Mildly affected FGFR2 cko cerebella had Bergmann glia cell defects within the anterior cerebellum but only faint alterations regarding cerebellar neuronal populations. Furthermore, FGFR2 cko displayed alterations in vertical and horizontal locomotion in the mHB. Both, the vertical and the horizontal locomotion, were reduced in the FGFR2 cko mice. Interestingly the vertical locomotion seems to be affected exclusively on board, in the centre of the test box.

The variability of cerebellar malformations among FGFR2 cko mice results most likely from the mixed genetic background. However, the fact that also the offspring of the same parents display different severity levels does not support this explanation. A further possibility would be a slightly variable onset of Cre recombinase expression among the FGFR2 cko mice. The expression of Cre recombinase driven by the *Nestin* promoter and the enhancer element from the second *Nestin* intron should start around embryonic day 11.5 in all CNS cells (Tronche et al., 1999). At this stage even a delay of some hours in Cre recombinase expression could potentially cause strong variability in the observed phenotypes. However, the differences in phenotype severity gave the opportunity to study distinct effect of FGFR2 inactivation on single cell types without disruption of the whole cerebellar organisation.

It is very likely that the primary defect in FGFR2 mutant mice lies in the development of the Bergmann glia monolayer. First of all in adult wt cerebellum *Fgfr2* is strongly expressed in the Purkinje cell layer but restricted to Bergmann glia cells whereas Purkinje cells do not express *Fgfr2* (Fig. 23). Furthermore, the altered morphology of Bergmann glia fibres (Fig. 13) could interfere with the Granule cell migration from the external to the internal GL. This hypothesis is supported by the observation that some Granule neurons, which are mispositioned within the ML of FGFR2 cko cerebella, show radial chain-like organisation

(Fig. 11, B). This is the exact position the cells would be at if their migration from the external GL inwardly was halted. Finally the disturbed migration of Granule neurons in turn could give rise to the observed alterations of Purkinje cell positioning. The incomplete Granule cell migration could lead to mispositioning of Purkinje cells by occupying space within the PCL. This could cause the observed dense packaging of the Purkinje cells (Fig. 11, A). It is likely that in severely affected FGFR2 cko cerebella most of the Bergmann glia fibres fail to reach the cerebellar surface. Consequently the Granule cell migration is almost completely abolished which then leads to the strong impact on the cerebellar structure (Fig. 64). The importance of neuronal cell migration, and its relationship to glia cells, in cerebellar development was demonstrated in many different mutant mice. The Reeler mutation affects the gene *Reelin*, coding for an extracellular protein, and results in disturbed neuronal migration and, besides other brain defects, in absent cerebellar foliation (D'Arcangelo and Curran, 1998; Goffinet et al., 1984). Complete ablation of proliferating astrocytes in a GFAP-TK mouse model leads to the disruption of the well defined cerebellar structure (Delaney et al., 1996). Probably the altered structure of the cerebellum upon astrocyte ablation was mainly due to the loss of Bergmann glia fibres. Furthermore, the elaboration of Purkinje cell dendrites and the number of Granule neurons was reduced in cerebella of GFAP-TK mice. Further studies will show if this is also the case in FGFR2 cko mice.

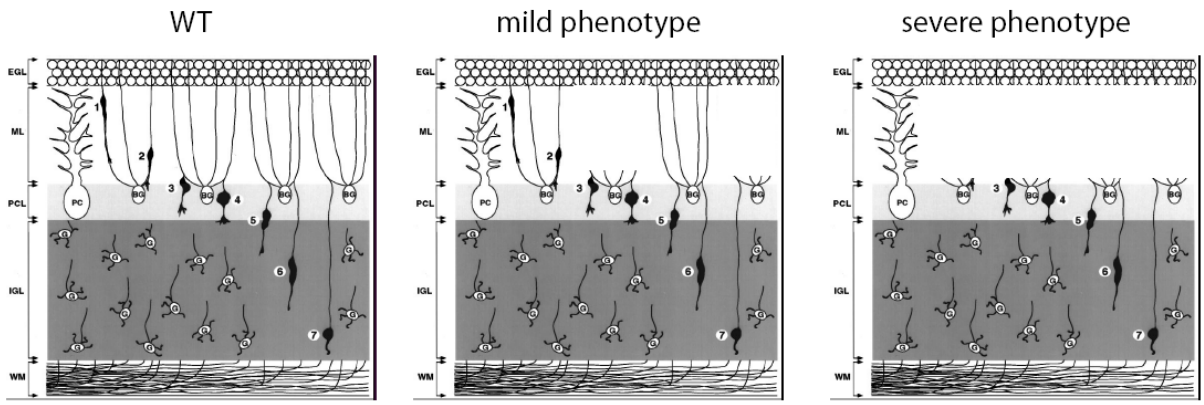

Figure 64. Model of cerebellar defects in *Fgfr2*$^{lox/lox}$*; Nestin-Cre* mice.
In postnatal wt cerebellum GC migrate from the EGL along Bergmann glia fibers through the ML and pass the PCL. Mature GC settle down in the IGL. Assuming a function of FGFR2 in Bergmann glia differentiation or fiber extension FGFR2 inactivation would result in fewer or shorter Bergmann glia fibers and hamper GC migration. Depending on the amount of affected Bergmann glia cells these disturbed GC migration could lead to mild or severe cerebellar defects. (Modified from Komuro and Rakic, 1998)

The analysis of young mice and embryos shows that the observed malformations in the cerebellum of adult mutants are probably caused by defects in the foliation process or by the incompetence of the different cell populations like Purkinje cells and Bergmann glia cells to find or keep their correct position (Fig. 11, 12, 13). The establishment of the Bergmann glia monolayer is regulated by Notch/RBP-J signalling. Conditional Notch1/2 double mutants and RBP-J mutants, generated using hGFAP-Cre mice, displayed similar Bergmann glia ectopia as seen in conditional *Fgfr2*$^{l/l}$*; Nestin-Cre* mutants (Komine et al., 2007). Interestingly, no alterations in cerebelli of Notch or RBP-J mutants were found before P1, indicating a normal Bergmann glia migration during embryonic development. Since in FGFR2 mutants already at E18 a cerebellar malformation can be observed (Fig. 27), FGFR2 should act upstream or in parallel in regulating Bergmann glia migration and differentiation. Additonally, FGFR2 could interact with the Shh pathway in regulating proper cerebellar development. It is known that mutants with impaired Shh signalling have cerebellar malformations similar to the cerebellar defects observed in this study in FGFR2 mutants (Blaess et al., 2006; Corrales et al., 2004). However, due to missing detailed molecular analysis of embryonic cerebelli it is not yet clear how FGFR2 is integrated in the genetic network which promotes cerebellum development.

The fact that inactivation of FGFR2 had such a clear effect on cerebellum morphology, and especially on Bergmann glia cells, was unexpected. Patterning and gross morphology of cerebella from mid- hindbrain specific FGFR2 cko mice was not altered as shown by Blak et al. (2007). However, in the mentioned study the focus was on mid-hindbrain development and patterning and thus a detailed analysis of Bergmann glia morphology was missing. Therefore I included in my analysis the mid-hindbrain specific FGFR2 cko mice used by Blak et al. (2007) to solve this discrepancy. I found also in these mid-hindbrain specific FGFR2 cko mice Bergmann glia defects (Fig. 14), although the impact on the cerebellum in general seemed to be less severe as compared to CNS specific FGFR2 cko cerebella, confirming the findings from Blak et al. (2007).

Furthermore, the ISH analysis of the four known FGF receptors in adult mouse brains showed co-expression of *Fgfr1, Fgfr2* and *Fgfr3* in PCL. The strong expression of three *Fgfrs* (*Fgfr1, Fgfr2* and *Fgfr3*) suggests receptor compensation (Fig. 23). The analysis of FGF signalling in FGFR2 cko cerebella revealed lower *Fgfr2* mRNA levels in PCL of FGFR2 cko cerebella. The amount of *Fgfr*2 mRNA inversely correlated with the occurring cerebellar defects. The *Fgfr2* ISH signal was diminished in PCL in the anterior part of mildly affected FGFR2 cko cerebella although both cell types, the Purkinje and Bergmann glia cell, were still present (Fig. 20). This indicated a repression of *Fgfr2* on the transcriptional level. The repression of

Fgfr2 and *Fgfr3* mRNA transcription by activated FGFR1 was described previously (Liu et al., 2003). *Fgfr3* expression was not repressed in FGFR2 cko PCL, although *Fgfr3* expression pattern was altered (Fig. 26). This result did not support the hypothesis that the weaker *Fgfr2* expression is caused by FGFR1 mediated transcriptional repression. There is no alteration in number of *Fgfr3* expressing cells but in positioning of these cells. It is highly likely that the mispositioned *Fgfr3* positive cells are Bergmann glia cells. Since there is a strikingly similar pattern of expression between *Fgfr3* and *Mkp3* we concluded that FGF signalling is active and that FGFR3 could mediate FGF signalling in affected regions of FGFR2 cko PCL.

As a behavioural consequence of CNS specific FGFR2 inactivation we found reduced vertical and horizontal locomotion (Fig. 29). Based on the above mentioned histological findings I interpret the behavioural impairments, especially regarding the vertical locomotion, as a result of cerebellar malformations in FGFR2 cko mice. I assume that the observed cerebellar defects impair three-dimensional movement coordination. My interpretation is supported by the extremely low number of rearing events of FGFR2 cko males in mHB. Actually, only one FGFR2 cko male showed rearing behaviour on board. Mice have to lift their forepaws for rearing and therefore would partially loose the contact to the ground. Assuming that the three-dimensional movement coordination in FGFR2 cko mice is disturbed, the ground contact would give a kind of additional orientation to the mouse. Close to the wall the rearing behaviour is not altered in FGFR2 cko mice. In this situation the wall could be used by FGFR2 cko mice as a guiding cue for vertical locomotion and help the mice to coordinate their vertical movements. The preference of FGFR2 cko males to stay close to the wall could be caused by altered Thigmotaxis, meaning the movement in response to contact. A possible correlation between Thigmotaxis and spatial learning in rats tested in Morris water maze was described previously (Venero et al., 2004).

I sought to determine whether the altered locomotor activity is associated with motor-coordination defects. The Rotarod task was used to address the question of impaired motor-coordination. The reason that the difference in Rotarod performance in males did not reach statistical significance could be due to the inhomogeneous FGFR2 cko group. The analysed mice in mHB and Rotarod included FGFR2 cko mice with severely and mildly affected cerebella (Fig. 10). Interestingly, the FGFR2 cko male with the best performance on Rotarod was the only FGFR2 cko male that showed rearing behaviour on board in mHB. This suggests that the behavioural impairments could correlate positively with the severity of cerebellar defects in CNS specific FGFR2 cko mice. Considering the anatomo-functional organisation of the cerebellum (Manni and Petrosini, 2004) there are probably other behavioural paradigms

which would reflect the severity of the cerebellar defect more clearly. It was shown that cerebellar malformations in *Zic3*-deficient mice caused alterations in eye movement without effecting Rotarod performance (Aruga et al., 2004). Therefore eye movement could be used as an additional parameter to assess the behavioural consequence of the described cerebellar defect in FGFR2 cko mice.

The FGFR2 mutants spent more time struggling in the FST, a test for depression-like behaviour (Fig. 30). However, since the mutants display also great behavioural alterations in many of the measured parameters in the mHB the results from the FST are not reliable in terms of increased or decreased depression-like behaviour. It reflects rather the strong impact of FGFR2 deletion on mouse behaviour in general.

I found interesting correlations between the cerebellar defects and behavioural alterations in FGFR2 cko mice. However, I can not exclude that effected cell populations from other brain regions in CNS specific FGFR2 cko mice contribute to the observed changes in behaviour. The dopaminergic, serotonergic and cholinergic neurotransmitter systems as assessed by ISH using probes against *Tyrosine hydroxylase (Th), Serotonin transporter (SERT)* and *vesicular Acetylcholine transporter (VAChT)*, respectively, seemed to be unaltered (Fig. 9). Further histological and behavioural studies are therefore needed. These studies should include additional behavioural paradigms like the Morris water maze and eye movement analysis but also FGFR2 cko mice with a more restricted Cre expression pattern.

5.1.1 FGFR2 in cerebellum development – outlook

The *Fgfr2*$^{l/l}$ *Nestin-Cre* mutants display cerebellar malformations, including mispositioning of Bergmann glia, Granule neurons and Purkinje cells. Analysis of embryonic cerebelli could solve the issue which cells are primary responsible for the observed cerebellar phenotype and at which developmental stage this phenotype begins. To determine if the observed phenotype is due to defects in differentiation and migration of Bergmann glia it would be helpful to analyse astroglia specific conditional FGFR2 mutants. One possibility is the generation of conditional mutants using *Glast-Cre-ER* mice (Mori et al., 2006). This would also allow analysing FGFR2 function in Bergmann glia in a time specific manner. Furthermore, it is necessary to analyse the expression of Notch pathway members during embryonic and early post-natal stages. This would allow us to analyse the relationship between Notch signalling

and FGF signalling during Bergmann glia differentiation and migration. Additionally, gene expression analysis of Reelin- and Integrin-dependent signalling pathways could show the migration properties of the cerebellar neuronal populations. A further interesting task is the analysis of forebrain structures. In the cerebral cortex similar layering processes like in the cerebellar cortex are occurring. Since we did not analyse the forebrain it is possible that layering defects are also present in the cerebral cortex. The adult neurogenesis could also be affected in FGFR2 mutants since *Fgfr2* is highly expressed in the SVZ and RMS and to a less extend in the SGZ of the dentate gyrus.

5.2 FGFR2 in Depression

This study reports the mainly redundant mRNA expression of *Fgfr1, Fgfr2*, and *Fgfr3* in six regions of the adult mouse brain, which are known to be involved in mood disorders. Although this suggests compensatory mechanisms FGFR2 deletion in mature forebrain neurons affected depression-like mouse behaviour in the FST. Furthermore, FGFR2 mutants display an altered acute response to fluoxetine administration in FST. Our data suggest a role of FGF signalling, and especially of FGFR2, in depression.

In FGFR2 forebrain mutants I found reduced FGFR2 protein levels in other brain regions than forebrain suggesting broader expression pattern of Cre than expected (Fig. 43). Therefore it is important to repeat this studies using Cre-expressing mice with more restricted and defined Cre-expression pattern or applying injections of Cre-expressing viruses to certain brain areas. Although the FGFR2 inactivation is not restricted to the forebrain the behavioural results show an involvement of FGFR2 in regulating depression-like behaviour and fluoxetine action in mice.

The broad expression pattern of *Fgf* family members in both, the adult mouse brain and the adult human brain, suggests important functions of this growth factor system in the adult brain (Belluardo et al., 1997; Gaughran et al., 2006). In this study *Fgfr* expression in six brain regions, which are known to be involved in depression, was analysed (Soares and Mann, 1997; Strakowski et al., 2005). *Fgfr2* mRNA is expressed in all six regions making the mouse a good model to study the function of FGFR2 in depression (Fig. 23, 35 - 41). I analysed the role of FGFR2 in depression by inactivating FGFR2 postnataly in mature forebrain neurons. FGFR2 forebrain mutants spent indeed less time with struggling in the FST, indicating increased depression-like behaviour (Fig. 52, A). The fact that FGFR2 inactivation had only a

subtle effect on depression-like behaviour in the FST could be due to compensatory mechanisms among the different FGFRs. Comparison of *Fgfr1, Fgfr2* and *Fgfr3* mRNA expression revealed a high degree of redundancy in almost all analysed brain regions. The redundancy of mRNA expression indicates that there is probably more than just one FGFR involved in depression. This is supported by the study of Evans et al. (2004) where they found the expression of several members of the *Fgf* family, including *Fgfr2* and *Fgfr3*, to be decreased in the prefrontal cortex and the cingulate cortex of depressed patients. Additionally, *Fgfr1* mRNA expression is found to be up regulated in the hippocampus of depressed patients (Gaughran et al., 2006). The heterogeneity of depression suggests that the onset of this disease, probably like in most other mood disorders, too, is caused or favoured by dysfunction of one or more complex genetic networks. However, the data from the FST with FGFR2 mutant mice together with the results of my mRNA expression analysis suggest that FGF signalling might be causatively involved in genetic predisposition to depression.

The involvement of FGFR2 in depression is further demonstrated by altered acute response to fluoxetine, a commonly used antidepressant drug (Fig. 52, B). The SSRI fluoxetine blocks Serotonin-reuptake and thereby increases the Serotonin level in the synaptic cleft. Fluoxetine had opposite effects in forebrain mutants and control animals in respect to struggling behaviour. This result suggests a function of FGFR2 in fluoxetine mediated antidepressant effects. One molecule which is known to be involved in both pathways, FGF signalling and fluoxetine mediated cellular response, is the extracellular signal-regulated kinase (ERK), a member of the MAPK family (Fumagalli et al., 2005; Kolch et al., 1993; Moodie et al., 1993; Stokoe and McCormick, 1997; Valjent et al., 2004). In rats chronic administration of fluoxetine leads to decreased levels of phosphorylated ERK (pERK), the active form of ERK protein, in hippocampus and frontal cortex (Fumagalli et al., 2005). Levels of pERK upon acute fluoxetine administration were not altered. However, in mice acute fluoxetine administration resulted in increased pERK levels in prefrontal cortex and hippocampal CA1 region (Valjent et al., 2004). Therefore, fluoxetine dependent regulation of pERK levels seems to depend on treatment duration, analysed brain region and species. Interestingly, in rats acute fluoxetine treatment leads to increased *Fgf2* levels in entorhinal cortex, whereas chronic fluoxetine treatment results in increased *Fgf2* in the hippocampus (Mallei et al., 2002). Thus, fluoxetine and FGF signalling, probably including FGFR2 activation, could cooperate in regulating pERK levels in certain brain areas.

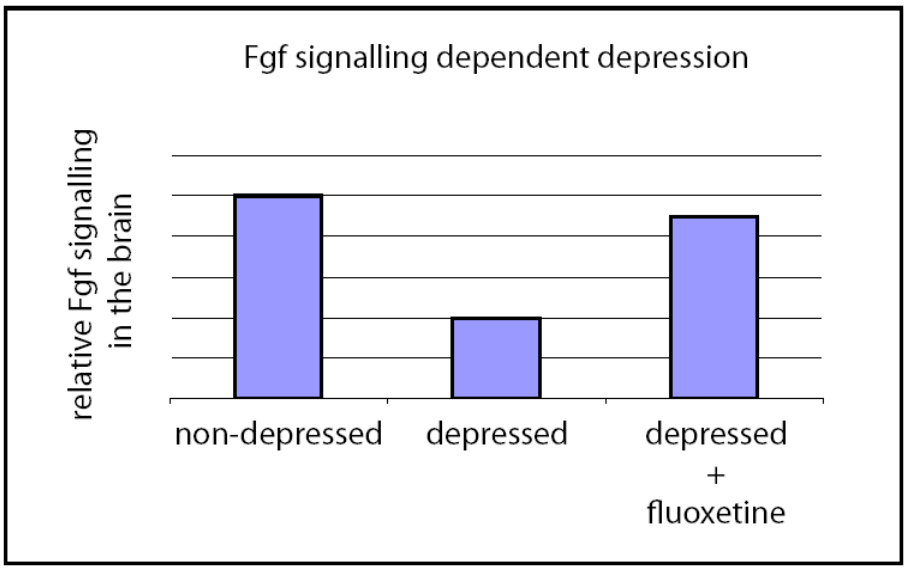

Figure 65. FGF signalling is reduced in depression.
Previously published data from depressed patients and experiments with rodents, together with the results from this study, suggest that low FGF signalling causes depressive disorder. In addition Treatment with antidepressants like fluoxetine could increase FGF signalling and attenuate depressive symptoms.

A candidate protein for a more direct interaction between fluoxetine and FGFR2 is the non-receptor tyrosine Src kinase Fyn. Fyn can bind via its SH2 domain to FGFRs (Kaabeche et al., 2004). This binding leads to increased Fyn kinase activity. On the other hand Fyn is also capable of binding via its SH3 domain the 5-HT_6 receptor (Yun et al., 2007). Binding of Fyn to the 5-HT_6 receptor increases the activity of both molecules. Interestingly, 5-HT_6 receptor stimulation has antidepressant-like effects in mice (Svenningsson et al., 2007). Therefore the role of FGFR2 in depression could be the modulation of 5-HT_6 receptor activity via the FGFR2-Fyn interaction. The Src kinase mediated phosphorylation and activation of FGFR2 upon 5-HT receptor activation with Serotonin was demonstrated in a recent study with rat C6 glioma cells by Tsuchioka and colleagues (Tsuchioka et al., 2008). Additionally, FGFR1 is also capable of binding Fyn and its expression is altered in depressed patients (Gaughran et al., 2006; Kilkenny et al., 2003). This suggests a general role of FGFR-Fyn interaction in depression. Interestingly, Fyn has been shown to promote neurite outgrowth. NCAM-dependent neurite outgrowth was inhibited in Fyn-deficient neuronal cell cultures (Beggs et al., 1994; Kolkova et al., 2000). The ability of the adult brain to generate new neurons is thought to be involved in antidepressant action of fluoxetine (Encinas et al., 2006; Sahay and Hen, 2007; Santarelli et al., 2003). However, neurite outgrowth is important for proper integration of newborn neurons into the existing neuronal network of the adult brain. Taken

together FGF signalling seems to be impaired in depressed patients and treatment with the antidepressant fluoxetine could normalise FGF signalling levels and reduce thereby depressive symptoms (Fig. 65).
However, the function of FGFR2 in depression could also be mediated by interactions with other proteins like CB1R or BDNF, both linked in various studies to depressive disorders (Bambico et al., 2007; Kozisek et al., 2008). Crosstalk between FGF signalling and endocannabinoid signalling regulates axonal growth (Williams et al., 2003). By adding CB1R antagonist to cultured cerebellar granule neurons N-cadherin/FGF2 dependent axonal growth was inhibited, whereas CB1R agonist could be used instead of N-cadherin/FGF2 to induce axonal growth. For BDNF pERK could be the link to FGF signalling. BDNF signalling and FGF signalling are acting both via pERK to induce cellular responses (Segal and Greenberg, 1996). Therefore the cooperation of FGF and BDNF signalling in regulating of pERK levels could be the basis of their interaction. A BDNF/FGF mediated pERK regulation was already suggested for their neuroprotective functions in hippocampal cultures (Johnson-Farley et al., 2007). Yet further studies are needed to analyse the co-expression and interaction of all the possible mediators of the FGFR2 function in fluoxetine action and in regulation of depression-like behaviour in mice.

The expression analysis of the three *Fgfrs* points to an important role of FGF signalling in adult neurogenesis. *Fgfr1* was strongly expressed in the subgranular zone of the dentate gyrus (DG) and only few positive cells for *Fgfr2* and *Fgfr3* were observed (Fig. 37). A strong expression of *Fgfr1* mRNA in the DG in rats was also found by Belluardo et al. (1997). However, in contrast to my results, no *Fgfr2* or *Fgfr3* positive cells in the DG were observed in the mentioned study. In the SVZ *Fgfr1* and *Fgfr3* are not or only weakly expressed whereas *Fgfr2* is expressed in the SVZ and in the RMS (Fig. 38, 39). A function of FGF signalling in both neurogenic regions of the adult brain, the hippocampal DG and the SVZ, is demonstrated in several studies. In rats intracerebroventricular infusion of FGF2 resulted in increased number of newly generated neurons and dendritic length in the DG and rat SVZ cultures treated with an FGFR inhibitor showed a decreased proliferation rate (Agasse et al., 2007; Rai et al., 2007). In adult mice immunohistochemical analysis revealed that FGFR2 positive cells in SVZ co-express GFAP, indicating that FGFR2 positive cells are slow-dividing neural stem cells (Zheng et al., 2004). In addition, adult conditional FGFR1 knockout mice, generated using *Nestin-Cre* mice, displayed decreased cell proliferation in the dentate gyrus (Zhao et al., 2007). These studies support the findings of my *Fgfr* expression

analysis and suggest that FGF signalling is necessary for adult neurogenesis, with FGFR1 mediating FGF signalling in the DG and FGFR2 in the SVZ.

The analysis of depression-related behaviour of FGFR2 forebrain mutants was the main interest in this study. However, I analysed also the behaviour in other tasks to get a more detailed insight into FGFR2 dependent modifications of mouse behaviour. I did not find any evidence for altered locomotion, motor-coordination, social, or anxiety-related behaviour in the mHB (Fig. 45). Interestingly, taking all the behaviour test results together, a slightly altered coping behaviour in FGFR2 forebrain mutants became obvious. Although in the mHB forebrain mutants display no altered locomotion or exploratory behaviour I found many significantly altered parameters in other tasks. Increased passive coping behaviour of FGFR2 forebrain mutants was found in Rotarod (more passive rotations; Fig. 46), SI (less interaction with an unfamiliar mouse; only females; Fig. 49), and FST (less struggling; Fig. 52, A) whereas more active coping behaviour was observed in LD (increased velocity and meander in lit compartment; Fig. 47) and in EPM (increased velocity in closed arm; Fig. 48). Upon injection of NaCl the time the forebrain mutants and control animals spent with struggling in the FST was not any more different, suggesting a strong response of forebrain mutants to the stressful handling before the test. This strong stress response in forebrain mutants resulted in compensation of the altered struggling behaviour seen in FST without injections (Fig. 52). Possibly FGFR2 inactivation leads to enhanced susceptibility to stress and the altered parameters are the behavioural outcome of this stress sensitivity of forebrain mutants. A function of FGF signalling in stress response has been suggested in previous studies. In rats escapable and inescapable stress (tail shock) resulted in increased *Fgf2* mRNA expression (Bland et al., 2007). An increased *Fgf2* mRNA level in the anterior cingulate cortex was observed in rats immediately after receiving the escapable tail shock as compared to rats without receiving tail shock. Different levels of *Fgf2* induction where found in several brain regions, including the hippocampus, and seem to depend on the stress (escapable or inescapable). Furthermore, FGF family members are expressed in a glucocorticoid dependent manner. Injection of adrenalectomised rats with a glucocorticoid receptor agonist resulted in increased basic FGF expression in the hippocampus and cortex (Hansson et al., 2000). A similar increase of *Fgf2* expression is also observed in several brain regions following acute restraint stress (Molteni et al., 2001). The hypothalamic–pituitary–adrenal (HPA) system operates to control glucocorticoid hormones secreted by the adrenal glands, which are the most important steroid hormones secreted during stress (McEwen, 1999; Strohle and

Holsboer, 2003). FGFR2 inactivation in forebrain mutants could interfere with glucocorticoid mediated stress response and thereby provoke altered coping behaviour.

5.2.1 FGFR2 in depression – outlook

The FGFR expression analysis revealed co-expression of the three *Fgfrs* in the six analysed brain regions, prefrontal cortex, cingulate cortex, hippocampus, amygdala, striatum and cerebellum. Together with the findings that in depressed patients the expression of all three receptors is altered and *Fgf2* expression is induced by fluoxetine a complex involvement of several FGF signalling members in depression is highly likely. Therefore it would be very interesting to analyse conditional FGFR2/3 double or FGFR1/2/3 triple mutants, generated using CamKII-Cre mice, and thereby avoid compensatory effects. This should lead to a stronger depression-like phenotype in mice since it would be more similar to the situation in depressed patients, where FGF signalling in general seems to be decreased. Unfortunately for Fgfr3 only complete null mutants are available. Therefore a fast strategy to generate FGFR2/3 double mutants is by using vectors for simultaneous expression of the two shRNA shFGFR2 and shFGFR3. I have cloned and tested the shRNA expression vectors for both *Fgfrs Fgfr2* and *Fgfr3*. The generation of conditional double knockdown mice has been established recently in our Institute and could be applied to generate FGFR2/3 double knockdown mice (Fig. 63) (Steuber-Buchberger et al., 2008).

It is also necessary to compare the pERK levels in FGFR2 forebrain mutants and in controls upon fluoxetine administration to decipher the possible effect of FGFR2 inactivation on acute cellular fluoxetine response. In addition it is important to identify which of the possible FGFR2 interaction partners are co-expressed in certain brain regions. Therefore, comparative expression analysis of *Fgfrs* together with *Fyn*, *5-HT$_6$ receptor*, *Bdnf* and its receptor *TrkB*, and *CB1R* should be done. In addition the expression of *Fgfrs* together with *Fyn* and *NCAM* in newly generated hippocampal neurons of the adult brain would give more information about possible FGFR functions in neurite growth of new neurons. Maybe also the analysis of fluoxetine effect in conditional FGFR1 and FGFR2 deficient mice regarding adult neurogenesis (dentate gyrus in FGFR1 mice; SVZ in FGFR2 mice) would help to understand the general role of FGFRs in generation of new neurons.

Finally, more behavioural and endocrinological parameters have to be analysed to get a more detailed picture of FGFR2 functions in the stress response.

5.2.2 P2RX7 and RNAi

I used the RMCE strategy to generate transgenic mice expressing U6 promoter driven *Wnt1* and *P2rx7* specific shRNAs from the *Rosa26* locus. RMCE works efficient and was already published by Hitz et al. (2007) to be feasible for the generation of shRNA transgenic mice. However, shWnt1 mice did not recapitulate the embryonic phenotype known from Wnt1 knockout mice (McMahon and Bradley, 1990; Thomas and Capecchi, 1990).

The reason why the shWnt1 knockdown mice were apparently normal was most likely due to the inefficient hairpin used to generate the shWnt1 mice. The first *in vitro* test, using the ß-Galactosidase (ß-Gal) based assay (Fig. 53, 55), showed strong silencing of the targeted *Wnt1* mRNA. I verified the results from the ß-Gal test by qReal-Time PCR quantifying the endogenous *Wnt1* mRNA. This second test showed that the used shRNA reduces the *Wnt1* mRNA by only 26% (Fig. 58). Therefore, the ß-Gal test system is not useful for our purposes. The discrepancy between the two different test systems and the failure to recapitulate the Wnt1 knockout phenotype make clear how important the pre-testing of target sequences is. In order to produce mice which are useful for further biological analysis the shRNA should be analysed as succesful as possible. Besides qReal-Time PCR the evaluation of knockdown efficiency on protein level by Western blot would have been an important additional *in vitro* test. Unfortunately there is no antibody against Wnt1 available that works in Western blots.

For the generation of shP2RX7 mice I tested the shRNA efficiency by qReal-Time PCR. Although the hairpin against *P2rx7* was cloned in the opposite direction (as compared to Rosa26 transcription and shWnt1 orientation) *P2rx7* mRNA level was strongly reduced suggesting independence of the U6-shRNA construct from the genomic environment within the Rosa26 locus. The *in vivo* silencing efficiency of the *P2rx7* hairpin differed between 88% in the brain and only 25% in the liver (Fig. 62, C, and D). One explanation for this difference could be an inhibited shP2RX7 expression in the liver or a stronger shP2RX7 expression in the brain and heart. However, since the *Rosa26* locus and the U6 promoter are both active in all tissues the shP2RX7 expression is rather not the reason (Hitz et al., 2007; Soriano, 1999). A further possibility is alternative splicing of the *P2rx7* mRNA. The qReal Time PCR was performed with primers binding to sequences in exon5 and exon6, respectively. The used *P2rx7* hairpin is directed against a sequence at the beginning of exon3. Therefore splicing out of exon3 would abolish *P2rx7* knockdown as measured by qReal Time PCR using the mentioned primers. Although 4 *P2rx7* isoforms are predicted (NM_001038845.2; NM_011027.2; NM_001038839.1; NM_001038887.1) a splice variant containing exon5 and

exon6 but lacking exon3 is not known. There are also several studies suggesting a role of double-stranded RNA adenosine deaminase (ADAR1) in RNAi and in microRNA processing and function (Bass, 2002). ADAR1 converts adenosines to inosines in double-stranded RNAs and thereby modifies the efficiency of siRNAs and microRNAs. If the used *P2rx7* hairpin could be a target for ADAR1 is not clear. Since the reduction of *P2rx7* mRNA was quite strong in the brain, these mice are a good model to study the role of P2RX7 in the adult brain and in particular in depression. The upcoming phenotypic analysis will be performed in collaboration with *Affectis Pharmaceuticals, Munich*. Upon quantification of knockdown efficiency in other tissues these mice could probably also be used for further tests to analyse the function of P2RX7 in the immune system or in activated microglia.

I further tested shRNAs directed against *Fgfr2* and *Fgfr3*, respectively (Fig. 63). Upon quantification of silencing efficiency I found hairpins against *Fgfr2* (54% knockdown) and *Fgfr3* (61% knockdown) which could be used for RMCE based generation of transgenic mice. Our observation with a ß-Gal expression plasmid was that approximately 90% of the ES cells contain the vector after electroporation (Data not shown). Therefore the silencing efficiencies of the tested shRNAs should be estimated with 60% for shFGFR2 and 70% for shFGFR3. My results together with other studies suggest that FGFR3 could partially compensate loss of FGFR2 in FGFR2 forebrain mutants (Fig. 35 - 41)(Evans et al., 2004). Assuming that all four FGFR2/3 alleles are involved in modifying depression-like behaviour in mice a conditional deletion of all four alleles would be needed to determine the function of FGF signalling in depression. In FGFR2 forebrain mutants only two alleles are deleted representing 50% reduction. The combination of shFGFR2/3 would reduce the expression of all four alleles by approximately 65% and probably induce a stronger phenotype in the FST and in response to fluoxetine. Further modifications of the tested hairpins would allow the generation of conditional knockdown mice or conditional shFGFR2/3 double knockdown mice. Generation of conditional double-knockdown mice, using the here presented U6 promoter based RMCE strategy, was already published by our group (Steuber-Buchberger et al., 2008). The conditional shFGFR2/3 double mutants, generated using Nex-Cre or CamKII-Cre mice, would be very helpful to decipher the proposed compensatory mechanisms of FGFRs in depression (Evans et al., 2004; Goebbels et al., 2006; Minichiello et al., 1999).

6 MATERIALS AND METHODS

6.1 Materials

6.1.1 Instruments and plastic ware

Materials	Supplier
autoclave	Aigner, type 667-1ST
balances	Sartorius, LC6201S, LC220-S
bottles for hybridization	ThermoHybaid
cassettes for autoradiography	Amersham, Hypercassette
cell culture dishes	Nunc
centrifuges	Sorvall, Evolution RC; Eppendorf, 5415D, 5417R; Heraeus, Varifuge 3.0R, Multifuge 3L-R
centrifuge tubes 15 ml, 50 ml	Falcon
chambers for electrophoresis (DNA)	MWG Biotech; Peqlab
cleaning columns	Amersham, MicroSpin S-300; Roche, mini Quick Spin Oligo Columns
confocal microscope	Olympus, equipped with the FluoView 1000 software
coverslips	Menzel Gläser, 24mm x 50mm; 24mm x 60mm
cryostat	Mikrom, HM560
cuvettes for electroporation	Biorad, 0.4 cm cuvettes
developer (in situ hybridization)	Kodak D19
developing machine	Agfa, Curix 60
digital camera	Zeiss, AxioCam MRc
electric homogenizer	IKA, Ultra-Turrax T25 basic
embedding pots	Polysciences, Peel-A-Way
fear potentiated startle apparatus	Med Associates Inc., Startle Stimulus Package PHM-255A, ANL-925C Amplifier
films for autoradiography	Kodak, Biomax MS, Biomax XAR, Biomax MR
films for chemiluminescence detection	Amersham, Hyperfilm
filter paper	Whatman 3MM (Kat.-Nr.:3030 917)
filter tips 20 µl, 200 µl, 1 ml	Art, Starlab
fixer (in situ hybridization)	Kodak fixer (Kat.-Nr.: 197 1720)
freezer (-20°C)	Liebherr
freezer (-80°C)	Heraeus HFU 686 Basic
fridges (4°C)	Liebherr
gel documentation system	Herolab, E.A.S.Y.
gel-/blottingsystem "Criterion" (protein)	BioRad
gel-/blottingsystem "Xcell SureLockTM Mini-Cell" (protein/RNA)	Invitrogen
glass pipettes	Hirschmann
glassware	Schott
gloves	Kimberley-Clark, Safeskin PFE, Safeskin, Nitrile
ice machine	Scotsman, AF 30
in situ robot	Tecan
incubators (for bacteria)	New Brunswick Scientific, innova 4230
incubators (for cells)	Heraeus
light source for microscopy	Leica KL 1500
liquid szintillation counter	Hidex, Triathler

luminometer	Berthold, Orion I
magnetic stirrer / heater	Heidolph, MR3001
microscope	Zeiss Axioplan 2
microwave oven	Sharp R-937 IN
motor pestle	Sigma
Neubauer counting chamber	Brand
nylon membrane for DNA transfers	Amersham, Hybond N Plus
one-way needles	Terumo, Neolus 20G, 27G
one-way syringes	Terumo, 1ml, 10ml, 20ml
oven for hybridization	Memmert, UM 400; MWG-Biotech, Mini 10; ThermoElectron, Shake'n'Stack
paraffin embedding machine	Leica, EG1160
Pasteur pipettes	Brand
PCR machine	Eppendorf, MasterCycler Gradient
PCR reaction tubes 0.2 ml	Biozym
pH-meter	InoLab, pH Level 1
photometer	Eppendorf, Biophotometer 6131
pipette tips	Gilson
pipette boy	Eppendorf, Easypet; Hirschmann, Pipettus akku
pipettes	Gilson; Eppendorf
plastic pipettes (1 ml, 5 ml, 10 ml, 25 ml)	Greiner
power supplies for electrophoresis	Consort, E443; Pharmacia Biotech, EPS200; Thermo, EC250-90, EC3000-90
PVDF membrane for Western blotting	Pall Biosciences
radiation monitor	Berthold, LB122
reaction tubes (0.5 ml, 1.5 ml, 2 ml)	Eppendorf
rotating rod apparatus	Bioseb, Letica LE 8200
shaker	Heidolph, Promax 2020
slide warmer	Adamas instrument, BV SW 85
slides	Menzel Gläser, Superfrost Plus
sonifier	Branson sonifier, cell disrupter B15
stereomicroscope	Zeiss, Stemi SV6
thermomixer	Eppendorf, comfort
tissue cassettes	Merck
tissue embedding molds	Polysciences, Inc.
ultramicrotom	Microm, HM 355S
UV-DNA/RNA-crosslinker	Scotlab, Crosslinker SL-8042; Stratagene, UV-Stratalinker 1800
UV-lamp	Benda, N-36
vortex	Scientific Industries, Vortex Genie 2
water bath	Lauda, ecoline RE 112; Leica, HI1210; Memmert, WB7
water conditioning system	Millipore, Milli-Q biocel

6.1.2 Chemicals

Chemicals	Supplier
[α-thio-35S]-ATP	Amersham
[α-thio35S]-UTP	Amersham
1kb+ DNA Ladder	Invitrogen
3,3'-diaminobenzidine (DAB)	Sigma
α-32P-dCTP	Amersham
acetic acid	Merck
acetic anhydride	Sigma
agarose (for gel electrophoresis)	Gibco Life Technologies, Biozym
ammonium acetate	Merck
ampicillin	Sigma
Ampuwa	Fresenius
bacto agar	Difco
bacto peptone	BD Biosciences
BCIP	Roche
bicine	Fluka
bis-tris	Sigma
β-Mercaptoethanol	Sigma, Gibco
boric acid	Merck
bovine serum albumin (BSA)	NEB (20 mg/ml), Sigma
bromphenol blue	Sigma
calcium chloride ($CaCl_2$)	Sigma
carrier DNA	Sigma
chlorobutanol	Sigma
Complete® Mini (protease inhibitors)	Roche
cresyl violet acetate	Sigma
CriterionTM XT Bis-Tris-gels, 10% (protein)	BioRad
dextran sulphate	Sigma
dithiotreitol (DTT)	Roche
DIG RNA Labeling Mix	Roche
DIG-11-UTP	Roche
DIG-labeled control RNA	Roche
DMEM	Gibco
DNase I, RNase free	Roche
DMSO	Sigma
dNTP (100 mM dATP, dTTP, dCTP, dGTP)	MBI
DPX	Fluka
EDTA	Sigma
EGTA	Sigma
ethanol absolute	Merck
ethidiumbromide	Fluka
ethylene glycol	Sigma
fetal calf serum (FCS)	PAN
Ficoll 400	Sigma
Fluoxetine HCl	Sigma
formamide	Sigma
freezing medium	Tissue Tek, OCT compound
FuGENE 6 transfection reagent	Roche
γ-32P-dATP	Amersham
gelatin	Sigma
glucose	Sigma
glutaraldehyde	Sigma
glycerol	Sigma
Hepes	Gibco
hydrochloric acid (HCl)	Merck
hydrogen peroxide, 30%	Sigma

iodacetamide	Sigma
isopropanol	Merck
kanamycin	Sigma
Levamisole	Sigma
magnesium chloride ($MgCl_2 \cdot 4H_2O$)	Merck
MEM nonessential aminoacids	Gibco
MES hydrate	Sigma
methanol	Merck
MOPS	Sigma
NBT (4-NBT)	Roche
Nonidet P40 (NP-40)	Fluka
NuPAGE® Novex Bis-Tris gels, 10% (protein)	Invitrogen
orange G	Sigma
PBS (for cell culture)	Gibco
PIPES	Sigma
Paraformaldehyde	Sigma
polyvinylpyrrolidone 40 (PVP 40)	Sigma
potassium chloride (KCl)	Merck
potassium ferricyanid ($K_3Fe(CN)_6$)	Sigma
potassium ferrocyanid ($K_4Fe(CN)_6 \cdot 3H_2O$)	Sigma
potassium hydroxid (KOH)	Sigma
potassium phosphate ($KH_2PO_4 \cdot H_2O$, K_2HPO_4)	Roth
pregnant mare's serum gonadotropin (PMSG)	Intervet
RapidHyb buffer	Amersham
Renaissance Individual Indirect Tyramide Reagent Pack	NEN
RNaseZAP®	Sigma
RotiHistoKit® I	Roth
RotiHistol®	Roth
salmon sperm DNA	Fluka
SeeBlue® Plus2 Prestained protein ladder	Invitrogen
skim milk powder	BD Biosciences
SmartLadder DNA marker	Eurogentec
sodium acetate (NaOAc)	Merck, Sigma
sodium chloride (NaCl)	Merck
sodium citrate	Sigma
sodium desoxycholate	Sigma
sodium dodecylsulfate (SDS)	Merck
sodium hydroxide (NaOH)	Roth
sodium phosphate ($NaH_2PO_4 \cdot H_2O$, Na_2HPO_4)	Sigma
spermidin	Sigma
sucrose	Sigma
TBE urea gels, 15% (RNA)	Invitrogen
TBE urea sample buffer (2x)	Invitrogen
triethanolamine	Merck
TriReagent	Sigma
Tris (Trizma-Base)	Sigma
Triton-X 100	Biorad
Trizol	Invitrogen
tRNA	Roche
trypsin	Gibco
tryptone	BD Biosciences
Tween 20	Sigma
xylol	Merck
yeast extract	Difco

Kits	Supplier
β-Gal reporter gene assay	Roche
DNA Maxi Prep Kit	Qiagen
DNA Highspeed Maxi Prep Kit	Qiagen
DNA Mini Prep Kit	Qiagen
ECL Detection Kit	Amersham
QIAquick Gel Extraction Kit	Qiagen
mirVana™ miRNA Isolation Kit	Ambion
NorthernMax®-Gly Kit	Ambion
PCR Purification Kit	Qiagen
RediPrime DNA Labeling Kit	Amersham
RNeasy Mini Kit	Qiagen
SuperScript First-Strand Synthesis System for RTPCR	Invitrogen
TOPO TA Cloning Kit	Invitrogen
Vectastain Elite ABC Kit	Vector Labs
Wizard Genomic DNA Purification Kit	Promega

Stock solutions

loading buffer (5x) for agarose gels (DNA):
15% Ficoll 400
200 mM EDTA
1 - 2% orange G

loading buffer (10x) for MOPS agarose gels (RNA):
50% Glycerol
1 mM EDTA, pH 8.0
0.25% Bromphenole blue
0.25% Xylene cyanol FF
in RNase free water

paraformaldehyde solution (PFA, 4%):
4% PFA w/v in PBS

PBS (1x):
171 mM NaCl
3.4 mM KCl
10 mM Na_2HPO_4
1.8 mM KH_2PO_4
pH 7.4

SSC (saline sodium citrate, 20x):
3 M NaCl
0.3 M sodium citrate
pH 7.0

sucrose solution (20% or 25%):
20% / 25% sucrose w/v in PBS

TAE (10x):
0.4 M Tris base
0.1 M acetate
0.01 M EDTA

TBE (10x):
0.89 M Tris base
0.89 M boric acid
0.02 M EDTA

TBS (10x):
0.25 M Tris-HCl pH 7.6
1.37 M NaCl

TBS-T (1x):
1 x TBS
0.05% Tween 20

TE (Tris-EDTA):
10 mM Tris-HCl pH 7.4
1 mM EDTA

Tris-HCl:
1 M Tris base
pH 7.5

solutions for work with Bacteria

LB medium (Luria-Bertani):
10 g Bacto peptone
5 g yeast extract
5 g NaCl
ad 1 l H_2O

LB agar:
98.5% LB medium
1.5% Bacto agar
pH 7.4

LB_{amp} medium:
LB medium with 50 µg/ml ampicillin

LB_{amp} agar:
LB agar with 100 µg/ml ampicillin

LB_{kan} medium:
LB medium with 25 µg/ml kanamycin

LB_{kan} agar:
LB agar with 50 µg/ml kanamycin

$CaCl_2$ solution:
60 mM $CaCl_2$
15% glycerol
10 mM PIPES pH 7.0
autoclave or filter sterile

Solutions for cell culture

F1 medium:
15% FCS (PAN)
20 mM Hepes
1x MEM nonessential aminoacids
0.1 mM β-mercaptoethanol
1500 u/ml LIF
in DMEM

feeder medium:
10% FCS in DMEM

freezing medium (1x):
15% FCS (PAN)
10% DMSO
in DMEM

Luciferase assay buffer:
25 mM glycylglycine
15 mM potassium-phosphate pH 8.0
4 mM EGTA
2 mM ATP
1 mM DTT
100 µM coenzyme A
75 µM luciferin
pH 8.0

gelatin solution:
1% gelatin in H_2O

Solutions for Southern blot

Church buffer:
0.5 M Na_2HPO_4
0.5 M NaH_2PO_4
1% BSA
7% SDS
1 mM EDTA pH 8.0
0.1 mg/ml salmon sperm DNA

Denaturation solution:
0.5 M NaOH
1.5 M NaCl

Neutralizing solution:
0.1 M Tris-HCl pH 7.5
0.5 M NaCl

Stripping solution:
0.4 M NaOH

Wash solution I:
2 x SSC
0.1% SDS

Wash solution II:
0.2 x SSC
0.1% SDS

Solutions for Western blot

Blocking solution milk:
4% skim milk powder in TBS-T

Blocking solution BSA:
5% BSA in TBS-T

Tris glycine blotting buffer (10x):
0.25 M Tris
1.92 M glycine

Tris glycine blotting buffer (1x):
10% 10 x blotting buffer
10% methanol

Laemmli buffer (5x):
313 mM Tris-HCl pH 6.8
50% glycerol
10% SDS
0.05% bromphenolblue
25% ß-mercaptoethanol

RIPA buffer:
50 mM Tris-HCl pH 7.4
1% NP-40
0.25% sodium desoxycholate
150 mM NaCl
1 mM EDTA
1 tablet Complete protease inhibitor
in 50 ml H_2O

NuPAGE transfer buffer (10x, for NuPAGE gels):
250 mM bicine
250 mM bis-tris
10 mM EDTA
0.05 mM chlorobutanol

NuPAGE transfer buffer (1x, for NuPAGE gels):
10% 10 x transfer buffer
10% methanol

MOPS running buffer (10x, for Criterion gels):
500 mM MOPS
500 mM Tris
1% SDS
10 mM EDTA
pH 7.7

10X MOPS:
0,2 M 3-Morpholinopropansulfonsäure
50 mM Natriumacetat
10 mM EDTA

MES running buffer (10x, for NuPAGE gels):
500 mM MES
500 mM Tris
1% SDS
10 mM EDTA
pH 7.2

Solution for ISH (DIG labelled probes)

2x PK buffer:
100 mM Tris
10 mM EDTA pH 8.0

PBT:
1 x PBS + 0.05% Tween20

5 x NTE:
2.5 M NaCl
50 mM Tris 8.0
25 mM EDTA

10 x TN:
1 M Tris
1.5 M NaCl
Solve TN 1h at 60^0C

TNT:
1 x TN + 0.05 % Tween-20

TNB:
1 x TN + 0.5 % Blocking reagent (NEN)

TMN (or MTN):
0,1 M Tris
0,1 M NaCl
0,05 M $MgCl_2$-$6H_2O$

Maleat buffer:
150 mM NaCl
100 mM Maleinsäure
pH 7.5

Blocking reagent in Maleat buffer:
Maleat buffer + 1% Blocking reagent (Roche).
Heat in water bath (60°C) to solve, store at 4°C and filter (45 µm) before use.

TBST:
TBS + 1% Tween20

Levamisol
200 mM Levamisol in H_2O

Proteinase K
2 mg/ml in H_2O

Solution for Immunohistochemistry

Cryo-protection solution:
30% ethylene glycol
30% glycerol
0.1M PBS

DAB stock solution:
1% DAB
in Tris-HCl, pH 7.4

Solution for Nissl staining

cresylviolet staining solution:
0.5% cresylviolet
2.5 mM sodium acetate
0.31% acetic acid
ad 500 ml H_2O
filter before use

Enzymes	Supplier
alkaline phosphatase	Shrimp alkaline phosphatase (SAP), Roche
DNase I (RNase-free)	Roche
Klenow fragment of DNA Polymerase I	NEB
PCR-Mastermix 5x	Eppendorf
polynucleotide kinase (PNK)	NEB
proteinase K	Roche
restriction enzymes	Roche, MBI, NEB
RNA polymerases (T7, SP6)	Roche
RNase A	Serva
RNasin RNAse inhibitor	Roche
RNeasy Mini Kit	Qiagen
T4 DNA ligase	NEB
terminal transferase	Roche

6.1.3 Antibodies

antigen	species	dilution	company
Calbindin D-28k	rabbit	1:2000	Swant (CB-38a)
Calbindin D-28k	mouse	1:2000	Sigma (C9848)
Calretinin	rabbit	1:2000	Swant (7699/4)
DIG-Pod, Fab Fragment	sheep	1:600	Roche (1207733)
Doublecortin (DCX)	goat	1:200	Santa Cruz (sc-8066)
FgfR2 (c-terminus)	rabbit	1:200	Santa Cruz (sc-122)
Glial fibrillary acidic prot. (GFAP)	mouse	1:100	Sigma (G3893)
HPRT	rabbit	1:400	Santa Cruz (sc-20975)
Neurofilament	mouse	1:50	DSHB (2H3)
Neuronal nuclei (NeuN)	mouse	1:200	Chemicon (MAB377)
Parvalbumin	rabbit	1:2000	Swant (PV28)
S100ß	mouse	1:1000	Sigma (S2532)

6.1.4 In situ probes

probe (gene)	NCBI Accession No.	Enzyme and RNA Polymerase for antisense probe	provided by
Engrailed1 (En1)	NM_010133	HindIII, T7	A. Joyner
Fgf8	NM_010205	PstI, T7	A. Tanaka
Fgfr1 (all isoforms)	NM_010206	NdeI, T7	R. Lauster
Fgfr2 (all isoforms)	BC091652	BamHI, T7	C. Dickson
Fgfr2 (exon5)	MMY16155	EcoRV, Sp6	A. Blak
Fgfr3 (all isoforms)	NM_008010	HindIII, T7	D. Ornitz
Fgfr4	NM_008011	NotI, T3	A. Blak
GAD65	MUSGAD65A	BamHI, T3	J. Guimera
MKP3	BC003869	SalI, T7	J. A. Belo
SERT	AF013604	HindIII, T7	C. Brodski
Sprouty1	NM_011896	EcoRI, T7	G. Martin
Sef1	AF459444	NcoI, Sp6	R. Friesel
TH	NM_009377	SphI, Sp6	J. Guimera
Wnt1	NM_021279	HindIII, T7	C. Brodski
VAChT	NM_021712	NotI, Sp6	C. Brodski

6.1.5 PCR primers and conditions

PCR	Primer	Sequence	Temp	Time	Cycles
Fgfr2 genotyping	R2 forward	CTAGGCCAGCTGGACCAGAC	94°C	1`	
	R2 reverse	CGTTCTCTGATGGGCCATTG	58°C	1`	35X
			72°C	1`30``	
Cre genotyping	pCre1	ATGCCCAAGAAGAAGAGGAAGGT	94°C	30``	
	pCre2	GAAATCAGTGCGTTCGAACGCTAGA	55°C	40``	30X
			72°C	1`	
RMCE genotyping (acceptor allele)	hygro1	GAAGAATCTCGTGCTTTCAGCTTCGATG	94°C	1`	
	hygro2	AATGACCGCTGTTATGCGGCCATTG	65°C	1`	30X
			72°C	1`	
shRNA genotyping	exneo2	GTTGTGCCCAGTCATAGCCGAATAG	94°C	1`	
	expgk3	CACGCTTCAAAAGCGCACGTCTG	65°C	1`	30X
			72°C	1`	
shRNA genotyping	U6 for	GAGGGCCTATTTCCCATGAT	94°C	1`	
	Rosa3`rev2	ACTCCCGCCCATCTTCTAG	57°C	1`	30X
			72°C	1`20``	
shRNA genotyping (inverted shRNA)	expgk3	CACGCTTCAAAAGCGCACGTCTG	94°C	1`	
	U6 for	GAGGGCCTATTTCCCATGAT	60,5°C	1`	35X
			72°C	1`30``	
shRNA genotyping (inverted shRNA)	U6 for	GAGGGCCTATTTCCCATGAT	94°C	1`	
	bpA for	GGGAGGATTGGGAAGACAAT	57°C	1`	30X
			72°C	1`	
semiq. RT-PCR P2rx7	P2X7_for	AAACAAAGTCACCCGGATCCA	94°C	1`	
	P2X7_rev	CCGTCACCTCTGCTATGCCTT	56°C	1`	30X
			72°C	45``	
semiq. RT-PCR HPRT	HPRT for	GTTGGATACAGGCCAGACTTTGT	94°C	1`	
	HPRT rev	CCACAGGACTAGAACACCTGCTA	56°C	1`	30X
			72°C	45``	

6.1.6 Sequencing primers

Sequencing reactions were performed by Sequiserve (Vaterstetten, Germany). The following standard primers were used for sequencing:

M13for	TGTAAAACGACGGCCAGT
M13rev	CAGGAAACAGCTATGACC
SP6	ATTTAGGTGACACTATAG
T7	TAATACGACTCACTATAGGG
T3	ATTAACCCTCACTAAAGGGA

6.1.7 shRNA sequences

The selection and design of shRNA target sequences was done using prediction programs e.g. from Sigma-Aldrich (http://www.sigmaaldrich.com/Brands/Sigma_Genosys/siRNA_Oligos) or Invitrogen (https://rnaidesigner.invitrogen.com/sirna/) or. These programs propose several possible shRNA sequences with different probabilities of their knockdown efficiency. I chose high ranked sequences beginning with a G with a length of 20 or 21 nt. All oligonucleotide sequences used in this study are presented with the upper sense strand and the lower antisense strand in 5` (left) → 3` (right) direction. The following colour code was used: green: sense sequence; black: loop region (HindIII recognition site is underlined); red: antisense sequence; and violet: linker sequence for cloning into the vector pBS-U6.

shWnt1/1

CTGCAGTGACAACATCGATTGAAGCTTGAATCGATGTTGTCACTGCAGCTTTTTTGGAAA

GATCTTTCCAAAAAAGCTGCAGTGACAACATCGATTCAAGCTTCAATCGATGTTGTCACTGCAGCG

shWnt1/2

CGTTCTGCACGAGTGTCTATGAAGCTTGATAGACACTCGTGCAGAACGCTTTTTTGGAAA

GATCTTTCCAAAAAAGCGTTCTGCACGAGTGTCTATCAAGCTTCATAGACACTCGTGCAGAACGCG

shWnt1/3

GTATTATCACCTTTCCTTGTGAAGCTTGACAAGGAAAGGTGATAATACCTTTTTTGGAAA

GATCTTTCCAAAAAAGGTATTATCACCTTTCCTTGTCAAGCTTCACAAGGAAAGGTGATAATACCG

shP2rx7/1

GAACTCATTCTTTGTCATGAGAAGCTTGTCATGACAAAGAATGAGTTCCTTTTTTGGAAA

GATCTTTCCAAAAAAGGAACTCATTCTTTGTCATGACAAGCTTCTCATGACAAAGAATGAGTTCCG

shP2rx7/2

GATGACAAGAACATGGATGAGAAGCTTGTCATCCATGTTCTTGTCATCCTTTTTTGGAAA

GATCTTTCCAAAAAAGGATGACAAGAACATGGATGACAAGCTTCTCATCCATGTTCTTGTCATCCG

shP2rx7/3

GACGTTGATCAAAGCCTTCGGAAGCTTGCGAAGGCTTTGATCAACGTCCTTTTTTGGAAA

GATCTTTCCAAAAAAGGACGTTGATCAAAGCCTTCGCAAGCTTCCGAAGGCTTTGATCAACGTCCG

shP2rx7/4

CATTGACTTGCTCATCAACAGAAGCTTGTGTTGATGAGCAAGTCAATGCTTTTTTGGAAA

GATCTTTCCAAAAAAGCATTGACTTGCTCATCAACACAAGCTTCTGTTGATGAGCAAGTCAATGCG

shP2rx7/5

CACAGTGAACGAGTATTACTGAAGCTTGAGTAATACTCGTTCACTGTGCTTTTTTGGAAA

GATCTTTCCAAAAAAGCACAGTGAACGAGTATTACTCAAGCTTCAGTAATACTCGTTCACTGTGCG

shP2rx7/6

CAAGTTGTCAAAGGCCAAGAGAAGCTTGTCTTGGCCTTTGACAACTTGCTTTTTTGGAAA

GATCTTTCCAAAAAAGCAAGTTGTCAAAGGCCAAGACAAGCTTCTCTTGGCCTTTGACAACTTGCG

shFgfr2/1

GGTGTTAATGTGGGAGATCTGAAGCTTGAGATCTCCCACATTAACACCCTTTTTTGGAAA

GATCTTTCCAAAAAAGGGTGTTAATGTGGGAGATCTCAAGCTTCAGATCTCCCACATTAACACCCG

shFgfr2/2

CACCAATGAACTGTACATGAGAAGCTTGTCATGTACAGTTCATTGGTGCTTTTTTGGAAA

GATCTTTCCAAAAAAGCACCAATGAACTGTACATGACAAGCTTCTCATGTACAGTTCATTGGTGCG

shFgfr2/3

CATCGCATTGGAGGCTATAAGAAGCTTGTTATAGCCTCCAATGCGATGCTTTTTTGGAAA

GATCTTTCCAAAAAAGCATCGCATTGGAGGCTATAACAAGCTTCTTATAGCCTCCAATGCGATGCG

shFgfr2/4

GCCTCAGCGTTCCTGAGCGGAAGCTTGCGCTCAGGAACGCTGAGGCCTTTTTTGGAAA

GATCTTTCCAAAAAAGGCCTCAGCGTTCCTGAGCGCAAGCTTCCGCTCAGGAACGCTGAGGCCG

shFgfr3/1

CAAGCACAAGAACATCATTAGAAGCTTGTAATGATGTTCTTGTGCTTGCTTTTTTGGAAA

GATCTTTCCAAAAAAGCAAGCACAAGAACATCATTACAAGCTTCTAATGATGTTCTTGTGCTTGCG

shFgfr3/2

CTCACCTGCAAGGATCTAGTGAAGCTTGACTAGATCCTTGCAGGTGAGCTTTTTTGGAAA

GATCTTTCCAAAAAAGCTCACCTGCAAGGATCTAGTCAAGCTTCACTAGATCCTTGCAGGTGAGCG

shFgfr3/3

GAGCTGATGGAAACTGATGAGAAGCTTGTCATCAGTTTCCATCAGCTCCTTTTTTGGAAA

GATCTTTCCAAAAAAGGAGCTGATGGAAACTGATGACAAGCTTCTCATCAGTTTCCATCAGCTCCG

shFgfr3/4

CAGTTGGTAGAGGATTTAGAGAAGCTTGTCTAAATCCTCTACCAACTGCTTTTTTGGAAA

GATCTTTCCAAAAAAGCAGTTGGTAGAGGATTTAGACAAGCTTCTCTAAATCCTCTACCAACTGCG

6.2 Methods

6.2.1 Molecular biology

6.2.1.1 General methods for the work with DNA

Determination of the concentration of nucleic acids

Concentrations of nucleic acids were determined by measuring the optical density (OD) in a photometer at the wavelength of 260 nm. OD260 of 1 corresponds to 50 µg double stranded DNA per ml, 33 µg single stranded DNA per ml, and 40 µg RNA per ml, respectively. Purity of DNA was assessed by the relation of OD260/OD280, which should not exceed a value of 1.8.

Preparation of plasmid DNA

DNA mini- or maxi-preps were carried out with the corresponding Qiagen kits following manufacturer's instructions. For mini-preps 2 ml of an overnight culture of bacteria were used, for maxi-preps 200 ml cultured bacteria were applied.

Isolation of genomic DNA

For isolation of genomic DNA from all kinds of tissues and ES cells (mouse tails, mouse brain tissue) the Wizard genomic DNA purification kit was used following manufacturer's instructions. To isolate genomic DNA from ES cells, cells from a 24- well or a 6-well were used. For mouse brain tissue, the brain (or parts of it) was first homogenized with a small motor pestle in PBS and then only a small portion of the homogenate was used for further proteinase K digestion and DNA extraction.

Precipitation of DNA

0.1 Vol. 3M sodium acetate (NaOAc), pH 5.2, and 3 Vol. 100% Ethanol (EtOH) were added to the solution containing the DNA to be precipitated. The mixture was shortly vortexed and incubated for 1 hour to overnight at -20°C. Then the DNA was pelleted at 14.000 x g for 10 min and washed with 70% EtOH. The pellet was air dried and solved in an appropriate buffer (e.g. TE).

Restriction digests of plasmid-DNA

Reaction conditions, amount of enzyme and type of buffer were applied following manufacturer's instructions. Samples were digested for 2 hours or overnight at 37°C (unless other temperature was recommended for the enzyme). For each µg of DNA and for each restriction site in the plasmid 2 u of enzyme were used. For the digestion of genomic DNA a separate protocol was used. If necessary, sticky vector ends were blunted with Klenow fragment of DNA polymerase I. Therefore, 5 u of Klenow and 25 nMol dNTPs were added after the restriction digest and incubated for 20 min at RT.

Gel electrophoresis of DNA fragments

For electrophoretical separation of DNA fragments according to their size, DNA samples were run on agarose gels and stained with ethidium bromide either in the gel itself or in the running buffer. Standard gels were of 1% agarose in 1x TAE buffer, for a better resolution of bands of similar size agarose concentrations of 2% were used. DNA samples were loaded on the gel with 5x loading buffer, the 1kb+ ladder or the Smartladder (for Southern blotting) were used as length standard and a voltage of 80- 120 V was applied for 30 min to several hours depending on the sizes of the DNA fragments to be separated. Pictures of the gels were taken on a UV desk with short wave UV radiation (254 nm).

Isolation of DNA fragments from agarose gels

To isolate DNA fragments of a specific size from agarose gels, the bands were visualized on long wave UV radiation (366 nm) to prevent damage of the DNA. The band of interest was cut out with a clean scalpel and elution of DNA was performed using the Qiagen Gel Extraction Kit following manufacturer's instructions.

Dephosphorylation of DNA fragments

During cloning of DNA fragments religation of an open vector should be minimized. With alkaline phosphatase (SAP, shrimp alkaline phosphatase) the terminal phosphates of the DNA can be removed, so that DNA ligase cannot join these ends with each other. For this purpose 0.1 u SAP were added to the vector DNA after digestion and incubated for 60 min at 37°C. For inactivation of the enzyme 5 mM EDTA pH 8.0 were added and the sample was heated to 75°C for 20 min.

Ligation of DNA fragments

To ligate a DNA fragment into a vector, linearised vector and insert DNA were used in a molar ratio of approximately 1:3. The reaction was performed by T4 DNA ligase at RT for 15 min for sticky ends and 30 min for blunt ends using 400 u and 100 to 200 ng of DNA in total. For the cloning of PCR fragments, the TOPO TA Cloning Kit was used. The linearised vector conjugated with Topoisomerase I allows subcloning without ligase. The reaction was performed following manufacturer's instructions.

Polymerase chain reaction (PCR)

For amplification of DNA fragments from either genomic DNA or vector DNA, polymerase chain reaction (PCR) was performed. About 20-400 ng of DNA template were used with the Eppendorf 5x PCR Mastermix in 25 µl total reaction volume. The following example program shows a general PCR program:

3 min	94°C	(initial melting of the template DNA)
1 min	94°C	(cyclic melting of the template DNA)
30 x 40 sec	xx°C	(annealing, dependent on primer sequence)
1 min	72°C	(template dependent elongation)
10 min	72°C	(terminal elongation / completion)
∞	4°C	(cooling until processing)

The specific conditions for each pair of primers are listed in materials.

6.2.1.2 General methods for the work with RNA

For all RNA work RNase free solutions, tubes and pipette tips were used. Glass and plastic equipment was cleaned with RNaseZAP® and fresh MilliQ water before use.

RNA extraction from cells and tissues

Cells were trypsinised and pelleted by centrifugation. Mice were asphyxiated with CO2, decapitated, and the brain was dissected removing bones and meninges. The whole brain or dissected parts of it were immediately frozen on dry ice or liquid nitrogen to prevent degradation of RNA. Tissue was processed directly or stored at -80°C.

Isolation of total RNA

Total RNA from cells or mouse tissue was extracted with RNeasy Mini Kit from Qiagen following manufacturer's protocol. RNA concentration was determined using a photometer, where an OD260 of 1 corresponds to 40 µg RNA per ml. RNA quality was controlled by electrophoresis. With non degraded RNA the ribosomal band are clearly visible under UV light after ethidium bromide staining. Isolated RNA was stored at -80°C if not processed immediately.

RNA agarose gels

RNase free 1xMOPS buffer containing 1% agarose was heated in a microwave and let cool down to 60°C. 3% Formaldehyde (37.5%) and ethidium bromide was added and filled into a clean gel chamber.

Reverse transcription (RT) of mRNA into cDNA

cDNA was generated by reverse transcription of mRNA by SuperScriptII, a reverse transcriptase. Approximately 1 µg of total RNA were incubated with random hexamer primers, dNTPs, SuperScriptII, and the corresponding buffers at 42°C following manufacturer's instructions. The RNA template was digested by RNase H incubation, and the quality of the cDNA was checked on an agarose gel before using it for further PCR reactions. 1 µl cDNA was used for semiquantitative RT PCR analysis.

Quantitative Real Time RT-PCR (qRT-PCR)

For qRT-PCR of *in vitro* samples cells were lysed using "Invisorb RNA Cell HTS 96-Kit/C" according to manufacturer's protocol (Invitec, Berlin, Germany). Lysates were stored at -80°C and qRT-PCR was performed by Cenix Biosciences (Dresden). The following primer pairs were used for *P2rx7* P2RX7-F 5`- ttgcacatgatcgtcttttcct -3` and P2RX7-R 5`- tgcagtgtcaaagatgctgtgt -3`. For qRT-PCR of *in vivo* samples RNA extraction from tissue was performed following RNeasy protocols (Qiagen) and RNA was stored at -80°C. For reverse transcription of RNA the High-Capacity cDNA Reverse Transcription Kit (Applied Biosystems) was used and qRT-PCR with Taqman universal PCR Master Mix (Applied Biosystems) was performed on a Thermo-Cycler (7900 HT Real-Time PCR System, Applied Biosystems). We used the Taqman(R) Gene Expression Assay for specific amplification of P2rx7 products (Assay Id: Mm00440582_m1; Applied Biosystems).

6.2.1.3 Methods for the work with bacteria

Production of competent bacteria

E.coli bacteria (DH5α) were cultivated on a LB agar plate without antibiotics overnight at 37°C. One single colony was inoculated to 5 ml LB medium and again incubated overnight on a shaker. 4 ml of this culture were added to 400 ml of fresh LB medium and incubated on a shaker for several hours. When the cell suspension reached absorption of 0.375 at 590 nm, but not higher than 0.4, bacteria were transferred to precooled 50 ml tubes, chilled on ice for 5-10 min and centrifuged (1,600x g, 7 min, 4°C). Each pellet was carefully resuspended in 10 ml ice-cold CaCl2 solution. Cells were centrifuged again (1,100x g, 5 min, 4°C) and each pellet was resuspended in 2 ml ice-cold CaCl2 solution. Bacteria were then ready for direct transformation or were aliquoted and frozen at -80°C.

Transformation of competent bacteria

50 µl suspension of competent bacteria were carefully thawed on ice and approximately 25 ng of plasmid DNA were added. The sample was mixed carefully and incubated on ice for 10 min. After a heat shock (90 sec at 42°C) and chilling on ice 1 ml LB medium were added. Bacteria were incubated at 37°C for 45 min gently shaking. Then the transformed bacteria were plated on LB plates containing an appropriate antibiotic and incubated overnight at 37°C.

6.2.1.4 Analysis of genomic DNA by Southern blotting

Restriction digest and blotting of genomic DNA

8-20 µg of genomic DNA were digested with an appropriate restriction enzyme in 30 µl total volume. For better restriction accuracy 3.3 mM spermidine was added to the sample and DNA was digested for 3 hours to overnight at 37°C. Cleaved DNA was run on a 0.8% agarose/TBE gel for 14 to 20 hours at 30 to 50 V, depending on the length of the expected bands. For a higher blotting efficiency of large DNA fragments, the gel was agitated in 0.25 M HCl for 30 min to depurinate the DNA. After a brief rinse in H2O, DNA on the gel was denatured for 1 hour in denaturing solution and neutralized again for 1 hour in neutralization solution. Single stranded DNA was then blotted overnight via capillary transfer using 20x SSC and a nylon membrane. After DNA transfer the membrane was briefly rinsed with 2x SSC and UV cross-linked, before proceeding with the hybridization.

Production of radioactive DNA probes

50-100 ng of DNA probe was radioactively labelled with α-32P-dCTP using the Rediprime II labelling kit following manufacturer's instructions. Unincorporated radioactive nucleotides were removed by centrifugation with a Microspin S-300 column. 1 µl of the probe was measured in a liquid scintillation counter to determine the labelling efficiency. 200,000-800,000 cpm/ml Church buffer were used for hybridization. Probe that was not used immediately was stored at -20°C for up to 2 weeks.

Hybridization

The membrane was prehybridised with Church buffer in a hybridization bottle for at least 1 hour at 65°C. After denaturing the labelled DNA probe at 95°C and chilling it on ice, the probe was added to the Church buffer and the membrane was hybridized at 65°C for 5 hours to overnight. To eliminate unspecifically hybridized probe, the membrane was washed with wash solution I 2 x for 30 min at 65°C. If necessary a third washing with wash solution II was added. If the membrane should be used again for hybridization with another probe after the first hybridization step, the old signal could be washed away with stripping solution. After 20 min at RT in the stripping solution the membrane was briefly rinsed with 2x SSC and hybridization was performed as described above, starting with prehybridising.

Autoradiography

The hybridized membrane was wrapped in transparent films and exposed to an autoradiography film for 1-3 days at -80°C. For weak signals the Biomax MS film was used together with a Biomax screen to intensify the signal 6x compared to a conventional film without enhancer screen. After exposition the film was developed in a developing machine.

6.2.1.5 Analysis of protein by Western blotting

Preparation of protein and determination of protein concentration

Tissue and protein samples were kept on ice during all steps of preparation. ES cells were homogenized in RIPA buffer by pipetting and cell debris in the homogenate was pelleted by centrifugation for 15 min at 4°C (13,000 rpm). For mouse brains (whole brains or brain parts), tissue was homogenized in RIPA buffer with a small motor pestle or an electrical homogenizer depending on the volume of buffer. For 1 g of tissue approximately 10 µl of buffer were used. DNA in the homogenate was sheared by sonification and cell debris was pelleted by centrifugation. The supernatant containing the proteins was removed and stored at -20°C. For determination of protein concentration with the BCA protein assay kit 1 µl of protein was mixed with 49 µl of RIPA buffer as diluent and 1 ml of BCA working reagent was added. Samples were incubated at 37°C in a water bath for 30 min, cooled down to RT and absorption was measured at 562 nm in a photometer. A BSA standard curve, included in each measurement, was used to correlate the absorption to the protein concentration.

SDS polyacrylamide gel electrophoresis (SDS-PAGE) and blotting

Proteins were separated according to their size with SDS-PAGE (Laemmli, 1970). The precasted gel systems from Invitrogen (NuPAGE® Novex) and Biorad (CriterionTM XT) were used. 50 µg of total protein were mixed with 1/5 of 5x Laemmli buffer, denatured at 95°C for 3-5 min, chilled on ice and loaded onto the gel. As molecular weight marker 5 µl of the SeeBlue® Plus2 standard were loaded. After running the gel at 200 V for 1-1.5 hours, the gel was blotted on a PVDF membrane, which has been activated by soaking in 100% methanol. Blotting was performed at 30 V for 1 hour with the module from Invitrogen or at 50 V for 2 hours to overnight with the Biorad apparatus. When the blotting time exceeded 2 hours, it was performed at 4°C, otherwise at RT.

Immunochemical reaction

After blocking the membrane with 4% skim milk (5% BSA for phospho-proteins) in TBS-T for ½ hour (RT) to overnight (4°C) to prevent unspecific signals, the membrane was incubated for 1 hour with the first antibody in TBS-T, washed with TBS-T, incubated with the second horseradish-peroxidase-conjugated antibody for 45 to 60 min in TBS-T and washed again with TBS-T. The detection reaction was initiated with ECL detection reagent following manufacturer's instructions and the membrane was exposed to a chemiluminescent film for 5 sec to several minutes, depending on the signal intensity. Films were then developed with a developing machine.

6.2.2 ES cell culture

Pluripotent embryonic stem (ES) cells represent the inner cell mass of blastocysts and are able to differentiate into divergent cell types *in vivo* as well as *in vitro*. Nevertheless it is possible to cultivate ES cells and keep them undifferentiated (Smith and Hooper, 1987; Williams et al., 1988). Therefore they are cultivated under special conditions. Here, the cultivating medium was supplemented with Leukemia inhibiting factor (LIF), specially tested fetal calf serum (FCS) was used, and ES cells were grown on feeder cells at 37°C and 5% CO2. During expansion, ES cells were splitted every two days to avoid confluent growing, which would give rise to differentiation of the cells. By injecting genetically modified ES cells into blastocysts, the ES cells can contribute to all cell lineages, including germ cells. After implanting of these early embryos into the uterus of pseudo-pregnant foster mothers, chimeras are born, which consist partly of cells derived from the blastocyst used for injection and partly of cells derived from the ES cells. Germline chimeras transmit an ES cell derived mutant chromosome to their progeny, which then consist to 100% of the mutant cells. The mouse ES cell line IDG3.2, used here, originates from the F1 generation of the mouse strains C57Bl/6J and 129SvEv/Tac. ES cells were not only used for the generation of genetically modified mice, but also for test experiments to determine the efficiency of different hairpin constructs. Whereas ES cells for mouse generation were always grown on a monolayer of feeder cells, ES cells for transient experiments were grown on gelatine coated cell culture dishes without feeder cells. Therefore the dish was coated with 1% gelatine solution before the solution was sucked off again and the ES cells were plated.

6.2.2.1 **Preparation of feeder cells**

Feeder cells are mouse fibroblast cells, which have been mitotically inactivated by mitomycin c treatment. Primary neomycin resistant fibroblasts were obtained from embryos of the transgenic mouse strain C57Bl/6J-Tg(pPGKneobpA)3Ems/J at the age of E14.5 to E16.5 under sterile conditions. Cultivated primary fibroblasts were expanded for two passages and grown on 10 cm cell culture dishes until confluence. Cells were incubated with medium containing 10 µg/ml mitomycin c for 2 hours at 37°C. After intensive washing with PBS, feeder cells were trypsinised and plated on a fresh culture dish or frozen at -80°C (in 1x freezing medium) for later use. Feeder cells were plated at a density of 2-2.5 x 104 cells/cm2 at least several hours (better one day) prior to plating of ES cells.

6.2.2.2 **Splitting of ES cells**

For expansion, cells were splitted every two days when colonies have grown nicely but not yet to confluence. The medium was suck off, cells were washed with PBS and trypsinised for 5 min at 37°C until cells detached from the surface. The reaction was stopped by adding an equal amount of medium to the cells and the suspension was resuspended carefully by pipetting and splitted on several fresh culture dishes depending on the desired amount of cells per dish. For determination of cell number, 10 µl of cell suspension were pipetted in a Neubauer counting chamber and ES cells were counted. The cell number of one quadrant multiplied by 10,000 corresponded to the number of cells in one ml cell suspension.

6.2.2.3 **Freezing and thawing of ES cells**

ES cells were stored -80°C for short term storage (up to 2-3 months) or in liquid nitrogen for long term storage. Cells were trypsinised as described in 5.2.2, centrifuged, resuspended in ice cold 1x freezing medium, and pipetted into a 2 ml cryovial. Vials were frozen in a freezing container at -80°C. Due to the isopropanol in the freezing container the temperature is lowered very slowly inside until it reaches the final temperature of the freezer after several hours. For long term storage, the vials were then transferred into liquid nitrogen. For freezing of cells on multi well plates, cells were trypsinised, resuspended with a small amount of

medium, and ice cold 2x freezing medium was added in a ratio of 1:1, so that the final concentration of freezing medium in each well was 1x. Plates were wrapped in cellulose and frozen at -80°C. The cellulose prevents the fast freezing of the cells. Cells were thawed in the water bath at 37°C, diluted with medium, centrifuged, resuspended in fresh medium, and plated on dishes with or without feeder cells. For small volumes of frozen cells, cells were diluted in a larger volume of medium and plated directly. For this procedure, medium was changed the next day as soon as possible to get rid of the DMSO from the freezing medium.

6.2.2.4 **Lipofection and electroporation of ES cells**

To introduce foreign DNA into cells, several vehicles can be used. The transfection reagent used here was FuGENE 6, a multi-component lipid-based reagent that can complex with DNA and transport it into cells. DNA was used as circular plasmid and also a mixture of several plasmids could be co-transfected. First, DNA had to be sterilized by precipitation. Therefore an appropriate amount of the DNA plasmid was precipitated and washed with ethanol as described elsewhere. Decanting of the ethanol and drying and dissolving of the DNA pellet in sterile H2O was performed under a laminar flow. For transfection, a DNA concentration of 100 ng/ µl was used.

One day prior to transfection, cells were plated on a gelatine coated 24-well plate (approx. 40,000 cells/well). For transfection, for each well 2 µl FuGENE 6 was mixed with 66 µl DMEM and incubated for 5 min at RT. The DNA was added to the FuGENE/ DMEM mixture and incubated for at least 15 min at RT. The old medium of the cells was exchanged by 600 µl fresh F1 medium and the FuGENE/DMEM/DNA mixture was added. Cells were grown overnight at 37°C, then the medium was changed to remove the FuGENE/DNA mixture. Two days after transfection, cells were harvested for analysis. A physical method to bring foreign DNA into ES cells is electroporation, in which the cell membranes are permeabilised transiently with short electrical impulses, so that DNA can pass through the emerging pores into the cell. Circular plasmid DNA stays transiently in the cells and linearised plasmids can be integrated into the genome. Also here co-transfection of several plasmids is possible. Co-transfection of a specially designed circular plasmid together with an expression vector for an integrase results in integration of a defined fragment of the circular plasmid into the genome of the cell, according to the recombination event catalyzed by the integrase. For each sample to be electroporated 10^6 - 10^7 ES cells have been used. Cells were harvested from their culture dish(es) by trypsination, centrifuged at 1,200 rpm for 5 min,

washed with PBS, centrifuged again and resuspended in 800 µl PBS containing the DNA to be electroporated. A maximum of 50 µg of total DNA was used for 10^7 cells; for lower cell numbers accordingly less DNA was used. The cell/DNA suspension was pipetted into an electroporation cuvette and electroporated with 300 V and 500 µF for 2 ms. For transient experiments, where a transfection efficiency as high as possible was needed, a voltage of 320 V was used for 3 ms. After transfection, cells were allowed to recover for 5 min at RT, diluted in medium and plated on 4-5 fresh culture dishes (when 10^7 cells have been used, otherwise on accordingly less dishes). For stable transfections dishes with feeder cells and for transient experiments gelatine coated plates were used. Cells were grown for two days at 37°C. For transient experiments, cells were harvested for analysis or were further grown in selection medium for stable experiments.

6.2.2.5 **Selection and picking of stably transfected clones**

For the selection of clones with stably integrated vector, two days after the transfection the specific antibiotic was added to the medium. Selection with the neomycin analogue Geneticin (G418) is based on the expression of a neomycin resistance gene from the vector after integration into the genome. With G418 at a concentration of 140 µg/ml in the medium, only resistant cells survive and can form colonies, whereas cells with no vector integrated die during selection. Selection medium was applied for 5-7 days until round, light breaking, and prominent colonies had formed and most of the single cells had died. Colonies were picked with a 20 µl pipette from the culture dish containing PBS into a 96-well plate containing 50 µl trypsin in each well to dissociate the colony. After a maximum time of 20 min in the trypsin, 50 µl medium was added, picked cells were resuspended and plated on a fresh 96-well plate with feeder cells in a total volume of 300 µl medium. Medium was changed the next day to remove dead cells and cells were expanded on larger wells as soon as the former wells have grown dense. Cells on 24-well plates were splitted onto several plates with feeder cells and plates coated with gelatine. Cells on a feeder layer were frozen at -80°C in 1x freezing medium or further expanded, and cells on gelatine coated plates were grown to confluence and used for DNA extraction and genotyping.

6.2.2.6 **Screening for recombined clones**

DNA was extracted from cells growing on gelatine coated plates to avoid extraction of DNA from feeder cells. ES cells were grown to confluence, washed twice with PBS, and either directly used for DNA extraction or frozen dry at -20°C. DNA extraction is described elsewhere. DNA was used for PCR analysis for an initial screening and for Southern blotting for confirmation.

6.2.2.7 **Chemiluminescence reporter gene assays (ß-Gal assay)**

To assess the activity of β-Galactosidase (β-Gal) and firefly-luciferase (Luc) after transfection of the corresponding expression plasmids, reporter gene assay for both genes were performed. The preparation of cell lysates and measurement of β-Gal activity were performed with the b-Gal reporter gene assay kit following the manufacturer's protocol. Thereby a substrate for β-Gal was added to 50 µl of the cell lysate, which resulted in light emission at 475 nm initiated by the cleaved substrate after a shift of the pH value. The intensity of the emitted light was measured for 5 sec in a plate luminometer. For the detection of Luc activity, 20 µl of each lysate were mixed with 100 µl Luciferase assay buffer and measured for 5 sec in the luminometer. The Luc oxidized the luciferin contained in the assay buffer, which then emitted light at 490 nm.

6.2.3 Histological methods

6.2.3.1 Perfusion and cutting

Mice were asphyxiated with CO2 and the thoracic cavity was opened to dissect the heart. A blunt needle was inserted through the left ventricle into the ascending aorta and the right atrium was snipped. Using a pump vessels were rinsed with PBS until the liver became pale and then perfusion was carried out with 4% paraformaldehyde (PFA)/PBS for approximately 5 min (10 ml/min). After perfusion was complete the mouse was decapitated and the brain was dissected removing bones and meninges. For postfixation the brain was kept in 4% paraformaldehyde/PBS for 1 hour at RT to overnight at 4°C, depending on the subsequent procedure. For Embryo preparation pregnant mice were asphyxiated with CO2 and Embryos were taken out and rinsed in cold PBS. The Embryos were decapitated and the brain was dissected removing bones and meninges and incubated in 4% PFA overnight at 4°C.

Paraffin sections

After perfusion brains were postfixed for 1-2 hours at RT, dehydrated in an ascending ethanol scale, and equilibrated and embedded in paraffin. Using an automated embedding machine, the program is as follows:

Step	Solution	Temp. (°C)	Time (min)
Dehydration:	30% EtOH	RT	90
Dehydration:	50% EtOH	RT	90
Dehydration:	75% EtOH	RT	90
Dehydration:	85% EtOH	RT	90
Dehydration:	95% EtOH	RT	90
Dehydration:	100% EtOH	RT	90
Dehydration:	100% EtOH	RT	60 under vacuum
Clarification:	RotiHistol	RT	60 under vacuum
Clarification:	RotiHistol	RT	60 under vacuum
Paraffination:	50% RotiHistol® / 50% paraffin	65	60 under vacuum
Paraffination:	paraffin	65	60 under vacuum
Paraffination:	paraffin	65	480 under vacuum
Embedding:	paraffin	65 to RT	

Paraffin embedded brain tissue was first mounted on a tissue cassette with paraffin and fixed on the microtome. 8 µm thick sections were cut and put into a water bath (37-42°C) for

flattening. Sections were mounted on slides and dried on a heating plate and/or in an incubator at 37°C. Slides with slices were stored at 4°C or directly used.

Frozen sections

After perfusion brains were postfixed for 1 hour at RT and equilibrated in 20% sucrose solution o/n at 4°C. For immunohistochemistry of phosphorylated proteins, solutions for perfusion were used ice-cold, brains were postfixed overnight at 4°C and 25% sucrose solution was used. Brains were frozen on dry ice or at 20°C and fixed on an object holder with freezing medium. On a cryostat slices of 30 or 40 µm were cut and collected in PBS. For storage longer than overnight the slices were kept in cryoprotection solution at -20°C.

6.2.3.2 ***in situ*** **hybridization on paraffin sections (radioactive)**

For the detection of mRNA expression on brain sections, radioactive ISH on paraffin section was performed. During the whole procedure RNase free solutions and materials were used to avoid degradation of the mRNA and the RNA probe.

Synthesis of ^{35}S labelled RNA probes

Radioactively labelled RNA probes for in situ hybridization were generated by *in vitro* transcription with an appropriate RNA polymerase in the presence of [α-thio35S]- UTP. As templates, plasmids containing part of the cDNA of the gene to analyze and promoters for the RNA polymerases T7 and SP6 were linearised shortly behind the end of the cDNA sequence with an appropriate restriction enzyme. A 1x transcription reaction was composed as follows:

3 µl	10x transcription buffer
3 µl	dNTP mix (rATP/rCTP/rGTP 10mM each)
1 µl	0.5 M DTT
1 µl	RNasin (RNase inhibitor; 40 u/µl)
1.5 µg	linearised plasmid DNA template
3 µl	[α-thio-35S]-UTP (12.5 mCi/mM)
x µl	H2O (total volume is 30 µl)
1 µl	RNA polymerase (T7 or SP6; 20 u/µl)

The reaction was incubated at 37°C for 3 hours in total. After the first hour another 0.5 µl of RNA polymerase was added to facilitate the transcriptional process. After transcription the DNA template was destroyed by adding 2 µl of RNase-free DNase I and incubation at 37°C for 15 min. Probes were purified with the RNeasy Mini Kit following manufacturer's instructions and activity was measured with a liquid scintillation counter. The probe was stored at -20°C up to five days.

Hybridization

The hybridisation temperature is about 25°C under the melting temperature of the probe. Before hybridization paraffin sections were dewaxed and pre-treated as follows:

Day 1

2 x 15 min	Rotihistol
2 x 5 min	100 % Ethanol
5 min	70 % Ethanol
3 min	DEPC-H_20
3 min	PBS/DEPC
20 min	4 % PFA/PBS
2 x 5 min	PBS/DEPC
7 min	20 µg/ml Proteinase K in Proteinase-K-buffer
5 min	PBS/DEPC
20 min	4 % PFA/PBS
5 min	PBS/DEPC
10 min	200 ml of rapidly stirring 0.1 M triethanolamine-HCl (pH 8) (TEA)
2 x 5 min	2x SSC
1 min	60 % Ethanol/DEPC
1 min	70 % Ethanol/DEPC
1 min	95 % Ethanol/DEPC
1 min	100 % Ethanol

Slides were air dried and used immediately for prehybridisation. For prehybridisation slides were incubated with Hyb-mix (without labelled riboprobe) for 1 h at hybridisation temperature. For hybridisation the following protocol was used:

- Make appropriate amount of hybridization mix containing 35000 to 70000 cpm/µl. Use 90 to 100 µl hybmix per slide (3,5 to 7 Million counts per slide).
- heat hybridisation mix containing the probe to 90 °C for 2 min.
- put shortly on ice, then on RT.
- after prehybridisation remove coverslip and as much liquid as possible. Go on immediately with hybridisation to avoid drying out!
- Take 90 to 100 µl of hybridisation mix containing 35000 to 70000 cpm/µl per slide, drop the solution on the slide and put coverslip carefully on it.
- Place slides carefully into a hybridisation chamber containing hybridisation chamber fluid to avoid drying out of the hybridisation mix.
- Incubate in an oven at 55-68°C for overnight (up to 20 hours).
- Hybridisation temperature is about 25C under the melting temperature of the probe, the higher the less background.

Day 2

4 x 5 min	RT	4xSSC
20 min	37 °C	NTE (20µg/ml RNaseA)
2 x 5 min	RT	2xSSC/1 mM DTT
10 min	RT	1xSSC/1 mM DTT
10 min	RT	0,5xSSC/1mM DTT
2 x 30 min	64 °C	0,1xSSC/1 mM DTT
2 x 10 min	RT	0,1xSSC
1 min	RT	30 % Ethanol in 300 mM NH_4OAc
1 min	RT	50 % Ethanol in 300 mM NH_4OAc
1 min	RT	70 % Ethanol in 300 mM NH_4OAc
1 min	RT	95 % Ethanol
2 x 1 min	RT	100 % Ethanol

Slides were air dried and exposed to an autoradiography film (BioMax MR) for 2 days. For a detailed analysis slides were dipped with a photo emulsion (diluted 1:1 with water) and stored at 4°C in the dark for an appropriate time depending on the signal intensity (estimated by the results from the film; in general 4 weeks). For developing, slides were equilibrated for 1 h to RT, developed for 5 min, rinsed in water and fixed for 7 min. After rinsing the slides for 25 min in floating tap water, remaining emulsion on the backside was scratch with a razor blade and slides were counterstained with cresyl violet.

6.2.3.3 Nissl staining (cresyl violet)

Nissl staining of Paraffin sections was performed according to the following protocol:

Staining:	1-5 min cresyl violet staining solution
Rinse:	H_2O
Clearing:	1 min 70% Ethanol until slide is clear
Clearing:	10-60 sec 96% Ethanol + 0.5% acetic acid
Dehydration:	2 x 1 min 96% Ethanol
Dehydration:	2 x 2 min 100% Ethanol
	2 x 10 min xylol

Slides were lidded immediately with DPX and dried o/n under the hood.

6.2.3.4 ***in situ*** hybridization on paraffin sections (DIG-labelled probes)

Probe labelling

20 µg of the probe containing plasmid were digested for at least 3h with appropriate restriction enzymes and for antisense probes. Upon heat inactivation the digestion was checked by electrophoresis on an agarose gel and the probe is cleaned up with the Wizard SV Gel & PCR Clean up kit (Promega) according to manufacturer's protocol. The purified probe can be stored at – 20°C and is used for reverse transcription:

Reverse transcription mix:

1 µg	linearised DNA (purified probe)
2 µl	10 x Transcription buffer (Roche)
2 µl	10 x DIG labeling Mix (Roche)
0.5 µl	RNase Inhibitor (Roche)
2 µl	T7, T3 or Sp6 RNA Polymerase
x µl	RNase free water (fill up to 20 µl)

The reverse transcription mix was incubated for 3h at 37°C RNase free DNaseI (Roche) was added to eliminate the DNA-template. The reaction was stopped by adding EDTA and stored at -80°C or the RNA probe was immediately purified with the RNeasy Mini kit. The reverse transcription products are checked on an agarose gel and the DIG-labelled control RNA kit (Roche) was used to ensure efficient DIG labelling of the probe.

Pre-treatment of Paraffin sections for ISH with DIG labelled probes:

Time	Treatment
2 x 20 min	Xylol
2 x 5 min	100 % Ethanol
5 min	95 % Ethanol
5 min	70 % Ethanol
3 min	H_20 (RNase free)
3 min	PBS
20 min	4 % PFA in PBS
2 x 5 min	PBS
2 min	60 % Ethanol
2 min	70 % Ethanol
2 min	95 % Ethanol
2 min	100 % Ethanol
	Air-dry

Protocol for ISH with DIG labelled probes on Paraffin sections:

Day1

cycles	**time**	**reagent**	**temp**
5	5 min	0.6 % H_2O_2/MeOH; no detergent	24 °
7	5 min	PBS	
2	5 min	0.2 N HCl	
4	5 min	PBS	
1	5 min	Proteinase buffer	
2	10 min	Proteinase K 20 µg/ml	
7	5 min	PBS	
2	10 min	4 % PFA	
7	5 min	PBS	
1	15 min	Hyb. Mix + DTT 1.5 mg/ml	24 °
1	30 min	Hyb. Mix	→64 °
1	6 h	Dig-Probes (150-) 300 ng/ml	64 °

Day2

cycles	time	reagent	temp
5	5 min	5 x SSC preheated (90 min in advance) to 64 ^{o}	64 ^{o}
5	10 min	Formamide I (2x SSC in 50 % Formamide)	
5	12 min	Formamide II (1x SSC in 50 % Formamide)	
4	8 min	0,1 x SSC	→25 ^{o}
4	5 min	NTE pH 7.6	
4	7 min	Iodacetamide, 20 mM	
4	5 min	NTE	
2	5 min	TNT p H 7.6	
3	10 min	4% Sheep Serum (filter 0.45 µm)	
4	5 min	TNT	
2	10 min	TNB blocking	
2	5 min	TNT	
2	5 min	Maleat Wash	
2	10 min	Maleat blocking	
2	5 min	Maleat Wash	
2	5 min	TNT	
3	5 min	TMN (no Levamisol)	
4	5 min	TNT	
4	10 min	TNB blocking	
2	30 min	Anti DIG-POD (1:600 or 0.2925 U/µl)	
6	5 min	TNT	
1	30 min	Tyramid-Biotin 1: 50 in TSA	
6	5 min	Maleat Wash	
2	30 min	Neutravidin-AP (Pierce; 31002) 1:750/2.85 µg/ml in MWB	
6	5 min	Maleat Wash	
4	5 min	TNT	
2	5 min	TMN	
2	15 min	NBT-BCIP in TMN + (+ 0.5 mg/ml Levamisol, BCIP 0.15ug/ml, NBT 0.4 ug/ml)	
4	5 min	Water I + 0.05 % Tween	
1	5 min	NTE	
1	20 min	4%PFA	
4	5 min	Water II	

6.2.3.5 **Immunhistochemistry on Paraffin sections**

Immunohistochemistry on Paraffin sections was performed in glass cuvettes (about 250 ml per cuvette) except blocking, antibody incubations, the ABC-reaction and the DAB-staining. As blocking solution 10% FCS with 0.05% Triton-X in 1x PBS was used. Primary and secondary antibodies were diluted in 10% FCS in 1x PBS. The DAB working solution was prepared by adding 1 ml DAB stock solution and 15 µl H_2O_2 (30%) to 19 ml o.1M Tris-HCl, pH 7.4 immediately before use.

Day1

1. dewaxing	Min. 45 min	Rotihistol or Xylol	
2. Rehydration	2 x 5 min	Ethanol 100%	
3.	2 x 5 min	Ethanol 96%	
4.	2 x 5 min	Ethanol 70%	
5. Rinse	10 min	Aqua dest	
6. wash	3 min	0.01 M Na-citrat, pH 6.0	
7. Antigen retrieval	5 min	Microwave at 100%	Attention: Times have to be determined for each microwave
8.	10 min	Cooling down	
9.	3 min	Microwave at 70%	
10.	20 min	Cool down	
11. wash	2 x 5 min	0.1M PBS	
12. destruction of endogenous peroxidases	5 min	0.1% H2O2 / PBS	Add H_2O_2 directly before use
13. wash	2 x 5 min	0.1M PBS	
14. blocking	1 hr	Blocking reagent	RT; humid chamber
15. 1st antibody	Over night	1st antibody	4°C; humid chamber

Day2

1. wash	3 x 5 min	PBS	
2. 2nd antibody	1 hr	2nd antibody	RT; humid chamber,
3. wash	3 x 5 min	PBS	
4. intensifying	30 min	ABC-solution	RT; humid chamber
5. wash	2 x 5 min	PBS	
6. wash	5 min	0.1M Tris-HCl	
7. DAB-staining		DAB-working solution	Humid chamber; Control intensity under microscope
8. stop staining	2 x 5 min	PBS	
9. dehydration	2 x 5 min	Ethanol 70%	
10.	2 x 5 min	Ethanol 96%	
11.	2 x 5 min	Ethanol 100%	
12.	2 x 5 min	Rotihistol or Xylol	
13. embedding		Rotihistokitt or DPX	

6.2.3.6 **Immunhistochemistry on frozen sections (free floating)**

In cryoprotection solution stored free-floating sections (40 µm in thickness) were first washed in 1x TBS, 6 x 15 min at RT or overnight at 4°C. Further steps were performed gently shaking at RT in 6-well or 12-well plates. Sections were blocked for 1h in 5% normal goat serum (NGS) in 0,2% Triton X100 in PBS (PBST) and incubated overnight with the primary antibody in 5% NGS in PBST overnight at 4°C on a shaker. The next day sections were washed 3 x 15min with PBST and incubated 45 min with a fluorescence-dye labelled secondary antibody in 5% NGS in PBST. Finally sections were washed 3 x 15 min in PBST and 3 x 10 min 1x PBS. During the second PBS washing step DAPI is added to PBS to label the DNA as counterstaining. Sections were mounted on slides, air-dried, and lidded with Aqua Poly/Mount (Polysciences, Inc.). During all steps the exposure of fluorescent dyes to bright light was reduced to a minimum.

6.2.4 Animal husbandry

Animal facilities

All mice were kept and bred in the GSF animal facility in accordance with national and institutional guidelines. Mice were group housed (if not mentioned else) with five mice per cage at maximum in open cages and maintained on a 12 hours light/dark cycle with food and water ad libitum. The temperature was 22 ± 2°C and relative humidity 55 ± 5%. For behaviour analyses in the German Mouse Clinic (GMC), mice were housed in individually ventilated cages (IVC) due to hygienical reasons. Animals were not transferred before the age of eight weeks to the GMC. For breeding single or double matings were set up and pups were weaned at an age of three weeks. At weaning mice got earmarks for identification.

6.2.4.1 Blastocyst injection and embryo transfer

For the production of mouse blastocysts (E3.5), female C57BL/6J mice were superovulated to increase the number of ovulated oocytes. Superovulation was performed with analoga of the gonadotropins follicle-stimulating hormone and luteinizing hormone. The hormones were injected intraperitoneally (i. p.) at noon, starting with 7.5 u of pregnant mare's serum gonadotropin (PMSG) to induce maturation of the follicles. 48 hours later 7.5 u of human chorion gonadotropin (hCG/Ovogest), which initiates the ovulation of the oocytes, were injected. After the injection of hCG, female mice were mated with one male of the same strain for one night. The uteri of pregnant females were dissected 3 days post coitum and blastocysts were flushed with M2 medium. One isolated blastocyst was fixed with one capillary of the micromanipulator and with a second capillary 10-20 mutant ES cells were injected into the blastocoel, where they will contribute to the inner cell mass. As foster mothers for these early embryos pseudo-pregnant CD1 females were used. Pseudo-pregnancy was achieved by mating the females to sterile, vasectomised males. For the embryo transfer under anaesthetic (dosage dependent on body weight, normally 0.25 ml of 1% ketamine and 0.1% rompun in isotonic saline solution), the retroperitoneal cavity of the foster mother was opened and ovaries and uterus were dissected. The proximal sides of the uterus were perforated with a thin canula and up to 10 manipulated blastocysts per side were transferred to the uterus via this opening. The surgery field was closed again with clips and the foster mothers were kept on warming plates until awakening. To avoid dehydration of the cornea and therefore prevent blindness of the mice, the eyes were kept wet with 0.9% NaCl during surgery.

6.2.4.2 **Establishment of new mouse lines**

16 days after embryo transfer chimeric mice were born. Since the wildtype cells from the blastocyst coded for black fur colour and the modified ES cells gave agouti fur colour, chimeric mice showed a mixture of black and agouti fur. The higher the contribution of ES cells was, the higher was the ratio of agouti to black fur. Chimeras were mated to wildtype C57Bl/6J mice to obtain offspring with germ line transmission of the modified allele. Mice, which have received the modified allele from their chimeric parent, were identified by genotyping.

6.2.4.3 **Behavioural testing**

All behavioural tests were performed in the german mouse clinic (GMC). Mice were transferred at the age of 8-10 weeks from the breeding facility to the GMC. First tests started after two weeks of accommodation for the animals. The test battery was divided into two batches, so that each batch of animals was subjected to a maximum of five of the eight single tests. Each batch of animals consisted of 10-15 mice for each sex and genotype (mutant / control) with a maximal difference in age of two weeks. Data were statistically analyzed using SPSS software. The chosen level of significance was $p < 0.05$.

Light-Dark box test

The test box was made of PVC and divided into two compartments, connected by a small tunnel (4 x 6 x 9 cm high). The lit compartment (29 x 19 x 24 cm high) was made of white PVC and was illuminated by cold light with 650 lux in the centre. The dark compartment (14 x 19 x 24 cm high) was made of black PVC and not directly illuminated (approx. 20 lux in the centre). The mouse was placed in the centre of the dark compartment and allowed to freely explore the apparatus for 5 min. Behaviours were observed by a trained observer sitting next to the box using a handheld computer. Data were analyzed with respect to (1) the number of entries, latency to first entry, and time spent in both compartments and the tunnel; and (2) the number of rearings in both compartments and the tunnel. An entry into a compartment was

defined as placement of all four paws into the compartment. Additionally, a camera was mounted above the centre of the test arena to videotape the trial, and the animal's locomotor path in the lit compartment was analyzed with a video-tracking system. The box was cleaned before each trial with a disinfectant.

Social discrimination test

Social memory was assessed using the social discrimination procedure described previously (Engelmann et al., 1995). As stimulus adult ovarectomised 129S1/SvlmJ female mice were used. Briefly, test animals were separated by transferring them to fresh cages 2 h before starting the session. The social discrimination procedure consisted of two 4 min exposures of stimulus animals to the test animal in the test animal's home cage. During the first exposure ("sampling") one stimulus animal was exposed to the test animal, and after a retention interval of 2 h, this stimulus animal was re-exposed to the test animal together with an additional, previously not presented stimulus animal during the second ("test") exposure. During each exposure the duration of investigatory behaviour of the test animal towards the stimulus animal(s) was recorded by a trained observer blind to the genotype with a hand-held computer. Significantly longer investigation duration of the unfamiliar stimulus animal compared to the familiar one (i.e., the conspecific previously presented during the sampling phase) was taken as an evidence for an intact recognition memory.

Tail suspension test

For testing tail suspension, the animal's tail tip was fixed with adhesive tape on the edge of a table. For 6 min, activity and immobility behaviour was observed by a trained observer using a hand-held computer. Data were analyzed with respect to (1) duration and frequency of activity or immobility periods; (2) total duration of each behaviour; and (3) latency to the first immobility period.

Modified Hole Board

The modified Hole Board (mHB) test was carried out in a improved version of the procedures described by Ohl et al. (2001). The test apparatus consisted of a box (150 x 50 x 50 cm) which was divided into a test arena (100 x 50 cm) and a group compartment (50 x 50 cm) by a transparent PVC partition (50 x 50 x 0.5 cm) with 111 holes (1 cm diameter) staggered in twelve lines to allow group contact. A board (60 x 20 x 2 cm) with 23 holes (1.5 x 0.5 cm) staggered in three lines with all holes covered by movable lids was placed in the middle of the test arena, thus representing the central area of the test arena as an open field. The area around the board was divided into twelve similarly sized quadrants by lines taped onto the floor of the box (Ohl et al., 2001). Both, box and board, were made of dark grey PVC. All lids were closed before the start of a trial. For each trial, an unfamiliar object (a blue plastic tube lid) and a familiar object (a metal cube, which was placed into the home cage three days before testing and removed again one day before testing; similar in size to the unfamiliar object) were placed into the test arena with a distance of 2 cm between them. The illumination levels were set at approximately 150 lux in the corners and 200 lux in the middle of the test arena.
At the beginning of the experiment, all animals of one cage were allowed to habituate to the test environment together in the group compartment for 20 min. Then each animal was placed individually into the test arena and allowed to explore it freely for 5 min, during which the cage mates stayed present in the group compartment. The animals were always placed into the test arena in the same corner next to the partition, facing the board diagonally. The two objects were placed in the corner quadrant diametrically to the starting point. During the 5 min trial, the animal's behaviour was recorded by a trained observer with a hand-held computer. Additionally, a camera was mounted 1.2 m above the centre of the test arena, and the animal's track was videotaped and its locomotor path was analyzed with a video-tracking system. After each trial, the test arena was cleaned carefully with a disinfectant.

Elevated plus maze

The test arena was made of light grey PVC and consisted of two open arms (30 x 5 x 0.3 cm) and two closed arms of the same size with 15 cm high walls. The open arms and accordingly the closed arms were facing each other connected via a central square (5 x 5 cm). The apparatus was elevated 75 cm above the floor by a pole fixed underneath the central square.

The illumination level was set at approx. 100 lux in the centre of the maze. For testing, each mouse was placed at the end of a closed arm (distal to the centre) facing the wall and was allowed to explore the maze for 5 min. A camera was mounted above the centre of the maze to video-monitor each trial by a trained observer in an adjacent room. The number of entries into each type of arm (placement of all four paws into an arm defining an entry), latency to enter the open arms as well as the time spent in the open and closed arms were recorded by the observer with a hand-held computer. After each trial, the test arena was cleaned carefully with a disinfectant.

Social interaction test

On two subsequent days before testing, mice were habituated separately to the test area (fresh cage with floor covered with bedding) for 10 min in moderate lighting conditions (40 lux) to enhance active interaction during testing (File and Hyde, 1978). For testing, two unfamiliar, weight-matched mice of the same sex and genotype were placed for 10 min into the known test area. The total time spent in active (grooming, sniffing the partner, crawling under and over) and passive social behaviour (sitting next to each other in physical contact) was recorded by a trained observer. As social interaction time of one individual depends on the partner's social activity, one dataset was recorded for each pair expressing the behaviour of both animals (Tonissaar et al., 2004).

Accelerating rotarod

Motor coordination and balance was assessed using a rotating rod apparatus. The rod diameter was approx. 4.5 cm made of hard plastic material covered by soft black rubber foam with lane widths of 5 cm. The test phase consisted of three trials separated by 15 min intertrial intervals (ITI). Per each trial, three mice were placed on the rod leaving an empty lane between two mice. The rod was initially rotating at constant speed (4 rpm) to allow positioning of all mice in their respective lanes. Once all mice were positioned, the trial was started and the rod accelerated from 4 rpm to 40 rpm in 300 sec. The latency and the speed at which each mouse fell off the rod were measured. Passive rotations were counted as a fall off and the mouse was removed from the rod carefully. After each trail the apparatus was disinfected and dried.

Forced swim test

The forced swimming procedure was adapted from Ebner et al. (Ebner et al., 2002). The forced swimming apparatus consisted of a cylindrical 10 l glass tank (24.5 cm in diameter) filled with water (25 ± 1°C) to a depth of 20 cm. A trained observer recorded the animal's behaviour in moderate lighting conditions (30 lux) for 6 min with a handheld computer according to one of the following behaviours: (1) struggling, defined as movements during which the forelimbs broke the water's surface; (2) swimming, defined as movement of the animal induced by movements of the fore and hind limbs without breaking the water surface; and (3) floating, defined as the behaviour during which the animal used limb movement just to keep its equilibrium without any movement of the trunk. After each trial, first the mouse was dried with a tissue and put in a new cage, second the water was renewed before continuing with testing.

7 REFERENCES

Agasse F, Nicoleau C, Petit J, Jaber M, Roger M, Benzakour O, Coronas V. 2007. Evidence for a major role of endogenous fibroblast growth factor-2 in apoptotic cortex-induced subventricular zone cell proliferation. Eur J Neurosci 26(11):3036-3042.

Anderson CM, Nedergaard M. 2006. Emerging challenges of assigning P2X7 receptor function and immunoreactivity in neurons. Trends Neurosci 29(5):257-262.

Arman E, Haffner-Krausz R, Chen Y, Heath JK, Lonai P. 1998. Targeted disruption of fibroblast growth factor (FGF) receptor 2 suggests a role for FGF signaling in pregastrulation mammalian development. Proc Natl Acad Sci U S A 95(9):5082-5087.

Aruga J, Ogura H, Shutoh F, Ogawa M, Franke B, Nagao S, Mikoshiba K. 2004. Locomotor and oculomotor impairment associated with cerebellar dysgenesis in Zic3-deficient (Bent tail) mutant mice. Eur J Neurosci 20(8):2159-2167.

Ashton JC, Darlington CL, Smith PF. 2006. Co-distribution of the cannabinoid CB1 receptor and the 5-HT transporter in the rat amygdale. Eur J Pharmacol 537(1-3):70-71.

Bambico FR, Katz N, Debonnel G, Gobbi G. 2007. Cannabinoids elicit antidepressant-like behavior and activate serotonergic neurons through the medial prefrontal cortex. J Neurosci 27(43):11700-11711.

Barden N, Harvey M, Gagne B, Shink E, Tremblay M, Raymond C, Labbe M, Villeneuve A, Rochette D, Bordeleau L, Stadler H, Holsboer F, Muller-Myhsok B. 2006. Analysis of single nucleotide polymorphisms in genes in the chromosome 12Q24.31 region points to P2RX7 as a susceptibility gene to bipolar affective disorder. Am J Med Genet B Neuropsychiatr Genet 141(4):374-382.

Barski JJ, Hartmann J, Rose CR, Hoebeek F, Morl K, Noll-Hussong M, De Zeeuw CI, Konnerth A, Meyer M. 2003. Calbindin in cerebellar Purkinje cells is a critical determinant of the precision of motor coordination. J Neurosci 23(8):3469-3477.

Bass BL. 2002. RNA editing by adenosine deaminases that act on RNA. Annu Rev Biochem 71:817-846.

Beggs HE, Soriano P, Maness PF. 1994. NCAM-dependent neurite outgrowth is inhibited in neurons from Fyn-minus mice. J Cell Biol 127(3):825-833.

Bellot F, Crumley G, Kaplow JM, Schlessinger J, Jaye M, Dionne CA. 1991. Ligand-induced transphosphorylation between different FGF receptors. EMBO J 10(10):2849-2854.

Belluardo N, Wu G, Mudo G, Hansson AC, Pettersson R, Fuxe K. 1997. Comparative localization of fibroblast growth factor receptor-1, -2, and -3 mRNAs in the rat brain: in situ hybridization analysis. J Comp Neurol 379(2):226-246.

Belvindrah R, Nalbant P, Ding S, Wu C, Bokoch GM, Muller U. 2006. Integrin-linked kinase regulates Bergmann glial differentiation during cerebellar development. Mol Cell Neurosci 33(2):109-125.

Belzung C, Griebel G. 2001. Measuring normal and pathological anxiety-like behaviour in mice: a review. Behav Brain Res 125(1-2):141-149.

Benedetti F, Serretti A, Pontiggia A, Bernasconi A, Lorenzi C, Colombo C, Smeraldi E. 2005. Long-term response to lithium salts in bipolar illness is influenced by the glycogen synthase kinase 3-beta -50 T/C SNP. Neurosci Lett 376(1):51-55.

Blaess S, Corrales JD, Joyner AL. 2006. Sonic hedgehog regulates Gli activator and repressor functions with spatial and temporal precision in the mid/hindbrain region. Development 133(9):1799-1809.

Blaess S, Graus-Porta D, Belvindrah R, Radakovits R, Pons S, Littlewood-Evans A, Senften M, Guo H, Li Y, Miner JH, Reichardt LF, Muller U. 2004. Beta1-integrins are critical for cerebellar granule cell precursor proliferation. J Neurosci 24(13):3402-3412.

Blak AA. 2005. Molekulare Faktoren, die die Entwicklung der Mittel-/Hinterhirnregion regulieren. Munich: Technical University Munich.

Blak AA, Naserke T, Saarimaki-Vire J, Peltopuro P, Giraldo-Velasquez M, Vogt Weisenhorn DM, Prakash N, Sendtner M, Partanen J, Wurst W. 2007. Fgfr2 and Fgfr3 are not required for patterning and maintenance of the midbrain and anterior hindbrain. Dev Biol 303(1):231-243.

Blak AA, Naserke T, Weisenhorn DM, Prakash N, Partanen J, Wurst W. 2005. Expression of Fgf receptors 1, 2, and 3 in the developing mid- and hindbrain of the mouse. Dev Dyn 233(3):1023-1030.

Bland ST, Tamlyn JP, Barrientos RM, Greenwood BN, Watkins LR, Campeau S, Day HE, Maier SF. 2007. Expression of fibroblast growth factor-2 and brain-derived neurotrophic factor mRNA in the medial prefrontal cortex and hippocampus after uncontrollable or controllable stress. Neuroscience 144(4):1219-1228.

Bourin M, Hascoet M. 2003. The mouse light/dark box test. Eur J Pharmacol 463(1-3):55-65.

Bremner JD, Narayan M, Anderson ER, Staib LH, Miller HL, Charney DS. 2000. Hippocampal volume reduction in major depression. Am J Psychiatry 157(1):115-118.

Broccoli V, Boncinelli E, Wurst W. 1999. The caudal limit of Otx2 expression positions the isthmic organizer. Nature 401(6749):164-168.

Brummelkamp TR, Bernards R, Agami R. 2002. A system for stable expression of short interfering RNAs in mammalian cells. Science 296(5567):550-553.

Bulanova E, Budagian V, Orinska Z, Hein M, Petersen F, Thon L, Adam D, Bulfone-Paus S. 2005. Extracellular ATP induces cytokine expression and apoptosis through P2X7 receptor in murine mast cells. J Immunol 174(7):3880-3890.

Burcescu I, Wigg K, King N, Vetro A, Kiss E, Katay L, Kennedy JL, Kovacs M, Barr CL. 2005. Association study of CREB1 and childhood-onset mood disorders. Am J Med Genet B Neuropsychiatr Genet 137(1):45-50.

Camps M, Chabert C, Muda M, Boschert U, Gillieron C, Arkinstall S. 1998. Induction of the mitogen-activated protein kinase phosphatase MKP3 by nerve growth factor in differentiating PC12. FEBS Lett 425(2):271-276.

Cavallaro U, Niedermeyer J, Fuxa M, Christofori G. 2001. N-CAM modulates tumour-cell adhesion to matrix by inducing FGF-receptor signalling. Nat Cell Biol 3(7):650-657.

Chen B, Dowlatshahi D, MacQueen GM, Wang JF, Young LT. 2001. Increased hippocampal BDNF immunoreactivity in subjects treated with antidepressant medication. Biol Psychiatry 50(4):260-265.

Chen SJ, Kao CL, Chang YL, Yen CJ, Shui JW, Chien CS, Chen IL, Tsai TH, Ku HH, Chiou SH. 2007. Antidepressant administration modulates neural stem cell survival and serotoninergic differentiation through bcl-2. Curr Neurovasc Res 4(1):19-29.

Chen ZY, Jing D, Bath KG, Ieraci A, Khan T, Siao CJ, Herrera DG, Toth M, Yang C, McEwen BS, Hempstead BL, Lee FS. 2006. Genetic variant BDNF (Val66Met) polymorphism alters anxiety-related behavior. Science 314(5796):140-143.

Chessell IP, Simon J, Hibell AD, Michel AD, Barnard EA, Humphrey PP. 1998. Cloning and functional characterisation of the mouse P2X7 receptor. FEBS Lett 439(1-2):26-30.

Chi CL, Martinez S, Wurst W, Martin GR. 2003. The isthmic organizer signal FGF8 is required for cell survival in the prospective midbrain and cerebellum. Development 130(12):2633-2644.

Choi HB, Ryu JK, Kim SU, McLarnon JG. 2007. Modulation of the purinergic P2X7 receptor attenuates lipopolysaccharide-mediated microglial activation and neuronal damage in inflamed brain. J Neurosci 27(18):4957-4968.

Corrales JD, Rocco GL, Blaess S, Guo Q, Joyner AL. 2004. Spatial pattern of sonic hedgehog signaling through Gli genes during cerebellum development. Development 131(22):5581-5590.

Crossley PH, Martinez S, Martin GR. 1996. Midbrain development induced by FGF8 in the chick embryo. Nature 380(6569):66-68.

Cryan JF, Page ME, Lucki I. 2005. Differential behavioral effects of the antidepressants reboxetine, fluoxetine, and moclobemide in a modified forced swim test following chronic treatment. Psychopharmacology (Berl) 182(3):335-344.

D'Arcangelo G, Curran T. 1998. Reeler: new tales on an old mutant mouse. Bioessays 20(3):235-244.

Delaney CL, Brenner M, Messing A. 1996. Conditional ablation of cerebellar astrocytes in postnatal transgenic mice. J Neurosci 16(21):6908-6918.

Deng C, Wynshaw-Boris A, Zhou F, Kuo A, Leder P. 1996. Fibroblast growth factor receptor 3 is a negative regulator of bone growth. Cell 84(6):911-921.

Deng CX, Wynshaw-Boris A, Shen MM, Daugherty C, Ornitz DM, Leder P. 1994. Murine FGFR-1 is required for early postimplantation growth and axial organization. Genes Dev 8(24):3045-3057.

Detke MJ, Rickels M, Lucki I. 1995. Active behaviors in the rat forced swimming test differentially produced by serotonergic and noradrenergic antidepressants. Psychopharmacology (Berl) 121(1):66-72.

Deuchars SA, Atkinson L, Brooke RE, Musa H, Milligan CJ, Batten TF, Buckley NJ, Parson SH, Deuchars J. 2001. Neuronal P2X7 receptors are targeted to presynaptic terminals in the central and peripheral nervous systems. J Neurosci 21(18):7143-7152.

Deussing JM, Wurst W. 2005. Dissecting the genetic effect of the CRH system on anxiety and stress-related behaviour. C R Biol 328(2):199-212.

Doetsch F, Garcia-Verdugo JM, Alvarez-Buylla A. 1997. Cellular composition and three-dimensional organization of the subventricular germinal zone in the adult mammalian brain. J Neurosci 17(13):5046-5061.

Doherty P, Walsh FS. 1996. CAM-FGF Receptor Interactions: A Model for Axonal Growth. Mol Cell Neurosci 8(2/3):99-111.

Ebner K, Wotjak CT, Landgraf R, Engelmann M. 2002. Forced swimming triggers vasopressin release within the amygdala to modulate stress-coping strategies in rats. Eur J Neurosci 15(2):384-388.

Echevarria D, Martinez S, Marques S, Lucas-Teixeira V, Belo JA. 2005. Mkp3 is a negative feedback modulator of Fgf8 signaling in the mammalian isthmic organizer. Dev Biol 277(1):114-128.

Echevarria D, Vieira C, Gimeno L, Martinez S. 2003. Neuroepithelial secondary organizers and cell fate specification in the developing brain. Brain Res Brain Res Rev 43(2):179-191.

Eiraku M, Tohgo A, Ono K, Kaneko M, Fujishima K, Hirano T, Kengaku M. 2005. DNER acts as a neuron-specific Notch ligand during Bergmann glial development. Nat Neurosci 8(7):873-880.

Elbashir SM, Harborth J, Lendeckel W, Yalcin A, Weber K, Tuschl T. 2001. Duplexes of 21-nucleotide RNAs mediate RNA interference in cultured mammalian cells. Nature 411(6836):494-498.

Encinas JM, Vaahtokari A, Enikolopov G. 2006. Fluoxetine targets early progenitor cells in the adult brain. Proc Natl Acad Sci U S A 103(21):8233-8238.

Erhardt A, Lucae S, Unschuld PG, Ising M, Kern N, Salyakina D, Lieb R, Uhr M, Binder EB, Keck ME, Muller-Myhsok B, Holsboer F. 2007. Association of polymorphisms in P2RX7 and CaMKKb with anxiety disorders. J Affect Disord 101(1-3):159-168.

Eswarakumar VP, Lax I, Schlessinger J. 2005. Cellular signaling by fibroblast growth factor receptors. Cytokine Growth Factor Rev 16(2):139-149.

Evans SJ, Choudary PV, Neal CR, Li JZ, Vawter MP, Tomita H, Lopez JF, Thompson RC, Meng F, Stead JD, Walsh DM, Myers RM, Bunney WE, Watson SJ, Jones EG, Akil H. 2004. Dysregulation of the fibroblast growth factor system in major depression. Proc Natl Acad Sci U S A 101(43):15506-15511.

Fasano S, Brambilla R. 2002. Cellular mechanisms of striatum-dependent behavioral plasticity and drug addiction. Curr Mol Med 2(7):649-665.

File SE, Hyde JR. 1978. Can social interaction be used to measure anxiety? Br J Pharmacol 62(1):19-24.

Ford-Perriss M, Abud H, Murphy M. 2001. Fibroblast growth factors in the developing central nervous system. Clin Exp Pharmacol Physiol 28(7):493-503.

Fortin D, Rom E, Sun H, Yayon A, Bansal R. 2005. Distinct fibroblast growth factor (FGF)/FGF receptor signaling pairs initiate diverse cellular responses in the oligodendrocyte lineage. J Neurosci 25(32):7470-7479.

Fumagalli F, Molteni R, Calabrese F, Frasca A, Racagni G, Riva MA. 2005. Chronic fluoxetine administration inhibits extracellular signal-regulated kinase 1/2 phosphorylation in rat brain. J Neurochem 93(6):1551-1560.

Furthauer M, Lin W, Ang SL, Thisse B, Thisse C. 2002. Sef is a feedback-induced antagonist of Ras/MAPK-mediated FGF signalling. Nat Cell Biol 4(2):170-174.

Gaiano N, Fishell G. 2002. The role of notch in promoting glial and neural stem cell fates. Annu Rev Neurosci 25:471-490.

Gaiano N, Nye JS, Fishell G. 2000. Radial glial identity is promoted by Notch1 signaling in the murine forebrain. Neuron 26(2):395-404.

Gaughran F, Payne J, Sedgwick PM, Cotter D, Berry M. 2006. Hippocampal FGF-2 and FGFR1 mRNA expression in major depression, schizophrenia and bipolar disorder. Brain Res Bull 70(3):221-227.

Gimeno L, Hashemi R, Brulet P, Martinez S. 2002. Analysis of Fgf15 expression pattern in the mouse neural tube. Brain Res Bull 57(3-4):297-299.

Goebbels S, Bormuth I, Bode U, Hermanson O, Schwab MH, Nave KA. 2006. Genetic targeting of principal neurons in neocortex and hippocampus of NEX-Cre mice. Genesis 44(12):611-621.

Goffinet AM, So KF, Yamamoto M, Edwards M, Caviness VS, Jr. 1984. Architectonic and hodological organization of the cerebellum in reeler mutant mice. Brain Res 318(2):263-276.

Gottesman, II, Gould TD. 2003. The endophenotype concept in psychiatry: etymology and strategic intentions. Am J Psychiatry 160(4):636-645.

Gould TD, Einat H, Bhat R, Manji HK. 2004. AR-A014418, a selective GSK-3 inhibitor, produces antidepressant-like effects in the forced swim test. Int J Neuropsychopharmacol 7(4):387-390.

Hack I, Hellwig S, Junghans D, Brunne B, Bock HH, Zhao S, Frotscher M. 2007. Divergent roles of ApoER2 and Vldlr in the migration of cortical neurons. Development 134(21):3883-3891.

Hack MA, Saghatelyan A, de Chevigny A, Pfeifer A, Ashery-Padan R, Lledo PM, Gotz M. 2005. Neuronal fate determinants of adult olfactory bulb neurogenesis. Nat Neurosci 8(7):865-872.

Hamburgh M. 1963. Analysis of the Postnatal Developmental Effects of "Reeler," a Neurological Mutation in Mice. a Study in Developmental Genetics. Dev Biol 19:165-185.

Hanafusa H, Torii S, Yasunaga T, Nishida E. 2002. Sprouty1 and Sprouty2 provide a control mechanism for the Ras/MAPK signalling pathway. Nat Cell Biol 4(11):850-858.

Hansson AC, Cintra A, Belluardo N, Sommer W, Bhatnagar M, Bader M, Ganten D, Fuxe K. 2000. Gluco- and mineralocorticoid receptor-mediated regulation of neurotrophic factor gene expression in the dorsal hippocampus and the neocortex of the rat. Eur J Neurosci 12(8):2918-2934.

Hasuwa H, Kaseda K, Einarsdottir T, Okabe M. 2002. Small interfering RNA and gene silencing in transgenic mice and rats. FEBS Lett 532(1-2):227-230.

Hatten ME, Heintz N. 1995. Mechanisms of neural patterning and specification in the developing cerebellum. Annu Rev Neurosci 18:385-408.

Hatten ME, Liem RK, Mason CA. 1986. Weaver mouse cerebellar granule neurons fail to migrate on wild-type astroglial processes in vitro. J Neurosci 6(9):2676-2683.

Hitz C. 2007. The role of MAP-Kinases in anxiety disorders and depression - studies with knockout and knockdown mouse models. Munich: Technical University Munich.

Hitz C, Wurst W, Kuhn R. 2007. Conditional brain-specific knockdown of MAPK using Cre/loxP regulated RNA interference. Nucleic Acids Res 35(12):e90.

Holick KA, Lee DC, Hen R, Dulawa SC. 2008. Behavioral effects of chronic fluoxetine in BALB/cJ mice do not require adult hippocampal neurogenesis or the serotonin 1A receptor. Neuropsychopharmacology 33(2):406-417.

Holsboer F. 2000. The corticosteroid receptor hypothesis of depression. Neuropsychopharmacology 23(5):477-501.

Holsboer F, Lauer CJ, Schreiber W, Krieg JC. 1995. Altered hypothalamic-pituitary-adrenocortical regulation in healthy subjects at high familial risk for affective disorders. Neuroendocrinology 62(4):340-347.

Hynes M, Porter JA, Chiang C, Chang D, Tessier-Lavigne M, Beachy PA, Rosenthal A. 1995. Induction of midbrain dopaminergic neurons by Sonic hedgehog. Neuron 15(1):35-44.

Hynes M, Ye W, Wang K, Stone D, Murone M, Sauvage F, Rosenthal A. 2000. The seven-transmembrane receptor smoothened cell-autonomously induces multiple ventral cell types. Nat Neurosci 3(1):41-46.

Inouye M, Oda SI. 1980. Strain-specific variations in the folial pattern of the mouse cerebellum. J Comp Neurol 190(2):357-362.

Ireland MF, Noakes PG, Bellingham MC. 2004. P2X7-like receptor subunits enhance excitatory synaptic transmission at central synapses by presynaptic mechanisms. Neuroscience 128(2):269-280.

Ishibashi M, McMahon AP. 2002. A sonic hedgehog-dependent signaling relay regulates growth of diencephalic and mesencephalic primordia in the early mouse embryo. Development 129(20):4807-4819.

Itoh N, Ornitz DM. 2004. Evolution of the Fgf and Fgfr gene families. Trends Genet 20(11):563-569.

Johnson-Farley NN, Patel K, Kim D, Cowen DS. 2007. Interaction of FGF-2 with IGF-1 and BDNF in stimulating Akt, ERK, and neuronal survival in hippocampal cultures. Brain Res 1154:40-49.

Jope RS, Roh MS. 2006. Glycogen synthase kinase-3 (GSK3) in psychiatric diseases and therapeutic interventions. Curr Drug Targets 7(11):1421-1434.

Kaabeche K, Lemonnier J, Le Mee S, Caverzasio J, Marie PJ. 2004. Cbl-mediated degradation of Lyn and Fyn induced by constitutive fibroblast growth factor receptor-2 activation supports osteoblast differentiation. J Biol Chem 279(35):36259-36267.

Kaga Y, Shoemaker WJ, Furusho M, Bryant M, Rosenbluth J, Pfeiffer SE, Oh L, Rasband M, Lappe-Siefke C, Yu K, Ornitz DM, Nave KA, Bansal R. 2006. Mice with conditional inactivation of fibroblast growth factor receptor-2 signaling in oligodendrocytes have normal myelin but display dramatic hyperactivity when combined with Cnp1 inactivation. J Neurosci 26(47):12339-12350.

Kato H, Sakai T, Tamura K, Minoguchi S, Shirayoshi Y, Hamada Y, Tsujimoto Y, Honjo T. 1996. Functional conservation of mouse Notch receptor family members. FEBS Lett 395(2-3):221-224.

Kawakami Y, Rodriguez-Leon J, Koth CM, Buscher D, Itoh T, Raya A, Ng JK, Esteban CR, Takahashi S, Henrique D, Schwarz MF, Asahara H, Izpisua Belmonte JC. 2003. MKP3 mediates the cellular response to FGF8 signalling in the vertebrate limb. Nat Cell Biol 5(6):513-519.

Kawamura H, Aswad F, Minagawa M, Malone K, Kaslow H, Koch-Nolte F, Schott WH, Leiter EH, Dennert G. 2005. P2X7 receptor-dependent and -independent T cell death is induced by nicotinamide adenine dinucleotide. J Immunol 174(4):1971-1979.

Kealey C, Reynolds A, Mynett-Johnson L, Claffey E, McKeon P. 2001. No evidence to support an association between the oestrogen receptor beta gene and bipolar disorder. Psychiatr Genet 11(4):223-226.

Khakh BS, North RA. 2006. P2X receptors as cell-surface ATP sensors in health and disease. Nature 442(7102):527-532.

Kilkenny DM, Rocheleau JV, Price J, Reich MB, Miller GG. 2003. c-Src regulation of fibroblast growth factor-induced proliferation in murine embryonic fibroblasts. J Biol Chem 278(19):17448-17454.

Kiselyov VV, Soroka V, Berezin V, Bock E. 2005. Structural biology of NCAM homophilic binding and activation of FGFR. J Neurochem 94(5):1169-1179.

Kolch W, Heidecker G, Kochs G, Hummel R, Vahidi H, Mischak H, Finkenzeller G, Marme D, Rapp UR. 1993. Protein kinase C alpha activates RAF-1 by direct phosphorylation. Nature 364(6434):249-252.

Kolkova K, Novitskaya V, Pedersen N, Berezin V, Bock E. 2000. Neural cell adhesion molecule-stimulated neurite outgrowth depends on activation of protein kinase C and the Ras-mitogen-activated protein kinase pathway. J Neurosci 20(6):2238-2246.

Komine O, Nagaoka M, Watase K, Gutmann DH, Tanigaki K, Honjo T, Radtke F, Saito T, Chiba S, Tanaka K. 2007. The monolayer formation of Bergmann glial cells is regulated by Notch/RBP-J signaling. Dev Biol 311(1):238-250.

Komuro H, Rakic P. 1998. Distinct modes of neuronal migration in different domains of developing cerebellar cortex. J Neurosci 18(4):1478-1490.

Konarski JZ, McIntyre RS, Grupp LA, Kennedy SH. 2005. Is the cerebellum relevant in the circuitry of neuropsychiatric disorders? J Psychiatry Neurosci 30(3):178-186.

Kornmann M, Beger HG, Korc M. 1998. Role of fibroblast growth factors and their receptors in pancreatic cancer and chronic pancreatitis. Pancreas 17(2):169-175.

Kouhara H, Hadari YR, Spivak-Kroizman T, Schilling J, Bar-Sagi D, Lax I, Schlessinger J. 1997. A lipid-anchored Grb2-binding protein that links FGF-receptor activation to the Ras/MAPK signaling pathway. Cell 89(5):693-702.

Kozisek ME, Middlemas D, Bylund DB. 2008. Brain-derived neurotrophic factor and its receptor tropomyosin-related kinase B in the mechanism of action of antidepressant therapies. Pharmacol Ther 117(1):30-51.

Kuhn R, Streif S, Wurst W. 2007. RNA interference in mice. Handb Exp Pharmacol(178):149-176.

Kumamaru E, Numakawa T, Adachi N, Yagasaki Y, Izumi A, Niyaz M, Kudo M, Kunugi H. 2008. Glucocorticoid Prevents Brain-Derived Neurotrophic Factor-Mediated Maturation of Synaptic Function in Developing Hippocampal Neurons through Reduction in the Activity of Mitogen-Activated Protein Kinase. Mol Endocrinol 22(3):546-558.

Kunath T, Gish G, Lickert H, Jones N, Pawson T, Rossant J. 2003. Transgenic RNA interference in ES cell-derived embryos recapitulates a genetic null phenotype. Nat Biotechnol 21(5):559-561.

Labasi JM, Petrushova N, Donovan C, McCurdy S, Lira P, Payette MM, Brissette W, Wicks JR, Audoly L, Gabel CA. 2002. Absence of the P2X7 receptor alters leukocyte function and attenuates an inflammatory response. J Immunol 168(12):6436-6445.

Laemmli UK. 1970. Cleavage of structural proteins during the assembly of the head of bacteriophage T4. Nature 227(5259):680-685.

Lam CS, Sleptsova-Friedrich I, Munro AD, Korzh V. 2003. SHH and FGF8 play distinct roles during development of noradrenergic neurons in the locus coeruleus of the zebrafish. Mol Cell Neurosci 22(4):501-515.

Lee NS, Dohjima T, Bauer G, Li H, Li MJ, Ehsani A, Salvaterra P, Rossi J. 2002. Expression of small interfering RNAs targeted against HIV-1 rev transcripts in human cells. Nat Biotechnol 20(5):500-505.

Leonardo ED, Hen R. 2006. Genetics of affective and anxiety disorders. Annu Rev Psychol 57:117-137.

Lickert H, Takeuchi JK, Von Both I, Walls JR, McAuliffe F, Adamson SL, Henkelman RM, Wrana JL, Rossant J, Bruneau BG. 2004. Baf60c is essential for function of BAF chromatin remodelling complexes in heart development. Nature 432(7013):107-112.

Liu A, Joyner AL. 2001. Early anterior/posterior patterning of the midbrain and cerebellum. Annu Rev Neurosci 24:869-896.

Liu A, Li JY, Bromleigh C, Lao Z, Niswander LA, Joyner AL. 2003. FGF17b and FGF18 have different midbrain regulatory properties from FGF8b or activated FGF receptors. Development 130(25):6175-6185.

Liu A, Losos K, Joyner AL. 1999. FGF8 can activate Gbx2 and transform regions of the rostral mouse brain into a hindbrain fate. Development 126(21):4827-4838.

Lopez AD, Mathers CD, Ezzati M, Jamison DT, Murray CJ. 2006. Global and regional burden of disease and risk factors, 2001: systematic analysis of population health data. Lancet 367(9524):1747-1757.

Lordkipanidze T, Dunaevsky A. 2005. Purkinje cell dendrites grow in alignment with Bergmann glia. Glia 51(3):229-234.

Lucae S, Salyakina D, Barden N, Harvey M, Gagne B, Labbe M, Binder EB, Uhr M, Paez-Pereda M, Sillaber I, Ising M, Bruckl T, Lieb R, Holsboer F, Muller-Myhsok B. 2006. P2RX7, a gene coding for a purinergic ligand-gated ion channel, is associated with major depressive disorder. Hum Mol Genet 15(16):2438-2445.

Lucki I. 1997. The forced swimming test as a model for core and component behavioral effects of antidepressant drugs. Behav Pharmacol 8(6-7):523-532.

Mallei A, Shi B, Mocchetti I. 2002. Antidepressant treatments induce the expression of basic fibroblast growth factor in cortical and hippocampal neurons. Mol Pharmacol 61(5):1017-1024.

Manni E, Petrosini L. 2004. A century of cerebellar somatotopy: a debated representation. Nat Rev Neurosci 5(3):241-249.

Maragnoli ME, Fumagalli F, Gennarelli M, Racagni G, Riva MA. 2004. Fluoxetine and olanzapine have synergistic effects in the modulation of fibroblast growth factor 2 expression within the rat brain. Biol Psychiatry 55(11):1095-1102.

Martinez S, Crossley PH, Cobos I, Rubenstein JL, Martin GR. 1999. FGF8 induces formation of an ectopic isthmic organizer and isthmocerebellar development via a repressive effect on Otx2 expression. Development 126(6):1189-1200.

Mason JM, Morrison DJ, Bassit B, Dimri M, Band H, Licht JD, Gross I. 2004. Tyrosine phosphorylation of Sprouty proteins regulates their ability to inhibit growth factor signaling: a dual feedback loop. Mol Biol Cell 15(5):2176-2188.

McEwen BS. 1999. Stress and hippocampal plasticity. Annu Rev Neurosci 22:105-122.

McMahon AP, Bradley A. 1990. The Wnt-1 (int-1) proto-oncogene is required for development of a large region of the mouse brain. Cell 62(6):1073-1085.

McMahon AP, Joyner AL, Bradley A, McMahon JA. 1992. The midbrain-hindbrain phenotype of Wnt-1-/Wnt-1- mice results from stepwise deletion of engrailed-expressing cells by 9.5 days postcoitum. Cell 69(4):581-595.

Mervaala E, Fohr J, Kononen M, Valkonen-Korhonen M, Vainio P, Partanen K, Partanen J, Tiihonen J, Viinamaki H, Karjalainen AK, Lehtonen J. 2000. Quantitative MRI of the hippocampus and amygdala in severe depression. Psychol Med 30(1):117-125.

Meyer JH, Ginovart N, Boovariwala A, Sagrati S, Hussey D, Garcia A, Young T, Praschak-Rieder N, Wilson AA, Houle S. 2006. Elevated monoamine oxidase a levels in the brain: an explanation for the monoamine imbalance of major depression. Arch Gen Psychiatry 63(11):1209-1216.

Meyers EN, Lewandoski M, Martin GR. 1998. An Fgf8 mutant allelic series generated by Cre- and Flp-mediated recombination. Nat Genet 18(2):136-141.

Millen KJ, Wurst W, Herrup K, Joyner AL. 1994. Abnormal embryonic cerebellar development and patterning of postnatal foliation in two mouse Engrailed-2 mutants. Development 120(3):695-706.

Millet S, Campbell K, Epstein DJ, Losos K, Harris E, Joyner AL. 1999. A role for Gbx2 in repression of Otx2 and positioning the mid/hindbrain organizer. Nature 401(6749):161-164.

Minichiello L, Korte M, Wolfer D, Kuhn R, Unsicker K, Cestari V, Rossi-Arnaud C, Lipp HP, Bonhoeffer T, Klein R. 1999. Essential role for TrkB receptors in hippocampus-mediated learning. Neuron 24(2):401-414.

Mjaatvedt AE, Cabin DE, Cole SE, Long LJ, Breitwieser GE, Reeves RH. 1995. Assessment of a mutation in the H5 domain of Girk2 as a candidate for the weaver mutation. Genome Res 5(5):453-463.

Mohammadi M, Dionne CA, Li W, Li N, Spivak T, Honegger AM, Jaye M, Schlessinger J. 1992. Point mutation in FGF receptor eliminates phosphatidylinositol hydrolysis without affecting mitogenesis. Nature 358(6388):681-684.

Molteni R, Fumagalli F, Magnaghi V, Roceri M, Gennarelli M, Racagni G, Melcangi RC, Riva MA. 2001. Modulation of fibroblast growth factor-2 by stress and corticosteroids: from developmental events to adult brain plasticity. Brain Res Brain Res Rev 37(1-3):249-258.

Moodie SA, Willumsen BM, Weber MJ, Wolfman A. 1993. Complexes of Ras.GTP with Raf-1 and mitogen-activated protein kinase kinase. Science 260(5114):1658-1661.

Moores TS, Hasdemir B, Vega-Riveroll L, Deuchars J, Parson SH. 2005. Properties of presynaptic P2X7-like receptors at the neuromuscular junction. Brain Res 1034(1-2):40-50.

Mori T, Tanaka K, Buffo A, Wurst W, Kuhn R, Gotz M. 2006. Inducible gene deletion in astroglia and radial glia--a valuable tool for functional and lineage analysis. Glia 54(1):21-34.

Muda M, Theodosiou A, Rodrigues N, Boschert U, Camps M, Gillieron C, Davies K, Ashworth A, Arkinstall S. 1996. The dual specificity phosphatases M3/6 and MKP-3 are highly selective for inactivation of distinct mitogen-activated protein kinases. J Biol Chem 271(44):27205-27208.

Muller MB, Wurst W. 2004. Getting closer to affective disorders: the role of CRH receptor systems. Trends Mol Med 10(8):409-415.

Mumm JS, Kopan R. 2000. Notch signaling: from the outside in. Dev Biol 228(2):151-165.

Nagy A, Rossant J, Nagy R, Abramow-Newerly W, Roder JC. 1993. Derivation of completely cell culture-derived mice from early-passage embryonic stem cells. Proc Natl Acad Sci U S A 90(18):8424-8428.

Naserke T. 2007. Specific and redundant functions of Fgf receptors in development of the midbrain and anterior hindbrain of the mouse. Munich: Technical University Munich.

Nelson JC, Charney DS. 1981. The symptoms of major depressive illness. Am J Psychiatry 138(1):1-13.

Nemeroff CB, Owens MJ, Bissette G, Andorn AC, Stanley M. 1988. Reduced corticotropin releasing factor binding sites in the frontal cortex of suicide victims. Arch Gen Psychiatry 45(6):577-579.

Nemeroff CB, Widerlov E, Bissette G, Walleus H, Karlsson I, Eklund K, Kilts CD, Loosen PT, Vale W. 1984. Elevated concentrations of CSF corticotropin-releasing factor-like immunoreactivity in depressed patients. Science 226(4680):1342-1344.

Nestler EJ, Carlezon WA, Jr. 2006. The mesolimbic dopamine reward circuit in depression. Biol Psychiatry 59(12):1151-1159.

Nie X, Luukko K, Kettunen P. 2006. FGF signalling in craniofacial development and developmental disorders. Oral Dis 12(2):102-111.

Norrholm SD, Ouimet CC. 2001. Altered dendritic spine density in animal models of depression and in response to antidepressant treatment. Synapse 42(3):151-163.

Oberdoerffer P, Kanellopoulou C, Heissmeyer V, Paeper C, Borowski C, Aifantis I, Rao A, Rajewsky K. 2005. Efficiency of RNA interference in the mouse hematopoietic system varies between cell types and developmental stages. Mol Cell Biol 25(10):3896-3905.

Ohbayashi N, Shibayama M, Kurotaki Y, Imanishi M, Fujimori T, Itoh N, Takada S. 2002. FGF18 is required for normal cell proliferation and differentiation during osteogenesis and chondrogenesis. Genes Dev 16(7):870-879.

Ohkubo Y, Uchida AO, Shin D, Partanen J, Vaccarino FM. 2004. Fibroblast growth factor receptor 1 is required for the proliferation of hippocampal progenitor cells and for hippocampal growth in mouse. J Neurosci 24(27):6057-6069.

Ohl F, Holsboer F, Landgraf R. 2001. The modified hole board as a differential screen for behavior in rodents. Behav Res Methods Instrum Comput 33(3):392-397.

Ornitz DM, Itoh N. 2001. Fibroblast growth factors. Genome Biol 2(3):REVIEWS3005.

Ornitz DM, Xu J, Colvin JS, McEwen DG, MacArthur CA, Coulier F, Gao G, Goldfarb M. 1996. Receptor specificity of the fibroblast growth factor family. J Biol Chem 271(25):15292-15297.

Paddison PJ, Caudy AA, Bernstein E, Hannon GJ, Conklin DS. 2002. Short hairpin RNAs (shRNAs) induce sequence-specific silencing in mammalian cells. Genes Dev 16(8):948-958.

Paddison PJ, Cleary M, Silva JM, Chang K, Sheth N, Sachidanandam R, Hannon GJ. 2004. Cloning of short hairpin RNAs for gene knockdown in mammalian cells. Nat Methods 1(2):163-167.

Papiol S, Arias B, Gasto C, Gutierrez B, Catalan R, Fananas L. 2007. Genetic variability at HPA axis in major depression and clinical response to antidepressant treatment. J Affect Disord 104(1-3):83-90.

Peters KG, Escobedo JA, Fantl WJ, Williams LT. 1992. Interactions of PDGF and FGF receptors with cytoplasmic signaling molecules. Cold Spring Harb Symp Quant Biol 57:63-66.

Phelps EA, LeDoux JE. 2005. Contributions of the amygdala to emotion processing: from animal models to human behavior. Neuron 48(2):175-187.

Porsolt RD, Anton G, Blavet N, Jalfre M. 1978. Behavioural despair in rats: a new model sensitive to antidepressant treatments. Eur J Pharmacol 47(4):379-391.

Porsolt RD, Le Pichon M, Jalfre M. 1977. Depression: a new animal model sensitive to antidepressant treatments. Nature 266(5604):730-732.

Posener JA, Wang L, Price JL, Gado MH, Province MA, Miller MI, Babb CM, Csernansky JG. 2003. High-dimensional mapping of the hippocampus in depression. Am J Psychiatry 160(1):83-89.

Prakash N, Brodski C, Naserke T, Puelles E, Gogoi R, Hall A, Panhuysen M, Echevarria D, Sussel L, Weisenhorn DM, Martinez S, Arenas E, Simeone A, Wurst W. 2006. A Wnt1-regulated genetic network controls the identity and fate of midbrain-dopaminergic progenitors in vivo. Development 133(1):89-98.

Prakash N, Wurst W. 2004. Specification of midbrain territory. Cell Tissue Res 318(1):5-14.

Raadsheer FC, Hoogendijk WJ, Stam FC, Tilders FJ, Swaab DF. 1994. Increased numbers of corticotropin-releasing hormone expressing neurons in the hypothalamic paraventricular nucleus of depressed patients. Neuroendocrinology 60(4):436-444.

Rai KS, Hattiangady B, Shetty AK. 2007. Enhanced production and dendritic growth of new dentate granule cells in the middle-aged hippocampus following intracerebroventricular FGF-2 infusions. Eur J Neurosci 26(7):1765-1779.

Rakic P, Sidman RL. 1973. Weaver mutant mouse cerebellum: defective neuronal migration secondary to abnormality of Bergmann glia. Proc Natl Acad Sci U S A 70(1):240-244.

Rhinn M, Brand M. 2001. The midbrain--hindbrain boundary organizer. Curr Opin Neurobiol 11(1):34-42.

Robertson SJ, Ennion SJ, Evans RJ, Edwards FA. 2001. Synaptic P2X receptors. Curr Opin Neurobiol 11(3):378-386.

Rowitch DH, McMahon AP. 1995. Pax-2 expression in the murine neural plate precedes and encompasses the expression domains of Wnt-1 and En-1. Mech Dev 52(1):3-8.

Rubinson DA, Dillon CP, Kwiatkowski AV, Sievers C, Yang L, Kopinja J, Rooney DL, Zhang M, Ihrig MM, McManus MT, Gertler FB, Scott ML, Van Parijs L. 2003. A lentivirus-based system to functionally silence genes in primary mammalian cells, stem cells and transgenic mice by RNA interference. Nat Genet 33(3):401-406.

Saab CY, Willis WD. 2003. The cerebellum: organization, functions and its role in nociception. Brain Res Brain Res Rev 42(1):85-95.

Saarimaki-Vire J, Peltopuro P, Lahti L, Naserke T, Blak AA, Vogt Weisenhorn DM, Yu K, Ornitz DM, Wurst W, Partanen J. 2007. Fibroblast growth factor receptors cooperate to regulate neural progenitor properties in the developing midbrain and hindbrain. J Neurosci 27(32):8581-8592.

Sahay A, Hen R. 2007. Adult hippocampal neurogenesis in depression. Nat Neurosci 10(9):1110-1115.

Sanada K, Gupta A, Tsai LH. 2004. Disabled-1-regulated adhesion of migrating neurons to radial glial fiber contributes to neuronal positioning during early corticogenesis. Neuron 42(2):197-211.

Santarelli L, Saxe M, Gross C, Surget A, Battaglia F, Dulawa S, Weisstaub N, Lee J, Duman R, Arancio O, Belzung C, Hen R. 2003. Requirement of hippocampal neurogenesis for the behavioral effects of antidepressants. Science 301(5634):805-809.

Schultz W. 2006. Behavioral theories and the neurophysiology of reward. Annu Rev Psychol 57:87-115.

Segal RA, Greenberg ME. 1996. Intracellular signaling pathways activated by neurotrophic factors. Annu Rev Neurosci 19:463-489.

Sgaier SK, Millet S, Villanueva MP, Berenshteyn F, Song C, Joyner AL. 2005. Morphogenetic and cellular movements that shape the mouse cerebellum; insights from genetic fate mapping. Neuron 45(1):27-40.

Sheline YI, Sanghavi M, Mintun MA, Gado MH. 1999. Depression duration but not age predicts hippocampal volume loss in medically healthy women with recurrent major depression. J Neurosci 19(12):5034-5043.

Shirayama Y, Chen AC, Nakagawa S, Russell DS, Duman RS. 2002. Brain-derived neurotrophic factor produces antidepressant effects in behavioral models of depression. J Neurosci 22(8):3251-3261.

Sim JA, Young MT, Sung HY, North RA, Surprenant A. 2004. Reanalysis of P2X7 receptor expression in rodent brain. J Neurosci 24(28):6307-6314.

Simeone A. 2000. Positioning the isthmic organizer where Otx2 and Gbx2meet. Trends Genet 16(6):237-240.

Skaper SD, Facci L, Culbert AA, Evans NA, Chessell I, Davis JB, Richardson JC. 2006. P2X(7) receptors on microglial cells mediate injury to cortical neurons in vitro. Glia 54(3):234-242.

Smith AG, Hooper ML. 1987. Buffalo rat liver cells produce a diffusible activity which inhibits the differentiation of murine embryonal carcinoma and embryonic stem cells. Dev Biol 121(1):1-9.

Smith KM, Ohkubo Y, Maragnoli ME, Rasin MR, Schwartz ML, Sestan N, Vaccarino FM. 2006. Midline radial glia translocation and corpus callosum formation require FGF signaling. Nat Neurosci 9(6):787-797.

Soares JC, Mann JJ. 1997. The anatomy of mood disorders--review of structural neuroimaging studies. Biol Psychiatry 41(1):86-106.

Solle M, Labasi J, Perregaux DG, Stam E, Petrushova N, Koller BH, Griffiths RJ, Gabel CA. 2001. Altered cytokine production in mice lacking P2X(7) receptors. J Biol Chem 276(1):125-132.

Soriano P. 1999. Generalized lacZ expression with the ROSA26 Cre reporter strain. Nat Genet 21(1):70-71.

Steuber-Buchberger P, Wurst W, Kuhn R. 2008. Simultaneous Cre-mediated conditional knockdown of two genes in mice. Genesis 46(3):144-151.

Stokoe D, McCormick F. 1997. Activation of c-Raf-1 by Ras and Src through different mechanisms: activation in vivo and in vitro. EMBO J 16(9):2384-2396.

Strakowski SM, Delbello MP, Adler CM. 2005. The functional neuroanatomy of bipolar disorder: a review of neuroimaging findings. Mol Psychiatry 10(1):105-116.

Strohle A, Holsboer F. 2003. Stress responsive neurohormones in depression and anxiety. Pharmacopsychiatry 36 Suppl 3:S207-214.

Suzuki T, Hide I, Ido K, Kohsaka S, Inoue K, Nakata Y. 2004. Production and release of neuroprotective tumor necrosis factor by P2X7 receptor-activated microglia. J Neurosci 24(1):1-7.

Svenningsson P, Tzavara ET, Qi H, Carruthers R, Witkin JM, Nomikos GG, Greengard P. 2007. Biochemical and behavioral evidence for antidepressant-like effects of 5-HT6 receptor stimulation. J Neurosci 27(15):4201-4209.

Tanaka M, Kadokawa Y, Hamada Y, Marunouchi T. 1999. Notch2 expression negatively correlates with glial differentiation in the postnatal mouse brain. J Neurobiol 41(4):524-539.

Thomas KR, Capecchi MR. 1990. Targeted disruption of the murine int-1 proto-oncogene resulting in severe abnormalities in midbrain and cerebellar development. Nature 346(6287):847-850.

Tonissaar M, Philips MA, Eller M, Harro J. 2004. Sociability trait and serotonin metabolism in the rat social interaction test. Neurosci Lett 367(3):309-312.

Trokovic R, Trokovic N, Hernesniemi S, Pirvola U, Vogt Weisenhorn DM, Rossant J, McMahon AP, Wurst W, Partanen J. 2003. FGFR1 is independently required in both developing mid- and hindbrain for sustained response to isthmic signals. EMBO J 22(8):1811-1823.

Tronche F, Kellendonk C, Kretz O, Gass P, Anlag K, Orban PC, Bock R, Klein R, Schutz G. 1999. Disruption of the glucocorticoid receptor gene in the nervous system results in reduced anxiety. Nat Genet 23(1):99-103.

Trullas R, Jackson B, Skolnick P. 1989. Genetic differences in a tail suspension test for evaluating antidepressant activity. Psychopharmacology (Berl) 99(2):287-288.

Tsai SJ, Wang YC, Hong CJ, Chiu HJ. 2003. Association study of oestrogen receptor alpha gene polymorphism and suicidal behaviours in major depressive disorder. Psychiatr Genet 13(1):19-22.

Tsuchioka M, Takebayashi M, Hisaoka K, Maeda N, Nakata Y. 2008. Serotonin (5-HT) induces glial cell line-derived neurotrophic factor (GDNF) mRNA expression via the transactivation of fibroblast growth factor receptor 2 (FGFR2) in rat C6 glioma cells. J Neurochem.

Turner CA, Akil H, Watson SJ, Evans SJ. 2006. The fibroblast growth factor system and mood disorders. Biol Psychiatry 59(12):1128-1135.

Valjent E, Pages C, Herve D, Girault JA, Caboche J. 2004. Addictive and non-addictive drugs induce distinct and specific patterns of ERK activation in mouse brain. Eur J Neurosci 19(7):1826-1836.

Venero C, Tilling T, Hermans-Borgmeyer I, Herrero AI, Schachner M, Sandi C. 2004. Water maze learning and forebrain mRNA expression of the neural cell adhesion molecule L1. J Neurosci Res 75(2):172-181.

Wahl MB, Deng C, Lewandoski M, Pourquie O. 2007. FGF signaling acts upstream of the NOTCH and WNT signaling pathways to control segmentation clock oscillations in mouse somitogenesis. Development 134(22):4033-4041.

Walf AA, Rhodes ME, Frye CA. 2004. Antidepressant effects of ERbeta-selective estrogen receptor modulators in the forced swim test. Pharmacol Biochem Behav 78(3):523-529.

Walsh FS, Meiri K, Doherty P. 1997. Cell signalling and CAM-mediated neurite outgrowth. Soc Gen Physiol Ser 52:221-226.

Wang VY, Zoghbi HY. 2001. Genetic regulation of cerebellar development. Nat Rev Neurosci 2(7):484-491.

Weller M, Krautler N, Mantei N, Suter U, Taylor V. 2006. Jagged1 ablation results in cerebellar granule cell migration defects and depletion of Bergmann glia. Dev Neurosci 28(1-2):70-80.

Wilkie AO. 2005. Bad bones, absent smell, selfish testes: the pleiotropic consequences of human FGF receptor mutations. Cytokine Growth Factor Rev 16(2):187-203.

Williams EJ, Walsh FS, Doherty P. 2003. The FGF receptor uses the endocannabinoid signaling system to couple to an axonal growth response. J Cell Biol 160(4):481-486.

Williams RL, Hilton DJ, Pease S, Willson TA, Stewart CL, Gearing DP, Wagner EF, Metcalf D, Nicola NA, Gough NM. 1988. Myeloid leukaemia inhibitory factor maintains the developmental potential of embryonic stem cells. Nature 336(6200):684-687.

Wong ML, Licinio J. 2001. Research and treatment approaches to depression. Nat Rev Neurosci 2(5):343-351.

Wurst W, Auerbach AB, Joyner AL. 1994. Multiple developmental defects in Engrailed-1 mutant mice: an early mid-hindbrain deletion and patterning defects in forelimbs and sternum. Development 120(7):2065-2075.

Wurst W, Bally-Cuif L. 2001. Neural plate patterning: upstream and downstream of the isthmic organizer. Nat Rev Neurosci 2(2):99-108.

Xu J, Liu Z, Ornitz DM. 2000. Temporal and spatial gradients of Fgf8 and Fgf17 regulate proliferation and differentiation of midline cerebellar structures. Development 127(9):1833-1843.

Yacubova E, Komuro H. 2003. Cellular and molecular mechanisms of cerebellar granule cell migration. Cell Biochem Biophys 37(3):213-234.

Yamaguchi TP, Harpal K, Henkemeyer M, Rossant J. 1994. fgfr-1 is required for embryonic growth and mesodermal patterning during mouse gastrulation. Genes Dev 8(24):3032-3044.

Ye W, Shimamura K, Rubenstein JL, Hynes MA, Rosenthal A. 1998. FGF and Shh signals control dopaminergic and serotonergic cell fate in the anterior neural plate. Cell 93(5):755-766.

Yoon K, Nery S, Rutlin ML, Radtke F, Fishell G, Gaiano N. 2004. Fibroblast growth factor receptor signaling promotes radial glial identity and interacts with Notch1 signaling in telencephalic progenitors. J Neurosci 24(43):9497-9506.

Yu Y, Ugawa S, Ueda T, Ishida Y, Inoue K, Kyaw Nyunt A, Umemura A, Mase M, Yamada K, Shimada S. 2008. Cellular localization of P2X7 receptor mRNA in the rat brain. Brain Res 1194:45-55.

Yue Q, Groszer M, Gil JS, Berk AJ, Messing A, Wu H, Liu X. 2005. PTEN deletion in Bergmann glia leads to premature differentiation and affects laminar organization. Development 132(14):3281-3291.

Yun HM, Kim S, Kim HJ, Kostenis E, Kim JI, Seong JY, Baik JH, Rhim H. 2007. The novel cellular mechanism of human 5-HT6 receptor through an interaction with Fyn. J Biol Chem 282(8):5496-5505.

Zhang X, Ibrahimi OA, Olsen SK, Umemori H, Mohammadi M, Ornitz DM. 2006. Receptor specificity of the fibroblast growth factor family. The complete mammalian FGF family. J Biol Chem 281(23):15694-15700.

Zhao M, Li D, Shimazu K, Zhou YX, Lu B, Deng CX. 2007. Fibroblast growth factor receptor-1 is required for long-term potentiation, memory consolidation, and neurogenesis. Biol Psychiatry 62(5):381-390.

Zheng W, Nowakowski RS, Vaccarino FM. 2004. Fibroblast growth factor 2 is required for maintaining the neural stem cell pool in the mouse brain subventricular zone. Dev Neurosci 26(2-4):181-196.

Zimmerman L, Parr B, Lendahl U, Cunningham M, McKay R, Gavin B, Mann J, Vassileva G, McMahon A. 1994. Independent regulatory elements in the nestin gene direct transgene expression to neural stem cells or muscle precursors. Neuron 12(1):11-24.

Zubenko GS, Hughes HB, 3rd, Stiffler JS, Brechbiel A, Zubenko WN, Maher BS, Marazita ML. 2003a. Sequence variations in CREB1 cosegregate with depressive disorders in women. Mol Psychiatry 8(6):611-618.

Zubenko GS, Maher B, Hughes HB, 3rd, Zubenko WN, Stiffler JS, Kaplan BB, Marazita ML. 2003b. Genome-wide linkage survey for genetic loci that influence the development of depressive disorders in families with recurrent, early-onset, major depression. Am J Med Genet B Neuropsychiatr Genet 123(1):1-18.

8 ABBREVIATIONS

°C	degree Celsius
µ	micro (10^{-6})
5-HT	5-hydroxytryptamine, serotonin
A	purine base adenine
A	ampere
Ac	acetate
ATP	adenosine triphosphate
attB	attachment site in the donor vector (RMCE)
attP	attachment site in the acceptor sequence (RMCE)
b-Gal	β-Galactosidase
bp	basepair
BSA	bovine serum albumin
c	centi (10^{-2})
C	pyrimidine base cytosine
C.elegans	Caenorhabditis elegans
C31Int	integrase from phage fC31
cDNA	copyDNA
Ci	Curie; 1 Ci = 3.7 x 10_{10} Bq
CNS	central nervous system
cpm	counts per minute
CREB	cAMP responsive element binding protein
CRHR	corticotropin releasing hormone (receptor)
c-terminus	carboxy terminus
CTP	cytosine triphosphate
Da	Dalton
DAB	3,3'-diaminobenzidine
DEPC	diethylpyrocarbonate
DMSO	dimethylsulfoxide
DNA	desoxyribonucleic acid
dNTP	desoxyribonucleotide triphosphate
dsRNA	double stranded RNA
DTT	1,4-dithiothreitol
E.coli	Escherichia coli
e.g.	exempli gratia, for example
EDTA	ethylendiamintetraacetate
EGTA	ethylenglycol-bis-(b-aminoethylether)-N,N,N´,N´-tetraacetate
ES cells	embryonic stem cells
EtBr	ethidium bromide
EtOH	ethanol
F	Farad
FCS	fetal calf serum
Fig.	figure
g	acceleration of gravity (9.81 m/s2)
g	gramme
G	purinbase guanine
GABA	g-aminobutyric acid
GMC	German mouse clinic
GSK3	glycogen synthase kinase 3
h	hour(s)
hCG	human chorion gonadotropin
HPRT	hypoxanthine phosphoribosyltransferase
IHC	immunhistochemistry
IMP	inositol monophosphatase
ISH	in situ hybridization

ITI	intertrial interval
IVC	indivudally ventilated cages
k.o.	knockout; organism, in which one gene is completely switched off
kb	kilobasepairs
kD	kilodalton
l	liter
lacZ	ß-Galactosidase
LB	Luria Broth
Li	lithium
LIF	leukemia inhibiting factor
Luc	firefly-luciferase
m	milli (10^{-3})
M	molar (mol/l)
mA	milli-ampere
MAPK	mitogen activated protein kinase
mHB	modified Hole Board
min	minute(s)
miRNA	micro RNA
mRNA	messenger ribonucleic acid
mut	mutant
n	nano (10^{-9})
n	sample size
neo	neomycin
NMDA	N-methyl-D-aspartate
NP-40	Nonidet P-40
nt	nucleotides
n-terminus	ammino terminus
o/n	over night
OD	optical density
ORF	open reading frame
P	postnatal day (P0 is the day of birth)
p	pico (10^{-12})
p	p-value for statistical analysis
PBS	phosphate buffered saline
PCR	polymerase chain reaction
PFA	paraformaldehyde
PMSG	pregnant mare's serum gonadotropin
RISC	RNA-inducing silencing complex
RMCE	recombinase mediated cassette exchange
RNA	ribonucleic acid
RNAi	RNA interference
rpm	rounds per minute
RT	room temperature
RT-PCR	reverse transcription PCR
SDS	sodium dodecyl sulfate
sec or s	second(s)
shRNA	short hairpin RNA
siRNA	short interfering RNA
SSC	sodium saline citrate
SSRI	selective serotonin reuptake inhibitor
T	pyrimidine base thymine
TAE	tris acetate with EDTA
TB	tris buffer
TBE	tris borate with EDTA
TBS	tris buffered saline
TBS(T)	tris buffered saline (with Tween)
TE	tris-EDTA
temp.	temperature
Tris	trishydroxymethyl-aminomethane
tRNA	tranfer ribonucleic acid
U	unit(s)
UTP	uracil triphosphate

UV	ultraviolet
V	volt
Vol.	volume or volumetric content
VPA	valproic acid
Wnt	wingless-type MMTV integration site family
wt	wildtype

9 ACKNOWLEDGMENTS / DANKSAGUNG

First of all I would like to express my gratitude to Prof. Wolfgang Wurst who accepted me as a student and provided me with excellent equipment and enjoyable atmosphere in his Lab.
I would like to thank my supervisor Dr. Ralf Kühn, who gave me the opportunity to develop my own ideas and patiently corrected my writing.
My cordial thanks go to Dr. Daniela Vogt Weisenhorn, who helped me with morphology and immunohistochemistry in all concerns. The scientific discussions with her were always very motivating and helped me to make the right decisions.
I thank the people from the behaviour group of the IDG for helping me practically with the behaviour tests. Special thanks go to Dr. Sabine M. Hölter and Magdalena Kallnik from the behaviour team of the IDG, who helped me with the analysis of the behaviour data.
My sincere thank goes to Annerose Kurz-Drexler for her help with cold in situ hybrisations and to all other colleagues who helped me practically or theoretically.
Especially, I want to mention some young and talented scientists: Florian Giesert, Dr. Barbara DiBenedetto, and Dr. Ravi Jagasia.

Here, I also want to thank the really important people in my life. I thank my parents, my brothers, and my sister for their continuing and absolute support during my University studies and my time as PhD student. Special thanks go to Konstantina for her support and appreciation.

Mein Dank gilt zuallererst Professor Dr. Wolfgang Wurst für die Möglichkeit meine Doktorarbeit an seinem Institut anzufertigen. Abgesehen von einem perfekt ausgestatteten Labor und einer netten Arbeitsatmosphäre bin ich besonders für die leider viel zu seltenen aber dennoch sehr hilfreichen Kommentare und Anregungen dankbar.
Meinem Betreuer Dr. Ralf Kühn möchte ich für die Möglichkeit danken, meine eigenen Ideen einzubringen und viel praktische Erfahrung zu sammeln. Darüber hinaus möchte ich mich für die sorgfältige Korrektur der Doktorarbeit bedanken.
Zu aufrichtigem Dank bin ich Dr. Daniela Vogt Weisenhorn verpflichtet. Ich habe von Ihr viel über Morphologie und histologische Verfahren gelernt, und die Diskussionen mit Ihr waren stets hilfreich und interessant.
Ich möchte mich auch bei den Leuten der Verhaltensgruppe des Instituts für Entwicklungsgenetik dafür bedanken, dass Sie mir einen Großteil der praktischen Durchführung der Verhaltenstests abgenommen haben. In dem Zusammenhang bedanke ich mich besonders bei Dr. Sabine M. Hölter und Magdalena Kallnik für die Hilfe bei der Auswertung der Verhaltenstests.
Annerose Kurz-Drexler möchte ich für ihre hilfreiche und freundliche Art danken und dafür die nicht-radioaktive (kalte) *in situ* Hybridisierungen für mich durchgeführt zu haben. Darüber hinaus möchte ich mich bei allen Kollegen bedanken, die mir praktisch oder theoretisch geholfen haben, und es mir ermöglicht haben, diese Arbeit anzufertigen. Besonders hervorheben möchte ich dabei die begnadeten Jungwissenschaftler, die mir auf freundschaftlicher Basis immer versucht haben, zu helfen: Florian Giesert, Dr. Barbara DiBenedetto und Dr. Ravi Jagasia.

Ich möchte mich an diese Stelle natürlich auch bei den wirklich wichtigen Menschen in meinem Leben bedanken. Bei meinen Eltern, meinen beiden Brüdern und meinem Schwesterchen möchte ich mich für die anhaltende und bedingungslose Unterstützung bedanken, die ich nicht nur während der Doktorarbeit, sondern auch schon in den Jahren des Biologie-Studiums erhalten habe. Besonders bedanken möchte ich mich bei Konstantina, die mit ihrer Unterstützung und ihrem Verständnis den erfolgreichen Abschluß der Doktorarbeit wesentlich erleichterte.

10 DECLARATION / ERKLÄRUNG

Sabit Delić
Kärntner Weg 15
40591 Düsseldorf

Düsseldorf, den 17.12.2008

Sehr geehrte Damen und Herren,

hiermit erkläre ich, Sabit Delić, dass die eingereichte Dissertation meine erste ist. Es gab keinen früheren Versuch eine Dissertation einzureichen oder sich einer Doktorprüfung zu unterziehen.
Ferner erkläre ich, dass die vorliegende Dissertation selbstständig und ohne unerlaubte Hilfe angefertigt worden ist. Die Dissertation wird vollständig eingereicht und wurde nicht in wesentlichen Teilen einer anderen Prüfungskommission vorgelegt.

Sabit Delić